

Liquefaction Susceptibility of Sand Including Fines

Hamza Saeed

Submitted to the
Institute of Graduate Studies and Research
in partial fulfillment of the requirements for the degree of

Master of Science
in
Civil Engineering

Eastern Mediterranean University
January 2020
Gazimağusa, North Cyprus

Approval of the Institute of Graduate Studies and Research

Prof. Dr. Ali Hakan Ulusoy
Director

I certify that this thesis satisfies all the requirements as a thesis for the degree of Master of Science in Civil Engineering.

Prof. Dr. Umut Türker
Chair, Department of Civil Engineering

We certify that we have read this thesis and that in our opinion it is fully adequate in scope and quality as a thesis for the degree of Master of Science in Civil Engineering.

Asst. Prof. Dr. Eriş Uygur
Co-Supervisor

Prof. Dr. Zalihe N. Sezai
Supervisor

Examining Committee

1. Prof. Dr. Zalihe N. Sezai

2. Assoc. Prof. Dr. Serhan Şensoy

3. Asst. Prof. Dr. Abdullah Ekinci

ABSTRACT

Liquefaction phenomenon associated with loss in shear strength of saturated sand is triggered due to monotonically increasing loads or propagation of seismic waves through granular structure under restricted drainage conditions. Such circumstances resulting in excess in pore-water pressure development within a soil-structure result in loss of confinement in soil strata due to decrease in intergranular forces transfer thus leading to strain-softening behaviour of soil matrix. This research focuses on effect of fines content with high plasticity on the liquefaction susceptibility of sand. The study simulates variation in soil composition by incorporating fines of 10, 20 and 30% by dry weight into sand-matrix. Fines are incorporated in three subgroups as silt, clay and equal proportions of silt and clay together to form a Sand-fines matrix. The instability characteristics of test specimen of soil-matrices are evaluated by subjecting them to monotonic and cyclic direct shear box tests and consolidated undrained triaxial tests. The tests specimens are prepared at initial relative densities of 35 % and 70% by dry funnel pluviation technique. Prior to shearing, specimens are consolidated under three different effective stresses of 50, 100 and 150 kPa. The results are analysed based on principles of critical state soil mechanics. The effect of fines addition on the soil fabric is also observed with the use of optical microscope. Amongst all soil groups experimented, Sand and clayey-silty Sand (10%) mixture prepared at loose state exhibited susceptibility for flow liquefaction. Critical state evaluations of all dense specimens indicating the stable response of specimens whilst loose specimens resulting in diverse characteristics. Apropos of loose specimens, liquefaction resistance increases of sand-fines mixture increases up to 20% of fines addition and

30% sand-fines mixtures are plotting in a close proximity of critical state line.

Keywords: Critical Void Ratio, Direct Shear Box Test, Fines Separation, Liquefaction, Sand with Fines, Steady State, Triaxial Test

ÖZ

Doymuş kumun kayma mukavemeti kaybıyla ilişkili sıvılaşma olgusu, monoton olarak artan yükler veya kısıtlı drenaj koşulları altında granül yapı boyunca sismik dalgaların yayılması nedeniyle tetiklenmektedir. Bir toprak yapısı içinde boşluk suyu basıncı gelişimine neden olan bu koşullar taneler arası kuvvetlerin transferindeki azalmaya bağlı olarak zemin tabakalarında hapsedme kaybı ile sonuçlanır, böylece toprak matrisinin deformasyon-yumuşama davranışına yol açar. Bu araştırma, yüksek plastisiteli ince tanecik içeriğinin kumun sıvılaşma duyarlılığına etkisi üzerine odaklanmaktadır. Bu çalışma, kuru ağırlıkça % 10, 20 ve % 30 oranında ince tanecikleri kum matrisine dahil ederek zemin bileşimindeki değişimini simüle eder. İnce tanecikler, silt, kil ve eşit oranlarda silt ve kil şeklinde bir Sand-fines matrisi oluşturmuş üç alt gruba teşkil edilmektedir. Toprak matrislerinin test örneğinin dengesizlik özellikleri, monotonik ve tekrarlı yüklemeli direkt kesme kutusu deneylerine ve konsolidasyonlu drenajsız üç eksenli deneylere tabi tutularak değerlendirilir. Deney numuneleri % 35 ve %70 başlangıç rölatif sıklık oranlarında kuru huni yayma tekniği kullanılarak hazırlanır. Kesme işleminden önce, numuneler 50, 100 ve 150 kPa'lık üç farklı efektif gerilme değerleri altında konsolide edilir. Sonuçlar, kritik zemin mekaniği prensiplerine dayanılarak analiz edilir. Optik mikroskop kullanılarak ince toz ilavesinin zemin taneciklerinin düzenlenmesi üzerindeki etkisi de gözlenir. Deney yapılan tüm toprak grupları arasında, gevşek halde hazırlanan Kum ve killi-siltli Kum (% 10) karışımı akış sıvılaşmaya yatkınlık göstermiştir. Tüm numunelerin kritik durum değerlendirmeleri, numunelerin kararlı yanıtını gösterirken, gevşek numuneler farklı özelliklere neden olur. Gevşek numunelerde, kum-ince tanecikleri karışımının sıvılaşma direnci artışları, % 20'ye

varan ince malzeme ilavesi ile artar ve % 30 kum-taneli karışımlar, kritik durum hattına yakın bir yerde yer alırlar.

Anahtar Kelimeler: Kritik Boşluk Oranı, Direk Kesme Kutusu Deneyi, İnce Tane Ayırıştırması, Sıvılaşma, İnce Tane İçerikli Kum, Denge Durumu, Üç Eksenli Deney

ACKNOWLEDGMENT

I would like to express my sincere appreciation and heartfelt gratitude to my greatest honourable mentors Professor Dr. Zalihe Nalbantođlu Sezai and Assistant Professor Dr. Eriř Uygur for their extraordinary kind support, patience and appreciation by sharing their pearls of wisdom to complete this comprehensive research work. Their encouragement throughout this journey undoubtedly amplified my interest for further research in geotechnical engineering.

I would also like to thank Civil Engineering Department academic staff for their great support and care taken during my study. A special thanks to laboratory engineer Mr. Ođün Kılıç and Mr. Orkan Lord for their kind technical assistance and support regarding experimental work.

Last but not least, I am thankful to my parents for their great support, prayers and motivation throughout this journey.

TABLE OF CONTENTS

ABSTRACT	iii
ÖZ	v
ACKNOWLEDGMENT	vii
LIST OF TABLES	xiv
LIST OF FIGURES	xv
LIST OF SYMBOLS	xxvii
LIST OF ABBREVIATION	xxix
1 INTRODUCTION	1
1.1 Scope and Objective	1
1.2 Dissertation Framework	4
2 LITERATURE REVIEW	6
2.1 Introduction	6
2.1.1 Flow Liquefaction	6
2.1.2 Cyclic Mobility	8
2.2 Liquefaction Susceptibility	8
2.2.1 Historical Criteria	9
2.2.2 Site Geological and Compositional Assessment	10
2.2.3 Critical State Framework	11
2.3 Liquefaction Failure	13
2.3.1 Flow liquefaction	13
2.3.2 Cyclic Mobility	16
2.4 Monotonic Undrained Response of Sand	19
2.4.1 Phase Transformations	19

2.5 Influence of Plastic Fines on Liquefaction Susceptibility	21
2.5.1 Influence of Fines Content on Liquefaction Susceptibility	26
2.6 Static Liquefaction Assessment Approach	29
2.6.1 State Parameter	30
2.7 Effect of Fines on Behavioural Properties of Sand	31
2.7.1 Inter-grain and Inter-fine State Concept	32
2.7.2 Transitional Fine Content, TFC	33
2.8 Specimen Reconstitution Techniques	37
3 RESEARCH METHODOLOGY	39
3.1 Introduction	39
3.2 Experimental Soils	39
3.2.1 Silver Beach Sand	39
3.2.1.1 Silver Beach Site Analysis	42
3.2.1.2 Mineralogical Analysis	42
3.2.2 Famagusta Bay Alluvial Clay	46
3.2.2.1 Mineralogical Analysis	48
3.3 Famagusta Shores Liquefaction Susceptibility Analysis	49
3.4 Testing Strategy	50
3.4.1 Experimental Program	51
3.5 Experiments Methodology	53
3.5.1 Specific Gravity	53
3.5.2 Particle Size Distribution	53
3.5.2.1 Dry Sieving	53
3.5.2.2 Wet Sieving	55
3.5.2.3 Hydrometer Analysis	55

3.5.3 Plasticity Tests	56
3.5.4 Relative Density	58
3.5.4.1 Maximum Void Ratio	58
3.5.4.2 Minimum Void Ratio	59
3.5.5 Chemical Tests.....	60
3.5.5.1 Cation Exchange Capacity	60
3.5.5.2 Specific Surface Area.....	62
3.5.5.3 Carbonate Content.....	64
3.5.5.4 Electrochemical Tests	65
3.6 Separation of Silt and Clay Fractions.....	66
3.6.1 Minuscule Stage Analysis	67
3.6.2 Intermediate Stage Analysis	69
3.6.3 Wide Scale Analysis	71
3.7 Consolidated Drained Direct Shear Box Test (CD-DST)	78
3.7.1 Sample Preparation	78
3.7.1.1 Loose Specimens Preparation	78
3.7.1.2 Dense Specimens Preparation	79
3.7.2 Application of the Normal Stress	80
3.7.3 Specimens Shearing Rate	81
3.8 Consolidated Drained Cyclic Direct Shear Box Test.....	81
3.9 Consolidated Undrained Triaxial Test.....	82
3.9.1 Specimen Preparation	82
3.9.2 Sample Saturation.....	83
3.9.3 Sample Consolidation.....	84
3.9.4 Shearing Rate.....	84

4 RESULTS AND DISCUSSION	87
4.1 Behavioural Characteristics of Sand Matrix with Fines.....	87
4.1.1 Effect of Fines on the Index Properties	87
4.1.2 Sand-Fines Matrix Optical Microscopic Analysis.....	93
4.2 Compositional Liquefaction Susceptibility Analysis	96
4.3 Drained Behaviour of Sand-Fines at Loose and Dense States	99
4.3.1 Effect of Fines on Initial States	99
4.3.2 Drained Response of Sand-Fines Mixtures	101
4.3.3 Drained Response of Sand.....	105
4.3.4 Drained Response of Silty Sand Matrix	106
4.3.4.1 Effect of 10% Silt Fractions in Sand Matrix.....	106
4.3.4.2 Effect of 20% Silt Fractions in Sand Matrix.....	107
4.3.4.3 Effect of 30% Silt Fraction in Sand Matrix.....	109
4.3.4.4 Critical State Analysis of Silty-Sand Matrix.....	110
4.3.5 Drained Response of Clayey-Silty Sand Matrix.....	113
4.3.5.1 Effect of 10% Clay and Silt Fractions in Sand Matrix.....	113
4.3.5.2 Effect of 20% Clay and Silt Fractions in Sand Matrix.....	114
4.3.5.3 Effect of 30% Clay and Silt Fraction in Sand Matrix	115
4.3.5.4 Critical State Analysis of Clayey-Silty Sand Matrix	117
4.3.6 Drained Response of Clayey Sand Matrix.....	119
4.3.6.1 Effect of 10% Clay Fractions in Sand Matrix	119
4.3.6.2 Effect of 20% Clay Fractions in Sand Matrix	121
4.3.6.3 Effect of 30% Clay Fractions in Sand Matrix	122
4.3.6.4 Critical State Analysis of Clayey-Silty-Sand Matrix	123
4.4.7 General Discussion of CD-DST Results.....	126

4.4 Cyclic Direct Shear Testing	128
4.4.1 Residual behaviour of Sand	129
4.4.2 Clayey-Sand Mixture	129
4.4.3 Silty- Sand Mixture	131
4.4.4 Clayey-Silty- Sand Mixture	134
4.5 Residual Behaviour Conclusive Remarks	136
4.6 Drained Strength Parameters Conclusive Remarks.....	139
4.7 Undrained Monotonic Behaviour	142
4.7.1 Initial State Analysis.....	142
4.7.2 Monotonic Loading Undrained Response of Sand.....	151
4.7.3 Critical and Steady State Analysis SP-Group.....	155
4.7.4 Monotonic Loading Undrained Response of Silty-Sand.....	157
4.7.4.1 Loose State	157
4.7.4.2 Dense State	163
4.7.4.3 Critical and Steady State Analysis SP-SM Groups.....	168
4.7.5 Monotonic Loading Undrained Response Clayey-Silty-Sand.....	174
4.7.5.1 Loose State	174
4.7.5.2 Dense State	179
4.7.5.3 Critical and Steady State Analysis SM-SC Group.....	184
4.7.6 Monotonic Loading Undrained Response of Clayey-Sand	190
4.7.6.1 Loose State	190
4.7.6.2 Dense State	195
4.7.6.3 Critical and Steady State Analysis SP-SC Groups.....	200
4.8 Visual Analysis of Liquified and Non-Liquified Groups.....	205
4.9 General Discussion of CU-Triaxial Test	211

4.10 Data Comparison of Direct Shear & Triaxial Test Results	213
5 CONCLUSIONS AND RECOMMENDATIONS	218
5.1 Conclusions	218
5.2 Recommendations	220
REFERENCES.....	222
APPENDICES	230
Appendix A: Optical Microscopic Analysis of Silver Beach Sand.....	231
Appendix B: Separated Soil Liquid Limit Linear Regression Analysis	235
Appendix C: Direct Shear Box Test Experiment Outcomes	236
Appendix D: Direct Shear Box Test Shear Stress versus Displacement Curves .	241
Appendix E: Critical State Parameters CU-TT	246

LIST OF TABLES

Table 1: Strain-softening susceptibility of fine-grained soils.	11
Table 2: SBS index properties.	41
Table 3: Alluvial Clay index properties.	48
Table 4: SBS Classification.	54
Table 5: Typical values of CEC and SSA of clay minerals	63
Table 6: Electrochemical properties of tested soils.....	65
Table 7: Index properties of separated fine proportions	74
Table 8: Index properties of sand-fine mixtures.	89
Table 9: Relative densities of sand-fines mixtures after consolidation.....	100
Table 10: Sand-fines groups shear strength parameters.....	101
Table 11: SP-SM state parameters.	112
Table 12: SM-SC State parameters.	119
Table 13: SP-SC state parameters.	125
Table 14: Post confining stress effect on initial states.	143
Table 15: Undrained static response of sand-fines mixtures.	147
Table 16: Steady state parameters of loose and dense sand.....	157
Table 17: Steady state parameters of silty-sand groups.	173
Table 18: Steady state parameters of clayey-silty sand mixture.	189
Table 19: Steady state parameters of clayey-sand groups.	205
Table 20: P-value significance analysis of Ψ for CD-DST and CU-TT.	217

LIST OF FIGURES

Figure 1: Upstream face San Fernando Dam flow liquefaction.....	2
Figure 2: Lake Merced, California 1957 lateral spreading	3
Figure 3: Lateral spreading Joban Motorway Japan 2011, $M_w = 9.0$	3
Figure 4: Undrained stress-strain behaviour of liquefied soil.....	7
Figure 5: Undrained stress path response of liquefied soil.	7
Figure 6: World-wide data for observed liquefaction at sites within the epicentral distance of earthquake.....	9
Figure 7: Gradation based liquefaction susceptibility of soils	10
Figure 8: (a)Stress-strain (b) Stress-void response of loose and dense sand under same effective stress.....	12
Figure 9: Flow liquefaction susceptibility concept	12
Figure 10: Loose saturated sand behaviour under monotonic undrained triaxial test	13
Figure 11: Undrained response of sand at different confining stress.....	15
Figure 12: Flow liquefaction surface and steady state.	16
Figure 13: Cyclic stress-strain response of Nevada Sand	17
Figure 14: Cyclic stress-path of Nevada Sand	17
Figure 15: Excess pore water pressure generation of Nevada Sand.	18
Figure 16: Flow liquefaction and cyclic mobility susceptible zones	18
Figure 17: Illustration of undrained shearing behaviour of sand soil	19
Figure 18: General monotonic undrained response of sand.....	20
Figure 19: Influence of clay fraction on undrained sand behaviour	22
Figure 20: Effect of clay content in sand on pore water pressure generation	22
Figure 21: Effect of fines on cyclic resistance of sand	23

Figure 22: Liquefaction resistance curves of sand-fines mixture at loose state.....	24
Figure 23: Liquefaction resistance curves of sand-fines mixture at medium dense state	24
Figure 24: Liquefaction resistance curves of sand-fines mixture at dense state	25
Figure 25: CSR versus PI of fines.....	25
Figure 26: sand with low plastic fines liquefaction potential curves	26
Figure 27: Undrained response of sand and sand with 15% fines.	27
Figure 28: Liquefaction resistance curves of sand-silt mixtures.....	28
Figure 29: Loose sand-fines mixtures undrained behaviour	29
Figure 30: QSS residual strength definition.....	30
Figure 31: Undrained stress-path	30
Figure 32: State parameter	31
Figure 33: (a) Inter-granular (b) Inter-fine void concepts.....	33
Figure 34: Binary packing for minimum void ratios.	35
Figure 35: Mixed soil classification.....	36
Figure 36: Sample reconstitution techniques schematic illustration.....	38
Figure 37: Sand sampling location.....	40
Figure 38: SBS sampling.	40
Figure 39: (a) Observation hole location (b) Site condition due to seasonal changes.	41
Figure 40: Famagusta Bay Delta 3D modelling.....	43
Figure 41: Famagusta Bay Delta contouring map.....	44
Figure 42: SBS Quartz minerals types.	44
Figure 43: SBS Particles shape.	45
Figure 44: Sand particles characterization	45

Figure 45: Sampling location of Alluvial Clay	46
Figure 46: Alluvial Clay strata.....	47
Figure 47: GWT location	47
Figure 48: Shallow earthquake magnitudes and epicentres distances from Famagusta	49
Figure 49: Famagusta shores susceptibility to liquefaction	50
Figure 50: State criterion evaluation strategy	52
Figure 51: SBS grain size distribution.	54
Figure 52: Alluvial Clay (a) composition (b) grains distribution	55
Figure 53: Alluvial Clay particle-size distribution curve.....	56
Figure 54: Alluvial soil flow curve for LL determination.	57
Figure 55: Clay minerals location on Casagrande’s Plasticity Chart.....	58
Figure 56: Schematic illustration for (a) e_{max} and (b) e_{min} determination.	60
Figure 57: MBAT titration process flowchart.....	61
Figure 58: Schematic illustration of EGME test.	64
Figure 59: Calibration curve and calcite equivalent of tested soils.	65
Figure 60: Alluvial Clay particle settlement versus time.....	66
Figure 61: Miniscule stage hydrometer analysis of separated silt.	68
Figure 62: Extracted silt grains sedimentation time.....	68
Figure 63: (a) Miniscule separation scale (b) Layers.....	69
Figure 64: Intermediate scale hydrometer analysis of separated silt.	70
Figure 65: (a) Intermediate scale (b) Siphon technique.	70
Figure 66: Crack patterns (a) Clay (b) Silt.....	71
Figure 67: Soil separation procedure flowchart.	72
Figure 68: Wide scale timeline of soil separation process.	72

Figure 69: Soil fine fractions (a) Miniscale (b) Intermediate (c) Wide Scales.....	73
Figure 70: Comparison of particle-size distribution of silt from different stages.....	73
Figure 71: Separated soil and soil mixtures hydrometer analysis results.	75
Figure 72: Separated soils flow curves.	75
Figure 73: Plasticity Chart (Das & Sobhan, 2014).	76
Figure 74: Separated soil and soil mixtures proportions (a) Silt (b) Clay and (c) 50% clay & 50% Silt.	76
Figure 75: Physicochemical properties comparison of separated and prepared soil .	77
Figure 76: Wide Scale.....	77
Figure 77: Schematic illustration of DFP technique.....	79
Figure 78: Schematic illustration of dense specimen preparation.	79
Figure 79: Fines inclusion in sand matrix.	80
Figure 80: (a) DFP Technique (b) Dense Sample preparations.	83
Figure 81: Triaxial base adapter.....	84
Figure 82: Summarized triaxial testing process.	85
Figure 83: Triaxial testing setup.	86
Figure 84: Soil groups USCS particles ranges distribution chart.	88
Figure 85: Variation of G_s with addition of fines.	90
Figure 86: Variation of e_{max} and e_{min} corresponding to fines content.	91
Figure 87: Fine-dominated groups liquid limits.....	92
Figure 88: SSA of Illite mineral containing fine-dominated groups.....	92
Figure 89: Sand-fines matrix (0 & 10%).	94
Figure 90: Sand-fines matrix (20 & 30%).	95
Figure 91: SP-SM group composition liquefaction analysis.....	96
Figure 92: SM-SC group composition liquefaction analysis	97

Figure 93: SP-SC groups compositional liquefaction analysis	97
Figure 94: Fines liquefaction susceptibility by Chinese Criteria.	98
Figure 95: Fines liquefaction susceptibility corresponding to 2 μ m presence.....	98
Figure 96: Internal frictional angles of Sand and silty-Sand groups.....	102
Figure 97: Internal frictional angles of Sand and clayey-silty-Sand groups.....	103
Figure 98: Internal frictional angles of Sand and clayey-Sand groups.	103
Figure 99: Variation of internal frictional angles of soil groups.....	104
Figure 100: Sand-fines groups peak/ultimate shear strength mobilisation.	104
Figure 101: Drained frictional angle of SP-SM for loose, residual and dense.	105
Figure 102: SP consolidated void ratios and CSL plot.	105
Figure 103: Drained frictional angle of SP-SM (10%) for loose, residual and dense.	106
Figure 104: SP-SM (10%) consolidated void ratios and CSL plot.	107
Figure 105: Drained frictional angle of SP-SM (20%) for loose, residual and dense.	108
Figure 106: SP-SM (20%) consolidated void ratios and CSL plot.	108
Figure 107: Drained frictional angle of SP-SM (30%) for loose, residual and dense.	109
Figure 108: SP-SM (30%) consolidated void ratios and CSL plot.	110
Figure 109: CSL plot of SP-SM-L Matrix with respect to e , σ'_n and f_c	110
Figure 110: CSL plot of SP-SM-D Matrix with respect to e , σ'_n and f_c	111
Figure 111: State parameters of SP-SM groups.....	112
Figure 112: Drained frictional angle of SM-SC (10%) for loose, residual and dense.	113
Figure 113: SM-SC (10%) consolidated void ratios and CSL plot.....	114

Figure 114: Drained frictional angle of SM-SC (20%) for loose, residual and dense.	114
Figure 115: SM-SC (20%) consolidated void ratios and CSL plot.....	115
Figure 116: Drained frictional angle of SM-SC (30%) for loose, residual and dense.	116
Figure 117: SM-SC (30%) consolidated void ratios and CSL plot.....	116
Figure 118: CSL plot of SP-SM-L Matrix with respect to e , σ'_n and f_c	117
Figure 119: CSL plot of SP-SM-L Matrix with respect to e , σ'_n and f_c	118
Figure 120: State parameters of SM-SC groups.	118
Figure 121: Drained frictional angle of SP-SC (10%) for loose, residual and dense.	120
Figure 122: SP-SC (10%) consolidated void ratios and CSL plot.....	120
Figure 123: Drained frictional angle of SP-SC (20%) for loose, residual and dense.	121
Figure 124: SP-SC (20%) consolidated void ratios and CSL plot.....	122
Figure 125: Drained frictional angle of SP-SC (30%) for loose, residual and dense.	122
Figure 126: SP-SC (30%) consolidated void ratios and CSL plot.....	123
Figure 127: CSL plot of SP-SC-L Matrix with respect to e , σ'_n and f_c	124
Figure 128: CSL plot of SP-SC-L Matrix with respect to e , σ'_n and f_c	124
Figure 129: State parameter pf SP-SC groups.	125
Figure 130: Variation of CSL lines of soil groups.....	126
Figure 131: State parameter variation with fines (Loose state).	127
Figure 132: State parameter variation with fines (Dense state).	128
Figure 133: Residual hysteresis loops of SP.	129

Figure 134: Residual hysteresis loops of SP-SC (10%).....	130
Figure 135: Residual hysteresis loops of SP-SC (20%).....	130
Figure 136: Residual hysteresis loops of SP-SC (30%).....	131
Figure 137: Residual hysteresis loops of SP-SM (10%).....	132
Figure 138: Residual hysteresis loops of SP-SM (20%).....	133
Figure 139: Residual hysteresis loops of SP-SM (30%).....	133
Figure 140: Residual hysteresis loops of SM-SC (10%).	134
Figure 141: Residual hysteresis loops of SM-SC (20%).	135
Figure 142: Residual hysteresis loops of SM-SC (30%).	135
Figure 143: SP-SM groups MDST and CDST ϕ'_{res} . comparison.....	136
Figure 144: SM-SC groups MDST and CDST ϕ'_{res} . comparison.	136
Figure 145: SP-SC groups MDST and CDST ϕ'_{res} . comparison.....	137
Figure 146: Residuals Comparison between TDST and CDST.....	138
Figure 147: MDST and CDST shear strength properties comparison.	138
Figure 148: Variation in frictional angles of SP-SM groups.	139
Figure 149: Variation in frictional angles of SM-SC groups.....	139
Figure 150: Variation in frictional angles of SP-SC groups.	140
Figure 151: Variation in cohesion with respect to fines content of SP-SM.....	141
Figure 152: Variation in cohesion with respect to fines content of SM-SC.	141
Figure 153: Variation in cohesion with respect to fines content of SP-SC.....	142
Figure 154: SP-SM direct shear and triaxial D_R comparison (Loose).	144
Figure 155: SP-SM direct shear and triaxial D_R comparison (Dense).....	144
Figure 156: SM-SC direct shear and triaxial D_R comparison (Loose).....	145
Figure 157: SM-SC direct shear and triaxial D_R comparison (Dense).	145
Figure 158: SP-SC direct shear and triaxial D_R comparison (Loose).	146

Figure 159: SP-SC direct shear and triaxial DR comparison (Dense).....	146
Figure 160: Undrained response of loose sand.	151
Figure 161: Excess pore-water pressure development in base sand.	151
Figure 162: Stress paths for loose sand.....	152
Figure 163: Undrained response of base sand.	152
Figure 164: Pore-water pressure development in dense sand.	153
Figure 165: Stress paths for dense sand.	153
Figure 166: SSL and FLS of Sand.	156
Figure 167: Steady state liquefaction susceptibility analysis.....	156
Figure 168: Undrained response of loose SP-SM (10%).....	158
Figure 169: Pore-water pressure development in loose state SP-SM (10%).	158
Figure 170: Stress paths of loose specimen SP-SM (10%).....	159
Figure 171: Undrained response of loose base SP-SM (20%).....	159
Figure 172: Pore-water pressure development in loose state SP-SM (20%).	160
Figure 173: Stress paths of loose specimen SP-SM (20%).....	160
Figure 174: Undrained response of loose base SP-SM (30%).....	161
Figure 175: Pore-water pressure development in loose state SP-SM (30%).	161
Figure 176: Stress paths of loose specimen SP-SM (30%).....	162
Figure 177: Undrained response of dense SP-SM (10%).	163
Figure 178: Pore-water pressure development in dense state SP-SM (10%).	163
Figure 179: Stress paths of dense specimen SP-SM (10%).....	164
Figure 180: Undrained response of dense SP-SM (20%).	164
Figure 181: Pore-water pressure development in dense state SP-SM (20%).	165
Figure 182: Stress paths of dense specimen SP-SM (20%).....	165
Figure 183: Undrained response of dense SP-SM (30%).	166

Figure 184: Pore-water pressure development in dense state SP-SM (30%).	166
Figure 185: SP-SM (30%) stress paths of dense specimen.	167
Figure 186: SSL comparison of SP-SM-L groups.	168
Figure 187: SSL comparison of SP-SM-D groups.	169
Figure 188: SSL cumulative plot of SP-SM groups.	169
Figure 189: SSL liquefaction susceptibility SP-SM (10%).	170
Figure 190: SSL liquefaction susceptibility SP-SM (20%).	170
Figure 191: SSL liquefaction susceptibility SP-SM (30%).	171
Figure 192: SP-SM state parameter.	171
Figure 193: SP-SM pore pressure ratio variation.	173
Figure 194: Undrained response of loose SM-SC (10%).	174
Figure 195: Pore-water pressure development in loose state SM-SC (10%).	174
Figure 196: Stress paths of loose specimen SM-SC (10%).	175
Figure 197: Undrained response of loose SM-SC (20%).	176
Figure 198: Pore-water pressure development in loose state SM-SC (20%).	176
Figure 199: Stress paths of loose specimen SM-SC (20%).	177
Figure 200: Undrained response of loose SM-SC (30%).	177
Figure 201: Pore-water pressure development in loose state SM-SC (30%).	178
Figure 202: Stress paths of loose specimen SM-SC (30%).	178
Figure 203: Undrained response of dense SM-SC (10%).	179
Figure 204: Pore-water pressure development in dense state SM-SC (10%).	179
Figure 205: Stress paths of dense specimen SM-SC (10%).	180
Figure 206: Undrained response of dense SM-SC (20%).	180
Figure 207: Pore-water pressure development in dense state SM-SC (20%).	181
Figure 208: Stress paths of dense specimen SM-SC (20%).	181

Figure 209: Undrained response of dense SM-SC (30%).....	182
Figure 210: Pore-water pressure development in dense state SM-SC (30%).....	182
Figure 211: Stress paths of dense specimen SM-SC (30%).....	183
Figure 212: SSL comparison of SM-SC-L groups.....	184
Figure 213: SSL comparison of SM-SC-D groups.	185
Figure 214: SSL cumulative plot of SM-SC groups.....	186
Figure 215: SSL liquefaction susceptibility SM-SC (10%).....	186
Figure 216: SSL liquefaction susceptibility SM-SC (20%).....	187
Figure 217: SSL liquefaction susceptibility SM-SC (30%).....	187
Figure 218: SM-SC state parameter.....	188
Figure 219: SM-SC pore pressure ratio variation.	189
Figure 220: Undrained response of loose SP-SC (10%).....	190
Figure 221: Pore-water pressure development in loose state SP-SC (10%).....	191
Figure 222: Stress paths of loose specimen SP-SC (10%).....	191
Figure 223: Undrained response of loose SP-SC (20%).....	192
Figure 224: Pore-water pressure development in loose state SP-SC (20%).....	192
Figure 225: Stress paths of loose specimen SP-SC (20%).....	193
Figure 226: Undrained response of loose SP-SC (30%).....	193
Figure 227: Pore-water pressure development in loose state SP-SC (30%).....	194
Figure 228: Stress paths of loose specimen SP-SC (30%).....	194
Figure 229: Undrained response of dense SP-SC (10%).	195
Figure 230: Pore-water pressure development in dense state SP-SC (10%).	196
Figure 231: SP-SC (10%) stress paths of loose specimen.	196
Figure 232: Undrained response of dense SP-SC (20%).	197
Figure 233: Pore-water pressure development in dense state SP-SC (20%).	197

Figure 234: Stress paths of dense specimen SP-SC (20%).	198
Figure 235: Undrained response of dense SP-SC (30%).	198
Figure 236: Pore-water pressure development in dense state SP-SC (30%).	199
Figure 237: Stress paths of dense specimen SP-SC (30%).	199
Figure 238: SSL comparison of SP-SC-L groups.	200
Figure 239: SSL comparison of SP-SC-D groups.	201
Figure 240: SSL cumulative plot of SP-SC groups.	201
Figure 241: SSL liquefaction susceptibility SP-SC (10%).	202
Figure 242: SSL liquefaction susceptibility SP-SC (20%).	202
Figure 243: SSL liquefaction susceptibility SP-SC (30%).	203
Figure 244: SP-SC state parameter.	204
Figure 245: SP-SC pore pressure variation.	204
Figure 246: Development of wrinkles on rubber membrane.	206
Figure 247: Soil specimen after liquefaction (Amini & Qi, 2000).	206
Figure 248: SM-SC (10%) limited liquefaction observation.	207
Figure 249: SM-SC liquefied soil at (a)100 kPa and (b)150 kPa.	208
Figure 250: SM-SC groups visual comparison.	208
Figure 251: (a) Liquefied SM-SC (10%) and (b) Non-liquified SM-SC (30%) loose specimens bulging.	209
Figure 252: Clayey-Silty-Sand particle separation: Microstructure analysis of soil specimen under 150kPa confining stress.	210
Figure 253: Variation of SSL of soil groups.	211
Figure 254: State parameters variation with fines at loose state.	212
Figure 255: State parameters variation with fines at dense state.	212

Figure 256: SP-SM state parameters comparison between CD (DST) and CU (TT).	213
Figure 257: SM-SC state parameters comparison between CD (DST) and CU (TT).	214
Figure 258: SM-SC state parameters comparison between CD (DST) and CU (TT).	214
Figure 259: CD (DST) and CU (TT) SM-SC-L state parameters comparison with f_c	215
Figure 260: CD (DST) and CU (TT) SM-SC-D state parameters comparison with f_c	215
Figure 261: CD-DST & CU-TT Ψ comparison.	216

LIST OF SYMBOLS

σ'_n	Effective Normal Stress
B	Skempton's pore-water pressure coefficient
Cc	Coefficient of curvature
Cu	Coefficient of uniformity
D_{max}	Maximum diameter
D_r	Relative density
e	Global void ratio
E	Modulus of Elasticity
e_c	Consolidated void ratio
e_f	Inter-fine void ratio
e_i	Initial void ratio
e_s	Inter-granular void ratio
G_s	Specific gravity
kPa	kilo Pascal
k Ω	kilo Ohms
pH	Potential of hydrogen
ppm	Parts per million
psu	Practical salinity unit
r_u	Pore-pressure ratio
u_f	Flow potential
w.c	Water content
Δu	Change in pore-water pressure
μ	Microns

μS	Micro Siemens
ρ	Density
τ	Shear Stress
ϕ	Internal Frictional Angle
Ψ	State Parameter

LIST OF ABBREVIATION

ASTM	American Society for Testing and Materials
BS	British Standards
CD	Consolidated Drained
CEC	Cation Exchange Capacity
CSL	Critical State Limit
CU	Consolidated Undrained
CVR	Critical Void Ratio
DST	Direct Shear Test
EC	Electrical Conductivity
EGME	Ethylene Glycol Monoethyl Ether
ER	Electrical Resistivity
FLS	Flow Liquefaction Surface
GWT	Ground Water Table
HDPE	High Density Polyethylene
LL	Liquid Limit
LS	Linear Shrinkage
MBAT	Methylene Blue Adsorption Test
MRDST	Multi-reversal Direct Shear Test
PI	Plasticity Index
PL	Plastic Limit
SAL	Salinity
SBS	Silver Beach Sand
SSA	Specific Surface Area

SSL	Steady State Line
TDS	Total Dissolved Solids
TFC	Threshold Fines Content
USCS	Unified Soil Classification System

Chapter 1

INTRODUCTION

1.1 Scope and Objective

In geotechnical earthquake engineering, liquefaction is one of the most complex and sceptical topics in terms of assessment criteria. During earthquake loading, excess machinery vibrations or rapid loadings on loose saturated sand, shear strength and stiffness of the soil are dramatically reduced and the soil tend to behave as an aqueous medium resulting in devastating, environmental and economic consequences on the structures. Liquefaction phenomenon first came to attention to geotechnical engineers dates back to earthquakes in Alaska, USA magnitude of 9.2 and Niigata, Japan magnitude of 7.5 in 1964. The drastic damages to structures such as buried structures floatation, foundation failures, structures sinking and slope failures were all liquefaction induced and observed in these events. In the present-day world, geological changes are causing frequent earthquakes and structures especially constructed on bays or offshores are highly vulnerable or susceptible to these events.

Liquefaction terminology was first cited by Mogami and Kubo (1953) and this terminology is associated with several aspects under undrained condition such as excessive deformations either due to monotonic or cyclic disturbance of saturated soil. In terms of dry cohesionless soils, said terminology is often confused due to similar behaviour as of saturated soils under both monotonic and cyclic loadings. The accurate

terminology associated in case of dry cohesionless soils is fluidization. For saturated soils, the liquefaction phenomenon is further divided into two categories:

- Flow liquefaction
- Cyclic mobility

Flow liquefaction as compared to cyclic mobility is less frequent but results in severe consequences. In the case of flow liquefaction, flow failures cause enormous instabilities in the soil leading towards dramatic effects on standing structures or slopes. The primary aspect for such case is due to lower shear strength of soil in the liquified state than the static equilibrium of a soil mass. In contrast with flow liquefaction, cyclic mobility also produces large deformations and, in this case, the static equilibrium of a soil mass is less than the shear strength of liquefied soil. The prime examples of flow liquefaction and cyclic mobility are illustrated in Figures 1 – 3 respectively.



Figure 1: Upstream face San Fernando Dam flow liquefaction (Geo-Slope International Limited).

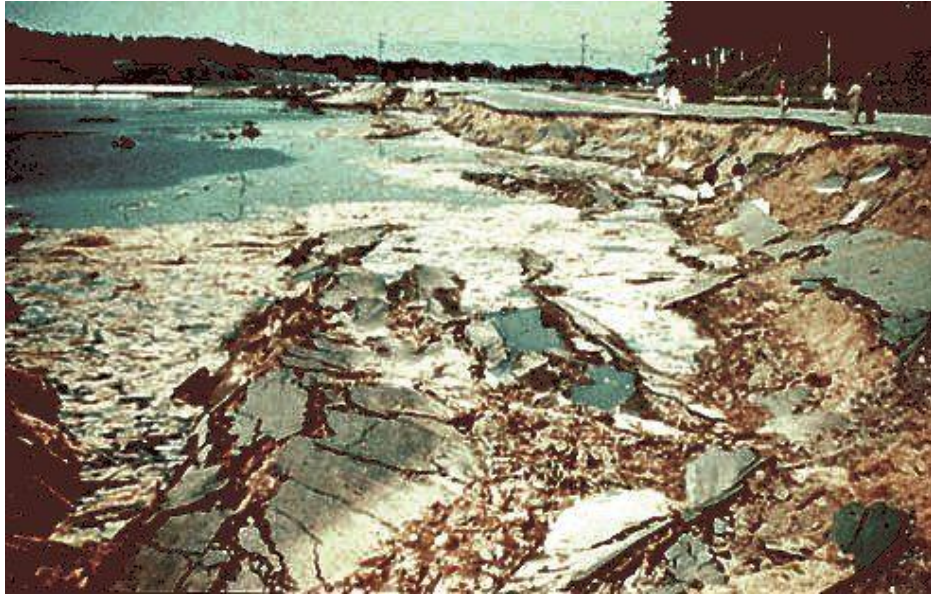


Figure 2: Lake Merced, California 1957 lateral spreading (Geo-Slope Limited).



Figure 3: Lateral spreading Joban Motorway Japan 2011, $M_w = 9.0$ (Dillerstone, 2011).

Static liquefaction occurs abruptly causing large displacements in soils. Influence of high plastic fines on static liquefaction is limited in the literature. However, the effect of low plastic fines has been widely discussed. The main focus in this dissertation study is to evaluate the shear strength properties and static liquefaction susceptibility

of Sand including high plastic fines. Sand samples along the coastline of Famagusta Bay are collected for this research and susceptibility of these to liquefaction is investigated. In order to study the effect of fines content on Sand behaviour, silt and clay fractions are added with varying percentages to form a set of manufactured samples. Silt and clay are separated and extracted from a natural clay through a separation process developed as part of this thesis. The test specimens are prepared to reflect various density states such as loose and dense. The laboratory testing programme included determination of physicochemical properties, monotonic Triaxial Compression and Direct Shear Box Tests along with cyclic (reversal) direct shear box tests. The core objectives of this research are as follows:

1. Develop a laboratory scale separation procedure for silt and clay fractions of a natural cohesive soil.
2. Investigate the effects of fines on soil fabric using optical microscope.
3. Investigate the changes in shear strength behaviour of manufactured soil specimens by monotonic triaxial tests, direct shear box tests and cyclic (reversal) direct shear box tests.
4. The results of this study will emphasize on the potential risk regarding the presence of fines in sands in the case of occurrence of liquefaction.

1.2 Dissertation Framework

The structure of the dissertation is outlined in the following:

Chapter 1 defines the primary purpose of the selected topic, information, background and its significance in geotechnical engineering field.

Chapter 2 includes a comprehensive literature review and fundamental concepts are extensively discussed including behaviour of Sand with fines under Monotonic and cyclic shear strength tests.

Chapter 3 comprises research methodology adopted to investigate the aforementioned objective.

Chapter 4 deals with the detailed evaluation of the results of experiments.

Chapter 5 concludes the findings of this thesis work and provides suggestions for further research.

Chapter 2

LITERATURE REVIEW

2.1 Introduction

In this chapter static liquefaction phenomenon and its significance in geotechnical engineering is discussed. A summary of the literature review on the available methods is done for the evaluation of liquefaction susceptibility is presented. In addition to this, previous studies related to the impact of fines inclusion in sand matrix are also presented.

Liquefaction phenomenon involves deformation of saturated soils when subjected to static or rapid loading, and repetitive disturbances under constrained drainage conditions. Based on the loading conditions, the liquefaction phenomenon is further categorized into two major categories; Flow liquefaction and Cyclic mobility. The primary aspect behind liquefaction phenomenon occurrence is generation of excess pore water pressure resulting in reduction in effective stress, thus abating confinement of strata. Such phenomena lead to soil behave as an aqueous medium exhibiting devastating effects on the structures.

2.1.1 Flow Liquefaction

Flow liquefaction can be triggered by several types of loadings such as static, constant/sustained loadings and dynamic loadings which can mobilize liquefied shear strength. The term flow liquefaction is associated to soils of low residual strengths where static equilibrium exceeds the shear strength of the liquefied soil. Flow

liquefaction. The flow liquefaction behaviour under undrained monotonic loading is presented in Figure 4 and Figure 5.

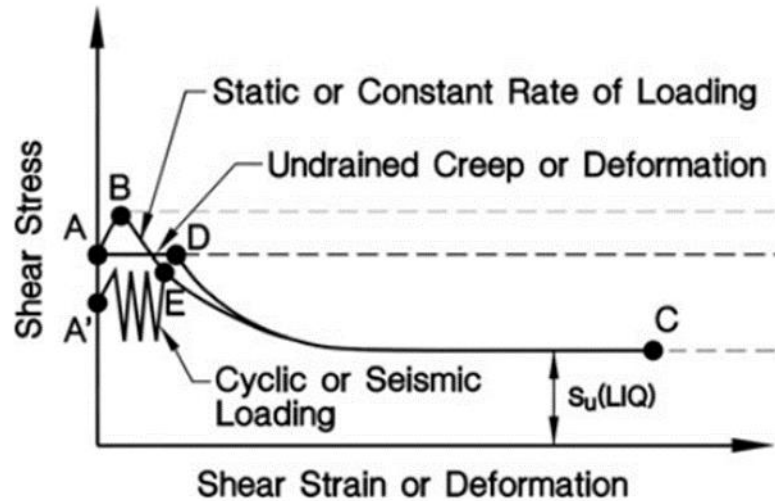


Figure 4: Undrained stress-strain behaviour of liquefied soil (Olson and Stark, 2003).

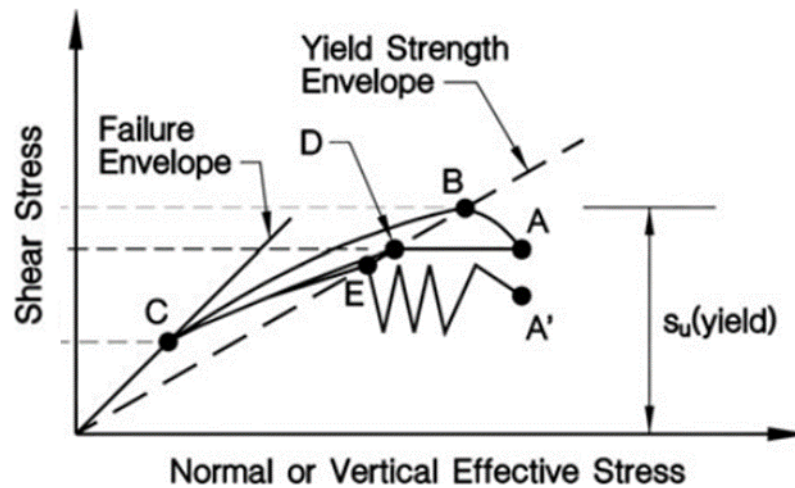


Figure 5: Undrained stress path response of liquefied soil (Olson and Stark, 2003).

In Figure 4, the stated loading scenarios are illustrated that can trigger flow liquefaction phenomenon. For instance, Point A represents current shear stress and strain in the soil element. Point A occurs if certain conditions are considered such as drainage is allowed. Yielding shear strength is presented as Point B on strength

envelope. Under undrained conditions, Point B is the maximum shear resistance a soil can mobilize. If the loading rate exceed beyond Point B, liquefaction is triggered where the soil matrix collapses. Points A and B are representing the static equilibrium (Static shear stress) high enough to trigger liquefaction associated to creep, deformation or shear strain. A point to be noted here the defined mechanisms are depicting anisotropic case study and similar behaviour is simulated in isotropic undrained testing (Explained in Section 2.4.1).

2.1.2 Cyclic Mobility

Cyclic mobility is typically associated with dynamic loadings such as earthquake or machine vibrations. In terms of cyclic mobility, static equilibrium of a soil mass is less than liquefied shear strength. In Figure 4 and Figure 5, cyclic behaviour of soil under undrained condition is illustrated. Point A' illustrates the current state of soil. In cyclic mobility, the intensity and duration of dynamic loading is the major criteria. If the duration is significant enough, causing excess pore water pressure generation thus Point A' shifts to Point E. At Point E, further application of load results in instability occurrence withing soil element thus, triggering liquefaction and Point E shifts to Point C.

2.2 Liquefaction Susceptibility

In order to evaluate liquefaction hazards, a systematic approach is followed. Traditional analyses approach involves the following steps:

- Analysing the historical aspect of the site. Numerous factors can be obtained from such analysis such as deposited soil which is directly linked with the configuration of site.
- Another factor is ground water table fluctuations.

- Among such factors the most crucial factor is the distance of the site from seismic zone. Several investigations regarding the liquefaction potential of site indicates that site within the certain distance (epicentral distance) of seismic zone is vulnerable to liquefaction effects (Novikova et al., 2006).
- Geological and compositional assessment of the site.
- Critical state framework analysis.

2.2.1 Historical Criteria

Site susceptibility to liquefaction phenomenon can be estimated by locating the coordinates of the selected area from epicentral distance. The compiled data is established from shallow earthquakes by Ambraseys (1988) and concludes that liquefaction is not observed beyond the epicentral distance. In Figure 6, regional liquefaction potential estimation for shallow earthquakes is illustrated.

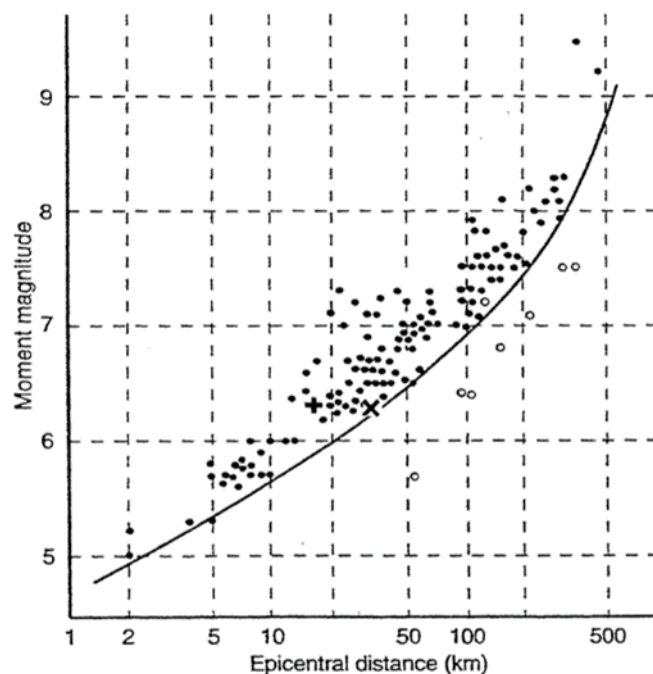


Figure 6: World-wide data for observed liquefaction at sites within the epicentral distance of earthquake (Ambraseys, 1988).

2.2.2 Site Geological and Compositional Assessment

Geological events of a particular site can also indicate the susceptibility of liquefaction such as deposition of the soil (Youd, 1991). Deposited soils such as fluvial and aeolian are highly susceptible and studies shows that in saturated alluvial deposits, liquefaction can also occur. One of the key assessments is primarily based on particle-size distribution of sand. Poorly graded sand that are deposited in loose state are mostly susceptible to liquefaction and in recent years, several studies performed on clean uniform sand and it is stated that uniform sands likely to liquefy. Liquefaction susceptibility can be predicted by gradation of a particular sand (Araujo & Ruiz, 2018). In Figure 7, soil susceptibility to liquefaction based on gradation is illustrated.

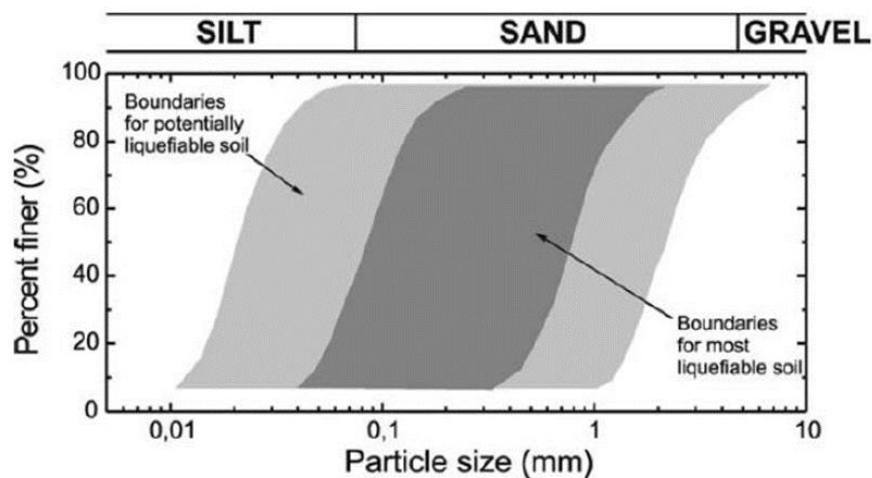


Figure 7: Gradation based liquefaction susceptibility of soils (Araujo & Ruiz, 2018).

In past studies, liquefaction assessment was only limited to coarser soils. Plastic soils, clay and silts were considered as non-liquefiable soils due to the fact that such soils exhibit cohesion factor which can nullify liquefaction phenomenon (Kramer, 2014). In recent years, it is observed that such soils can exhibit similar characteristics as of coarser soils. The said behaviour is termed as strain-softening and is observed in soils

with high activity. Wang, 1979 and U.S. Army Corps of Engineers (Chang, 1987; Koester, 1988) states that fine-grained soil can be susceptible to such behaviour if the criteria are met as mentioned in Table 1.

Table 1: Strain-softening susceptibility of fine-grained soils.

Parameters	Chinese Criteria	U.S. Corps of Engineers
Fines content (<0.005 μ m)	$\leq 15\%$	$\leq 10\%$
Liquid limit	$\leq 35\%$	$\leq 36\%$
Natural water content	$\geq 0.9LL$	$\geq 1.1LL$
Liquidity index	≤ 0.75	---

LL: Liquid Limit.

2.2.3 Critical State Framework

Evaluation of liquefaction susceptibility of a particular soil depends on its initial state. Here the initial state refers to density and stress state prior to the earthquake. The generation of excess pore water pressure during earthquake entirely relies on density of the soil and stress conditions (Kramer, 2014).

A commonly known aspect of shearing of a granular soil is that, for a certain effective stress at large strains the soil will reach to its critical state. Loose and dense sand when sheared tend to contract and dilate respectively. Critical void ratio is dependent on mean effective stress applied on the soil and as the stress increases, the volumetric contraction of a particular loose specimen becomes smaller (Taylor, 1948; Jefferies & Been, 2016). The said behaviour theory was first established by Casagrande in 1936 after conducting consolidated drained direct shear box tests and triaxial tests on

initially loose and dense sands (Figure 8). From Figure 8 (b), critical void ratios (CVR) of specimens under different normal and confining stresses (σ') can be obtained and CVR line can be established. CVR line marks the boundary between two initial states (consolidated void ratio, $e_{D/L}$ and critical void ratio, e_c) and liquefaction susceptibility of a particular soil based on its initial state can be obtained as shown in Figure 9.

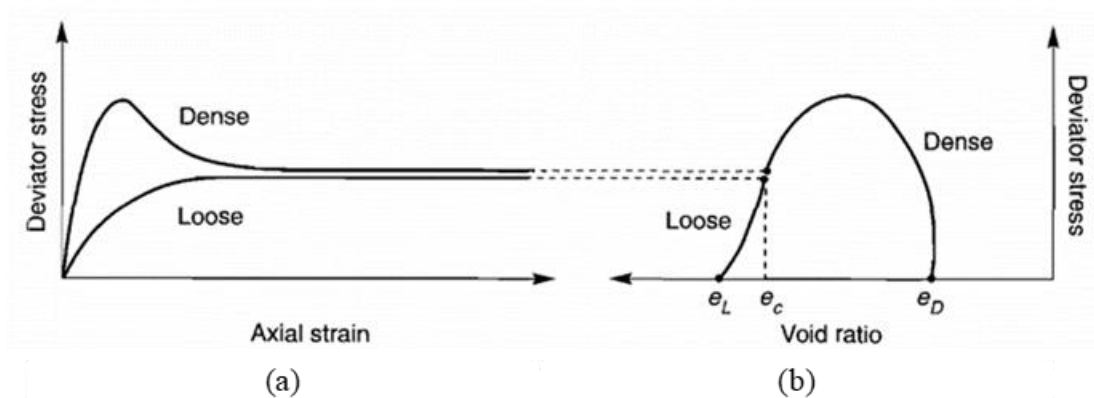


Figure 8: (a) Stress-strain (b) Stress-void response of loose and dense sand under same effective stress (Casagrande, 1936).

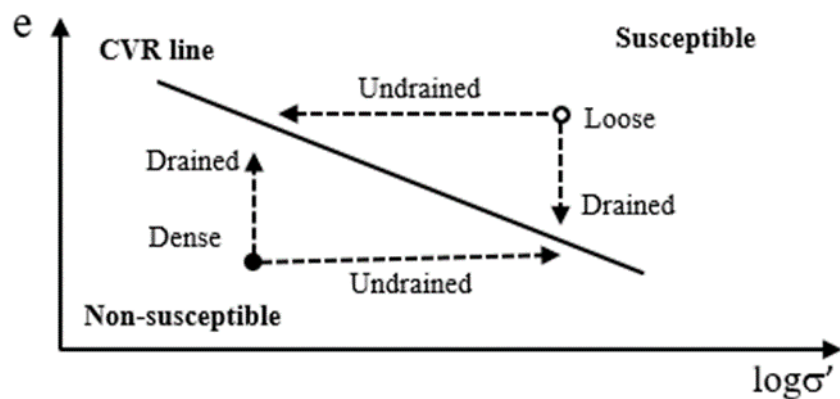


Figure 9: Flow liquefaction susceptibility concept (Kramer, 2014).

2.3 Liquefaction Failure

2.3.1 Flow liquefaction

Liquefaction of a particular soil requires substantial disturbance to occur. As discussed earlier, cyclic mobility is analogous to earthquake event or repeated disturbances while flow liquefaction can be triggered by several aspects. These aspects include blasting, pile driving application, machine vibrations, etc. which are all non-seismic induced vibrations. To evaluate the flow liquefaction, stress path can identify stability and instability occurrence within the soil.

The flow liquefaction concept is best illustrated by Kramer (2014) in Figure 10. Figure 10 (a – d) represents the shear stress ($\sigma_d/2$) – strain (ϵ), stress path (q-p space), pore water pressure – strain and steady state curves (void ratio – effective stress), respectively to represent an illustration of flow liquefaction.

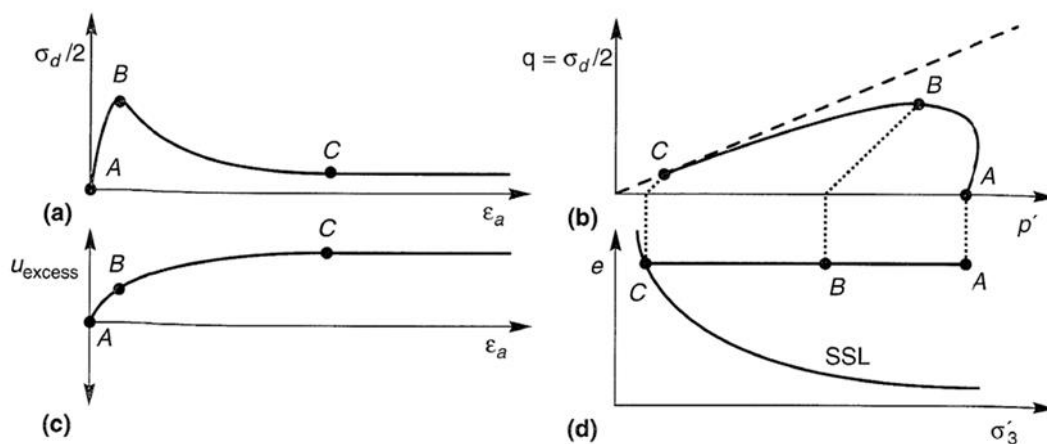


Figure 10: Loose saturated sand behaviour under monotonic undrained triaxial test (Kramer, 2014).

In Figure 10 (a), loose saturated specimen behaviour under monotonic loading is explained. At point A, the specimen is at isotropically consolidated state in drained

condition. When the soil is sheared, it will exhibit contractive behaviour up to Point B. At this stage, there is a build-up of excess pore water pressure, however stable. The instability occurs if the soil is sheared further causing considerable increase in the excess pore water pressure, with a dramatical decrease in the mobilized shear stress as the soil reaches to the steady state (Point C). There onwards, the soil is said to be liquefied, and this mechanism of liquefaction is termed as flow liquefaction.

In Figure 10 (b), pore water pressure response of loose saturated sand is presented. Point A is representing the consolidated state of soil (afore-shearing or drained equilibrium). Point B, as discussed, the soil is exhibiting shear resistance therefore the pore water pressure ratio (r_u) is considerably less than 1. Such behaviour in liquified soil is achieved at relatively low strain. As the shearing prolongs, at Point C, r_u value is equal to or greater than 1 thus, exhibiting liquefaction phenomenon. The excess pore water pressure ratio is defined as:

$$r_u = \frac{u_{\text{excess}}}{\sigma'_{30}} \quad (2.1)$$

where;

u_{excess} : Excess pore water pressure.

σ'_{30} : Initial effective confining pressure.

From Equation 2.1, the pore pressure ratio is directly proportional to excess pore water ratio indicating that for liquefiable soils, at Point C, the pore water pressure is equal to or greater than initial effective confining stress directly linking to loss of confinement at Point C. Such weakening of confinement in soils leads to collapse or flow failure.

In terms of stress-path evaluation, (Figure 10-b) similar behaviours as discussed can be plotted cumulatively. In addition to this, in stress-path, flow liquefaction surface (FLS) or collapse surface of a liquefiable soil can be constructed by obtaining yield strengths (Point B, Figure 10-b) by testing the specimens at similar initial void ratio under different confining stresses. Figure 11, illustrates the behaviour of 5 different sand specimens at the same void ratio under different confining stress.

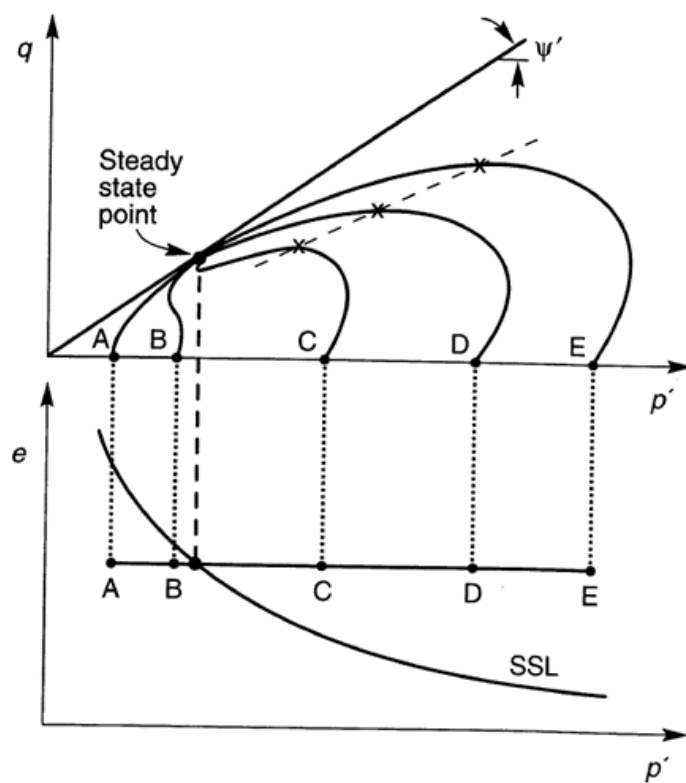


Figure 11: Undrained response of sand at different confining stress (Kramer, 2014).

From Figure 11, Specimens A and B are exhibiting dilative behaviour and based on their steady states achieved, A and B specimens are plotting below steady state line (SSL). C, D and E specimens, undrained response is exhibiting contractive response and are plotting above SSL. In contractive specimens, all specimens reach ultimate or peak strength and afterwards ultimately reaching to steady state. From the ultimate

points obtained in stress-path space, FLS is plotted in Figure 12. Stable or Unstable states of a particular soil is a boundary pronounced by FLS line and defines the state where liquefaction can trigger.

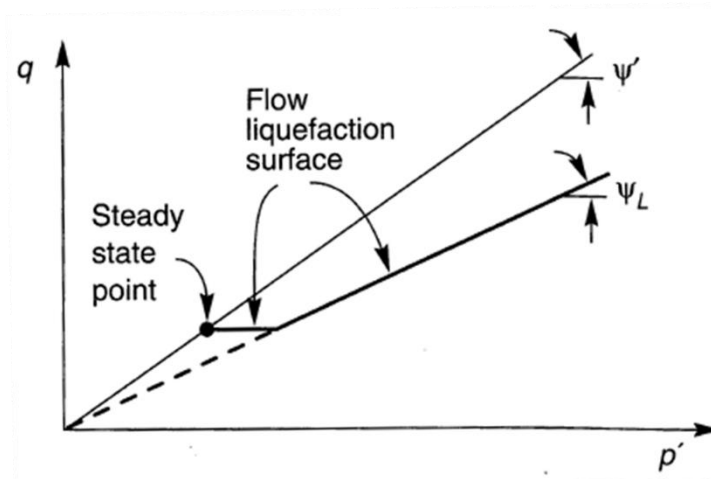


Figure 12: Flow liquefaction surface and steady state (Kramer, 2014).

Depending on the initial states of a particular soil, if the stress path reaches FLS, soil is susceptible to liquefaction. Another aspect observed in Figure 12, for very loose specimens tested under very low confining stress, the no significant difference is observed between SSL and FLS, therefore for such case, FLS is projected to the origin point and experimental results can be truncated at such levels (Specimen A and B, Figure 11).

2.3.2 Cyclic Mobility

Cyclic mobility as compared to flow liquefaction can occur in both contractive and dilative soils. Cyclic mobility can occur under similar conditions of flow liquefaction. Cyclic liquefaction phenomenon is illustrated in Figure 13. In Figure 13, cyclic triaxial results of Nevada Sand is presented [Arulanandan and Scott, 1993 (Retrieved from (Jefferies & Been, 2016))]. The stress-strain response of medium dense Nevada Sand

illustrates that soil is exhibiting stable response for first eight cycles and in 9th cycle, failure occurs. The failure in cyclic testing is associated with the increment of strain.

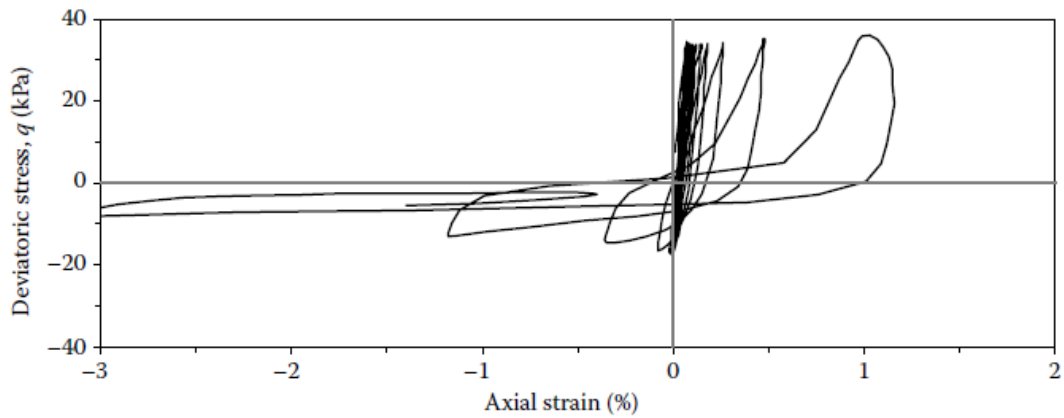


Figure 13: Cyclic stress-strain response of Nevada Sand
(Adapted from: Jefferies & Been, 2016).

In terms of pore water pressure and stress-path, gradual reduction of effective stress (p') is observed due to gradual build-up of excess pore water pressure. The reduction in effective stress due to pore water pressure ultimately reaches to critical state (Figure 14 and Figure 15).

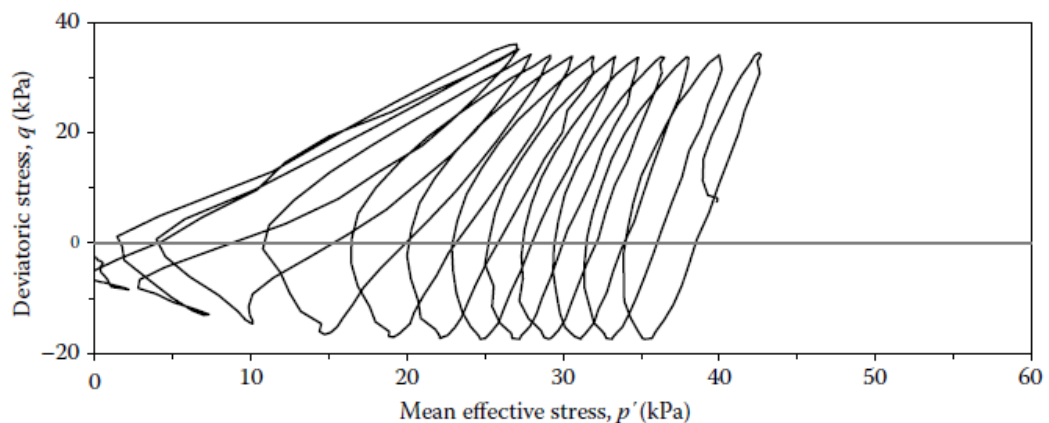


Figure 14: Cyclic stress-path of Nevada Sand
(Adapted from: Jefferies & Been, 2016).

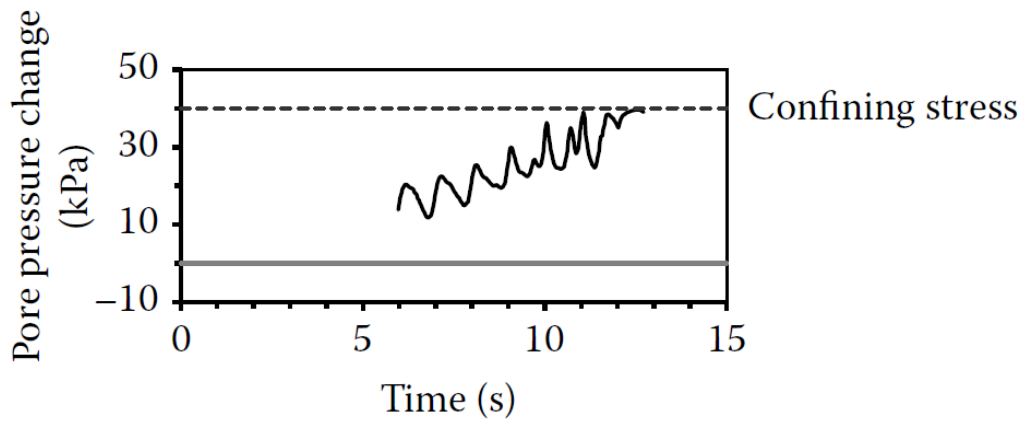


Figure 15: Excess pore water pressure generation of Nevada Sand.
 (Adapted from: Jefferies & Been, 2016).

Effective stress-path under cyclic loadings (Figure 14) will temporarily shift to the left ultimately reaching FLS (Figure 15). As it touches FLS, temporary instabilities will occur in soil matrix.

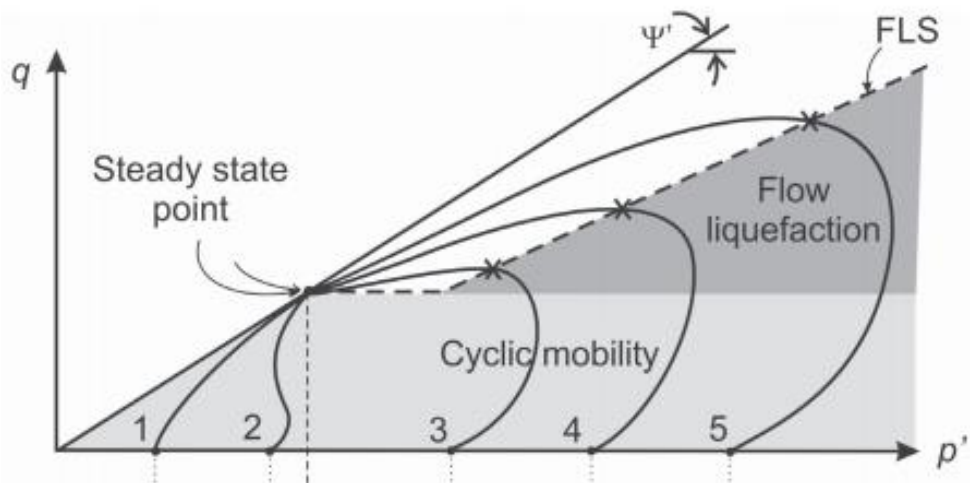


Figure 16: Flow liquefaction and cyclic mobility susceptible zones (Kramer, 1996).

In Figure 16, comparison between flow liquefaction and cyclic mobility occurrence zones are illustrated. The initial states of a soil if plots in the either region, soil is likely to liquefy under either flow or cyclic liquefaction.

2.4 Monotonic Undrained Response of Sand

In contrast to cyclic mobility, flow liquefaction phenomenon is infrequent yet yielding in most devastating consequences. Static gravity force is the dominant factor in flow liquefaction and to assess such behaviour, monotonic undrained triaxial test is routinely adopted. The illustration of the undrained shearing behaviour of sand test is presented in Figure 17.

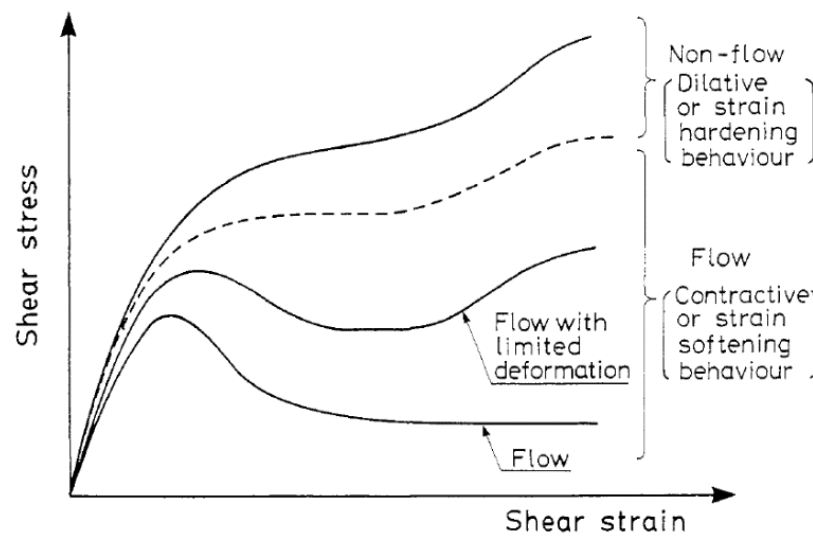


Figure 17: Illustration of undrained shearing behaviour of sand soil (Ishihara K. , 1996).

2.4.1 Phase Transformations

During undrained shearing of sand, three phases are commonly observed, ultimate, quasi and critical states. If the sand exhibits no change in stress after reaching ultimate state including pore-pressure equilibrium, such state is referred as steady state (Figure 18-a). The steady state normally occurs at large strains and such phenomenon is observed for dense sands (Yoshimine & Ishihara, 1998). For loose and medium dense sands, (Alarcon-Guzman et al., 1988) pointed out phase transformation occurrence in soil where soil exhibits low effective stress initially and afterwards, dilative behaviour

occurs (Figure 18-b). Another case associated with loose sands is the quasi-steady state, in which the shear stress and effective mean stress of a particular soil increases followed by a drop where both stresses reaching minimum. After exhibiting limited flow deformation, the contractive behaviour of the soil is transformed to dilative behaviour and reaching ultimate steady state (Figure 18-c). Total liquefaction or strain-softening behaviour is observed when stresses after increment, reduces significantly and reaching to critical steady state (Figure 18-d).

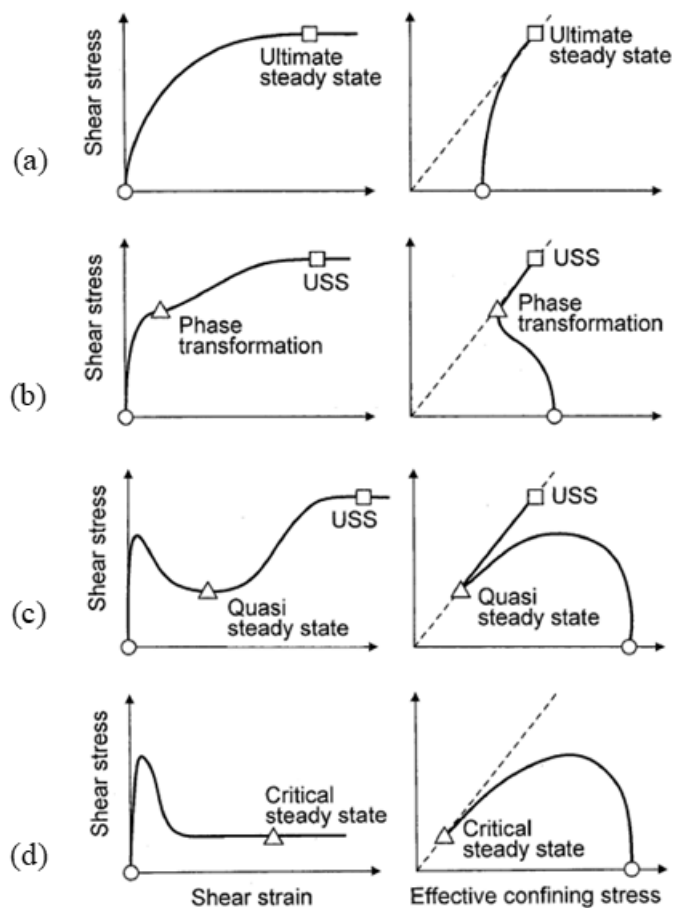


Figure 18: General monotonic undrained response of sand (Yoshimine & Ishihara, 1998).

2.5 Influence of Plastic Fines on Liquefaction Susceptibility

Considering the field conditions especially artificial fill deposits or reclaimed sites, clay and silt fractions are commonly observed with sand particles. In such cases the fines content might change the sand soil behaviour significantly due to increase in the plasticity.

Research study by Bouferra & Shahrour (2004), focusing on clayey sand mixtures upto 15% of fines addition in sand using monotonic undrained triaxial tests states that liquefaction susceptibility of mixed soil increases as the fine content increases based on low plastic fines (Figure 19). In this study the microstructure of the soil is the key parameter for the assessment and results shows that the increase of clay (kaolinite) fractions reduces the dilatency of sand particles. In Figure 20, the effect of clay content in sand on pore water generation in undrained loading is presented. It is observed that for clean sands, increase in effective stress (Figure 19) is due to decrease in pore water pressure developed indicating improvement in resistance to liquefaction. Whereas, as the clay content increases, the fines reduces the dilative behaviour thus extending the phase of increase in positive pore water pressure development. Such behaviour is associated to role of fines in transformation of soil fabric structure leading to more compressible behaviour. In addition to flow liquefaction assessment, cyclic mobility of sand containing 10% of clay content is also assessed (Figure 21). The soil mixture is tested under three cyclic stress ratios of 0.1, 0.2 and 0.4. Figure 21 illustrates that presence of clay at 5% reduces liquefaction resistance. The 5% clay content behaviour is described in contrast to 15% clay content presence where liquefaction resistance reduces significantly due to excess pore water generation ultimately reaching effective confining stress value.

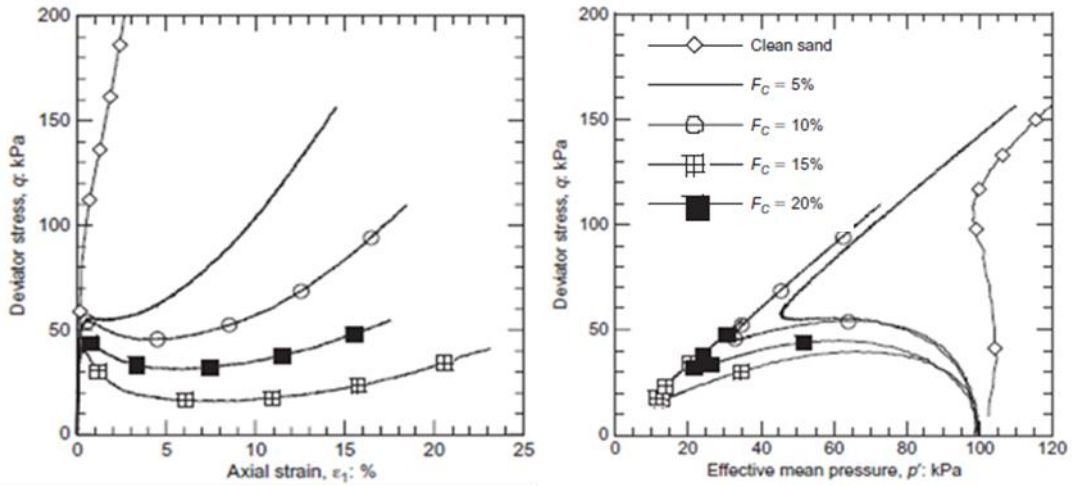


Figure 19: Influence of clay fraction on undrained sand behaviour (a) Deviator stress (b) Stress paths (Bouferra & Shahrour, 2004).

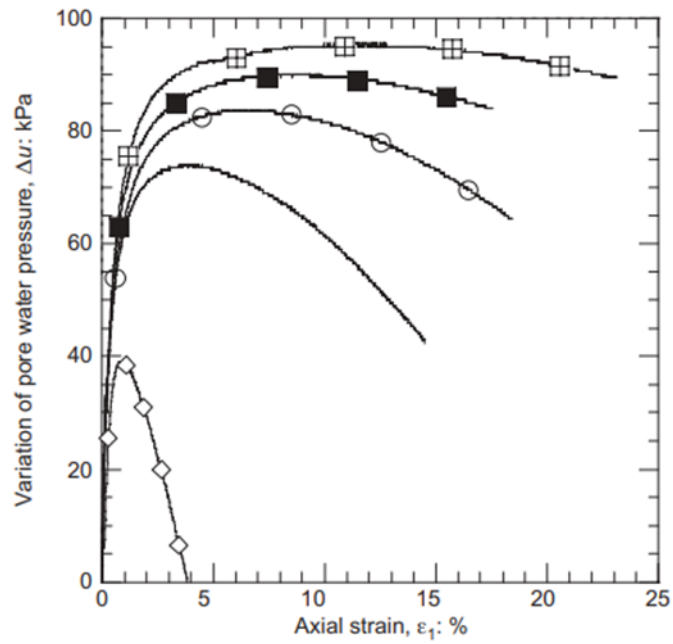


Figure 20: Effect of clay content in sand on pore water pressure generation (Bouferra & Shahrour, 2004).

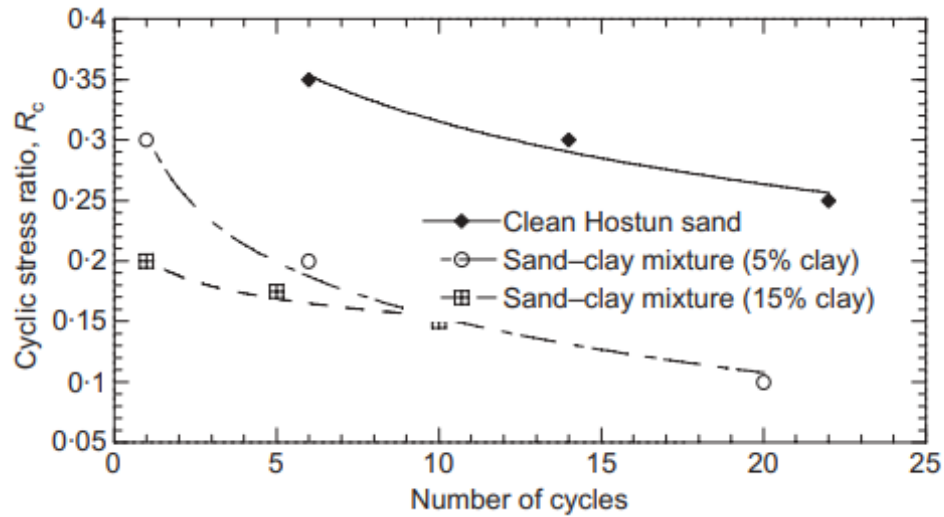


Figure 21: Effect of fines on cyclic resistance of sand (Bouferra & Shahrour, 2004).

Park & Kim (2013) carried out series of undrained cyclic triaxial tests on sand containing silt and clay minerals such as kaolinite and bentonite. The ratio of the fines in this study is kept constant at 10 % and the plasticity of the soil is varied. The research concluded that as the Plasticity Index of a particular soil mixture increases, the liquefaction susceptibility is also increased. In addition, it is also stated that regardless of initial states of soil specimen used (loose or dense), the liquefaction resistance of fines decreases significantly as the PI increases. Specimens in this research were reconstituted at three different states, loose, medium dense and dense. Figure 22, illustrates the effect of silt, kaolinite and bentonite-silt content (PI of 8, 18 and 50 respectively) at loose state on cyclic behaviour of sand. From Figure 22, it is observed that fines content slightly influenced the liquefaction resistance. In Figure 23 and Figure 24, influence of fines at medium and dense state is presented and from cyclic stress ratio, plot illustrates reduction in liquefaction resistance of soil mixtures with high plasticity. In Figure 25, relationship between liquefaction resistance and Plasticity Index is presented and from the plot, the difference between loose and medium to dense state is significant while difference between medium and dense state is marginal.

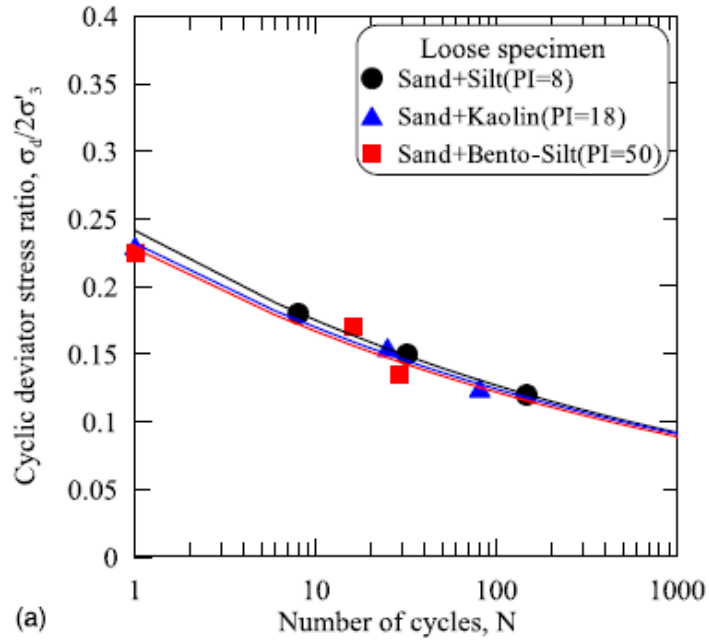


Figure 22: Liquefaction resistance curves of sand-fines mixture at loose state (Park & Kim, 2013).

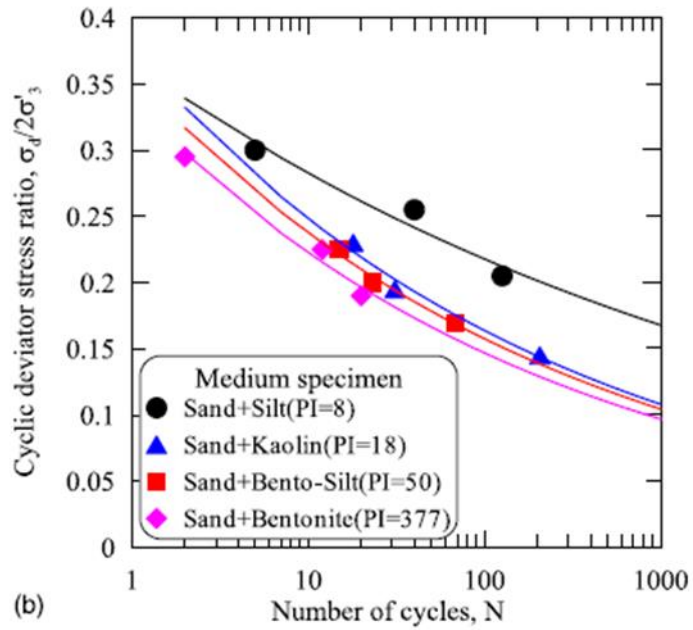


Figure 23: Liquefaction resistance curves of sand-fines mixture at medium dense state (Park & Kim, 2013).

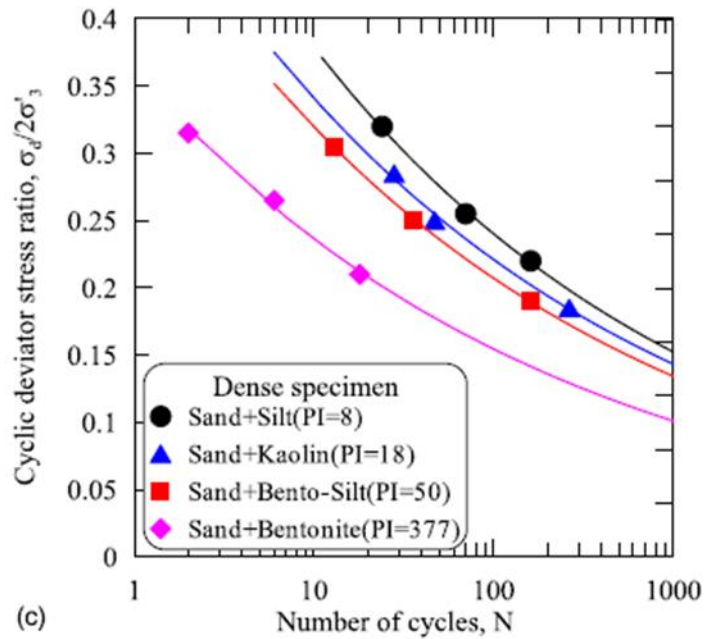


Figure 24: Liquefaction resistance curves of sand-fines mixture at dense state (Park & Kim , 2013).

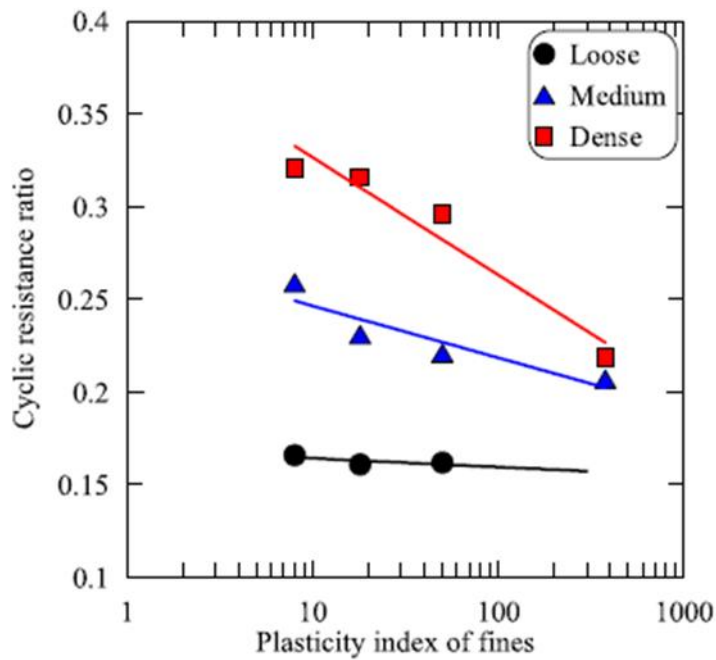


Figure 25: CSR versus PI of fines (Park & Kim , 2013).

Benghalia et al. (2014) conducted a research study about the effect of low plastic fines on liquefaction resistance of sandy soils. They reported that as the fines content is increased beyond a threshold limit, the liquefaction is decreased. In the study sand soil

of various composition are tested. The results have shown that not only nature of fine particles dominates liquefaction behaviour but also microstructure of the soil matrix plays an important role.

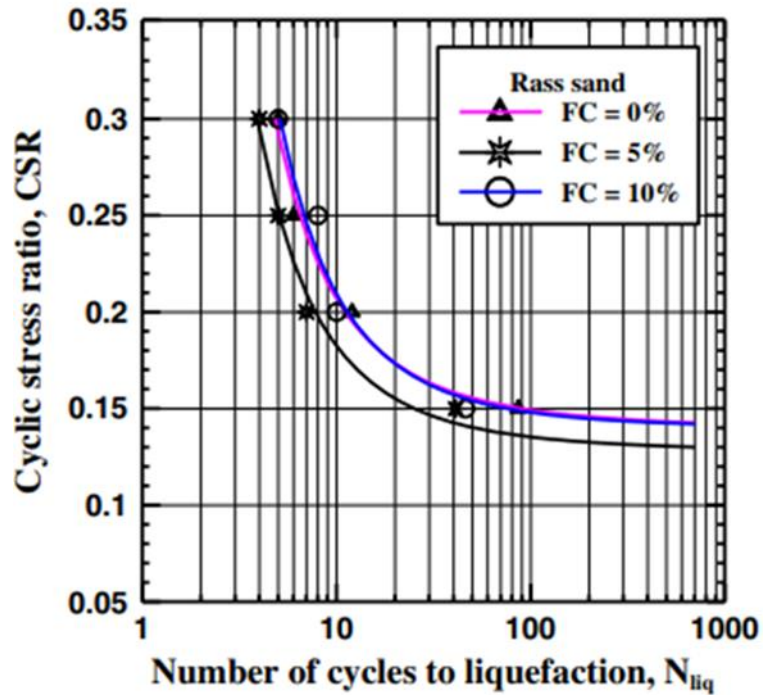


Figure 26: sand with low plastic fines liquefaction potential curves
Benghalia et al. (2014).

In aforementioned studies the base of the study is primarily focused on low plastic fines. However, Guo & Prakash (1999) states that increment of fine percentage with leads to more compressible behaviour and low PI range of fines reduces the liquefaction resistance whereas, PI with high plasticity ranges increases liquefaction resistance.

2.5.1 Influence of Fines Content on Liquefaction Susceptibility

In plastic fines, as the fines content increases several factors are involved such as PI, void ratio and water retention capacity of fines which govern the pore-pressure generation, strain softening and hardening behaviour. In case of non-plastic fines, the pore-pressure generation is similar to somewhat of Sandy soil however, the crucial

aspect is the void ratio and particle shape factor. The point of contact forces between sand grains is a key assessment regarding the microstructure where the increase in non-plastic silt fractions plays a significance role. Several investigations regarding the influence of non-plastic silts on Sand undrained response are linked with sample reconstitution technique. Other key factors such as grain-size distribution and amount of fines content are considered as well. Numerous researches performed on amount of fines content have conflicting results. For instance, Chien et al. (2002), Xenaki & Athanasopoulos (2003) and Rahman & Lo (2014) reported that as the fine content increases the liquefaction susceptibility increases (Figure 27).

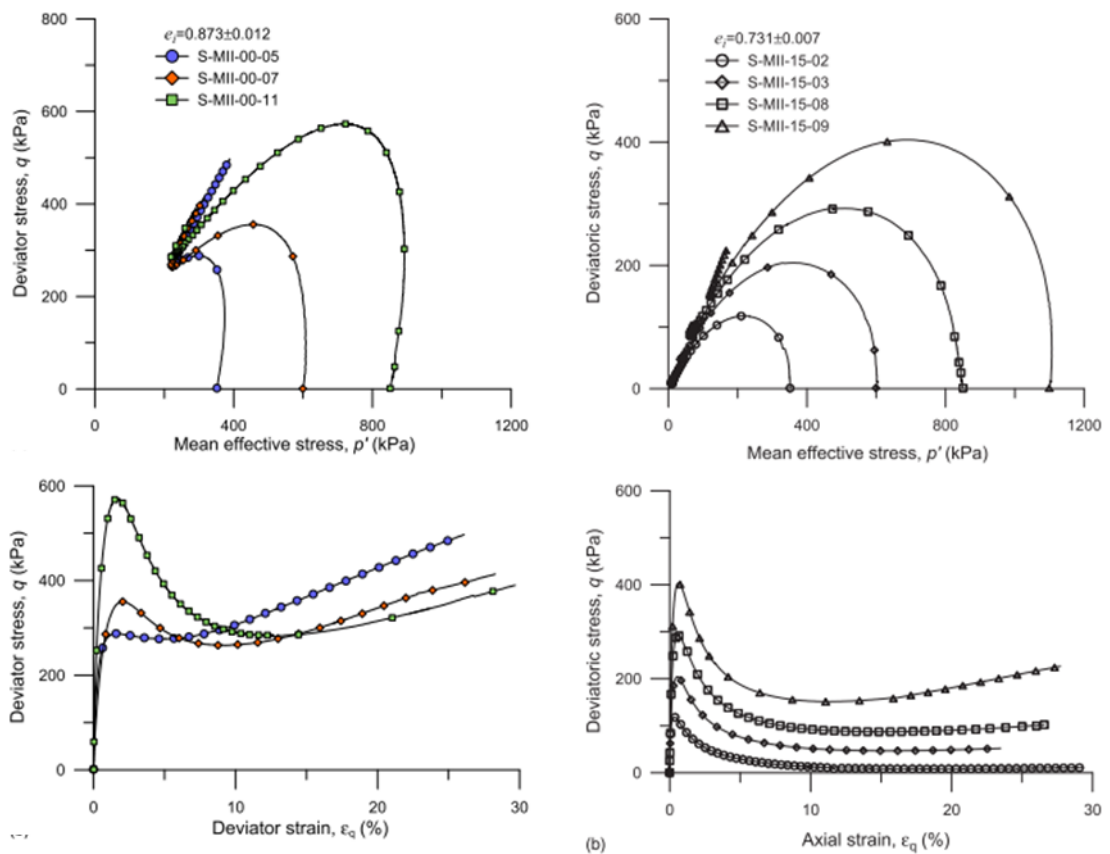


Figure 27: Undrained response of sand and sand with 15% fines. (Rahman & Lo, 2014).

Other researchers (Amini & Qi, 2000) concludes that lower percentages of fines exhibit liquefaction phenomenon (10%) and compared to higher content (50%) liquefaction resistance increases (Figure 28).

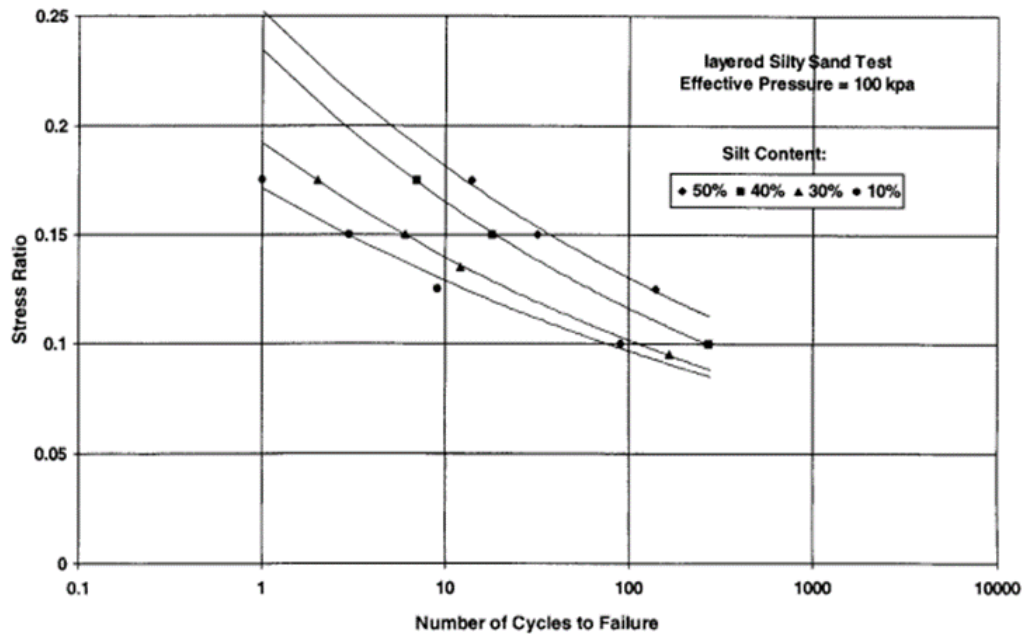


Figure 28: Liquefaction resistance curves of sand-silt mixtures (Amini & Qi, 2000).

Wang & Wang (2010), Polito & Martin (2001) and states that soil with fine fractions up to a certain threshold shows deformations and afterwards exhibiting stable behaviour. Another case observed by Tana et al. (2015) where sand with kaolinite and bentonite mixtures undrained response is studied and concludes that liquefaction resistance increased up to threshold fine content and resistance decreased with further inclusion of fine percentage. Same observations were obtained by adding non-plastic fines into sand matrix by Monkul et al. (2017) (Figure 29).

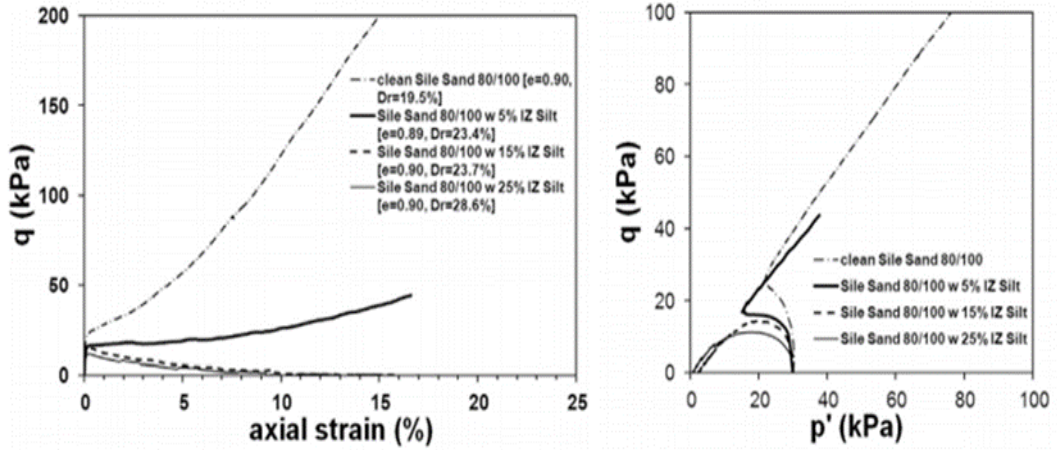


Figure 29: Loose sand-fines mixtures undrained behaviour (Monkul et al.; 2017).

2.6 Static Liquefaction Assessment Approach

As discussed earlier, to assess the undrained response of sand under monotonic loading, as soil is sheared beyond the peak point (Figure 30) shear strength drops significantly to a constant state for loose state termed as steady-state shear strength. The undrained behaviour of a particular soil is assessed by plotting deviator stress versus axial strain, change in pore-water pressure versus axial strain and stress path (q - p') planes. From q - p' planes stability, instability and steady states are assessed and one of the most prominent method to analyse static liquefaction behaviour. From Figure 31, the instability occurs when a particular soil ability of sustaining stresses or applied load is reduced due to large pore-water pressure generation and large plastic strains in soil element occurs.

The said steady state or residual strength is obtained as follows:

$$S_{us} = \left[\frac{q_s}{2} \right] \cos \phi_s \quad (2.2)$$

$$S_{us} = \left[\frac{M}{2} \right] \cos \phi_s p'_s \quad (2.3)$$

where, $M = \frac{6 \sin \phi_s}{3 - \phi_s}$ (2.4)

ϕ_s : Phase transformation angle.

p'_s : Effective mean principal stress.

q'_s : Deviator stress.

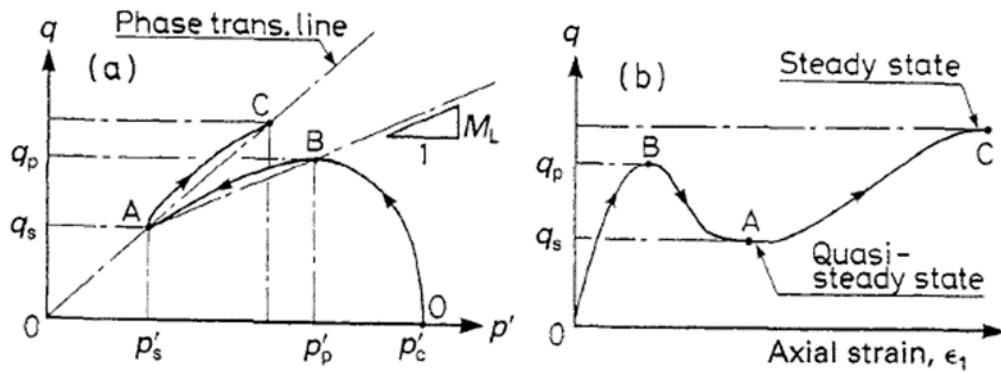


Figure 30: QSS residual strength definition (Ishihara ,1996).

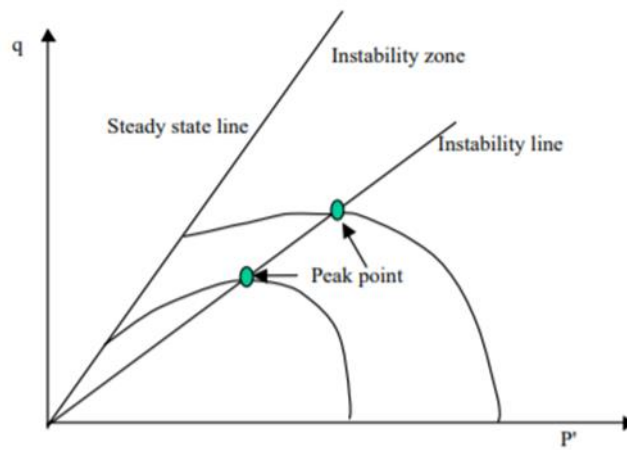


Figure 31: Undrained stress-path (Yang, Sandven, & Grande, 2006)

2.6.1 State Parameter

Comparison between initial state and critical state of a soil can also be a good indication of a soil illustrating whether liquefaction is expected or not. The state parameter (Ψ) is defined as:

$$\Psi = e - e_{ss} \quad (2.5)$$

where;

e : Initial void ratio

e_{ss} : Steady state void ratio

From Equation 2.5, flow liquefaction is associated with positive value and non-flow behaviour with negative values (Jefferies & Been, 2016). In Figure 32, the state parameter associated behaviour are illustrated.

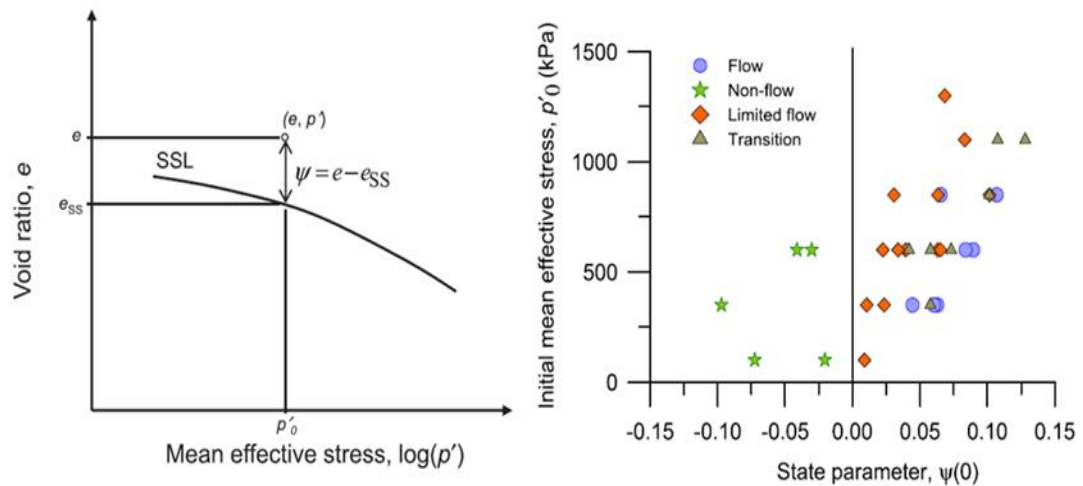


Figure 32: State parameter (Rahman & Lo, 2014).

2.7 Effect of Fines on Behavioural Properties of Sand

Mechanical properties of any soil are entirely dependent on the behavioural aspect of soil. Inclusion of fines into sandy soils can alter the behaviour completely. Numerous researchers (Lade & Yamamuro 1997; Yang, Lacasse, & Sandven 2006) categorize sand and fines mixtures into two groups, sand-dominated and fine-dominated. Generally, soils are either fine-grained (clays and silts) or coarse-grained (gravels and sands) based on their proportions. Based on mixing proportions or ratio of fines, mixed

soil exhibit different in behaviour. These mixed soils are termed as intermediate soil (Kim, Kim, & Zhuang, 2016).

To investigate the behaviour of mixed soils in terms of low or high fines content, transitional fine content (TFC) indicator is used to assess the dominated group (Lade et al., 1998).

2.7.1 Inter-grain and Inter-fine State Concept

Thevanayagam (1998) proposed the concept of inter-grain void ratio which refers to intergranular and interfine void ratios. Intergranular void ratio (e_s) in case of low fines content in sand is defined as:

$$e_s = \frac{e + f_c}{1 - f_c} \quad (2.5)$$

where;

e : void ratio of the mixture.

f_c : fines content (decimals).

The primary aspect in intergranular void ratio is directly linked with the voids where fine particles are assumed as voids. In such case, fine particles are hypothetically assumed that they will not contribute to shear resistance.

Interfine void ratio is associated for sand with high fines content and is defined as:

$$e_f = \frac{e}{f_c} \quad (2.6)$$

In case of fine dominated soil, sand particles are considered as voids and will not contribute to shear resistance of soil. The inter-granular and inter-fine concepts are illustrated in Figure 33 (a) and (b) respectively. In such cases, the fine content is referred to non-plastic particle sizes less than 75 microns. Kuerbis et al. (1988); Marto

et al. (2015) & Kim et al. (2016) suggests that similar theory can also be considered for plastic fines and additionally states a unique relation between void ratio and consolidation characteristics of plastic fines.

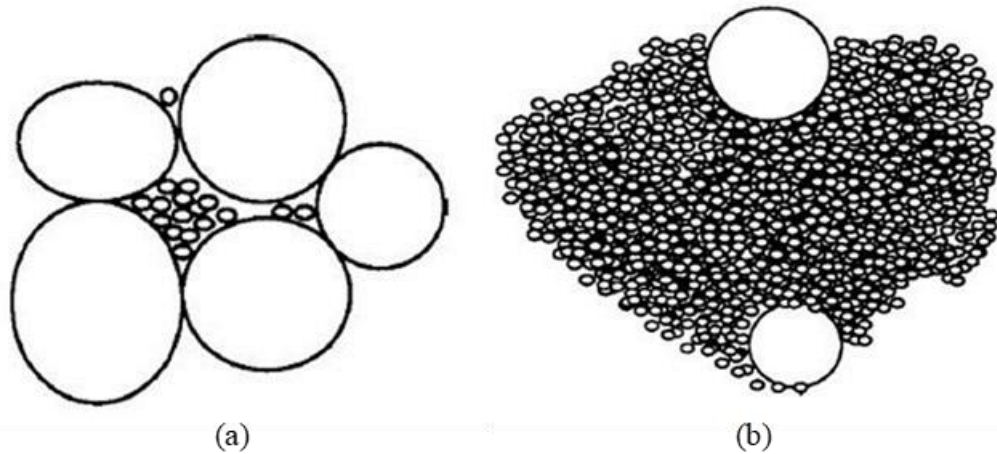


Figure 33: (a) Inter-granular (b) Inter-fine void concepts (Thevanayagam, 1998).

2.7.2 Transitional Fine Content, TFC

Sample reconstituion technique is directly associated with soil fabric which influences the behavioural aspect of soil mixtures. Transitional fine content (TFC) is considered as a key parameter indicating the presence of fine above or below the threshold content rather than fines proportions in sand matrix. The general definition behind TFC determination is when the voids between sand grains are entirely filled with fine grains. Such case is termed as binary packing suggested by Lade et al. (1998) and illustrated in Figure 21. TFC is calculated with different fine propotions in terms of mass percentage as follows:

$$TFC = \frac{M_{fines}}{M_{total}} = \frac{G_f}{\left(\frac{G_s(1+e_f)}{e_s}\right) + G_f} \quad (2.7)$$

where;

M_f : Fines dry mass

M_{total} : Mixture total dry mass

G_f : Fines specific gravity

G_s : Sand specific gravity

e_f : void ratio of fines

e_s : void ratio of sand

It is noted from Equation 2.7 and Figure 34 that, TFC is entirely dependent on maximum and minimum void ratios of sand and fines. The degree of compaction for sandy soil is generally measured by relative density parameter (D_r). However the relative density parameter is only applicable for sand matrix composed of less than 5% of fines. The modified equation to evaluate relative density in terms of granular void ratio is as follows:

$$D_{rg} = \frac{e_{\max H} - e_g}{e_{\max H} - e_{\min H}} \quad (2.8)$$

where;

$e_{\max H}$ and $e_{\min H}$: maximum and minimum void ratios of coarse grains.

e_g : granular void ratio.

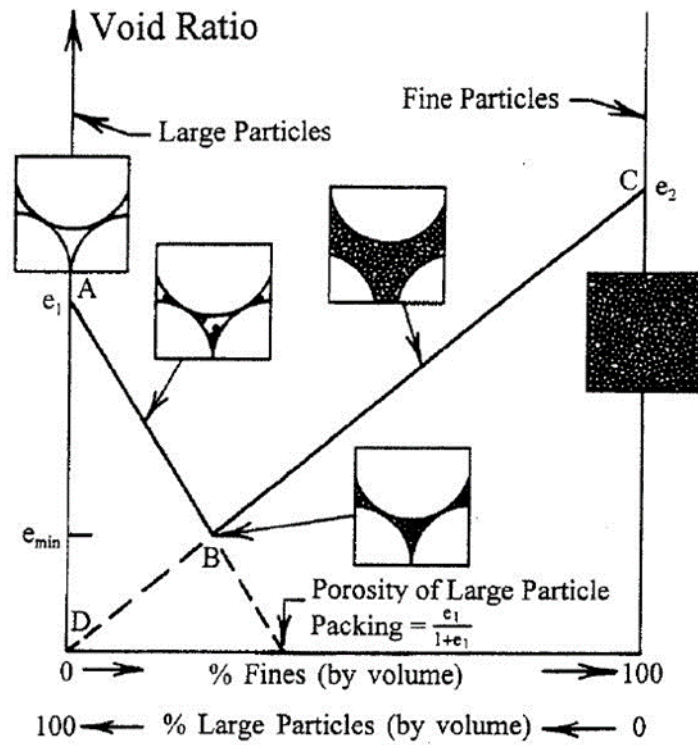
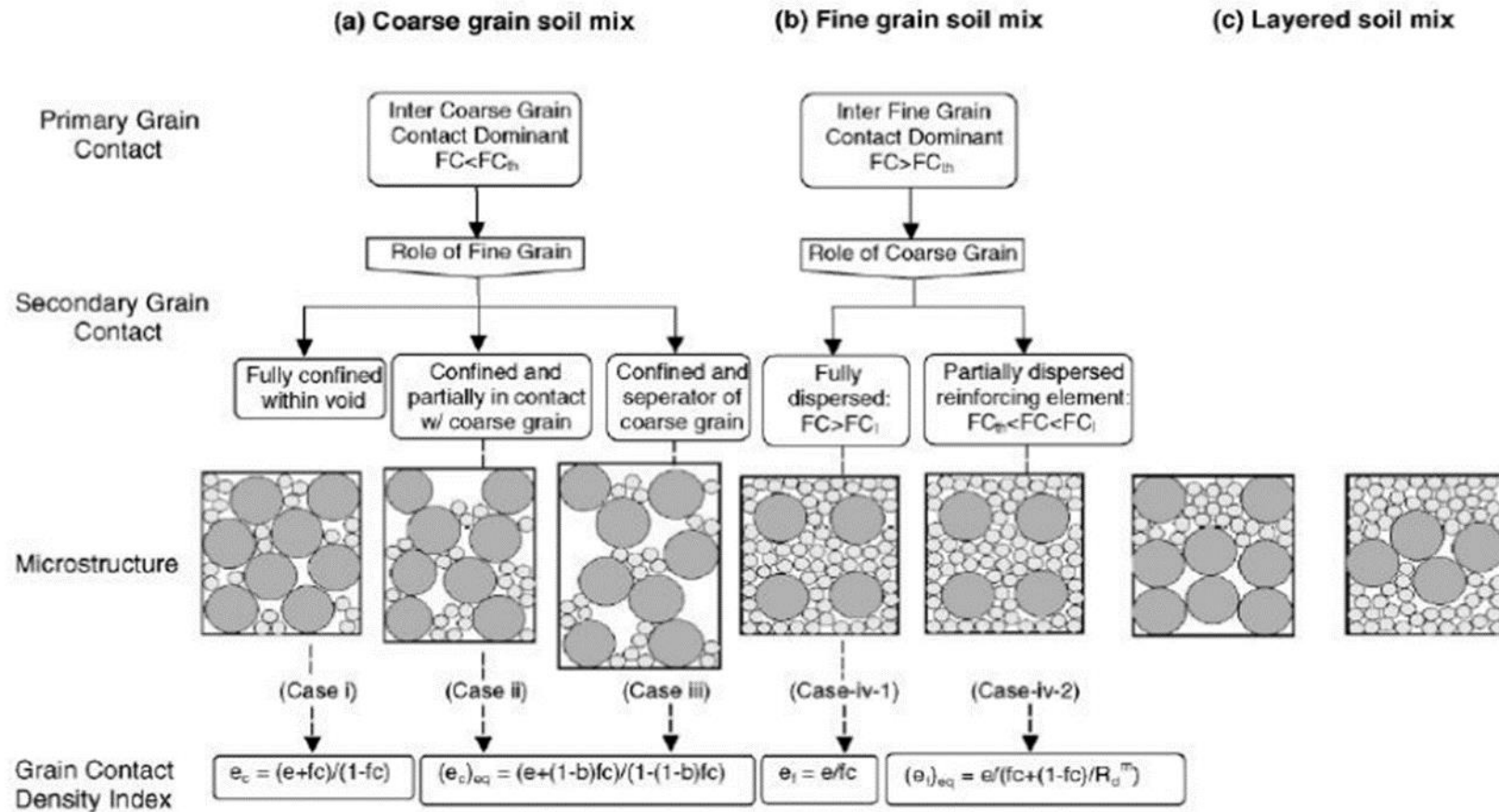


Figure 34: Binary packing for minimum void ratios (Lade et al. 1998).

Based on inter-granular and inter-fine concepts, Thevanayagam et al. (2002) proposed a mixed soil classification system based on their conceptual fabric patterns as illustrated in Figure 35.



b =portion of the fine grains that contribute to the active intergrain contacts; e =global void ratio; FC =fine grains content; FC_{th} =threshold fine grains content, $FC_{th} < (100e/e_{max,HF})\%$; FC_1 =limit fines content, $FC_1 > 100(1-\pi(1+e)/(6s^3))\% > FC_{th}$; m : reinforcement factor; $R_d = D/d$ =particle size disparity ratio; $s=1+a/R_d$, $a=10$; $e_{max,HF}$: the maximum void ratio of host fine

Figure 35: Mixed soil classification (Thevanayagam et al. 2002)

2.8 Specimen Reconstitution Techniques

Investigation of liquefaction phenomenon in element testing is directly linked with the sample reconstitution technique and specimen preparation method governs the stress-strain behaviour of samples. For coarse soils, several preparation techniques are proposed such as dry deposition, air pluviation, mixed dry deposition, water sedimentation and slurry techniques. Different sample reconstitution techniques yield in different fabric structure of soil and governs the behavioural aspect (Mulilis et al. 1997; Ladd 1977). Specimens reconstituted in wet deposition and slurry techniques are fully saturated before triaxial cell assembly. Numerous researches have been conducted to study the effect of preparation technique and yet contradictions among these studies exists. For instance, samples prepared by employing dry pluviation techniques elevates the initiation of liquefaction (Yamamuro, Wood, & Lade, 2008). Another study related with samples prepared by sedimentation method states that liquefaction phenomenon is more elevated than those samples prepared by other methods such as wet and dry depositions (Zlatovic & Ishihara, 1997). Experimental study related with wet deposition shows that liquefaction resistance is less than samples prepared by dry deposition technique (Ishihara, 1993; Della et al. 2009).

The experimental results shows that mechanical behaviour of the soil is directly dependant on its initial state . The initial state of the soil is referred to cumulative factors such as initial void ratio and effective stress applied, geometric arrangement of the soil particles and soil fabric patterns.

In this dissertation study, the reconstitution method applied is dry funnel deposition (dry pluviation). Dry pluviation technique simulates conditions similar to in-situ

grain structure and as mentioned earlier that alluvial and marine soils are mostly prone to liquefaction phenomenon therefore low input energy should be simulated (Lade & Yamamuro,1997). In Fiure 36, schematic illustration of sample reconstitution techniques are presented.

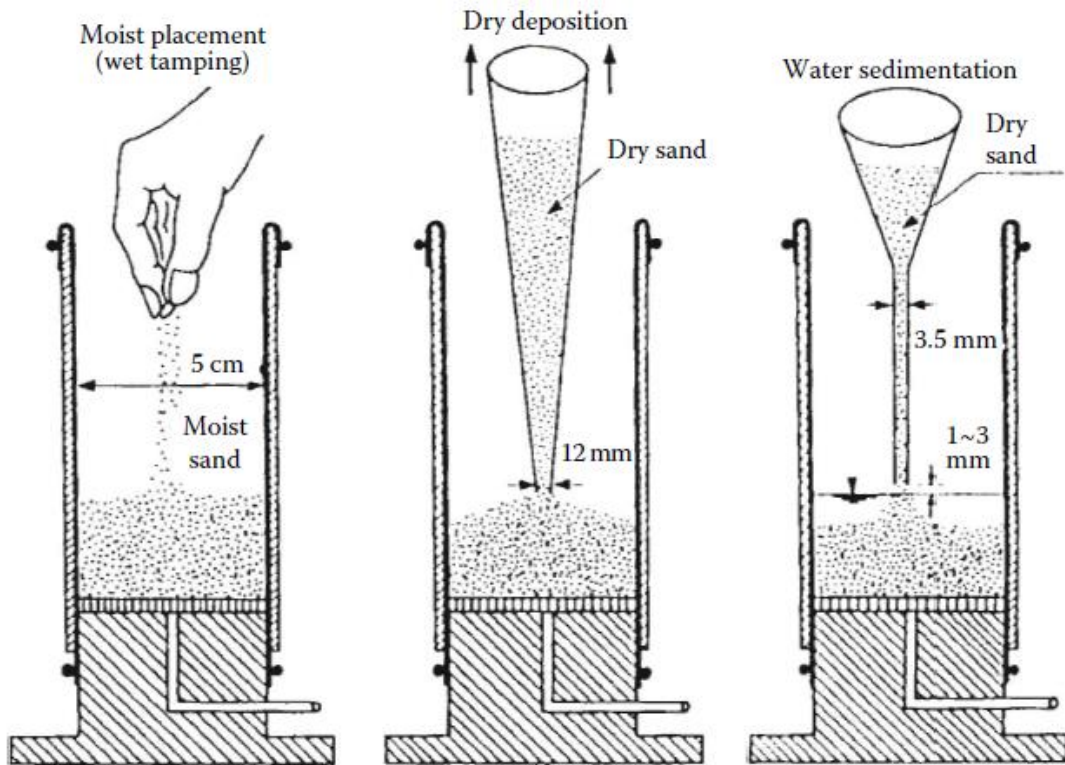


Figure 36: Sample reconstitution techniques schematic illustration (Adapted from: Jefferies & Been, 2016) .

Chapter 3

RESEARCH METHODOLOGY

3.1 Introduction

In this chapter, information about the materials selected for this research and testing strategy are presented. All tests are conducted in accordance with American Society of Testing and Materials (ASTM) and British Standards (BS). A laboratory testing program is designed to enable measurement of influence of plastic fines on the liquefaction behaviour of Silver Beach Sand, Famagusta.

3.2 Experimental Soils

In this study, two types of soils are used. Primary soil is sand, obtained from Silver Beach and secondary soil is Alluvial Clay from Eastern Mediterranean University Campus.

3.2.1 Silver Beach Sand

Silver Beach Sand (SBS) is obtained from Famagusta Bay Delta and the sampling location is shown in Figure 37. Soil samples are obtained from four different locations ranging from depths of 0.5 to 1 meter below ground level in the form of disturbed samples. These samples are collected in High Density Polyethylene (HDPE) containers to avoid any contamination and were transported to Soil Mechanics Laboratory, EMU. Physical and chemical properties of SBS soil are highlighted in Table 2. A qualitative assessment of mineralogy is carried out by optical microscope and the observations are made with available quartz mineral database (Hershel

Friedman, 2010). The field observations at the sampling location are presented in Figure 38 and Figure 39.



Figure 37: Sand sampling location (Google Maps, 2019).



Figure 38: SBS sampling.



Figure 39: (a) Observation hole location (b) Site condition due to seasonal changes.

Table 2: SBS index properties.

Properties	Values
Specific Gravity ^a , G_s	2.712
In-situ density ^b , $\rho_{in-situ}$ (g/cm^3)	1.77
In-situ moisture content, $w_{cinsitu}$ (%)	5
Coefficient of uniformity ^c , C_u	1.32
Coefficient of curvature ^c , C_c	0.92
Soil classification ^d	SP
Minimum void ratio ^e , e_{min}	0.95
Maximum void ratio ^e , e_{max}	0.63
Minimum dry density, $\rho_{d,min}$ (g/cm^3)	1.39
Maximum dry density, $\rho_{d,max}$ (g/cm^3)	1.66
Carbonate content ^f (g)	0.6
Electrical conductivity ^g , EC (μS)	3110
Electrical resistivity ^g ER ($k\Omega$)	0.346
pouvoir Hydrogène ^h , pH	8.39

a. ASTM D854-14

b. ASTM D1556-15

c. ASTM D6913-17

d. USCS

e. Lade and Yamamuro-1997

f. ASTM D4373-14

g. ASTM D1125-14

h. ASTM D4972-13

3.2.1.1 Silver Beach Site Analysis

Depth to ground water (GWT) is an important indicator to estimate the liquefaction potential of soil especially when there are huge fluctuations in GWT as discussed in Chapter 2. In Figure 38, the estimated depth of sampling is 0.5 to 1 meters and presence of GWT is not observed and the sand samples were obtained during summer period where the in-situ conditions were partially saturated. A site visit was held after 4 months during winter period and great difference was observed in the depth of GWT. Three of the sampling locations were eroded off and increase in GWT was observed at fourth sampling location as shown in Figure 39(a). The GWT depth is obtained through drilling the bore hole by hand-held auger and samples were secured to evaluate the physical properties after increment of GWT. The bore holes were also drilled in other locations rather than sampling areas to investigate the GWT increment and the location of GWT was approximately similar in all cases. The samples obtained from bore holes exhibited no significant difference in physical properties except that the carbonate content was slightly higher than previous analysis performed before winter. The primary reason behind increase in carbonate content is based on the density of the carbonates (seashells), as per due to lower density of crushed seashells, the tendency of carbonates to the surface increases. For the purpose of the analysis in this research, it is fair to assume that the GWT is at ground surface.

3.2.1.2 Mineralogical Analysis

Mineralogy plays a vital role in defining engineering properties of a soil. The geological setting of the site hints deposition of various types of minerals. A map of Famagusta Bay Delta and a contour map of ground surface levels are presented in Figure 40 and Figure 41 respectively.

Optical Microscopic analysis is conducted to determine the minerals distribution (Appendix A-1 to A-4). The optical microscope magnification power includes ocular and objective power. The microscope model and magnification details are as follows:

- i. Model: Novex: 86.025
- ii. Ocular Magnification power = x10
- iii. Objective Magnification power:
 - Red Band = x 4
 - Yellow Band = x 10

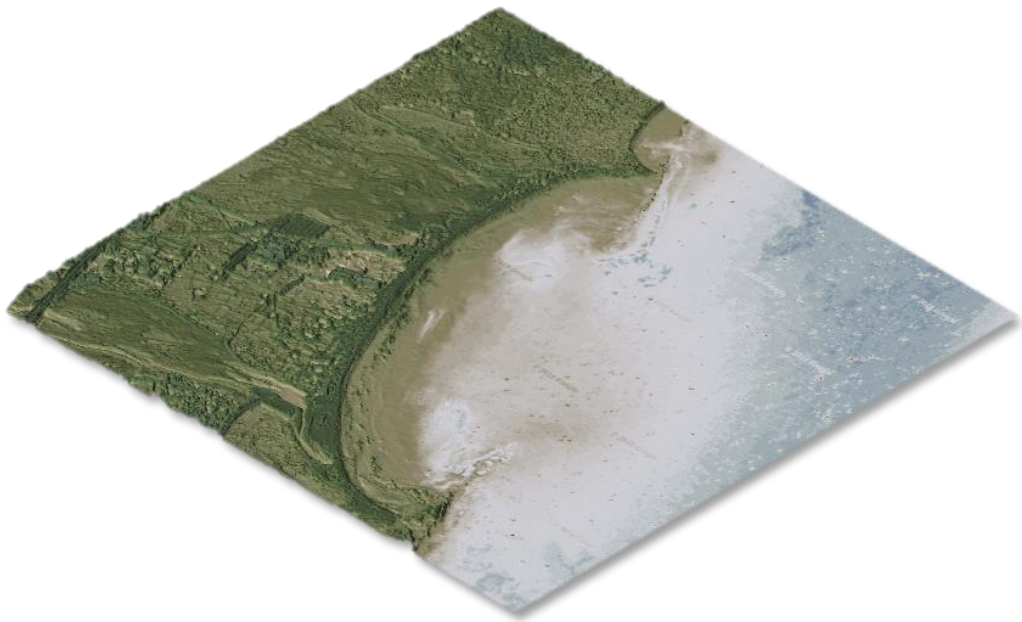


Figure 40: Famagusta Bay Delta 3D modelling (Height Mapper[®]).

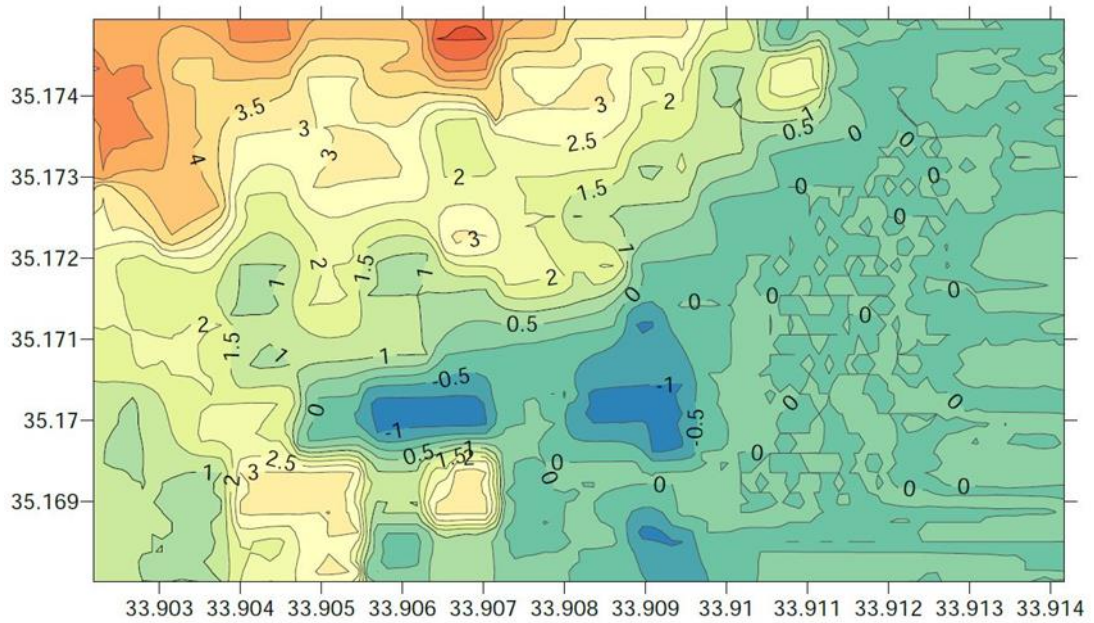


Figure 41: Famagusta Bay Delta contouring map (Surfer 13).

The mineralogical analysis is based on sieving the sand through consecutive sieves (425, 355, 250, 212, 180, 150, 125, 106, 90 and 75 μm) and a representative portion of sieved soil is obtained. From the available data base of quartz minerals (Hershel Friedman, 2010), different types of quartz minerals are illustrated in Figure 42.

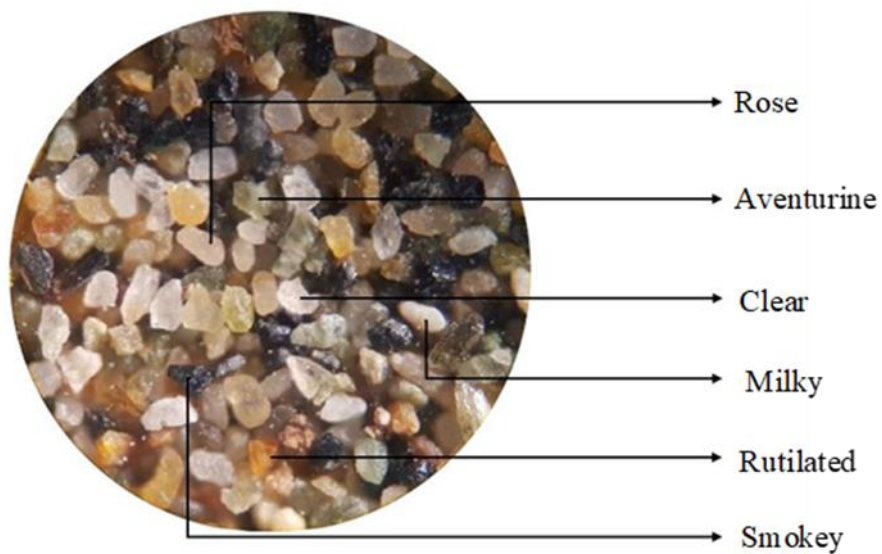


Figure 42: SBS Quartz minerals types (Hershel Friedman, 2010).

Clear and rose quartz minerals are in abundant and observed in all categories. Smokey quartz mineral is more frequent in smaller diameters (D_{max} less than 90 microns) and minor in above than 90 microns. Carbonates are mostly present in 425 microns sieve and very few traces of quartz mineral are observed. The reflective property of minerals is one of the main indicators for comparison and for this purpose, the emitting source of light was from top of microscope. The particle shape of sand grains is presented in Figure 43.

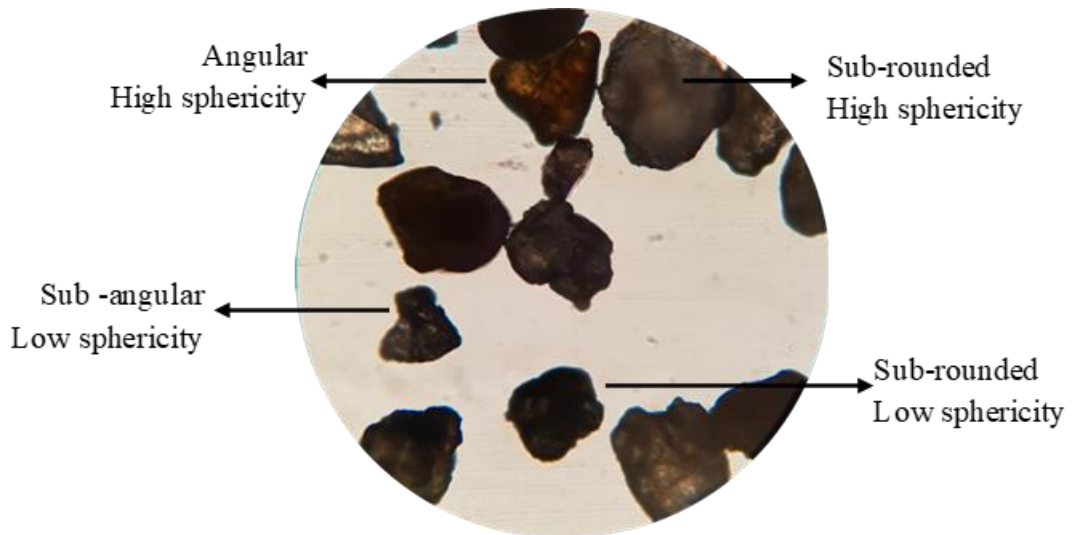


Figure 43: SBS Particles shape.

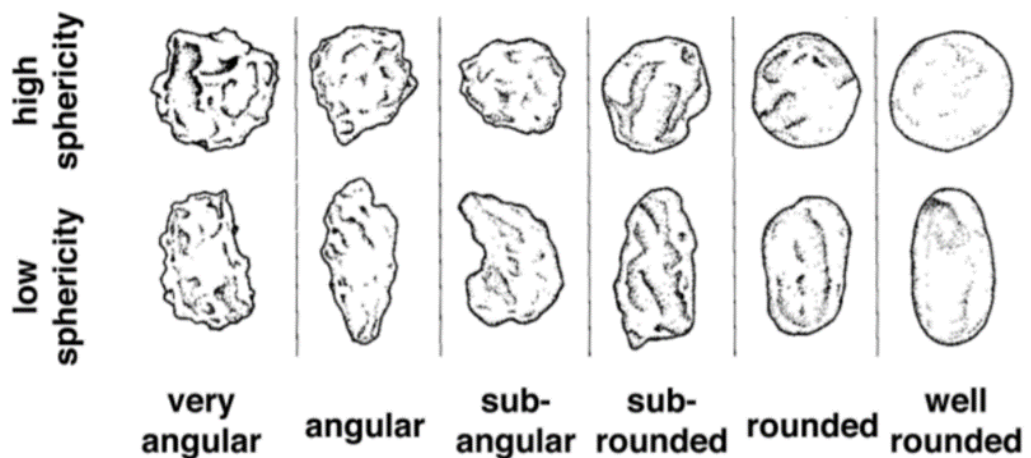


Figure 44: Sand particles characterization (Saputra, 2016).

3.2.2 Famagusta Bay Alluvial Clay

Secondary soil is Famagusta Bay Alluvial Clay which is used to obtain to mix into Sand samples. The samples are retrieved from a depth of approximately 2.5 meters. GWT seepage is observed at 3 meters. In Figure 45, the approximate sampling location is shown while in Figure 46 and Figure 47, soil strata and GWT depth are presented, respectively.

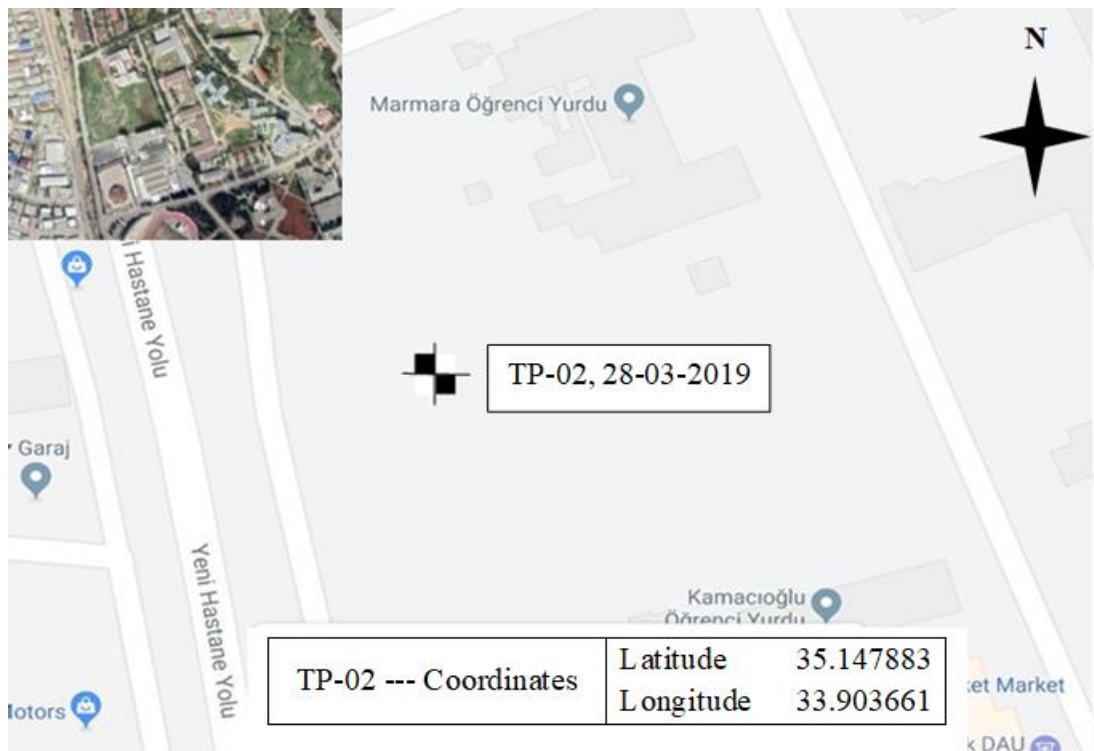


Figure 45: Sampling location of Alluvial Clay (Google Maps, 2019).

The samples are excavated by backhoe excavator, collected in HDPE bins and transported to Soil Mechanics Laboratory, EMU. In Table 3, physical and chemical properties of Alluvial Clay are tabulated. This soil is comprised of approximately equal percentages of silt and clay. Therefore, equal proportions of silts and clays can be

obtained from separation procedure developed for this study. Detailed explanation of the separation procedure will be given in following sections.



Figure 46: Alluvial Clay strata.



Figure 47: GWT location

Table 3: Alluvial Clay index properties.

Properties	Values
Specific Gravity ^a , G_s	2.575
In-situ moisture content, w.c (%)	28
In-situ density, $\rho_{in-situ}$ (g/cm ³)	1.89
Liquid Limit ^b , LL (%)	53
Plastic Limit ^b , PL (%)	25
Plasticity Index ^b , PI (%)	28
Linear Shrinkage ^c , LS (%)	15
Classification ^d	CH
Cation Exchange Capacity ^e , CEC (meq/100g)	20
Specific Surface Area ^f , SSA (m ² /g)	142
Carbonate Content ^g	0.245
Electrical conductivity ^h , EC (μ S)	6880
Electrical resistivity ^h , ER (k Ω)	0.13
pouvoir Hydrogène ⁱ , pH	8.15

a. ASTM D854 – 14

b. ASTM D4313 – 17

c. BS 1377-2 – 1990

d. Unified Soil Classification System (USCS)

e. ASTM Geotechnical Testing Journal, Methylene Blue Adsorption Test (MBAT)

f. ASTM Geotechnical Testing Journal, Ethylene Monoethyl Ether (EGME)

g. ASTM D4373 – 14

h. ASTM D1125 – 14

i. ASTM D4972 – 13

3.2.2.1 Mineralogical Analysis

The mineralogical composition of Alluvial Clay is obtained indirectly by conducting chemical tests. From these tests, values of SSA and CEC indicated that the soil comprises Illite mineral. Another indirect estimation can also be established from

Atterberg limit which indicated that the soil plasticity behaviour is likely to be governed by Illite.

3.3 Famagusta Shores Liquefaction Susceptibility Analysis

Liquefaction susceptibility analysis initiates with a response that either the deposited soil is susceptible to liquefaction or not. Several factors are considered in such analysis by locating the co-ordinates of the site (Famagusta) and in-situ density of the soil. The deposited soil in-situ density from Table 2 is $\rho_b = 1.77 \text{ g/cm}^3$ ($\rho_d = 1.43 \text{ g/cm}^3$) stating that sand is naturally deposited in a loose state, which indicates the vulnerability of the site to liquefaction based on its distance from epicentres. In Figure 48, approximated co-ordinates from historical shallow earthquake epicentres of Famagusta Bay Delta is illustrated and from Ambraseys, 1988 chart (Figure 49) illustrating that site is vulnerable to liquefaction phenomenon based on all criteria considered.

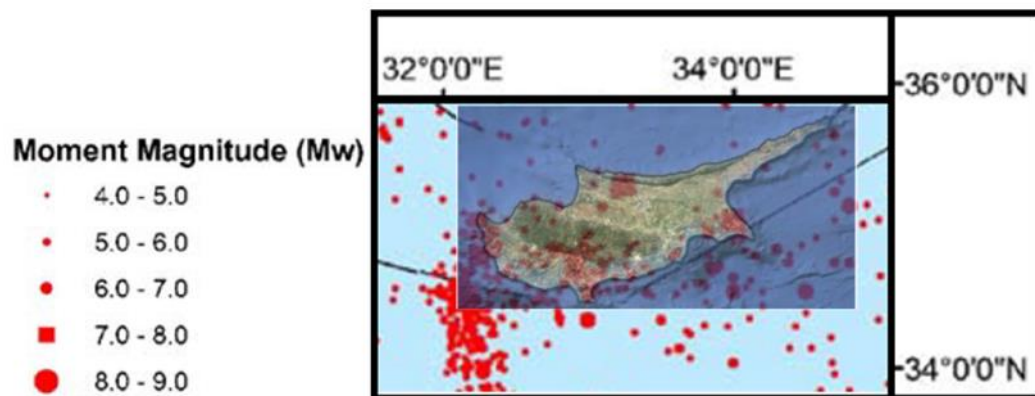
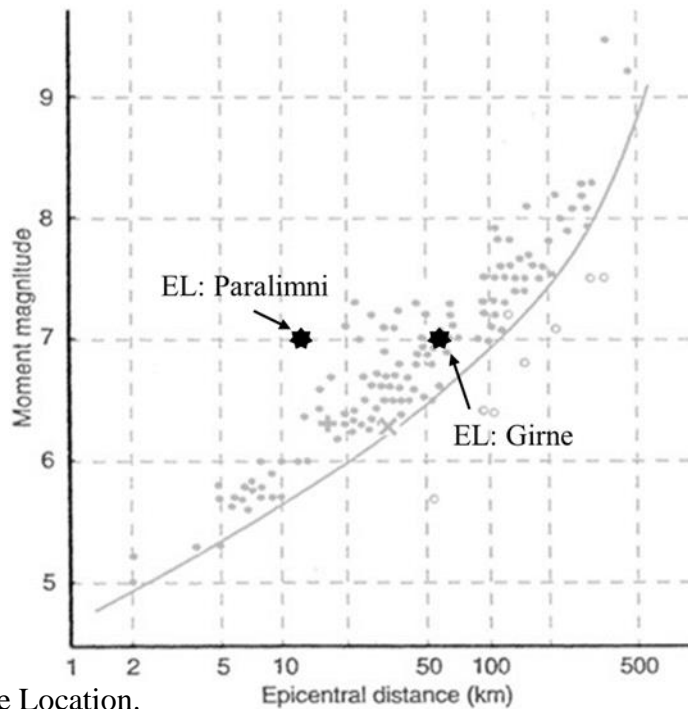


Figure 48: Shallow earthquake magnitudes and epicentres distances from Famagusta (Cagnan and Tanircan, 2010).

In Figure 49, the analysis is done based on maximum inland historical earthquake experienced ($M_w = 7.0$) and the closest epicentres. The selected epicentres are Girne and Paralimni located approximately 60 and 16 kilometres away from Famagusta.



*EL: Epicentre Location.

Figure 49: Famagusta shores susceptibility to liquefaction (Ambraseys, 1988).

The graph illustrates that the selected epicentres are plotted above the observed liquefied sites and from such observations, considering the calculated in-situ relative density, the vulnerability of the site is high. After establishing the initial analysis, the next procedure involves element testing as aforementioned.

3.4 Testing Strategy

In this section, a detailed strategy is set forth to estimate the liquefaction potential of the soil. The laboratory testing programme will include determination of index density properties of samples, monotonic triaxial compression and direct shear test along with the cyclic (multi-reversal) direct shear tests. The thesis program is divided into three phases as presented as follows:

1st Phase:

- Field analysis and observations.
- Sample collection.

2nd Phase:

- Physicochemical properties evaluation.
- Establishing experimental program.
- Separation and extraction of silts and clays from original soil.

3rd Phase:

- Experimental analysis.
- Evaluation of soil groups prone to liquefaction.

3.4.1 Experimental Program

In order to investigate the effect of fines content on the liquefaction susceptibility, silt and clay will be added to sand samples with varying percentages to form a set of manufactured samples representing a typical variation of Sand with fines. The test specimens are prepared to reflect various density states such as loose and dense. The varying percentages of fines includes silts and clays which are extracted from Alluvial Clay through a separation process developed which will be described in section 3.6. Upon completion of separation process, testing groups are developed as shown in Figure 50.

The main aim of the established strategy is to investigate the soil liquefaction potential for Sand containing various properties of fines in loose and dense states. The Direct Shear Box Tests under three different normal stresses (50, 100 and 150 kPa) are performed for evaluation of behaviour for monotonic and cyclic loading. Triaxial compression tests are also performed under three different confining pressures (50, 100 and 150 kPa) for the measurement of shear strength properties.

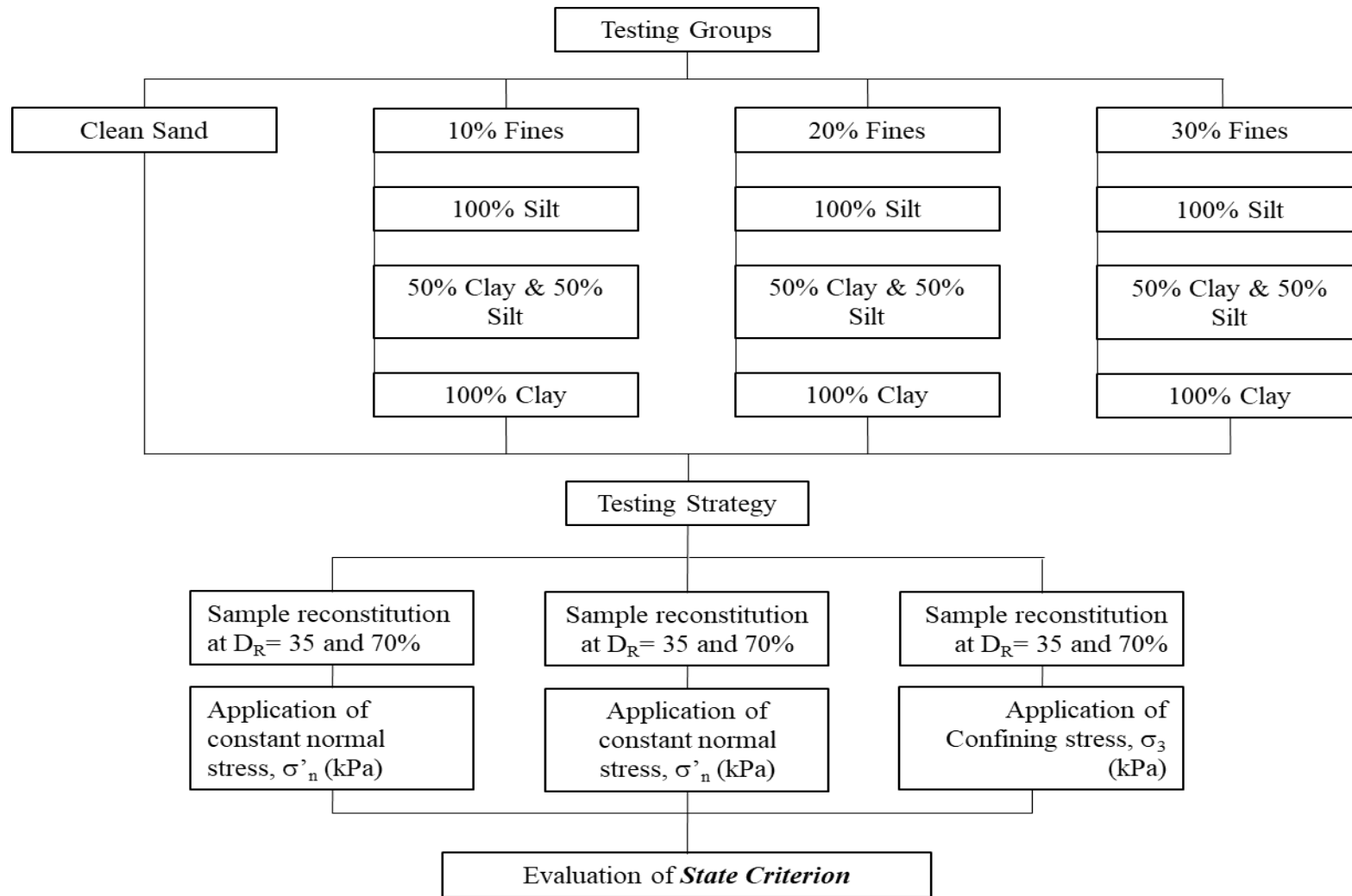


Figure 50: State criterion evaluation strategy

3.5 Experiments Methodology

This section elaborates the procedures taken into consideration to evaluate required parameters in a comprehensive manner.

3.5.1 Specific Gravity

The specific gravity (G_s) of soil solids is obtained by the procedure described in ASTM D854-14. A slight deviation from the standard is made by using 100 mL pycnometer. Oven-dried soil at $100 \pm 10^\circ\text{C}$ sieved through 4.75mm sieve soaked in distilled water for 1 day ahead of vacuum pressure application to remove trapped air bubbles in voids. In case of Alluvial Clay, soil is mechanically pulverized and the same procedure is practiced to obtain G_s .

3.5.2 Particle Size Distribution

The particle size distribution is obtained by dry and wet-sieving procedures based on the soil type and designated standards were followed accordingly.

3.5.2.1 Dry Sieving

Particle gradation of SBS soil is done according to the guidelines presented in ASTM D6913-17. The soil is oven-dried at $100 \pm 10^\circ\text{C}$ in thermostatically controlled oven overnight prior to conduct the test. The particle-size distribution is presented in Figure 51 and classification of soil parameters are tabulated in Table 4.

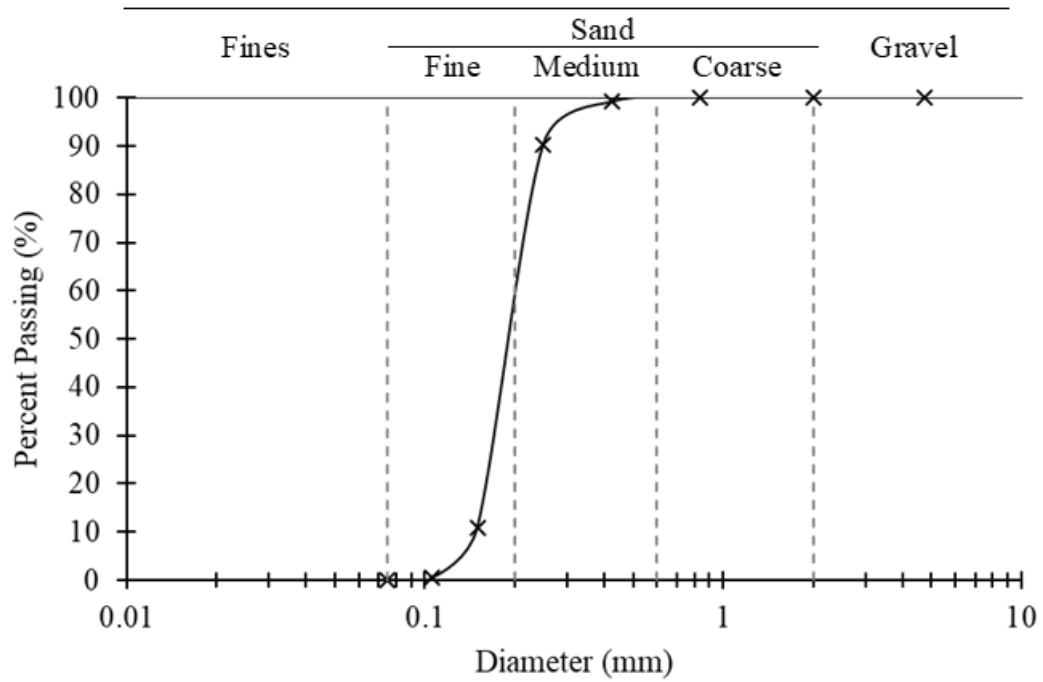


Figure 51: SBS grain size distribution.

Table 4: SBS Classification.

Parameters	Values
Diameter corresponding to 10% finer, D_{10} (mm)	0.148
Diameter corresponding to 30% finer, D_{30} (mm)	0.170
Diameter corresponding to 50% finer, D_{50} (mm)	0.197
Diameter corresponding to 60% finer, D_{60} (mm)	0.200
Uniformity Coefficient, C_u	1.35
Curvature Coefficient, C_c	0.98
Fines content (%)	0.10
Soil Category	Fine to Medium, Clean Sand
Soil Classification	Poorly Graded Sand, SP

3.5.2.2 Wet Sieving

ASTM D1140-17 guidelines are followed to determine the amount of soil particles passing sieve no. 200 (75 μ). The test is conducted on various fine-grained soil before proceeding with hydrometer analysis in order to observe the amount of material retained on No. 200 sieve and Alluvial Clay is selected for the aforementioned purpose. Prior to washing, soil is soaked in dispersing agent (Test method-B) for 2 hours and frequently agitated to ensure complete separation of particles. In Figure 52 (a), coarse and fine particles percentages of Alluvial is illustrated.

3.5.2.3 Hydrometer Analysis

Alluvial Clay gradation analysis is performed according to ASTM D7928-17 guidelines. Prior to sedimentation process, the soil is oven-dried in a thermostatically controlled oven at 100 \pm 10 $^{\circ}$ C overnight and the experiment is performed in a temperature-controlled room ranging between 20 to 23 $^{\circ}$ C. The particle size distribution curve of Alluvial Clay is shown Figure 53.

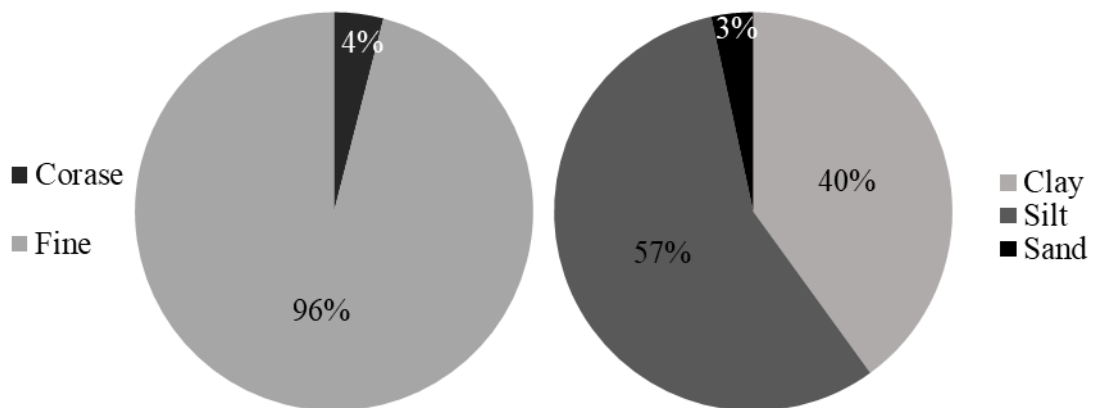


Figure 52: Alluvial Clay (a) composition (b) grains distribution

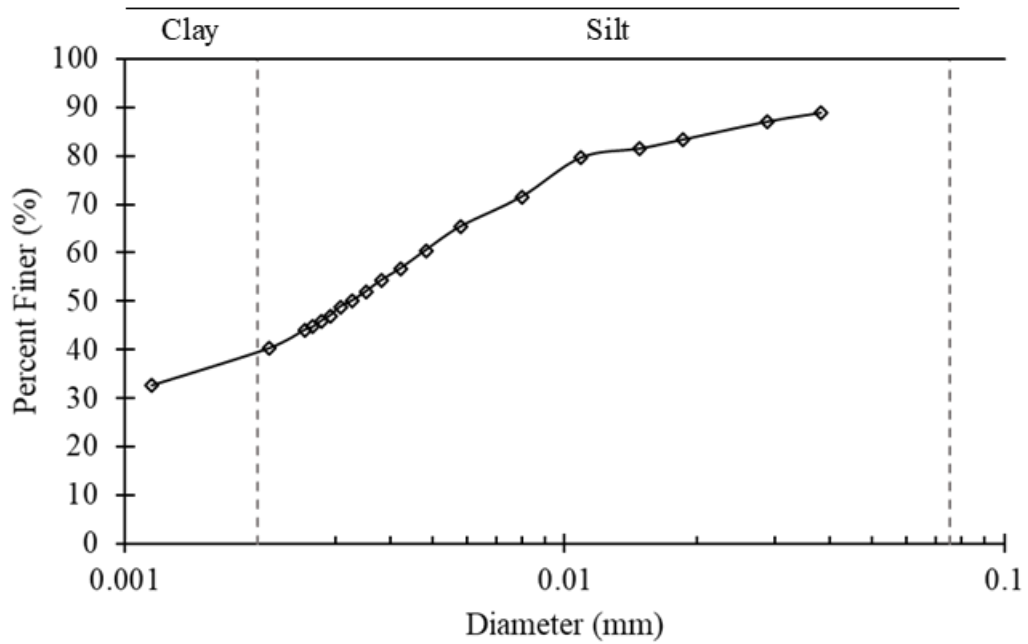


Figure 53: Alluvial Clay particle-size distribution curve.

3.5.3 Plasticity Tests

Atterberg's Limits are obtained by the procedures outlined in ASTM D4318-17. Liquid limit (LL) of the soil is obtained by linear regression analysis through multipoint method using Casagrande's device where the water content versus number of drops for different specimens are plotted in semi-logarithmic graph. Dry preparation technique of soil is applied where, oven-dried specimens (50°C) are mixed with adequate amount of different water content and were allowed to soak in a polyethylene bag overnight prior to conduct the test. In Figure 54, semi-logarithmic plot to obtain LL is shown.

Plastic limit (PL) of soil is obtained by rolling a thread of soil until noticeable cracks are detected or soil crumbles before reaching approximately 3 mm in diameter.

BS 1377-2-1990 guidelines were implemented to conduct linear shrinkage (LS) test where, the oven dried soil is mixed with distilled water at liquid limit water content. After overnight soaking period, the soil is moulded and placed at room temperature for a period of 24 hours until the soil shrinks from the walls of mould and then placed in 50°C oven. The length of the specimen is measured after 24 hours, then placed in 100°C oven and the final length of specimen is recorded and linear shrinkage value is measured.

From Casagrande’s plasticity chart (Figure 55), common minerals present in fine-grained soil can be estimated and is the simplest approach. From PI and LL of Alluvial Clay soil, the point lies above the A-Line which indicates the presence of Illite mineral. Classification of Alluvial Clay is tabulated in Table 3.

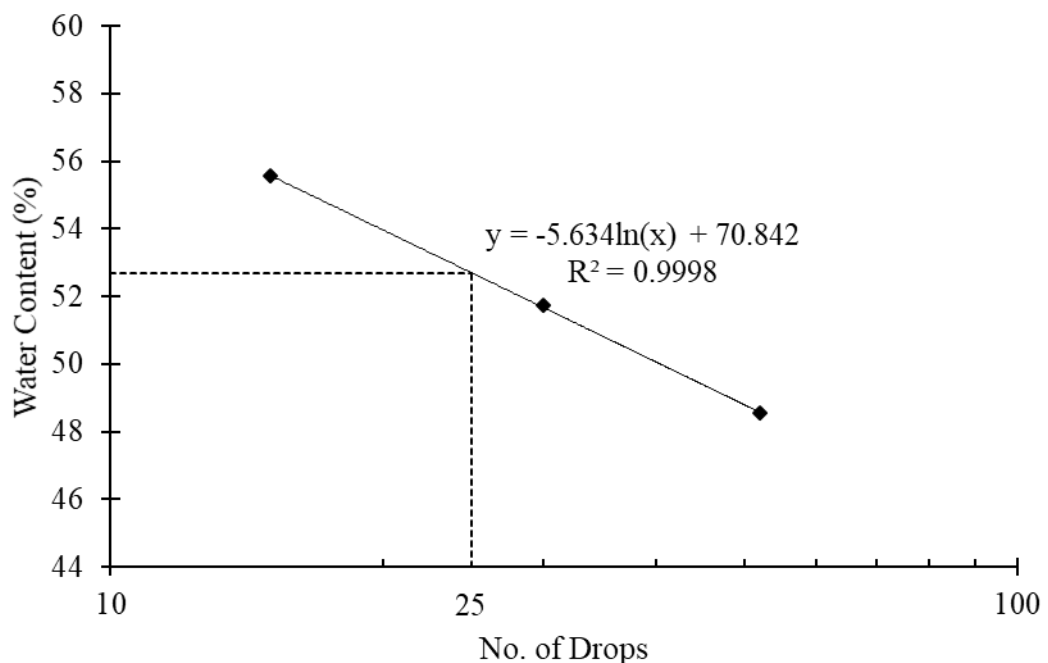


Figure 54: Alluvial soil flow curve for LL determination.

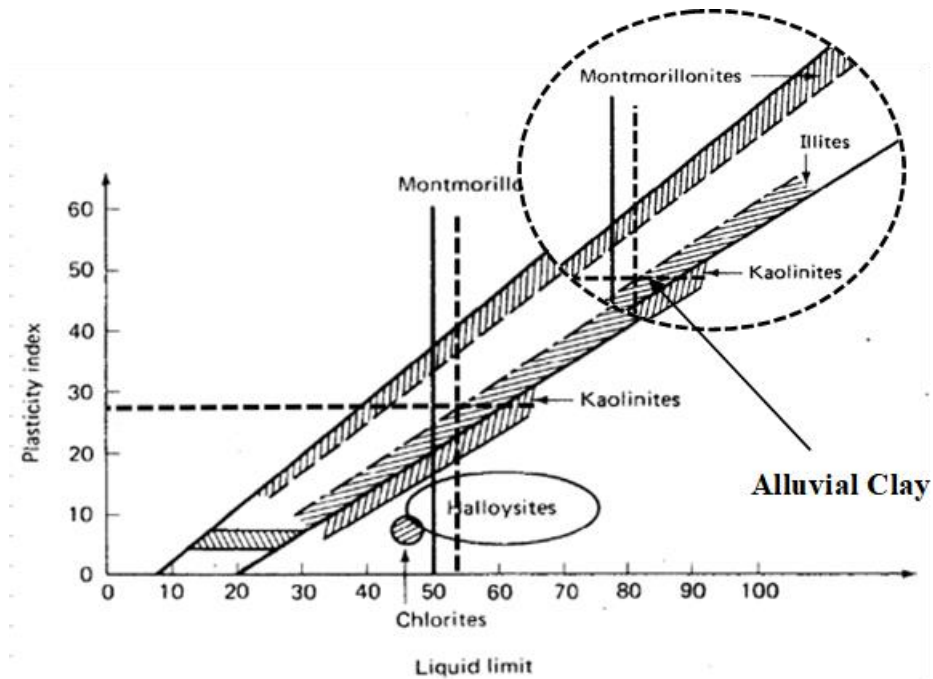


Figure 55: Clay minerals location on Casagrande's Plasticity Chart (Holtz & Kovacs, 1981).

3.5.4 Relative Density

Relative density (D_R) of SBS soil groups are obtained by a method proposed by Lade & Yamamuro (1997). The primary reason behind adopting the mentioned method is due to presence of fines in sand matrix whereas conventional methods are only applicable for sand containing fines up to 15%. Apart from following the aforementioned method, ASTM D4253 and 4254 – 16 methods were also followed and similar values for e_{max} were observed except that e_{min} values differ due to crushing of carbonates in soil. It is also noticed that with ASTM D4253 and 4254-16 methods, when the 20% fines were added, the loss of finer material in the form of dust escaped from spacings and accumulated at the top of base plate.

3.5.4.1 Maximum Void Ratio

The maximum void ratio (e_{max}) is obtained by placing 800 grams of soil incrementally in a 1000 mL graduated cylinder. The cylinder is covered with a rubber stopper and

turned upside-down or tipped over for a period of one minute (each second one rotation) and the final reading is observed on the cylinder as shown in Figure 56(a).

3.5.4.2 Minimum Void Ratio

The minimum void ratio (e_{\min}) is obtained in a similar manner except that instead of turning upside-down, the poured soil is tapped with rubber hammer until no further settlement of soil is observed (Figure 56-b). One of the advantages of this method is that there will be no particle breakage especially when soil contains high degree of carbonates.

From obtained reading on graduated cylinder, the dry densities of soil and void ratios are calculated as follows:

$$\rho_{d,\min} = \frac{M}{V} \quad , \quad \rho_{d,\max} = \frac{M}{V} \quad (3.1)$$

$$e_{\max} = \frac{G_s}{\rho_{d,\min}} - 1 \quad , \quad e_{\min} = \frac{G_s}{\rho_{d,\max}} - 1 \quad (3.2)$$

where;

M: Mass of dry soil used.

V: Volume of soil (mL = cm³).

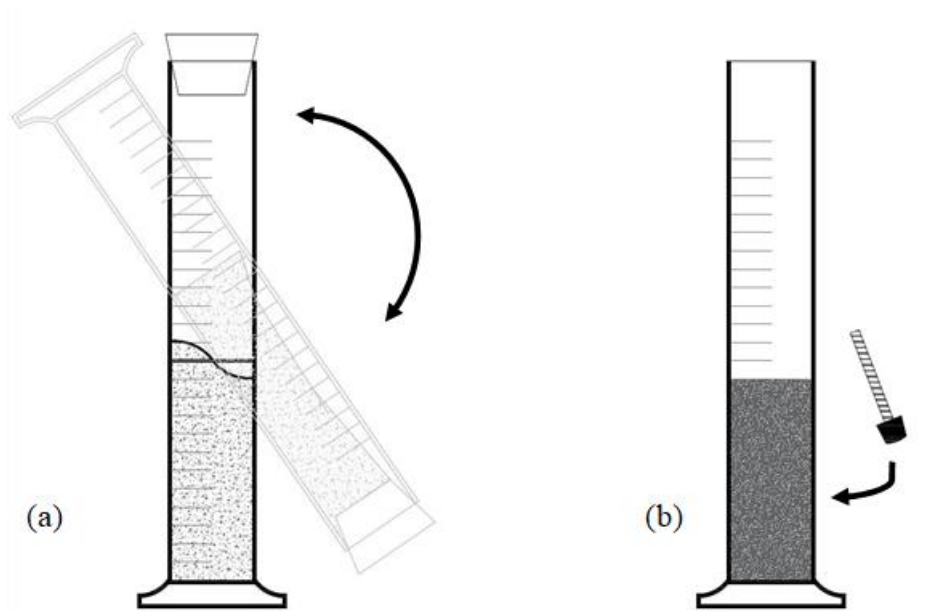
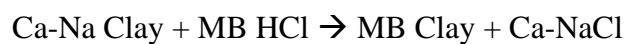


Figure 56: Schematic illustration for (a) e_{\max} and (b) e_{\min} determination.

3.5.5 Chemical Tests

3.5.5.1 Cation Exchange Capacity

The quantitative mineralogical analysis of fine-grained soil can be estimated by means of chemical tests and from the techniques available for chemical analysis, the degree of accuracy is good. One of the quantitative measurement's technique for clay minerals is through cation exchange capacity (CEC), expressed in terms of milliequivalent per 100 grams (mEq/100g). Alluvial Clay, CEC is determined by method suggested by AFNOR (1988) through Methylene Blue Adsorption Test (MBAT). The method is based on the replacement of the natural cations of clays by methylene blue dye. The replacement of cations chemical reaction in the solution is as follows:



A simple flowchart of the procedure is illustrated in Figure 57. The CEC of a given clayey soil is measured by tendency of clay minerals to adsorb methylene blue in an aqueous solution.

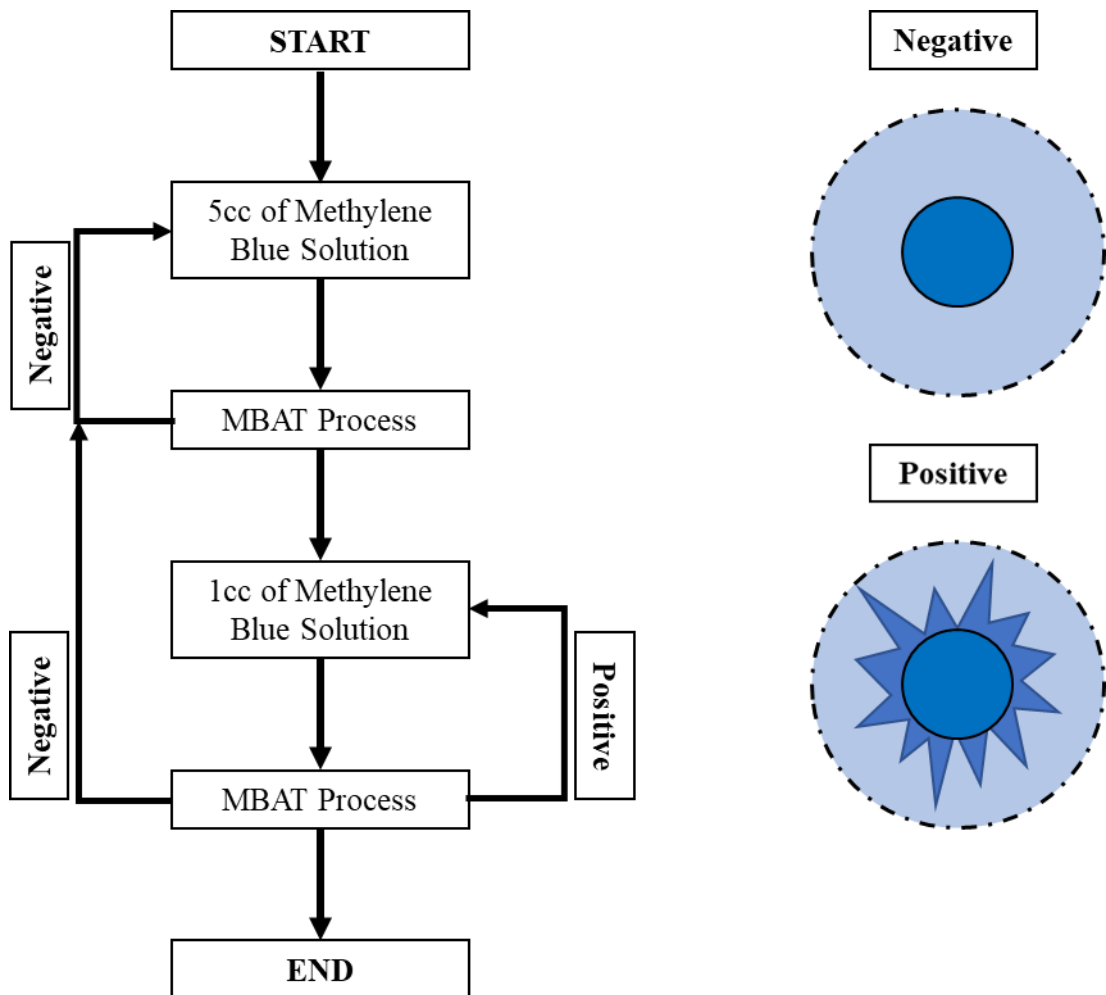


Figure 57: MBAT titration process flowchart (AFNOR, 1988).

The primary principle behind MBAT phenomenon is that, it quantifies the amount of methylene blue that covers the surface of clay minerals (ionic absorption). During the titration process, the methylene blue releases cations and ions are exchanged with negative charged clay particles. During the mentioned process, the main indicator is that when ion exchange capacity is reached, the formation of light blue halo (sunshine

pattern) around the blue strain appears (Figure 57). The CEC (mEq/100g) is estimated from MBAT test as follows:

$$CEC = \frac{100}{W_M} V_{cc} N_{mb} \quad (3.3)$$

where;

W_M : mass of clay specimen (g).

V_{cc} : The volume of Methylene Blue titrant, mL.

N_{mb} : Normality of Methylene Blue substance (meq/mL).

and

$$N_{mb} = \frac{\text{Weight of Methylene Blue (g)}}{320} \frac{100-X}{100} \quad (3.4)$$

where;

X: Moisture content of the methylene blue content (%).

320: Molecular mass of methylene blue.

3.5.5.2 Specific Surface Area

Apart from CEC of soil and clay fraction presence in the soil, index properties of soil are significantly dominated by surface area of soil. Surface area of soil is primarily associated with particle-size distribution and is considered as intrinsic property. One of the most prominent method to obtain specific surface area (SSA) of fine-grained soil is by adsorption of polar liquid. SSA of alluvial clay is measured through a method proposed by Cerato & Lutenege (2002) and in this testing method, ethylene glycol monoethyl ether (EGME) is incorporated to the soil. EGME as compared to ethylene glycol is a very volatile polar liquid at room temperature, it has higher vapour pressure and excess liquid evaporates much faster than ethylene glycol under controlled conditions. The capability of this method application in determining SSA ranges from 15 to 800 m²/g.

SSA by EGME method is obtained by placing 1 g of oven-dried (100°C) soil passed through sieve no. 40 in a glass tare and approximately 3 mL of polar liquid is smeared all over the soil. The saturated sample is then placed in a desiccator containing desiccant and the final reading is recorded when equilibrium is achieved between 2 reading intervals. Figure 58 represents schematic illustration of EGME test arrangement and Table 5 shows typical CEC and SSA for common clay minerals are presented (Baker, et al., 2017).

The SSA of a given soil is calculated as follows:

$$SSA = \frac{W_a}{f W_s} \quad (3.5)$$

where,

W_a : Weight of EGME retained by sample (g) = Final slurry weight – W_s

W_s : Weight of added dry soil (g)

f : 0.000286, Weight of EGME required to form a monomolecular layer on a square meter of surface (m^2/g)

Table 5: Typical values of CEC and SSA of clay minerals (Baker, et al., 2017).

Mineral Type	CEC (mEq/100g)	SSA (m^2/g)
Kaolinite	3 – 15	10 – 15
Illite	10 – 40	80 – 120
Montmorillonite	80 – 100	700 – 800

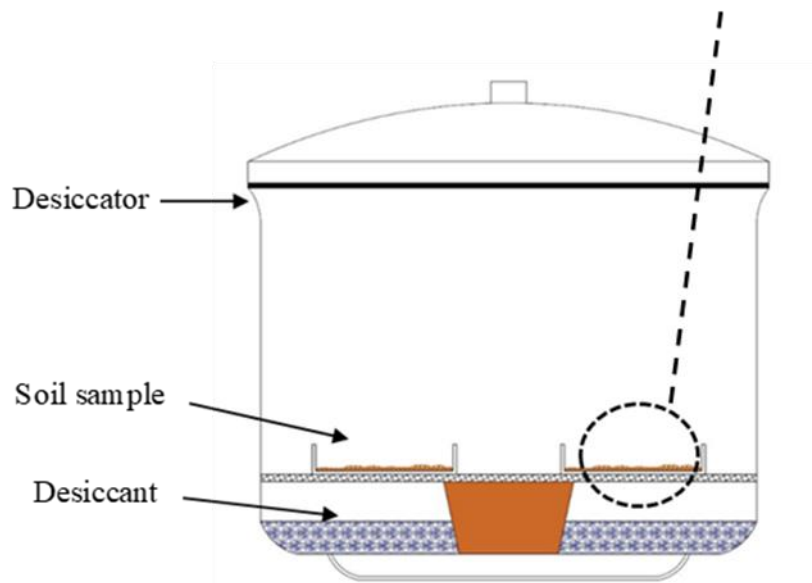
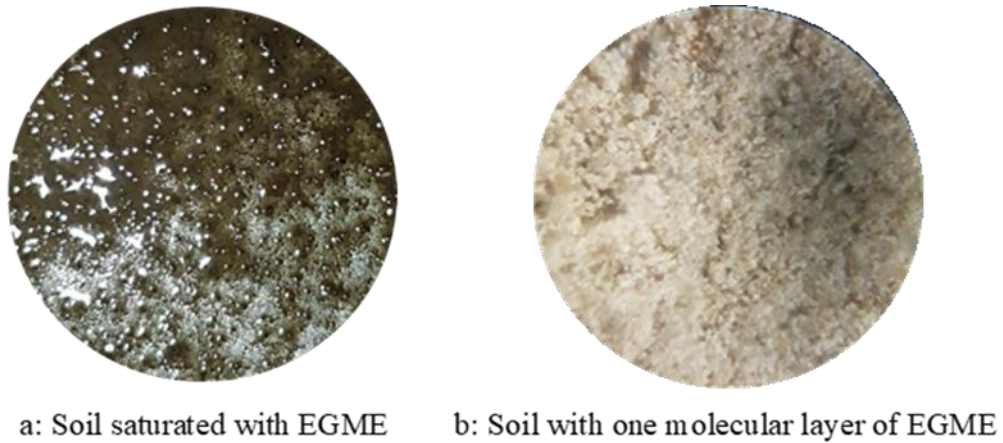


Figure 58: Schematic illustration of EGME test.

3.5.5.3 Carbonate Content

Carbonate content of SBS and Alluvial Clay is obtained in accordance with the guidelines presented in ASTM D4373-13. The fundamental concept involves determination of calcite equivalent present in soil. The procedure requires calibration by using anhydrous calcium carbonate to obtain calibration through production of carbon dioxide gas by mixing with an agent hydrochloric acid (HCl). Soil specimen with an approximate mass of 1 ± 0.01 g is placed in the reactor (reaction cylinder) which is mixed with an approximately 20 ± 2 mL of HCl (1M solution). As the reaction initiates in the reactor the pressure generated by CO₂ production is measured. The

pressure reading is monitored until it is stabilized (10 minutes) from which calcite equivalent is obtained. In Figure 59, calibration curve is plotted and the calcite equivalent for both SBS and Alluvial Clay soils are shown.

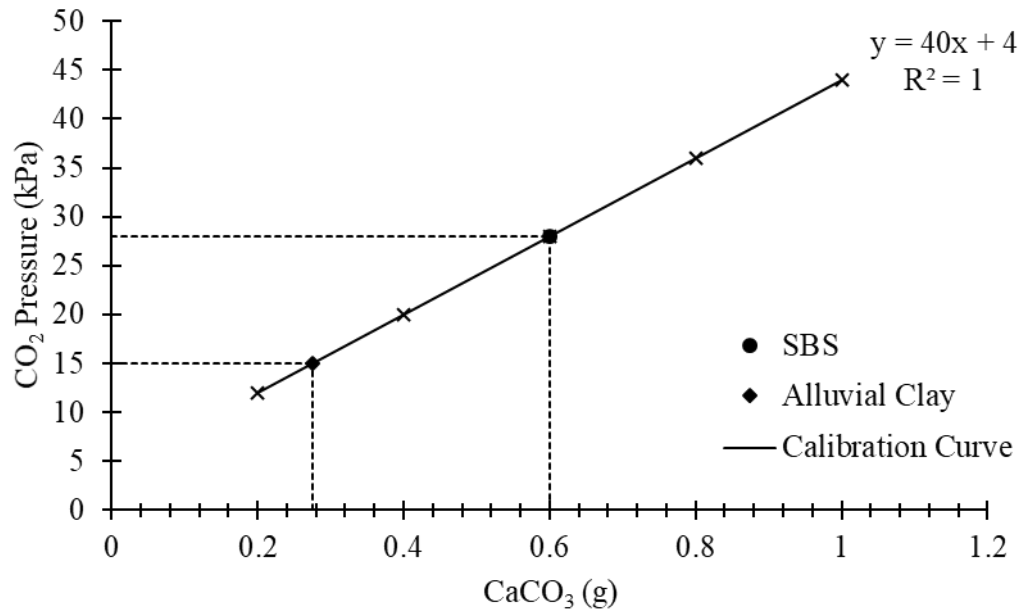


Figure 59: Calibration curve and calcite equivalent of tested soils.

3.5.5.4 Electrochemical Tests

Electrochemical tests; pH, electrical conductivity (resistivity) tests are performed in accordance with ASTM D4972-13 and ASTM D1125-14.

Table 6: Electrochemical properties of tested soils.

Property	Soil Type	
	SBS	Alluvial Clay
Potential of Hydrogen, pH	8.39	8.15
Electrical Conductivity, EC (μ S)	3110	6880
Electrical Resistivity, ER (k Ω)	0.346	0.13
Total Dissolved Solids, TDS (ppm)	-	3720
Salinity, SAL (psu)	-	4.80

3.6 Separation of Silt and Clay Fractions

A method for separation of fines fractions of Alluvial Clay is developed in order to separate silt and clay size particles from soil at laboratory scale. The separated fines were mixed with sand in various proportions to represent typical soil mixtures which can be found in the site. The mixtures produced can be classified as sandy Silt or Silty Sand, sandy Clays or clayey Sand and clayey-silty Sand or sandy Clay-Silt.

The primary idea of soil separation procedure is adopted from a well-known analysis technique known as “Sedimentation Analysis”. The fundamental aspect in this analysis is based around Stokes Law which is very reliable in determination of particle-size distribution through distribution of sedimentation of particles with time. After selection of the preferred soil, the particle sedimentation with respect to time is plotted as shown in Figure 60.

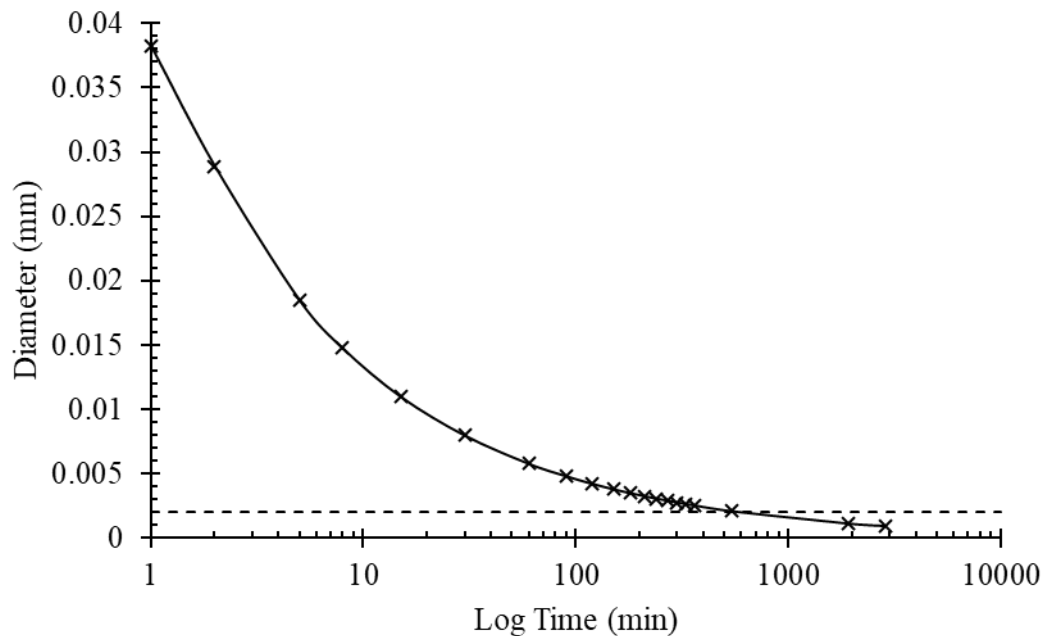


Figure 60: Alluvial Clay particle settlement versus time.

The total time required for sedimentation of silt grains can be obtained from Figure 58. Based on trial procedures, three stages miniscule, intermediate and wide scale of treatment for separation of fines is developed. In all stages of treatment, dispersing agent, sodium hexametaphosphate and sodium carbonate is used as dispersing agent.

3.6.1 Minuscule Stage Analysis

In minuscule stage, 50 grams of dispersed soil is mixed with water (6 times of soil mass) to form a soil suspension which allowed sufficient time for silt fractions to accumulate at the bottom of cylinder. Several samples were tested in order to obtain adequate amount for hydrometer analysis to validate the testing procedure. Another primary indicator of separated soil in transparent container is the visibility of layers in the solution (Figure 63-b). After the required time is achieved, the extraction process of silt and clay proportions requires extreme caution not to disturb the settled soil and this process is done with the help of syringes. The collected material is then submerged into distilled water to remove the excess salts from the soil and for this purpose, pH value (Neutral ≈ 7.0) indication is very helpful. Conservatively, a thin layer on top of silt is discarded to avoid extraction of particles from clay layer. The hydrometer test is then performed on the collected proportions and the result of separated soil at miniscule stage is plotted in Figure. In order to validate the extraction procedure at a required time, sedimentation of separated soil with respect to time is plotted in Figure 62.

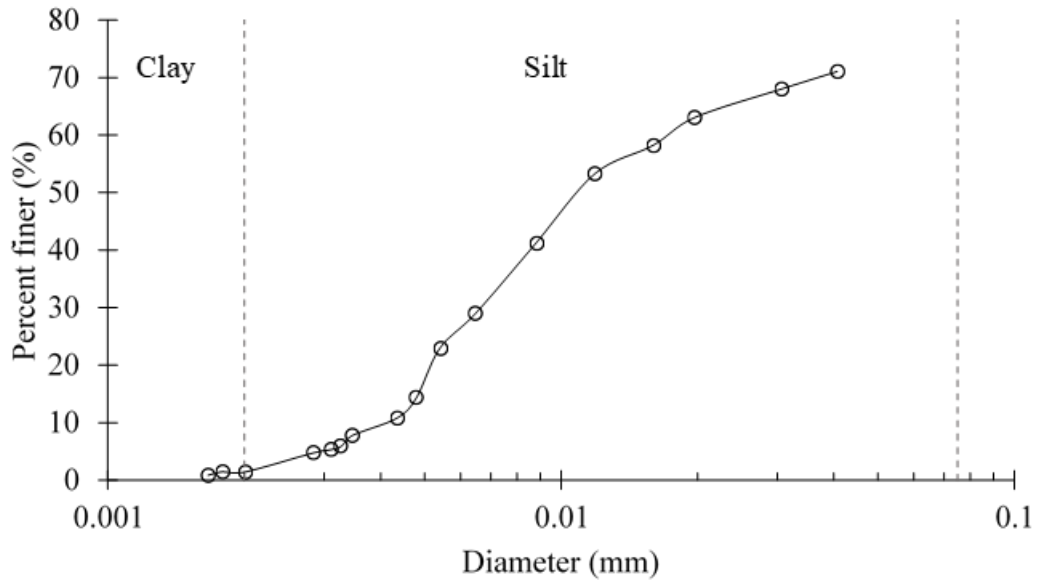


Figure 61: Miniscule stage hydrometer analysis of separated silt.

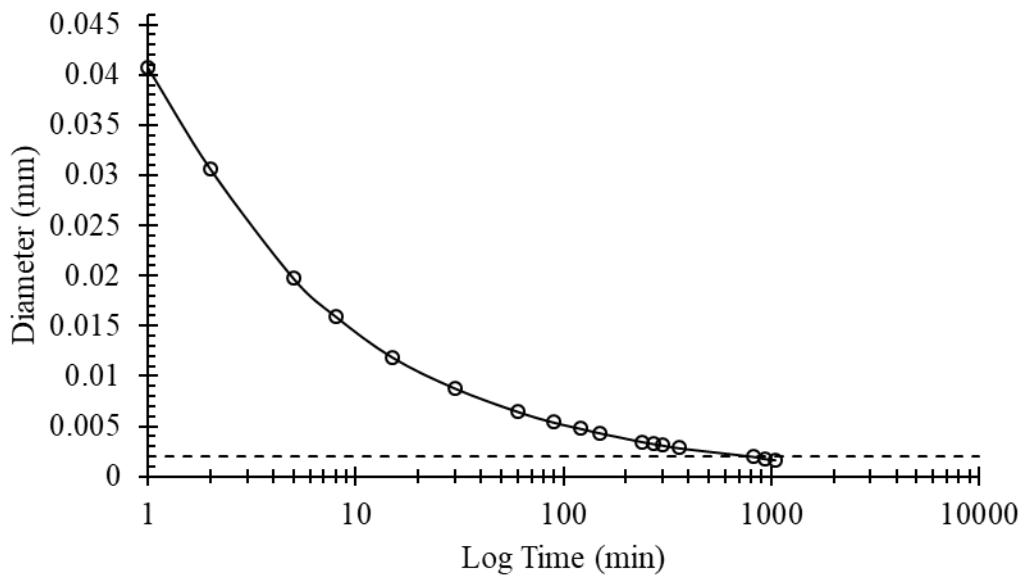


Figure 62: Extracted silt grains sedimentation time.

The settlement rate differs from the original analysis, which may be due to temperature differences of soil composition and the variation in the hydrometer analysis. In addition to this, Alluvial Clay comprises approximately equal proportions in terms of mass, whereas, Figure analysis is based on 50 grams of separated silt fractions.

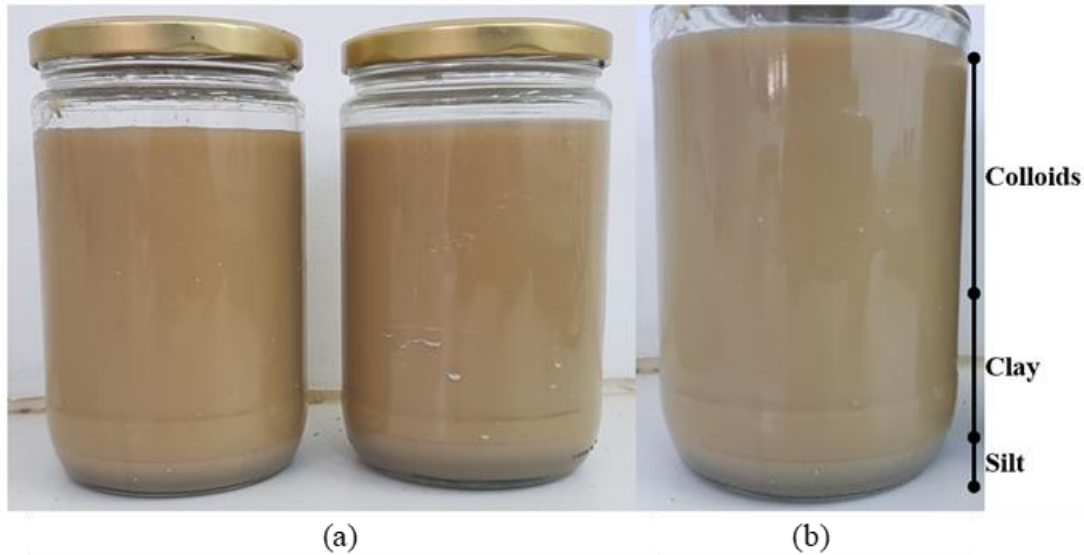


Figure 63: (a) Miniscule separation scale (b) Layers.

3.6.2 Intermediate Stage Analysis

The second stage (intermediate stage) involves improvement of the effectiveness of the method developed for separation of silt and clay size fractions. In this stage the primary aim is to obtain adequate amount of fines in shorter period and to develop a fast extraction process. As compared to miniscule stage, 135 grams of dispersed soil is mixed with water (6 times of soil mass) in a 1 litre capacity container and after a required time, extraction process initiated. As previously mentioned, firstly the colloids and clays are extracted because of nature of clay particles. As clay size particles remains in Brownian motion, extraction of them from a suspension is easier. One of the effective techniques employed in this case is by applying Siphon's technique to transfer liquid substance from one container at higher elevation to another container at lower elevation as shown in Figure 65(b). By employing this technique, the suspended clay suspension is transferred to another container at a faster rate by the action of gravity. After collection of silts and clays, the dried soil is washed in a similar manner as previously mentioned. The separated proportions from each container are

mixed together for homogeneity purpose and index properties were evaluated before initiating for final stage. In Figure 64, hydrometer analysis is plotted and crack patterns of separated fines are shown in Figure 66.

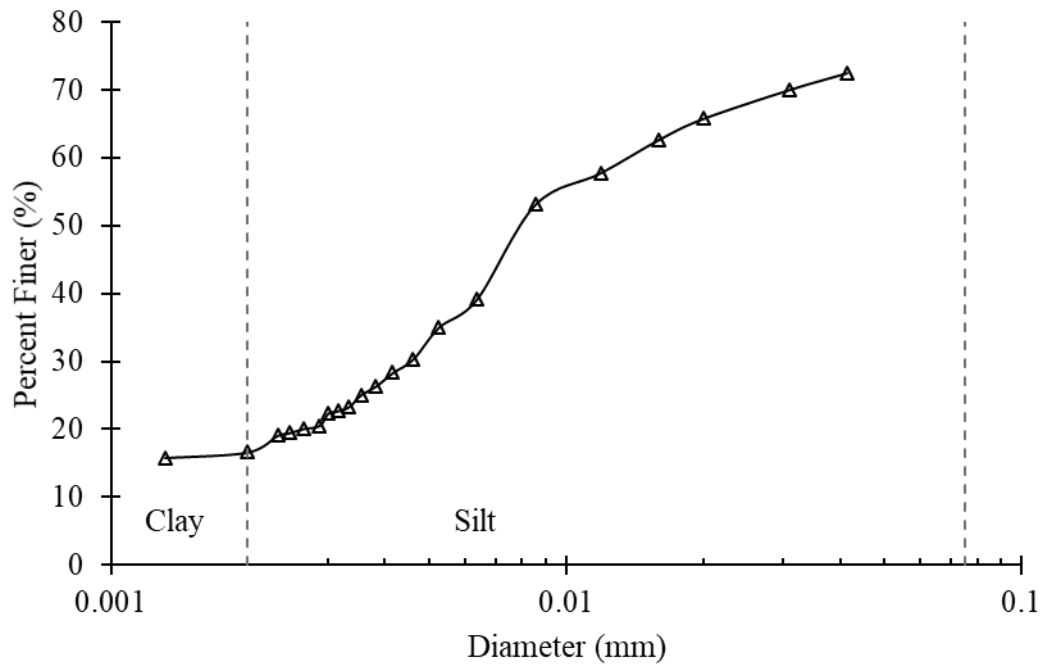


Figure 64: Intermediate scale hydrometer analysis of separated silt.

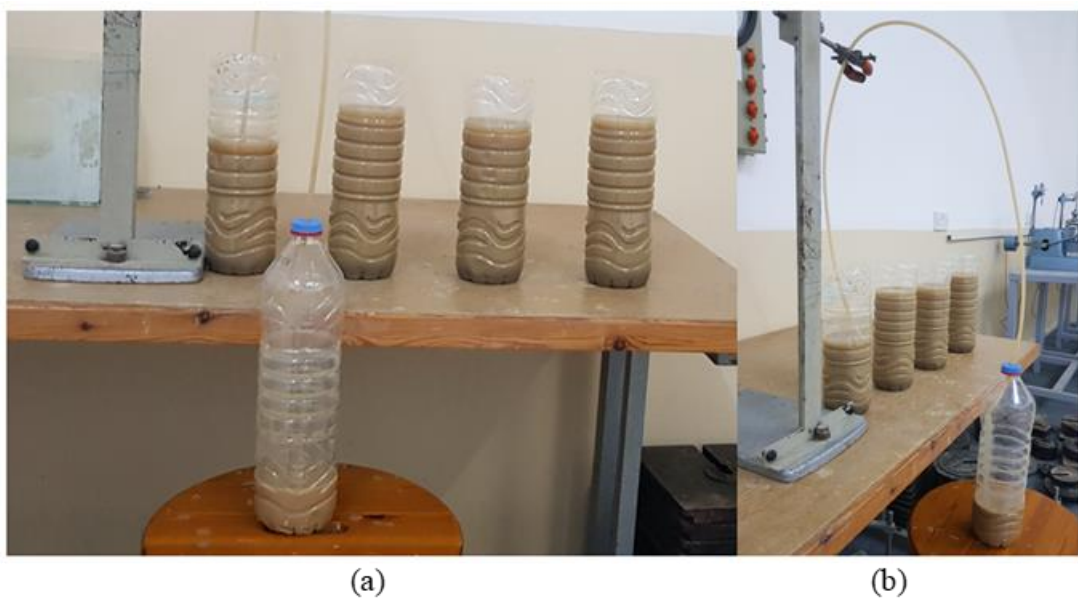


Figure 65: (a) Intermediate scale (b) Siphon technique.

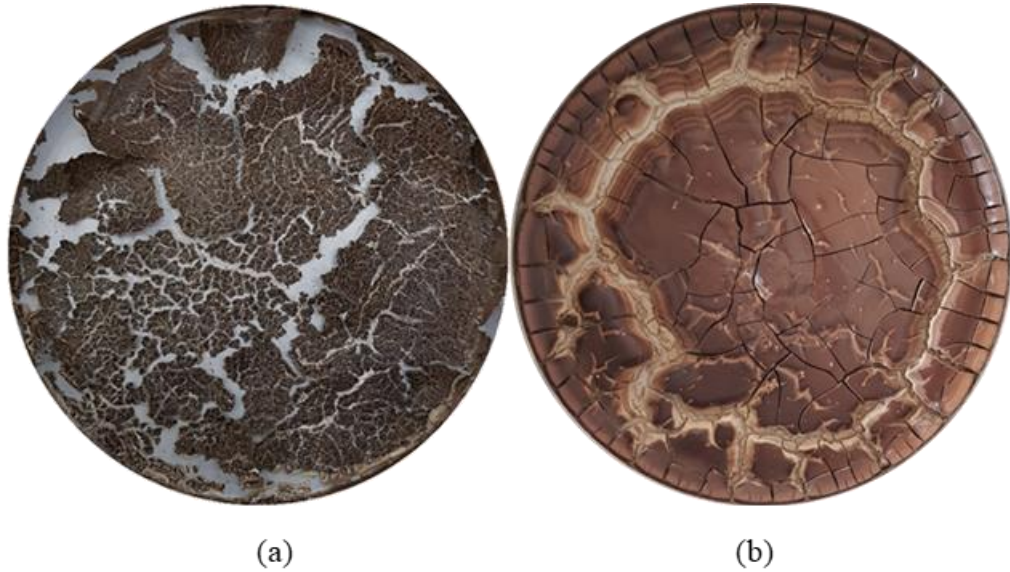


Figure 66: Crack patterns (a) Clay (b) Silt.

As it can be observed in Figure 64, at intermediate scale the soil proportions as compared to miniscule stage differs by approximately 7 percent, which might be due large quantity soil extraction. During small scale, the control of sample characteristics is primarily easier due to step by step extraction process, whereas during the application of siphon technique, some of the clay particles might get mixed due to slight disturbance between suspended layers. Although the difference is not significant, further adjustments can be applied by eliminating the vibration caused initially when a small vacuum is applied for transferring the suspension.

3.6.3 Wide Scale Analysis

Subsequent to intermediate stage after assessing the method effectiveness, wide scale separation is initiated in a similar manner. To ensure the homogenous mixture of separated fines, silts and clays were mixed individually after collecting desired amount for further testing. In Figure 67 summarized flow chart of separation process is illustrated. After assessing the outcomes and the effectiveness of separation technique developed to separate silt and clay fractions, the general procedure is summarized in Figure 68.

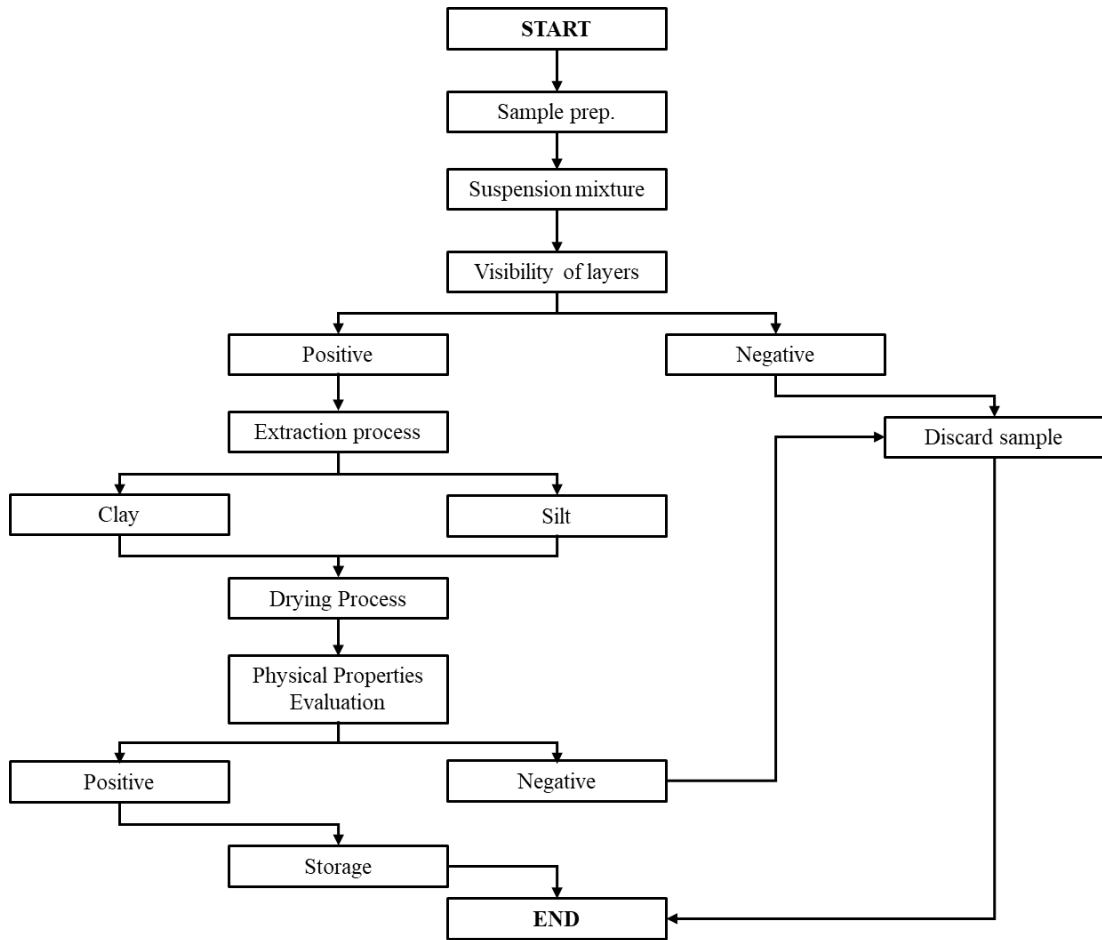


Figure 67: Soil separation procedure flowchart.

DAYS								
1	2	3	4	5	6	7	8	
Sample prep.	Suspension mixture	Extraction process						
		Clay	Drying Process			Physical Properties evaluation	Storage	
		Silt	Drying Process	Physical Properties evaluation	Storage			

Figure 68: Wide scale timeline of soil separation process.

Based on soil groups, the physical properties of respective fine proportions are tabulated in Table 7. Separated silt and clay from each stage is illustrated in Figure 69 and Figure 70.

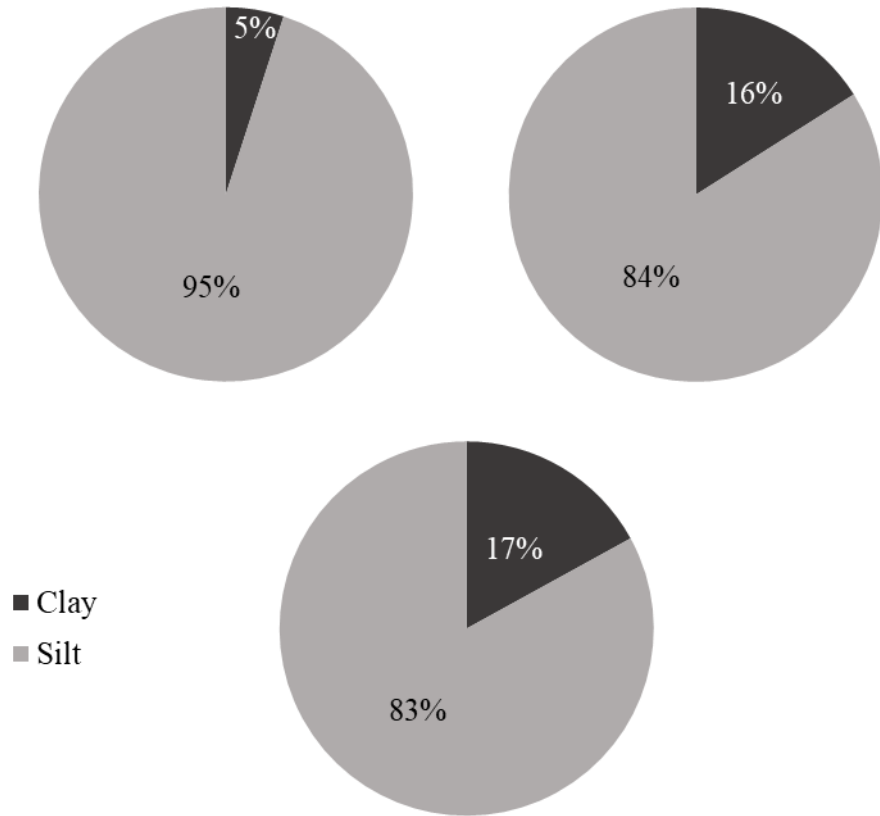


Figure 69: Soil fine fractions (a) Miniscule (b) Intermediate (c) Wide Scales.

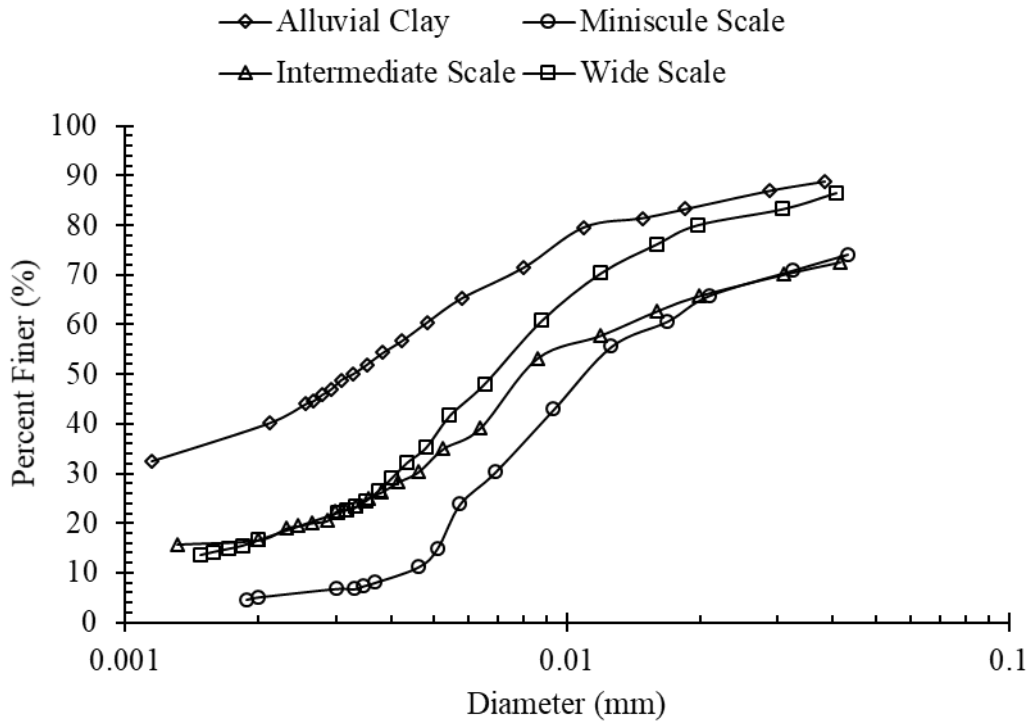


Figure 70: Comparison of particle-size distribution of silt from different stages

Table 7: Index properties of separated fine proportions.

Properties	Fine Proportions			
	Alluvial Clay	Silt	50/50 Silt & Clay	Clay
Specific Gravity, G_s	2.575	2.611	2.609	2.598
Liquid Limit, LL (%)	53	52	52	56
Plastic Limit, PL (%)	25	33	31	27
Plasticity Index, PI (%)	28	19	21	29
Linear Shrinkage, LS (%)	16	15	15	12
Classification	CH	MH	MH	CH
Specific Surface Area, SSA (m^2/g)	111	19	86	146

Hydrometer results for separated soil and soil mixture prepared are presented in Figure 71. Figure 72 shows the flow curves of the separated soils for liquid limit determination and the plasticity index of these soils are shown in the plasticity chart (Figure 73). The linear regression equations corresponding to each soil type is presented in Appendix B.

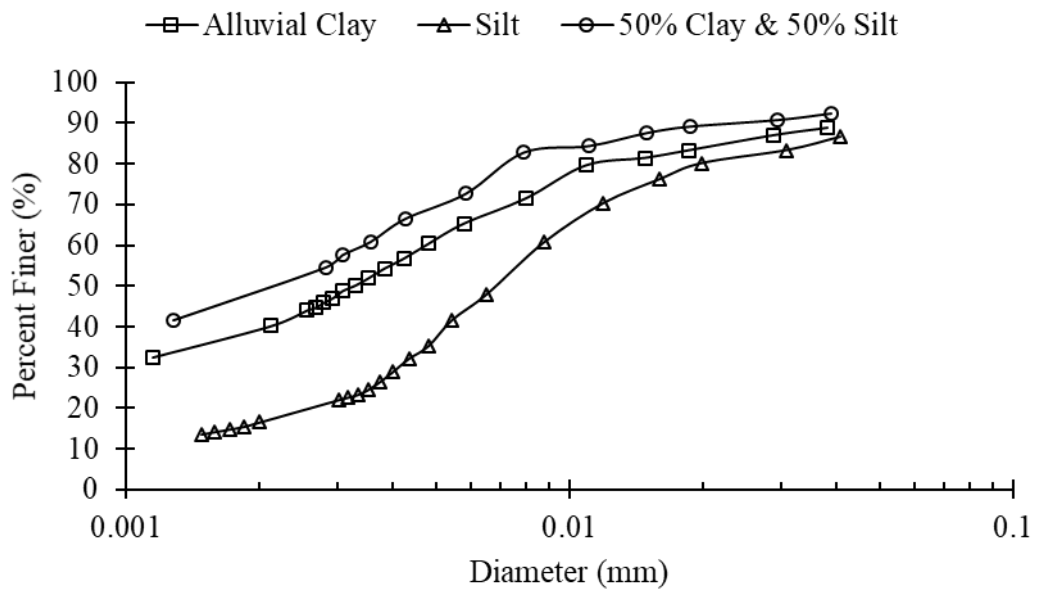


Figure 71: Separated soil and soil mixtures hydrometer analysis results.

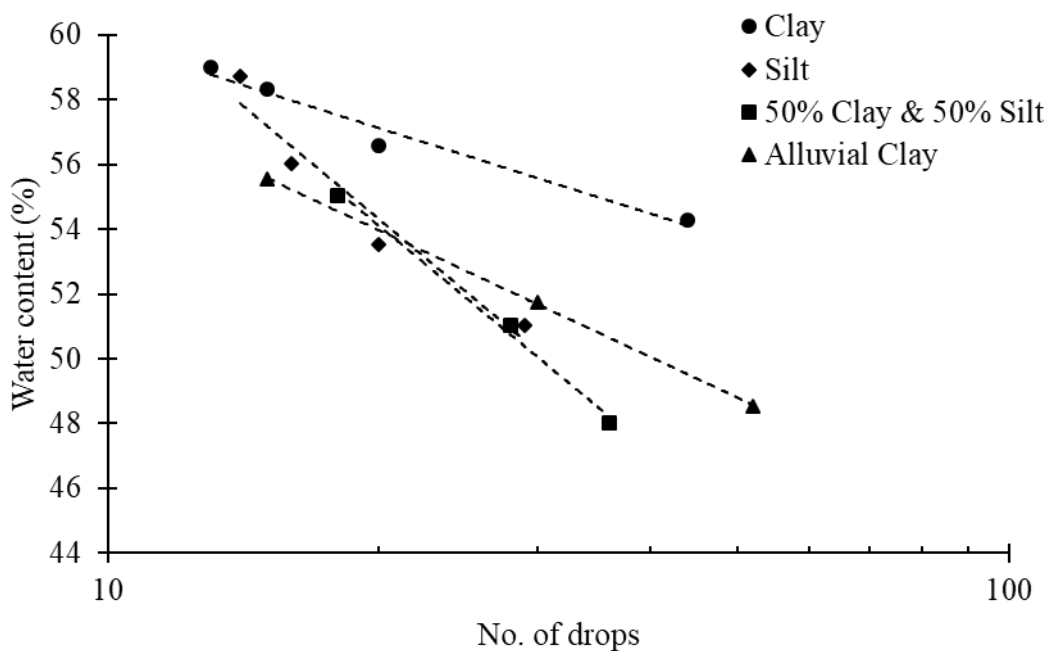


Figure 72: Separated soils flow curves.

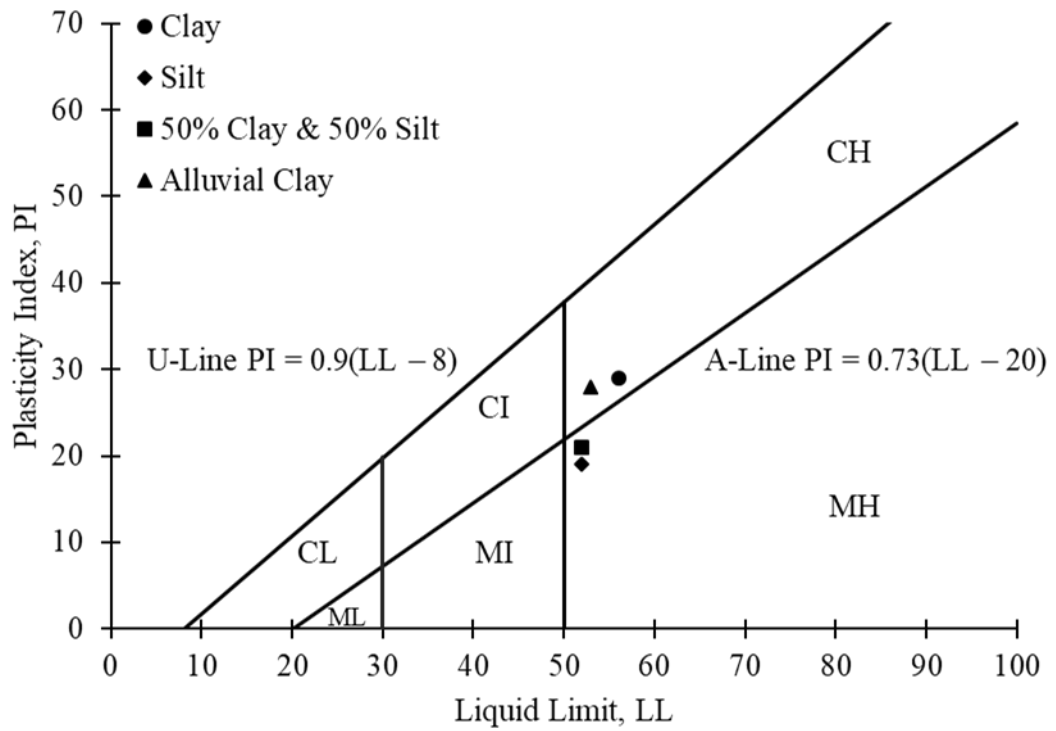


Figure 73: Plasticity Chart (Das & Sobhan, 2014).

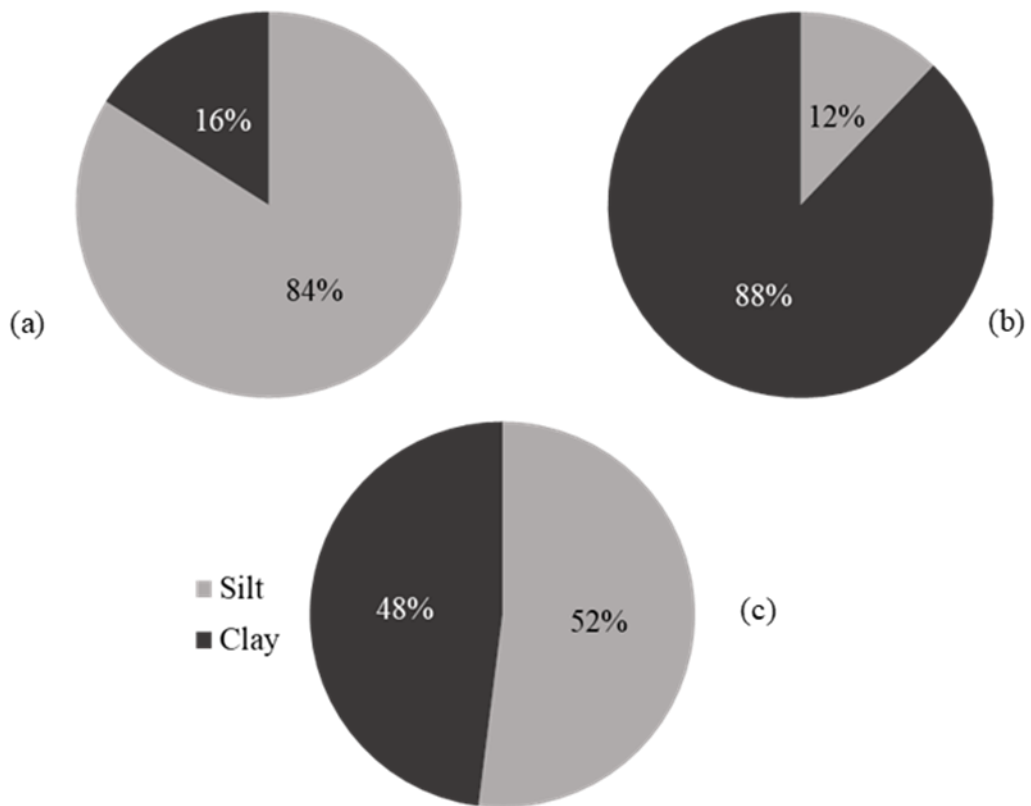


Figure 74: Separated soil and soil mixtures proportions (a) Silt (b) Clay and (c) 50% clay & 50% Silt.

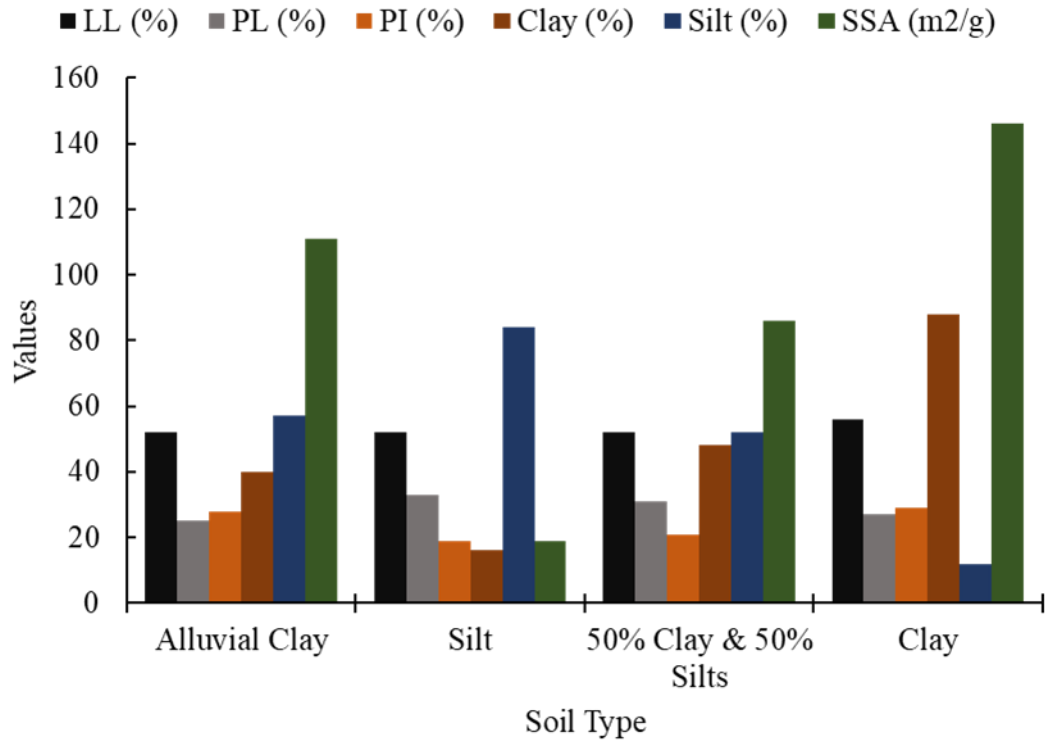


Figure 75: Physicochemical properties comparison of separated and prepared soil mixture.



Figure 76: Wide Scale.

3.7 Consolidated Drained Direct Shear Box Test (CD-DST)

CD-DST's of soil groups are performed according to guidelines presented in ASTM D3080-11 in a strain-controlled direct shear testing device. Detailed information related to sample conditions are provided in this section. The soil samples are tested at two relative densities, 35 % and 70%.

3.7.1 Sample Preparation

In this section, the employed specimen preparation techniques for loose and dense specimens are presented.

3.7.1.1 Loose Specimens Preparation

Oven-dried specimens (100°C) are poured into the shear box with dimensions of 60 mm by 60 mm by employing dry-funnel pluviation (DFP) technique to reconstitute loose specimens. DFP technique helps provide a uniform distribution of soil particles and preparation of identical specimens. In this technique, the soil is poured into the funnel and funnel is raised slowly. Pouring of specimens from low height helps with preparation of loose specimen where the height of the funnel tip is kept very low (Quasi-nil) in order to avoid segregation of particles. In Figure 77, schematic illustration of DFP technique is shown. The samples at lower relative densities are prepared directly into the DST machine setup in order to avoid any disturbance while transferring the direct shear box. In order to validate the preparation of homogenous preparations of soil samples, three samples are prepared before shearing process. After the application of constant normal stress if similar initial settlement is observed then the specimen is regarded as identical. Otherwise, if the difference exceeds $\pm 10\%$, the sample is discarded and re-evaluation is performed. The primary reason of setting $\pm 10\%$ difference is due to homogenous preparation of specimen to confirm the initial void ratio since initial void ratio is one of the key aspects in this study.

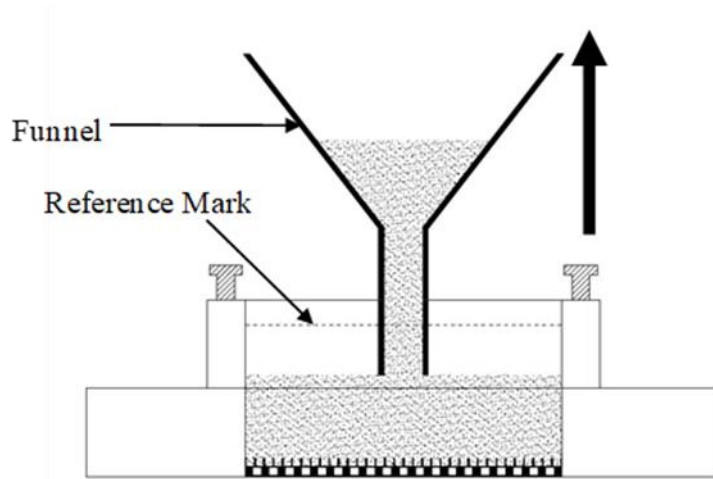


Figure 77: Schematic illustration of DFP technique.

3.7.1.2 Dense Specimens Preparation

Dense specimens are prepared by pouring soil in three successive layers and tamped in a consistent manner until desired relative density is achieved (Figure 78). To achieve the uniform distribution of fine particles in Sand matrix, Sand with fines are poured to a set height limit and tamped accordingly to achieve desired relative density.

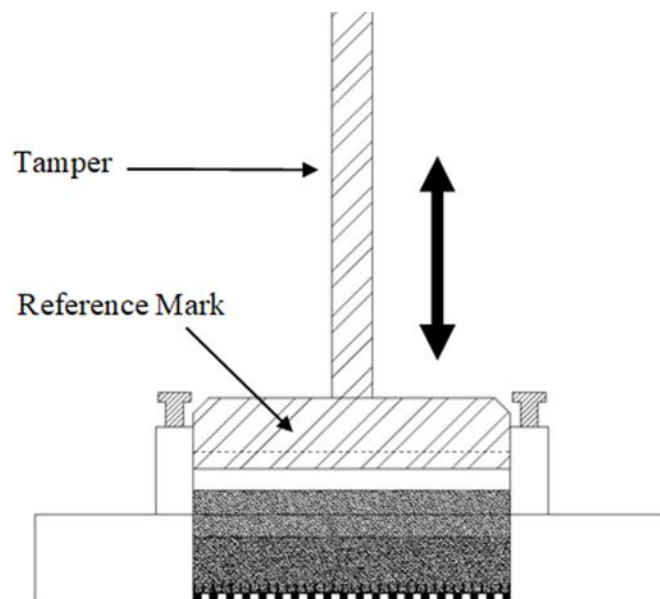


Figure 78: Schematic illustration of dense specimen preparation.

Specimens with fines are prepared by dry weight for example, 10% sand-fine mixture contains 90% sand + 10% fines, 20% sand-fine mixture is composed of 20% fines + 80% sand and 30% fine + 70% sand for 30% sand-fine mixture. the method used for preparation of soil mixes are presented in Figure 79. Soil samples with fines were agitated through mechanical end-over-end mixer at 27 rpm for 10 minutes in 1 litre glass jar to obtain homogenous sand-fines mixtures for relative density test and manually agitated for element tests in small glass cylinders.



Figure 79: Fines inclusion in sand matrix.

3.7.2 Application of the Normal Stress

In all cases, the soil specimens are subjected to three normal stresses 50, 100 and 150 kPa to represent the shallow depths of Silver Beach site. After sample preparation at required relative density, top shearing plate and loading cap are placed with extreme caution to avoid changes in initial conditions. The loading frame is adjusted at top of the loading cap and levelled so that no excess moment is exerted to the specimens. The desired loads are applied incrementally changes in initial conditions of soil specimens

are recorded. The details of changes in relative densities of each soil group is discussed in detail in results and discussion section (Chapter 4).

A point to be noted here, since after TFC, the sand-fine groups is fine-dominated therefore, the test is performed under both dry and saturated states for comparison reasons. The results plotted for base-sand and TFC of all groups are in dry state.

3.7.3 Specimens Shearing Rate

All soil groups are subjected to a constant shearing rate of 1mm/min for dry cases. Several types of soil mixtures such as clayey sands, silty sands, etc. can be tested under dry states specifically if drained behaviour of a particular soil is under consideration (Vallejo & Mawby, 2000; Monkul, 2013). The tests in dry states is evaluated primarily due to variation in degree of saturation of sand specimens with different fines content and especially partial drainage development during shearing process. This partial drainage can be associated with gap between upper and lower boxes which is difficult to adjust especially when fines content increases as fines can escape, causing a shift in shear failure, which is not favourable for cyclic (multi-reversal) direct shear testing.

3.8 Consolidated Drained Cyclic Direct Shear Box Test

In traditional translational direct shear testing, a specimen cannot be subjected to large displacements due to tilting of loading cap which can result in erroneous evaluations such as residual strength parameters. In order to overcome such cases, the split box is reversed to its origin and sheared repeatedly until the residual parameters becomes constant or distinct. The drawback in Cyclic Direct Shear Box Test, after the first cycle (in case of dense specimens) usually a small peak value is observed in second run and if the gaps between split boxes is more than the standardized specifications, the loss in material can also occur. In CD-CDST, only dry soil groups are tested and subjected to a constant displacement rate of 1mm/min in both forward and reverse direction with

no standby time due to absence of pore water pressure. In this dissertation study, the travel limit of shear box is set to 6 mm.

3.9 Consolidated Undrained Triaxial Test

CU-triaxial tests are carried out in a strain-controlled triaxial testing device and ASTM D4767-11 guidelines are followed. The testing strategy in CU-test is similar with CD-DST tests here, Specimens are subjected to confining pressures of 50, 100 and 150 kPa. The test setup is illustrated in Figure 87.

3.9.1 Specimen Preparation

In CU-test, specimen preparation plays a critical aspect and affects the final outcomes of testing's as described in Chapter 2. DFP technique is employed for loose specimens and specimens are directly prepared in split mould (Figure 82-a). Prior preparation of dry specimens, porous discs along with filter papers are first saturated in a distilled water. The saturated porous disc and filter paper are placed on the base of the cell and then rubber membrane is stretched over a split mould. The dry soil is then poured into the mould by employing DFP technique using funnel with additional tube attached at tip (Figure 80-a) and after targeted relative density is achieved, filter paper, porous disc and loading cap were placed on top of the specimen. The specimen's dimensions are prepared at an aspect ratio of 2 :1 (76 mm in height and 38 mm in diameter). After specimen preparation, a vacuum pressure of 20 kPa is applied to the base to support the specimen as shown in Figure 82(c). The vacuum pressure applied to the specimen was monitored through pore-pressure transducer. After specimen preparation is completed the triaxial cell is mounted on the base and cell is filled with de-aired distilled water. Prior to saturation stage, the specimen is subjected to 20 kPa of confining stress and vacuum inlet is closed. At this stage the specimen is held without vacuum pressure. It is necessary to apply the same confining stress as of vacuum

pressure because it nullifies any changes in initial conditions of specimen. The base adapter configuration is illustrated in Figure 81.

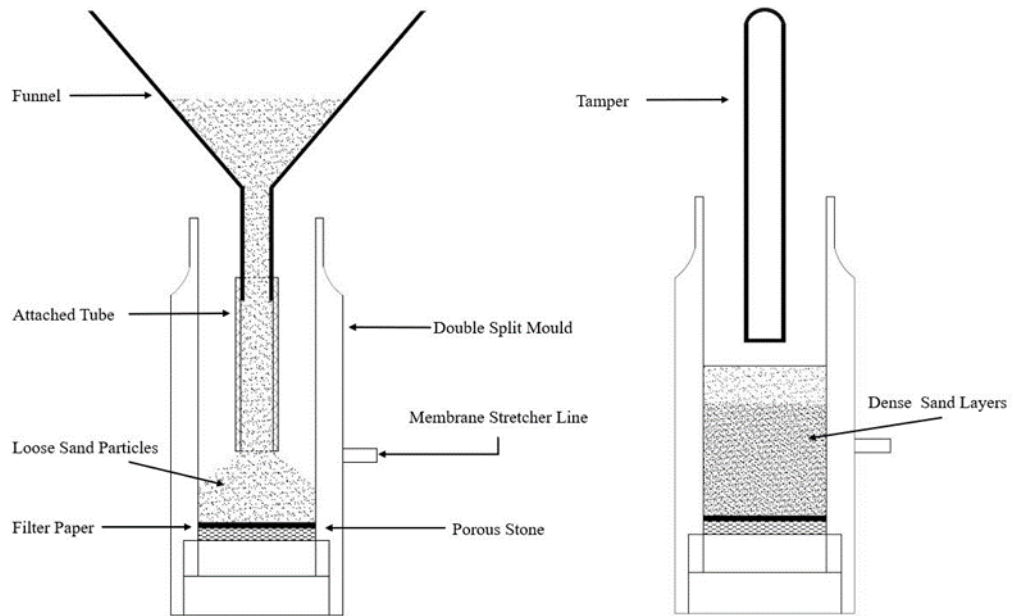


Figure 80: (a) DFP Technique (b) Dense Sample preparations.

3.9.2 Sample Saturation

Specimen is saturated with back pressure application. In order to overcome the negative pressure inside the specimen, de-aired distilled water is percolated from top of the specimen under the action of gravity (Figure 82-d). After pore-water pressure is stabilized, back pressure saturation procedure is initiated. Special care is taken throughout this process regarding the difference between cell pressure and back pressure, which is kept at a maximum 20 kPa to avoid over-consolidation of specimens. The samples are considered saturated when the resulting B-value check is equal to or greater than 0.95.

3.9.3 Sample Consolidation

The specimens are isotropically consolidated after full saturation is ensured. The specimens are subjected to three effective stresses 50, 100 and 150 kPa. The samples are considered consolidated under two conditions such as; no further volume change is observed and zero excess pore water pressure is maintained.

3.9.4 Shearing Rate

Once the consolidation stage is completed, the drainage lines of back pressure unit is closed and the specimens are subjected to relatively slow deformation rate at a strain rate of 0.5 mm/min, slow enough for pore-pressure equalization. Another reason behind slow deformation rate is the increase in volumetric contraction of sand (Lade & Yamamuro ,1997). Post shearing specimen behaviour of loose (Bulged) and dense specimens (Shear Plane) is illustrated in Figure 82(e) and Figure 82(f).

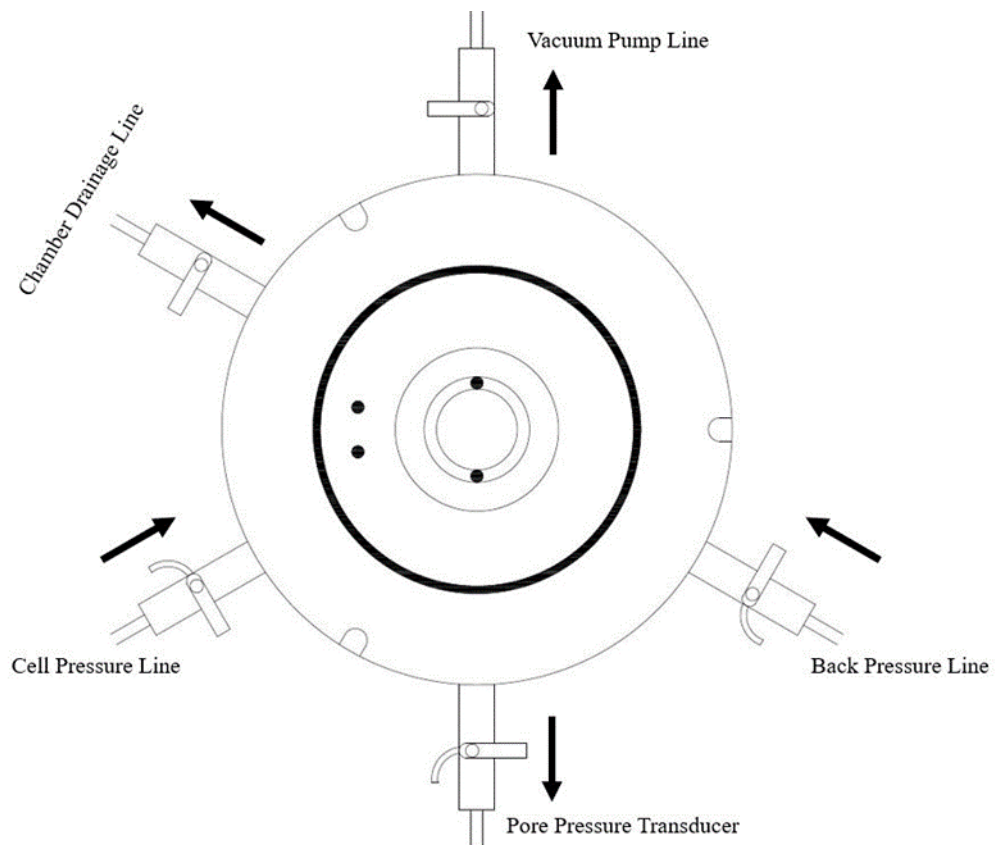


Figure 81: Triaxial base adapter.

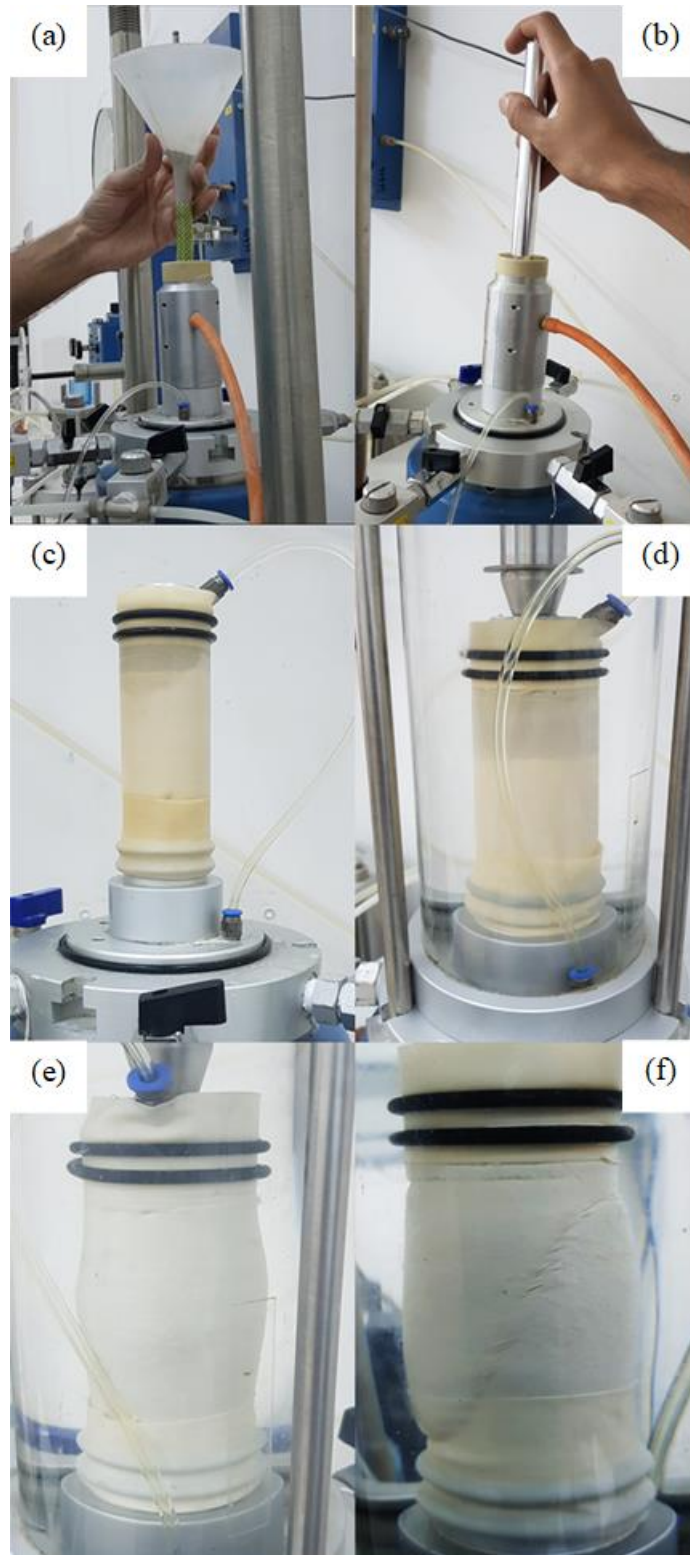


Figure 82: Summarized triaxial testing process.

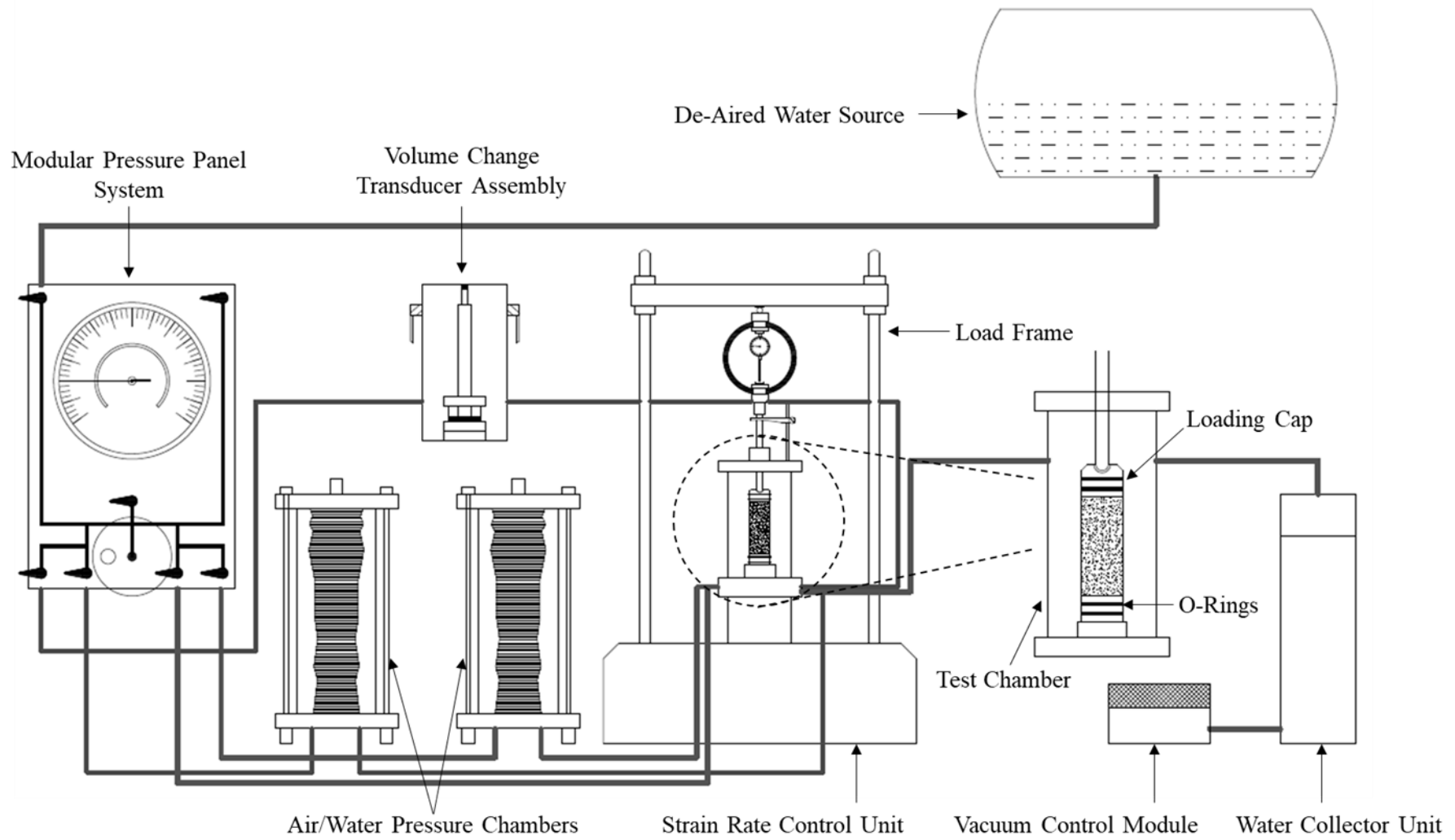


Figure 83: Triaxial testing setup.

Chapter 4

RESULTS AND DISCUSSION

In this chapter discussion of the experimental results and their analysis are presented. The behaviour of sand due to inclusion of fines, seismology of Cyprus and liquefaction prediction models are interpreted in detail. The microstructural behaviour of the test soil groups and impact of this on the shear strength mobilisation are also examined. The primary focus of this chapter study is to provide a detailed liquefaction of the Famagusta beach Sand.

4.1 Behavioural Characteristics of Sand Matrix with Fines

Presence of fines in sand matrix not only affects the soil classification but also alters the shear strength mobilization. The soil fabric is therefore, studied in the evaluation of the mechanisms triggering liquefaction.

4.1.1 Effect of Fines on the Index Properties

Table 8 summarizes the results of index tests. As discussed in Section 3.6, the separated fines are mixed with Sand to form silty or clayey Sand matrix. In Figure 84, the experimental soil groups are classified according to USCS and the proportions of fines in a particular sand-fines mixture is illustrated.

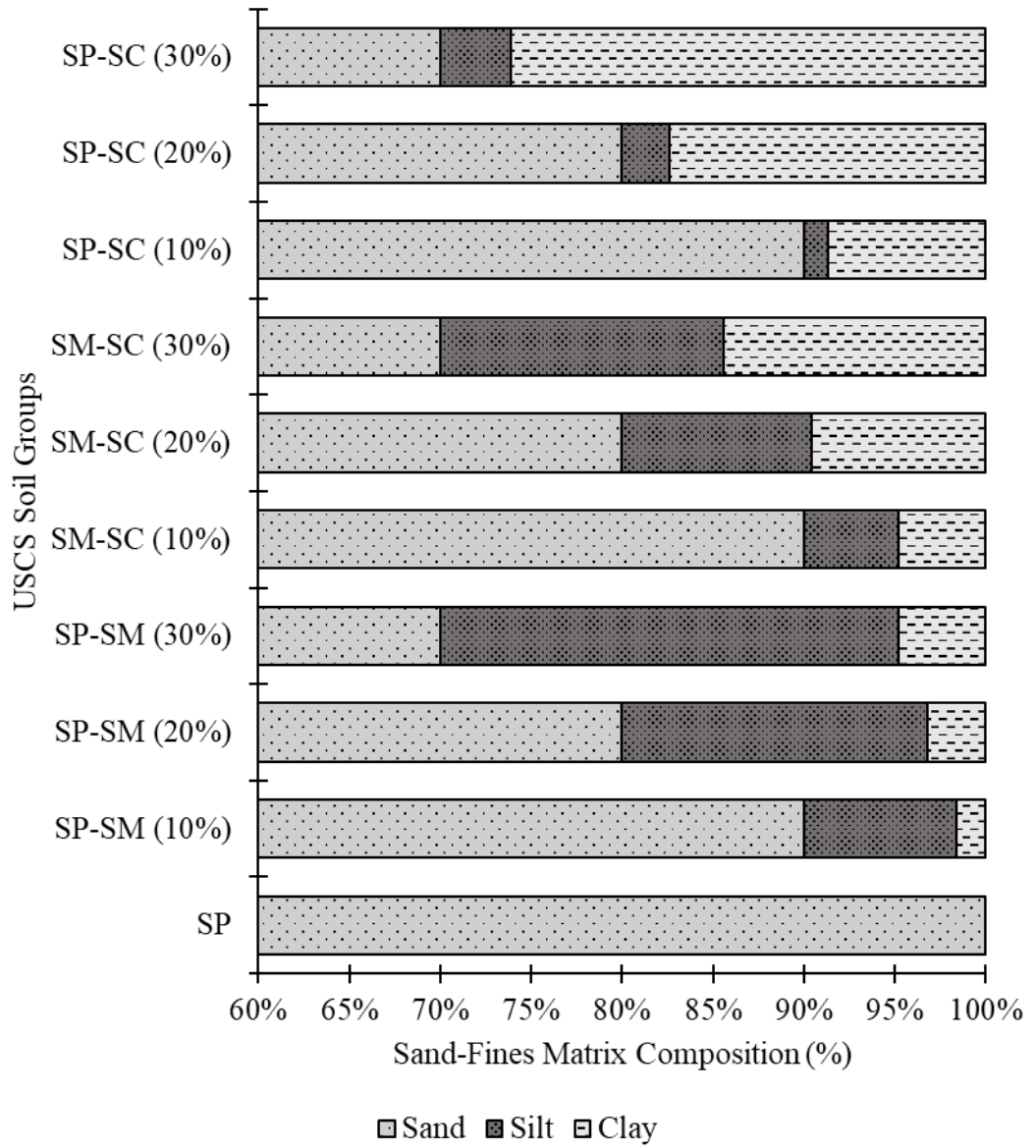


Figure 84: Soil groups USCS particles ranges distribution chart.

Table 8: Index properties of sand-fine mixtures.

Properties	Sand-fines mixture category												
	SP	SP-SM			MH	SM-SC			MH	SP-SC			CH
	0%	10%	20%	30%	100%	10%	20%	30%	100%	10%	20%	30%	100%
G_s	2.712	2.68	2.66	2.65	2.611	2.67	2.65	2.64	2.609	2.65	2.63	2.62	2.598
e_{max}	0.95	0.93	0.95	1.06	1.35	0.93	0.96	1.05	1.32	0.88	0.95	1.04	1.28
e_{min}	0.63	0.62	0.65	0.69	0.75	0.61	0.65	0.68	0.71	0.59	0.64	0.67	0.70
$\rho_{d,min}$ (g/cm ³)	1.39	1.39	1.36	1.29	1.11	1.38	1.35	1.29	1.14	1.41	1.35	1.28	1.14
$\rho_{d,max}$ (g/cm ³)	1.66	1.65	1.61	1.57	1.49	1.66	1.60	1.57	1.54	1.66	1.60	1.56	1.53
LL (%)	-	-	10.4	14.7	52	-	10.4	15.6	52	-	11.2	16.8	56
PL (%)	-	-	6.6	8.9	33	-	6.2	9.5	31	-	5.4	10.2	27
PI (%)	-	-	3.8	5.8	19	-	4.2	6.3	21	-	5.8	8.7	29
LS (%)	-	-	1.0	2.0	15	-	1.0	2.0	15	-	2.0	5.0	12
D ₁₀ (mm)	0.148	0.070	0.0066	0.0043	-	0.060	0.0023	-	-	0.055	-	-	-
D ₃₀ (mm)	0.170	0.165	0.150	0.072	-	0.167	0.151	0.068	-	0.165	0.150	0.075	-
D ₅₀ (mm)	0.197	0.190	0.180	0.168	-	0.192	0.180	0.166	-	0.193	0.180	0.165	-
D ₆₀ (mm)	0.205	0.200	0.195	0.187	-	0.205	0.195	0.183	-	0.205	0.192	0.185	-
C _u	1.35	2.85	29.55	43.50	-	3.42	84.78	-	-	3.73	-	-	-
C _c	0.98	1.94	17.48	6.45	-	2.27	50.83	-	-	3.77	-	-	-
USCS	SP	SP-SM	SP-ML	SP-ML	MH	SM-SC	SP-CL/ML	SP-CL/ML	MH	SP-SC	SP-CL	SP-CL	CH
SSA (m ² /g)	-	-	-	-	19	-	17.2	22	86	-	29.2	48	146

- NA/Not Applicable

In Figure 85, change in specific gravity (G_s) with respect to fines addition to sand is illustrated. As compared to the native Sand, silt, clayey- silty and clay group indicated a drop in G_s values indicating a greater volume occupied by fines as compared to Sand for equal dry mass.

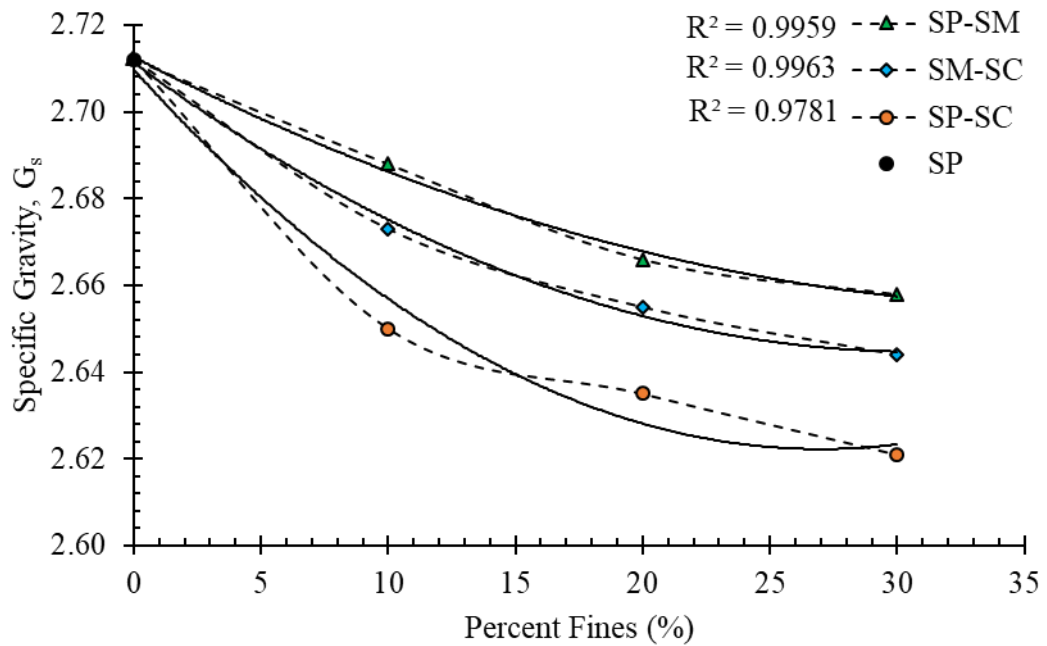


Figure 85: Variation of G_s with addition of fines.

Effect of fines content on index void ratios are presented in Figure 86. The added fines improved the mix by reducing the index limits up to 10%, beyond which fines dominate the density states. At 10% fines addition, the void between Sand grains are entirely filled with fines, hence in terms of soil index states it can be said that the up to 10% fines addition, the soil group is Sand-Dominated and onwards, Fine-Dominated.

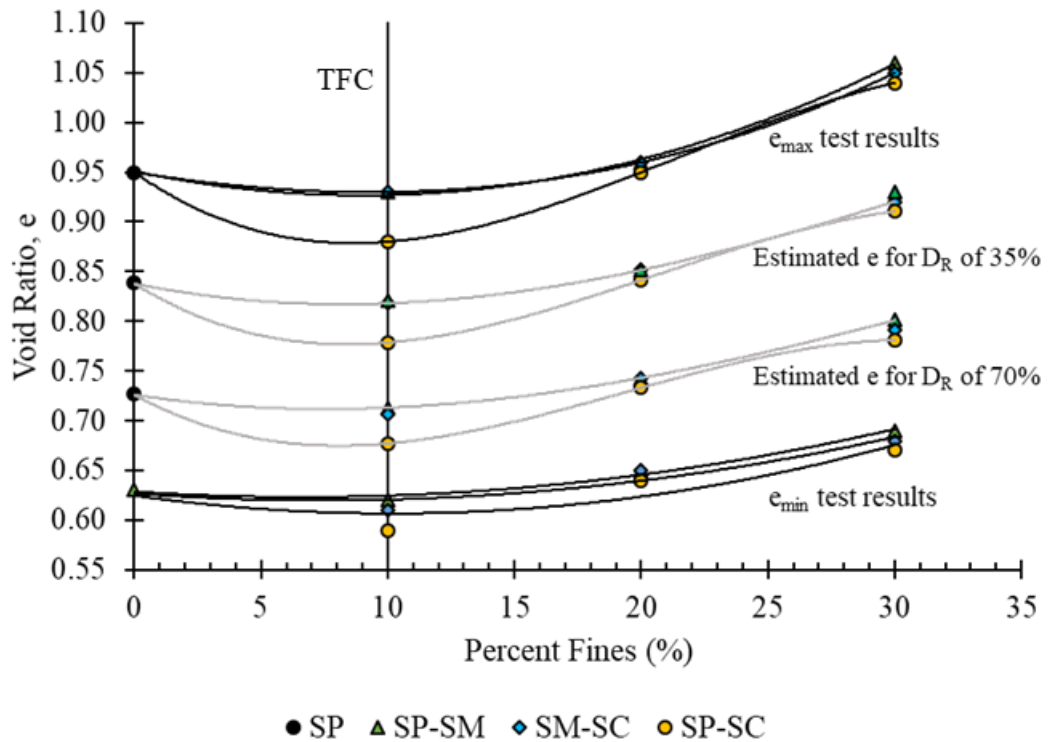


Figure 86: Variation of e_{\max} and e_{\min} corresponding to fines content.

In order to make observations on the soil particles arrangements at macroscale, microscopic analyses are performed which are presented in Figure.

In the interpretation of plasticity test results, the Sand grains are hypothetically assumed as voids between fines particles after threshold fines content (TFC). Hence, fine particles are considered to influence the patterns in soil fabric and contribute to engineering properties. Liquid Limit (LL) and Plasticity Index (PI) test results with respect to fines content are presented in Figure 87.

For Fine-Dominated groups, the intrinsic property, specific surface area (SSA) test results are presented in Figure 88. In Figure 88, silty-clayey SAND and clayey- SAND are only plotted since the application of EGME method on MH group is not applicable due to very low presence of Illite mineral.

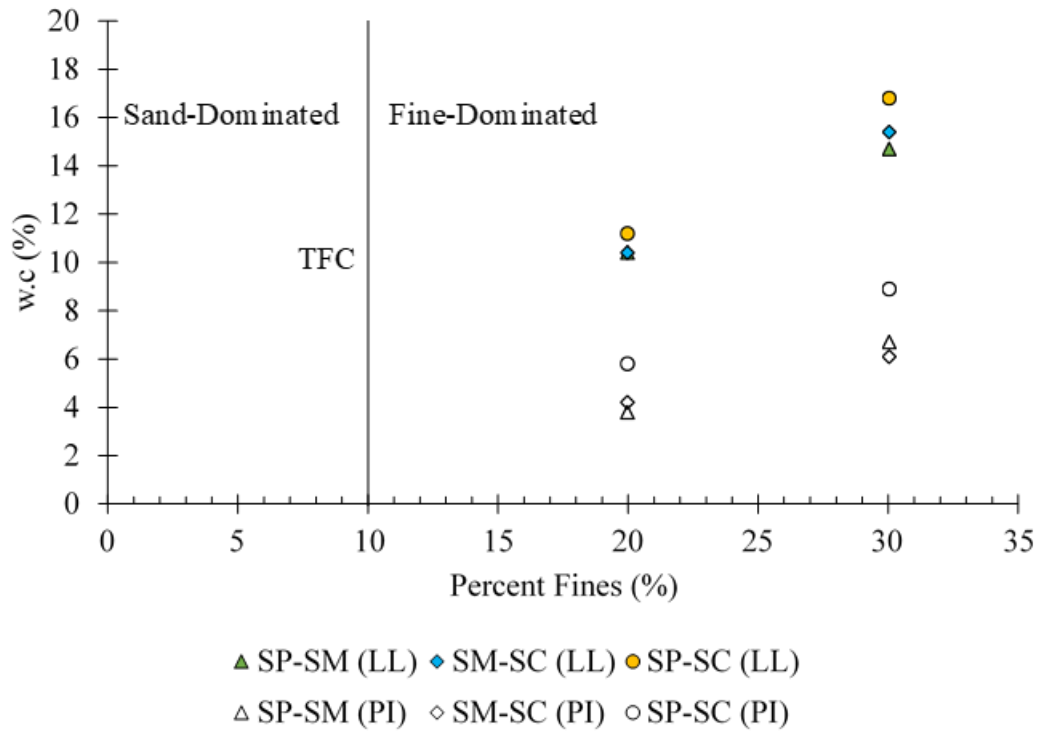


Figure 87: Fine-dominated groups liquid limits.

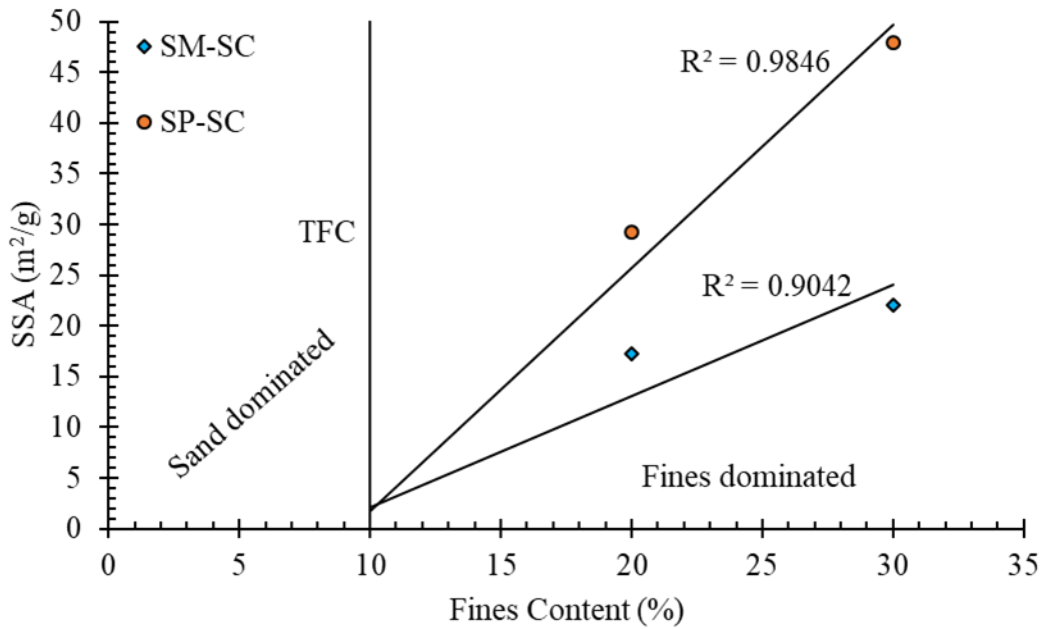


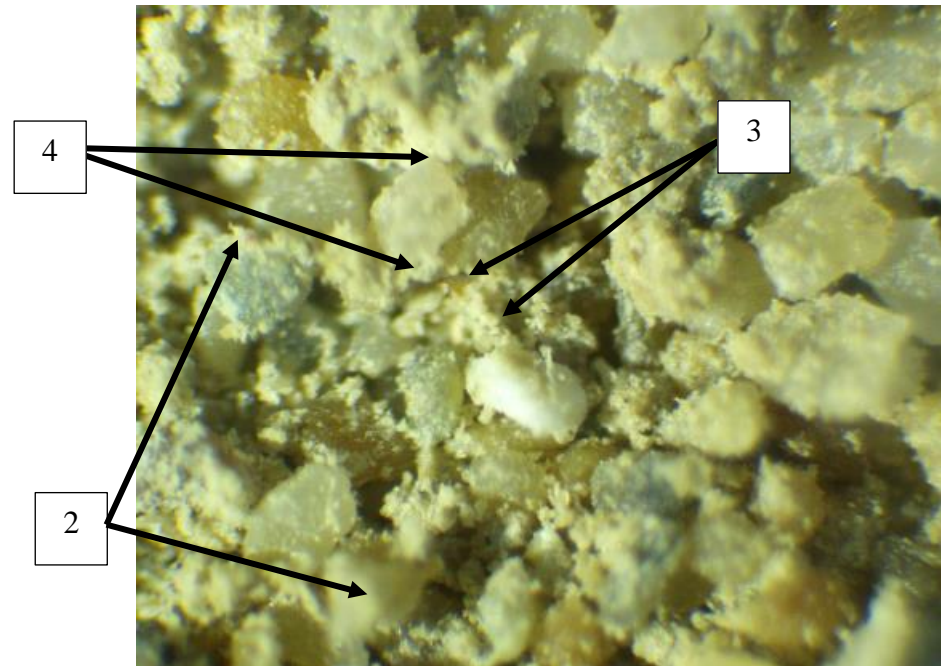
Figure 88: SSA of Illite mineral containing fine-dominated groups.

4.1.2 Sand-Fines Matrix Optical Microscopic Analysis

Alteration of sand matrix due to different fines natures addition is illustrated in Figures 89 – 90. The presented images are analysed at consolidated void ratios under 50 kPa of effective normal stress in direct shear box to understand the sand and fine dominancy criteria.



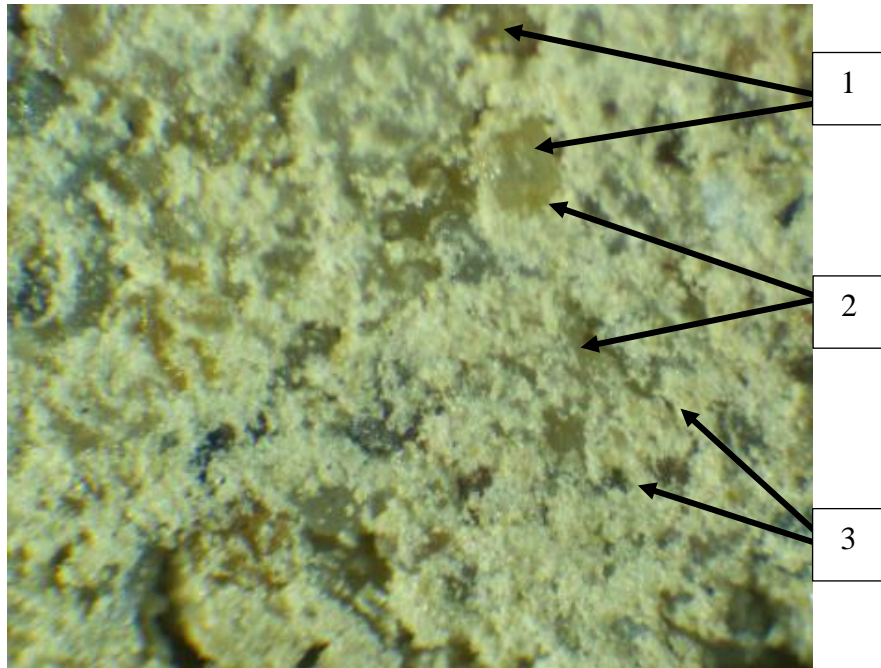
Sand matrix



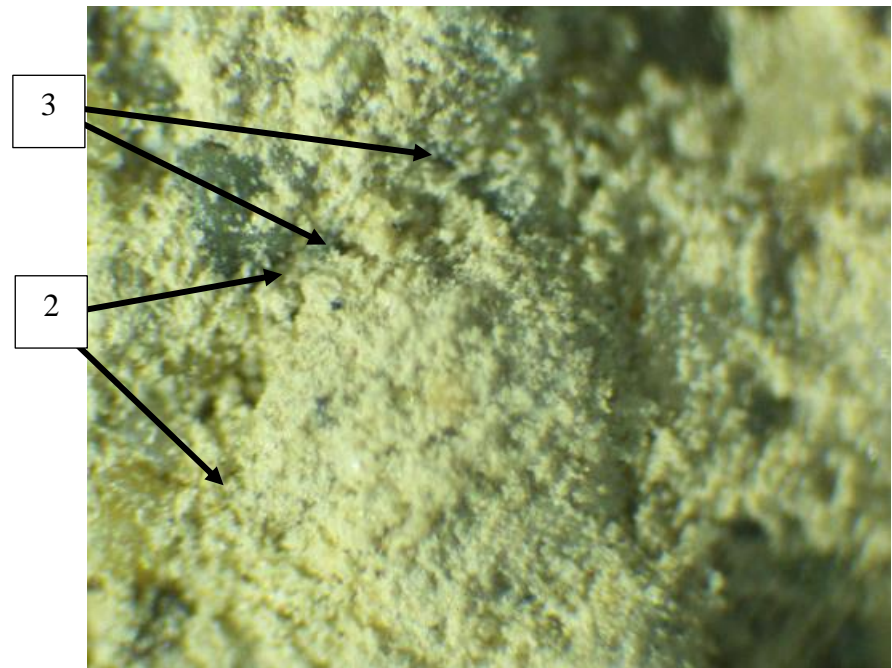
Threshold Fines Content 10% sand-fines matrix

- 1) Point of contact forces.
- 2) Sand-Grains.
- 3) Fines in-between pores.
- 4) Separation between point of contact forces for sand grain.

Figure 89: Sand-fines matrix (0 & 10%).



Fines dominated 20% sand-fines matrix



Fines dominated 30% sand-fines matrix

- 1) Sand Grains.
- 2) Increase in sand grains point of contact distances.
- 3) Micro-pores.

Figure 90: Sand-fines matrix (20 & 30%).

4.2 Compositional Liquefaction Susceptibility Analysis

Figure 91 – 93 relates to liquefaction analysis based on particle-size gradation and in Figures 94 – 95, Chinese criteria is followed to assess liquefaction phenomenon based on liquid limit. The particle size gradation-based analysis of sand indicates the susceptibility of liquefaction on basis of its uniformity. However, soils with wider size gradation curves here also been reported as liquefied in the literature. Therefore, an assessment merely based on uniformity may not be adequate. In addition, Chinese Criteria assessment is performed, results of which are presented in Figure 94.

Since after TFC, the sand-fines matrix is dominated by fine particles which alters the soil matrix behaviour completely, it is necessary to analyse the potential liquefaction susceptibility based on liquid limit and clay fraction presence.

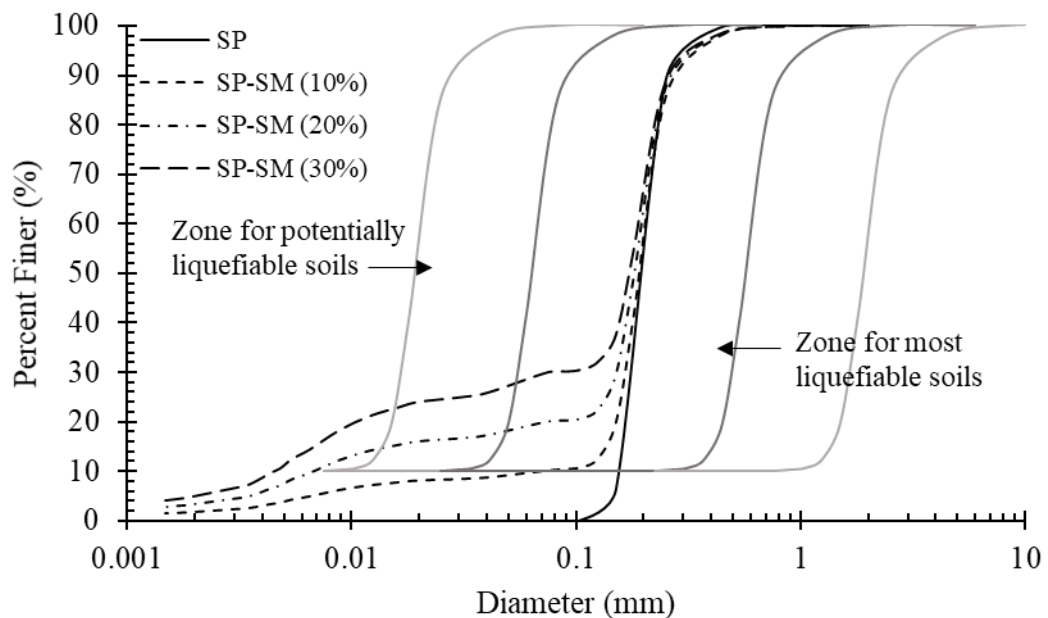


Figure 91: SP-SM group composition liquefaction analysis (Araujo & Ruiz, 2018).

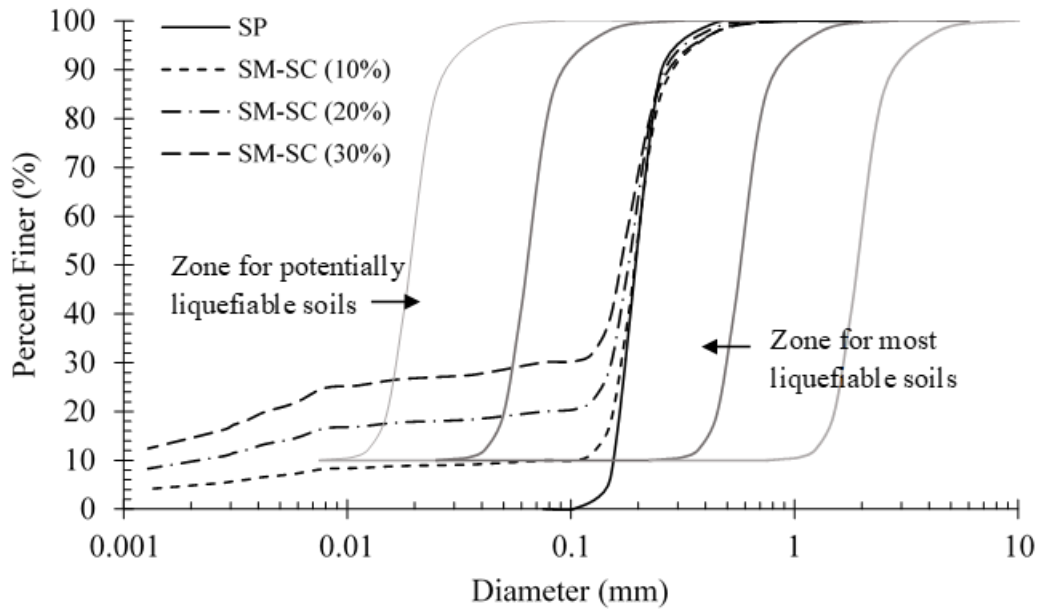


Figure 92: SM-SC group composition liquefaction analysis (Araujo & Ruiz, 2018).

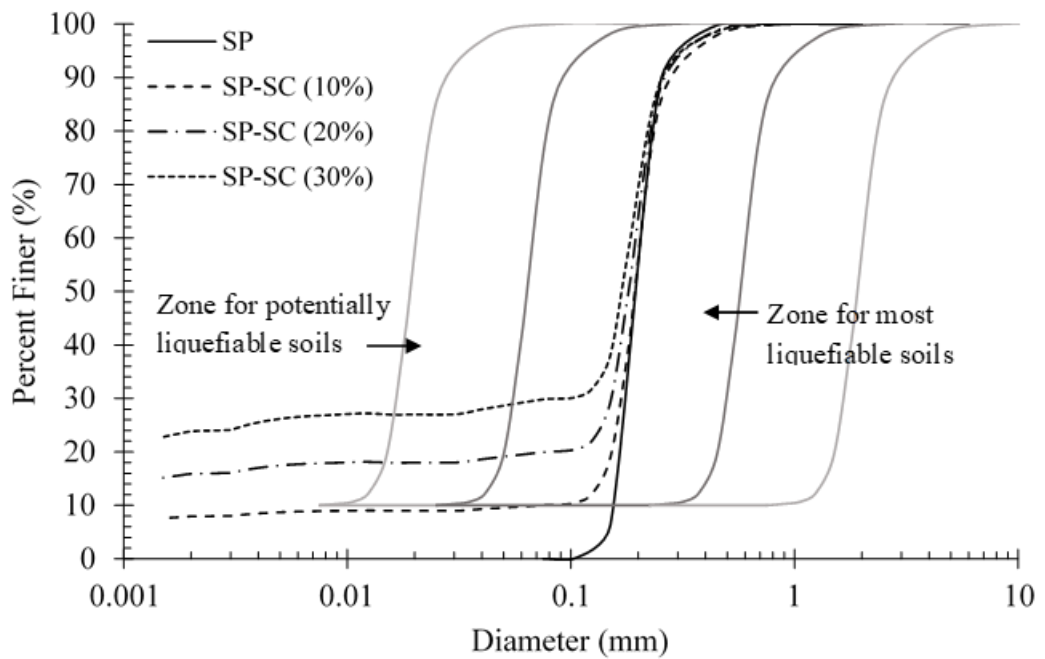


Figure 93: SP-SC groups compositional liquefaction analysis (Araujo & Ruiz, 2018).

Since after TFC, the sand-fines matrix is dominated by fine particles which alters the soil matrix behaviour completely, therefore it is necessary to analyse the potential liquefaction susceptibility based on liquid limit and clay fraction presence.

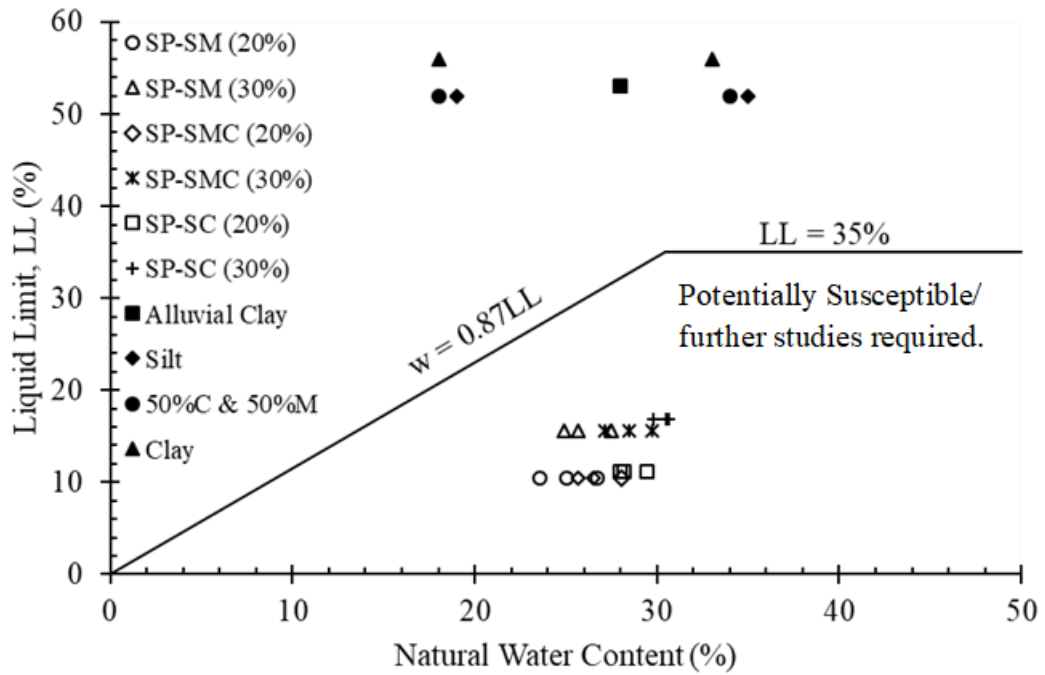


Figure 94: Fines liquefaction susceptibility by Chinese Criteria.

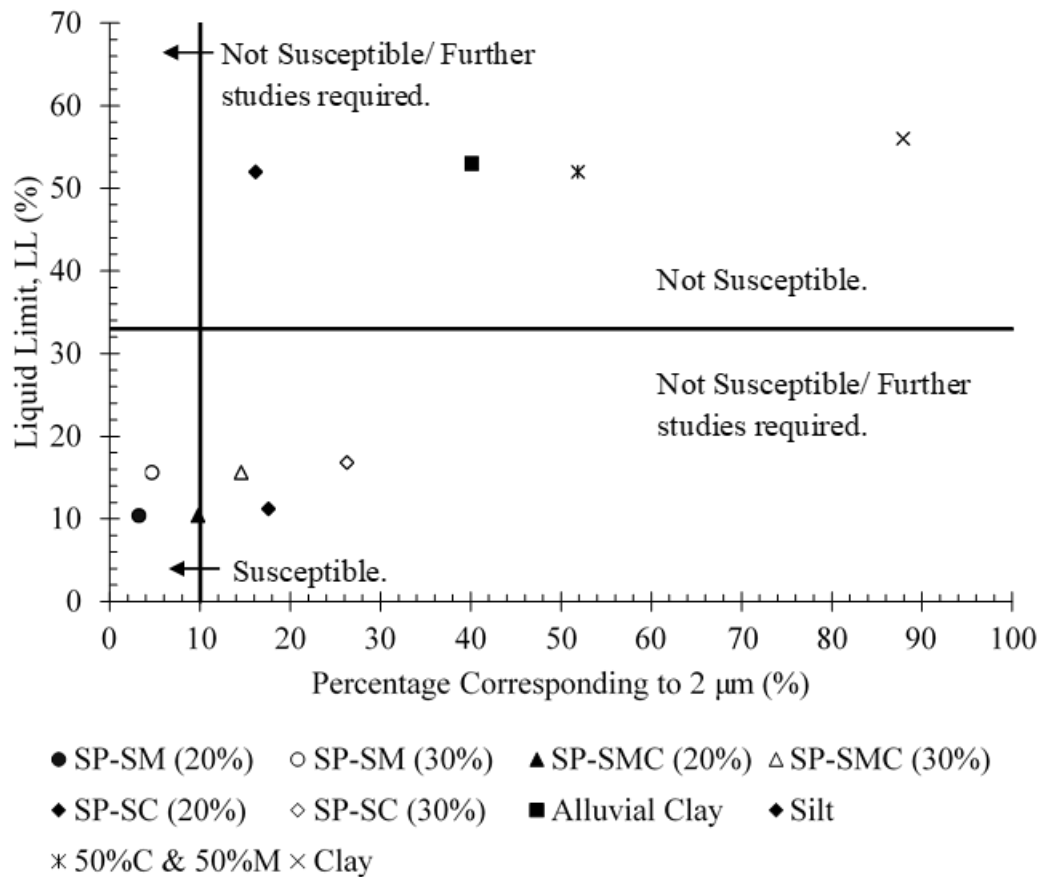


Figure 95: Fines liquefaction susceptibility corresponding to $2\ \mu\text{m}$ presence.

Further to the assessment using Chinese criteria, an assessment based on Clay percentage is also performed based on. This analysis is based on saturated state of soil considering ground water table at ground surface. The results indicated that all soil groups are potentially susceptible for liquefaction (Figure 94). However, as these methods of assessment are originally for fine-grained soils therefore, further testing is required to assess the applicability of such criteria for sand-plastic fines mixtures.

4.3 Drained Behaviour of Sand-Fines at Loose and Dense States

Drained behaviour of sand-fines mixtures is tested in Direct Shear Box Test and the analysis of experimental results are based on critical state soil mechanics in order to depict the contractive and dilative behaviour for assessment of liquefaction susceptibility. Furthermore, the said testing method is conducted to observe the effectiveness of outcomes in order to predict the static liquefaction phenomenon and later validating the data from undrained behaviour.

4.3.1 Effect of Fines on Initial States

As discussed earlier, initial state of the specimen governs the engineering properties of a particular soil based on the applied stress. Although the test specimens are prepared at relative densities of 35% and 70% the normal stress applied at the initial stage significantly increased these relative densities prior to shearing as presented in Table 9.

The increase in the fines fraction resulted to a more compressible behaviour, such that at high percentage of fractions and normal stress, the loose state behaviour is transformed into densest state. Such exhibited behaviour is due to rearrangement of the fabric, thus resulting in complete eradication of voids at loose state. Since the relative densities are transformed greatly, it can be argued that the liquefaction

susceptibility is also reduced. However, the shear mobilisation is very related with the initial condition, hence shear strength is not likely to be affected by this initial compression.

Table 9: Relative densities of sand-fines mixtures after consolidation.

Group	Applied effective normal stress, σ'_n (kPa)					
	Loose			Dense		
	50	100	150	50	100	150
Relative Density, D_R (%)						
SP	54	59	62	84	88	90
SP-SM (10%)	70	81	84	87	89	95
SP-SM (20%)	80	90	94	96	98	101
SP-SM (30%)	89	92	96	95	99	107
SM-SC (10%)	63	70	75	86	92	95
SM-SC (20%)	69	81	89	94	95	102
SM-SC (30%)	71	80	90	93	95	102
SP-SC (10%)	56	59	64	85	93	95
SP-SC (20%)	56	66	68	88	92	96
SP-SC (30%)	64	65	70	87	90	93

4.3.2 Drained Response of Sand-Fines Mixtures

The detailed experimental results for loose and dense specimens are presented in Appendix C and D. Appendix D comprises shear stress versus axial displacement and Appendix C comprises shear strength parameters. A summary of the shear strength parameters for all groups are presented in Table 10.

Table 10: Sand-fines groups shear strength parameters.

Group	$\phi'_{\text{peak/ultimate}}$ (Degrees)	ϕ'_{residual} (Degrees)	$\epsilon_{\text{peak/ultimate}}$ (%)	c' (kPa)	c'_{res} (kPa)
SP-L	32	-	4.90	0.7	-
SP-D	40	36	1.92	1.3	0.4
SP-SM-L (10%)	29	-	7.30	0.5	-
SP-SM-D (10%)	35	28	2.83	3.9	3.3
SP-SM-L (20%)	29	-	8.60	1.0	-
SP-SM-D (20%)	34	27	3.97	4.4	4.4
SP-SM-L (30%)	30	-	9.40	2.3	-
SP-SM-D (30%)	32	29	6.20	6.7	4.7
SM-SC-L (10%)	29	-	5.87	0.6	-
SM-SC-D (10%)	37	30	2.25	3.2	3
SM-SC-L (20%)	32	-	7.16	2.5	-
SM-SC-D (20%)	36	28	3.60	5.9	3.1
SM-SC-L (30%)	32	-	8.50	5.7	-
SM-SC-D (30%)	38	28	5.20	9.7	3.4
SP-SC-L (10%)	29	-	5.10	1.3	-
SP-SC-D (10%)	36	28	2.30	3.0	2.7

Table 10 (cont.): Sand-fines groups shear strength parameters.

Group	$\phi'_{\text{peak/ultimate}}$ (Degrees)	ϕ'_{residual} (Degrees)	$\epsilon_{\text{peak/ultimate}}$ (%)	c' (kPa)	c'_{res} (kPa)
SP-SC-L (20%)	28	-	6.30	3.6	
SP-SC-D (20%)	34	29	2.80	3.4	2.1
SP-SC-L (30%)	30	-	6.40	2.3	-
SP-SC-D (30%)	32	29	3.80	6.7	4.7

Variation of internal frictional angles of all soil groups is presented in Figures 94 - 96. As compared to sand, the mobilised peak shear strength decreases as fines content increases. The reduction in peak shear strength is directly associated with the cohesion factor due to plastic nature of fines.

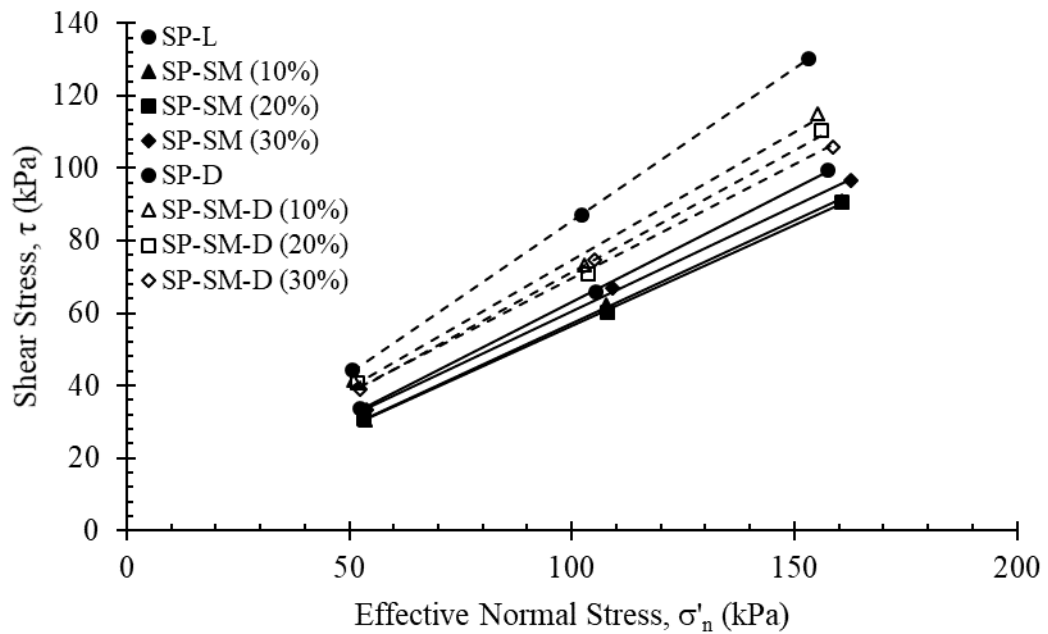


Figure 96: Internal frictional angles of Sand and silty-Sand groups.

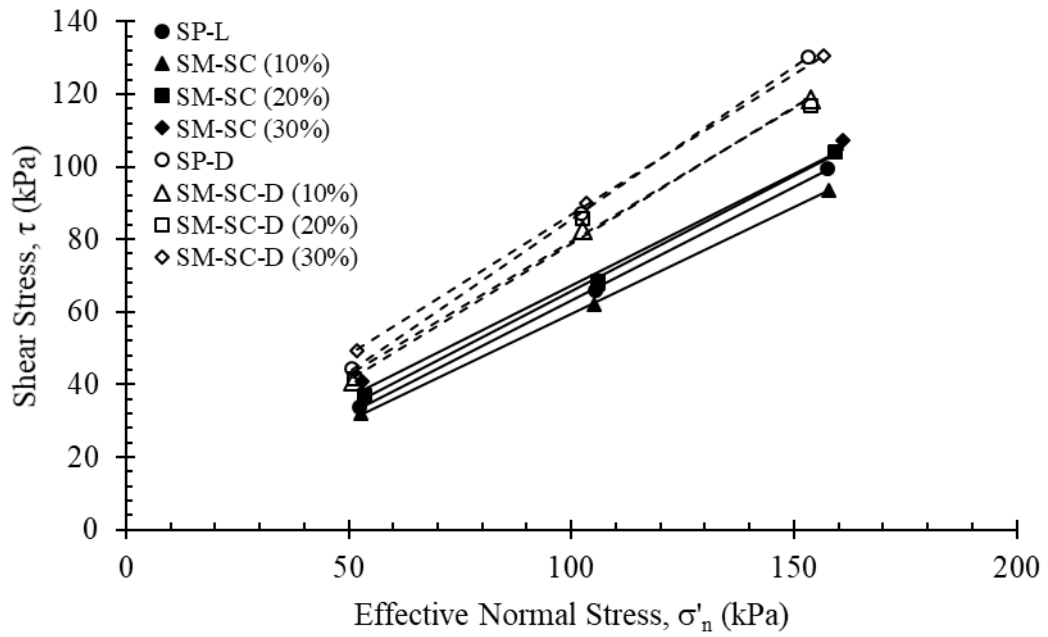


Figure 97: Internal frictional angles of Sand and clayey-silty-Sand groups.

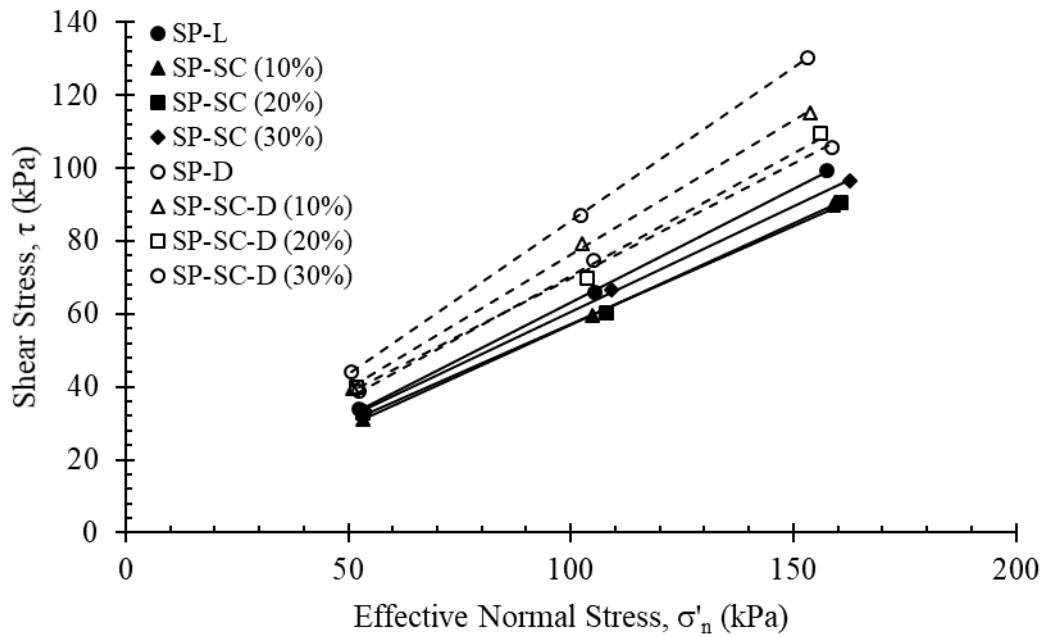


Figure 98: Internal frictional angles of Sand and clayey-Sand groups.

In Figure 100, peak shear strength mobilized reciprocal to axial strain (%) with respect to fines content is illustrated.

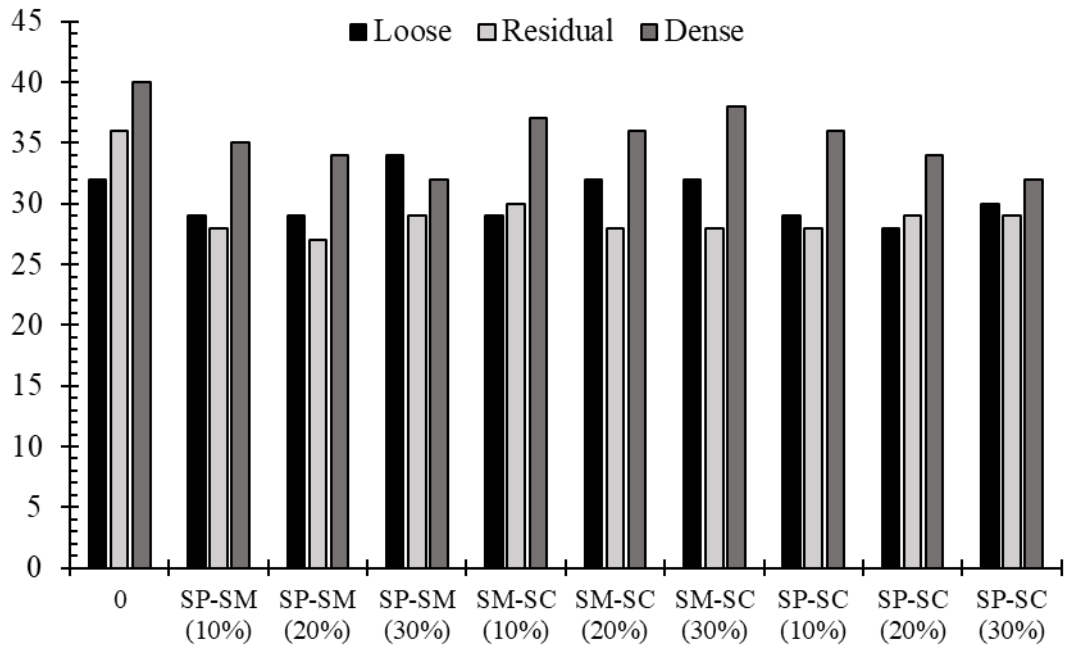


Figure 99: Variation of internal frictional angles of soil groups.

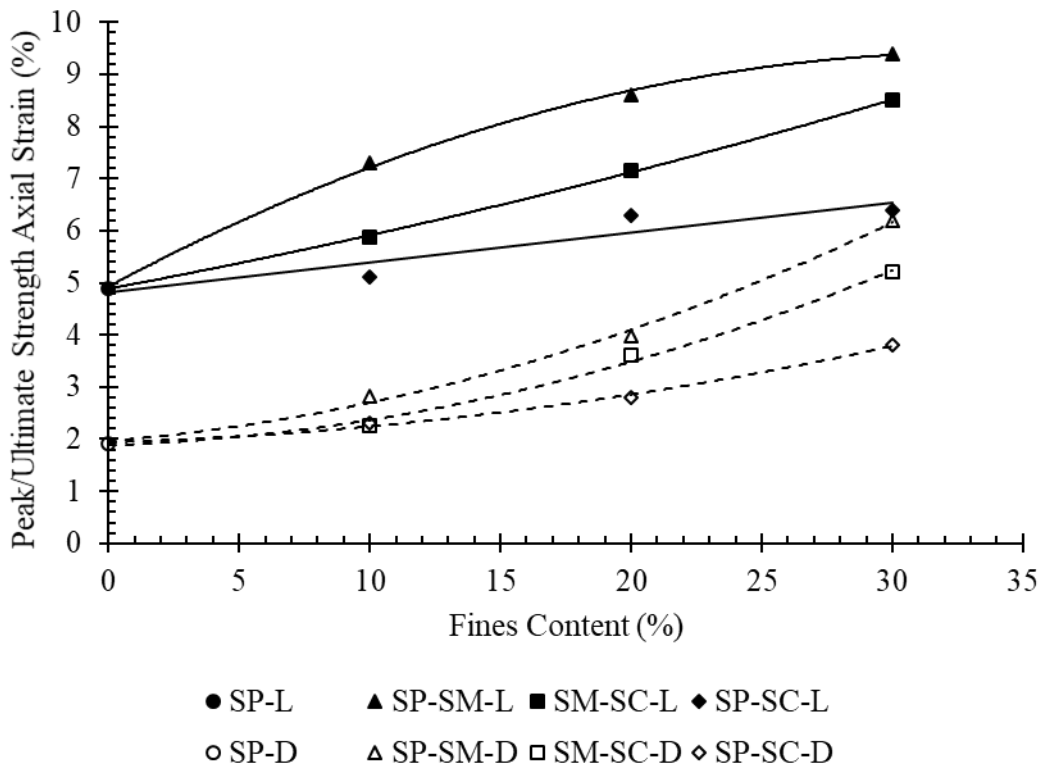


Figure 100: Sand-fines groups peak/ultimate shear strength mobilisation.

4.3.3 Drained Response of Sand

In Figure 101, internal frictional angles for loose, residual and dense Sand are illustrated and Figure 102 presents initial and critical state plots.

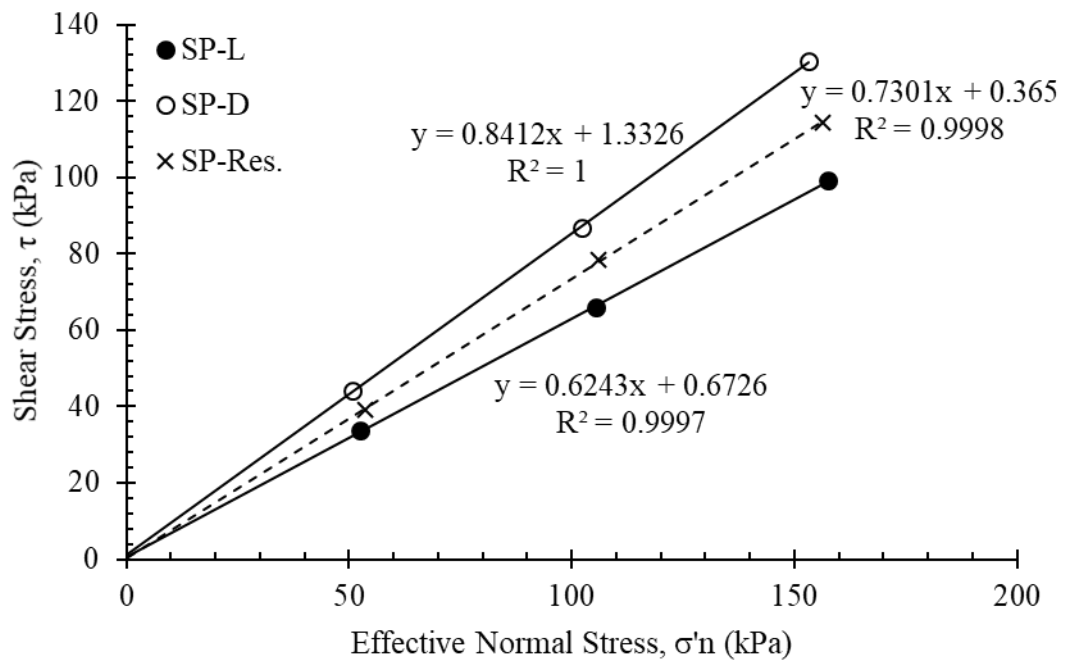


Figure 101: Drained frictional angle of SP-SM for loose, residual and dense.

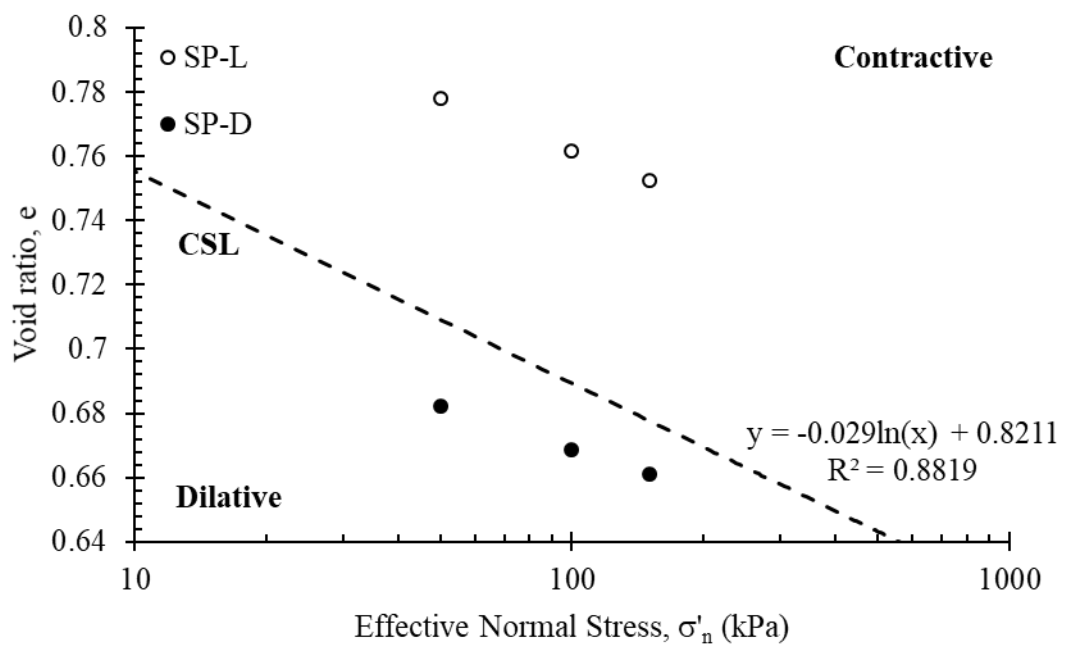


Figure 102: SP consolidated void ratios and CSL plot.

From Figure 102, the CSL plot indicates that the initially loose specimens even after initial compression are exhibiting contractive behaviour. In order to obtain CSL of a particular soil, a homogenous preparation is required to obtain accurate values of final void ratios. By establishing CSL, the void ratios plotting above will exhibit contractive behaviour and the initial states plotting below CSL will exhibit dilation phenomenon. Since initial states of SP-L specimens are exhibiting contractive behaviour, the soil is susceptible to static liquefaction.

4.3.4 Drained Response of Silty Sand Matrix

4.3.4.1 Effect of 10% Silt Fractions in Sand Matrix

In comparison with SP groups, the added silt fractions have led to an increase in compressibility, causing a significant change in the initial state such that even results from loose specimens plotted below critical state line. In Figure 103 and Figure 104, internal frictional angle and critical state plots are presented for silty-Sand (10%).

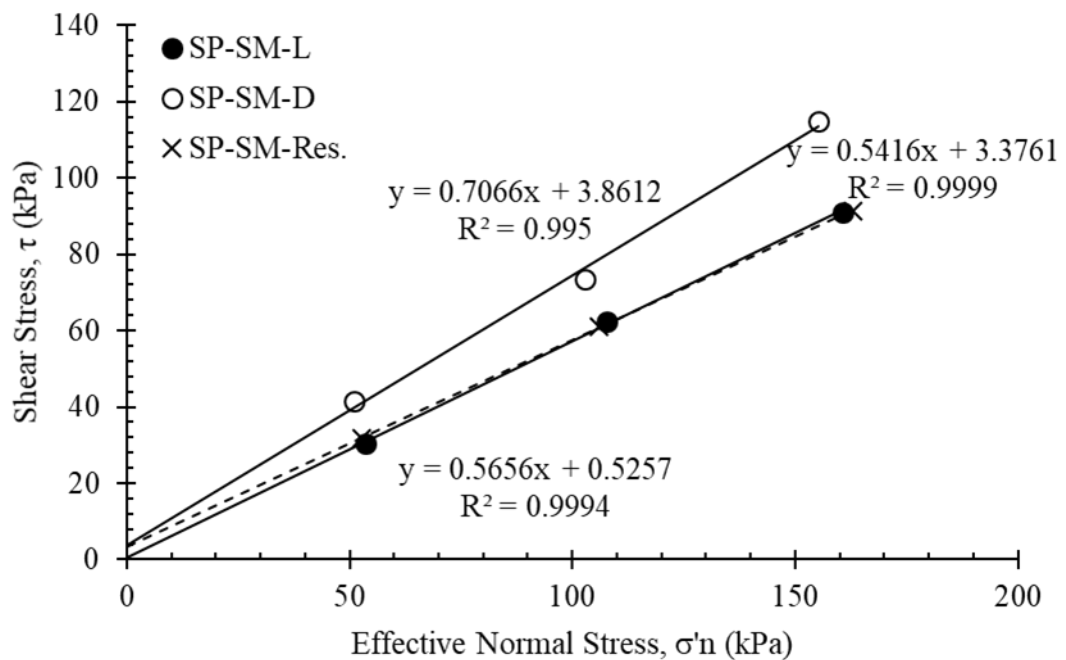


Figure 103: Drained frictional angle of SP-SM (10%) for loose, residual and dense.

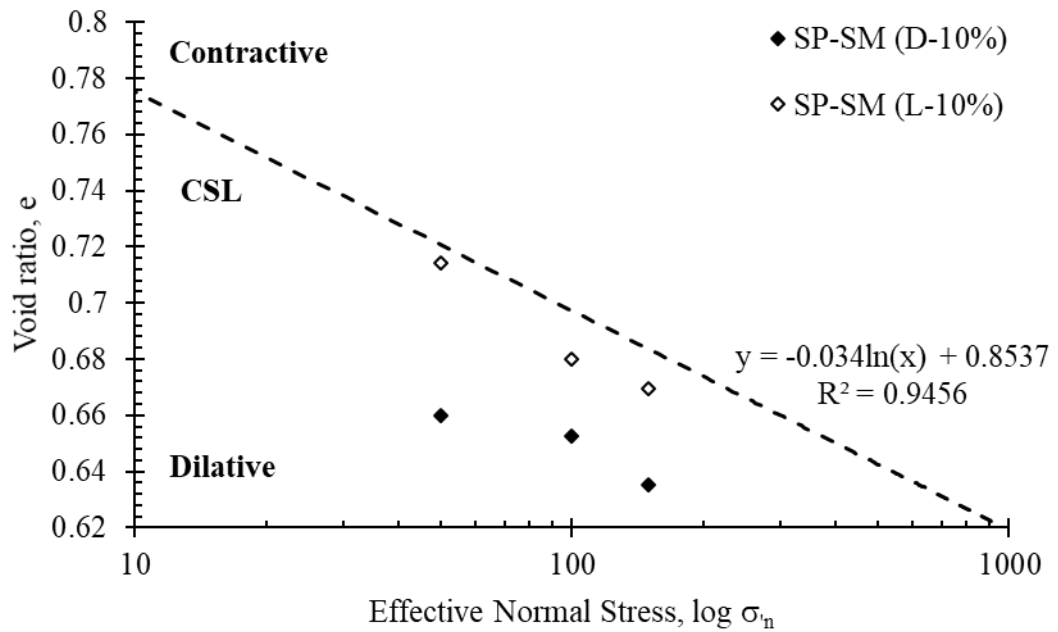


Figure 104: SP-SM (10%) consolidated void ratios and CSL plot.

4.3.4.2 Effect of 20% Silt Fractions in Sand Matrix

Effect of 20% addition of silt fractions into Sand matrix is presented in this section. Silty-sand matrix containing 20% of silt particles entirely alters the behaviour after threshold fines content and in this case, the soil matrix is dominated by fines. Since the sand particles are not actively participating in shear strength of soil, the fines are exhibiting lower shear stress values compared to sand matrix indicating the sliding mechanism of silt particles resulting in reduced friction between surfaces of silts. In Figure 105 and Figure 106, internal frictional angles and critical state plots are illustrated. The initial states of SP-SM (20%) are plotting below CSL line for loose and dense states. The loose specimens exhibiting characteristics similar to 10% silt addition due to compressibility.

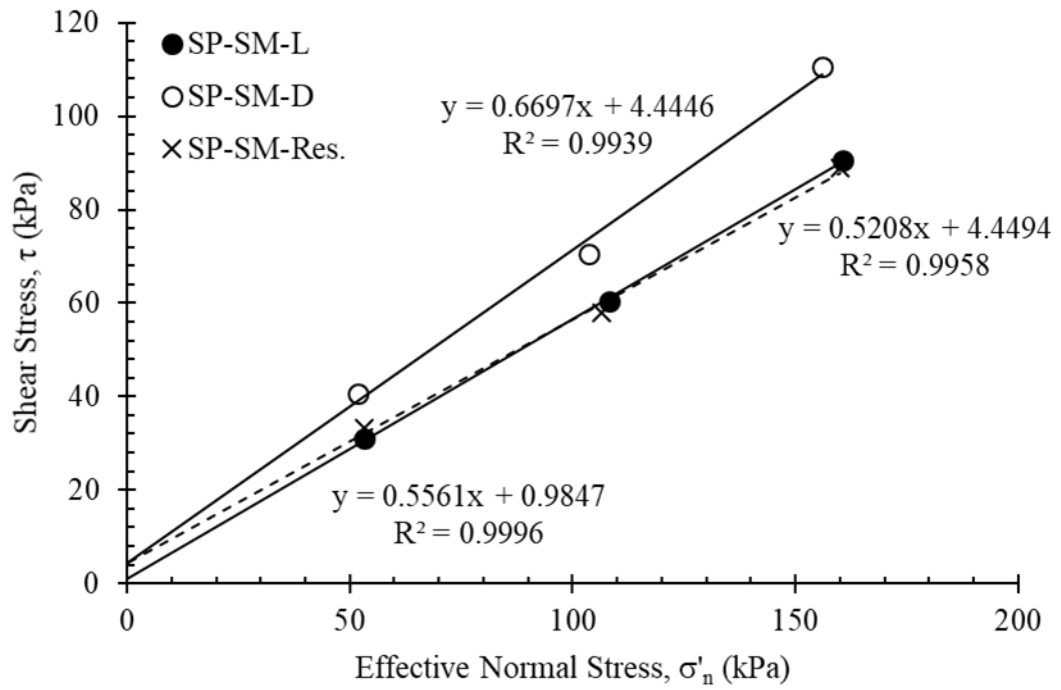


Figure 105: Drained frictional angle of SP-SM (20%) for loose, residual and dense.

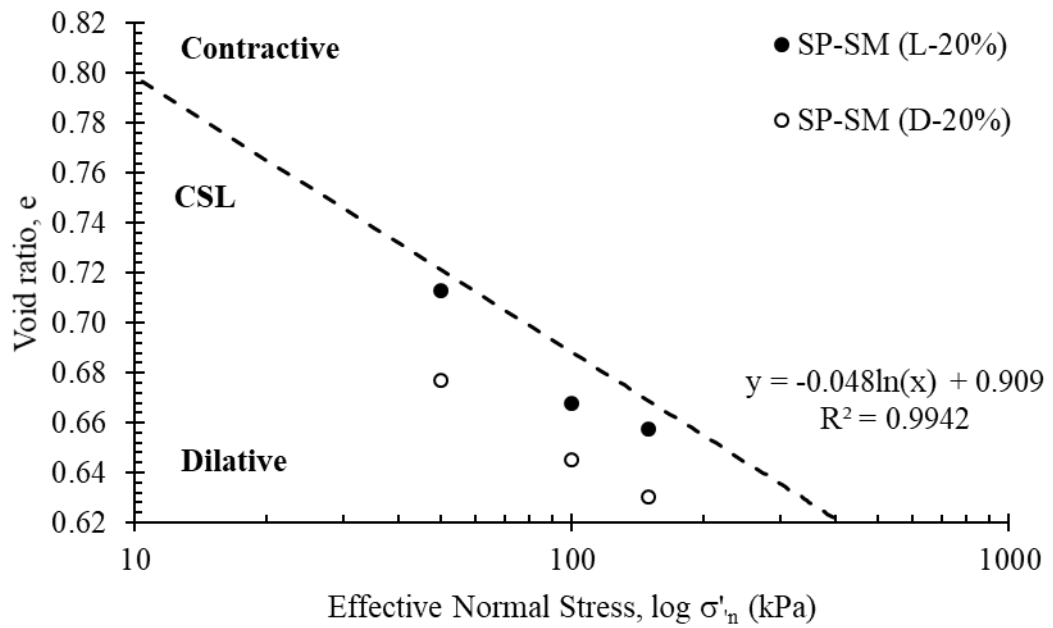


Figure 106: SP-SM (20%) consolidated void ratios and CSL plot.

4.3.4.3 Effect of 30% Silt Fraction in Sand Matrix

Figure 107 illustrates that internal friction angles for loose and dense specimens and CSL plot is presented in Figure 108. As the fines content increased, mobilized shear stress of both loose and dense specimens are approximately exhibiting similar characteristics and resulting in shifting of peak value further indicating the reduction in failure envelope (Appendix D).

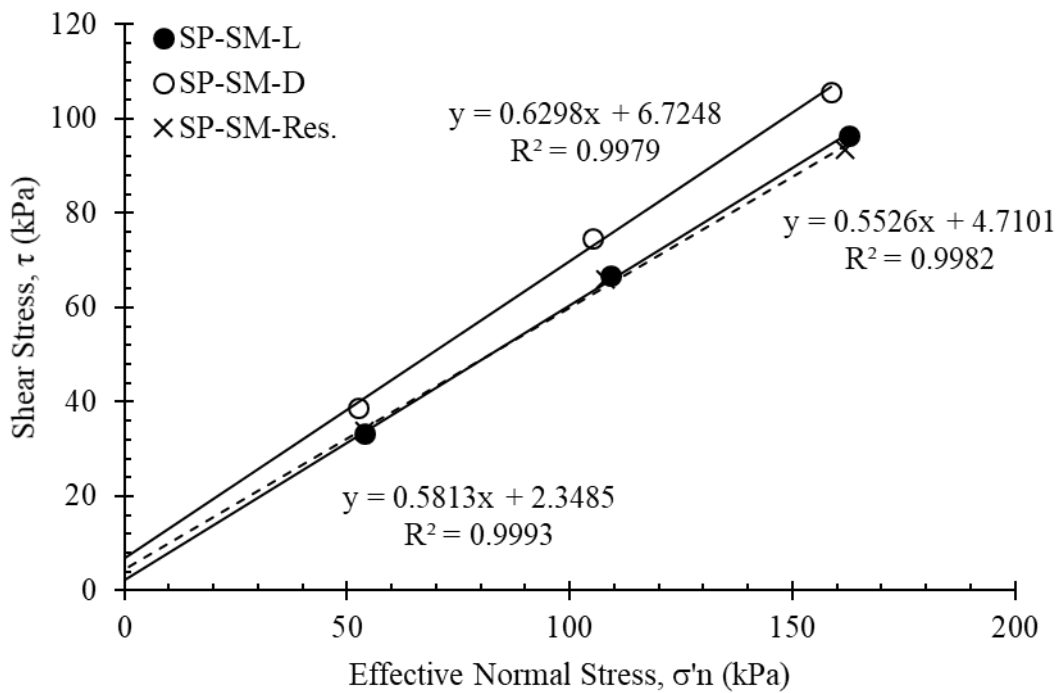


Figure 107: Drained frictional angle of SP-SM (30%) for loose, residual and dense.

From CSL analysis (Figure 108), due to initial compression of loose specimen, initial states are plotting in dilative region. As compared to 10% and 20% dense specimens, the initial states of dense specimens are shifted above plotting close to CSL.

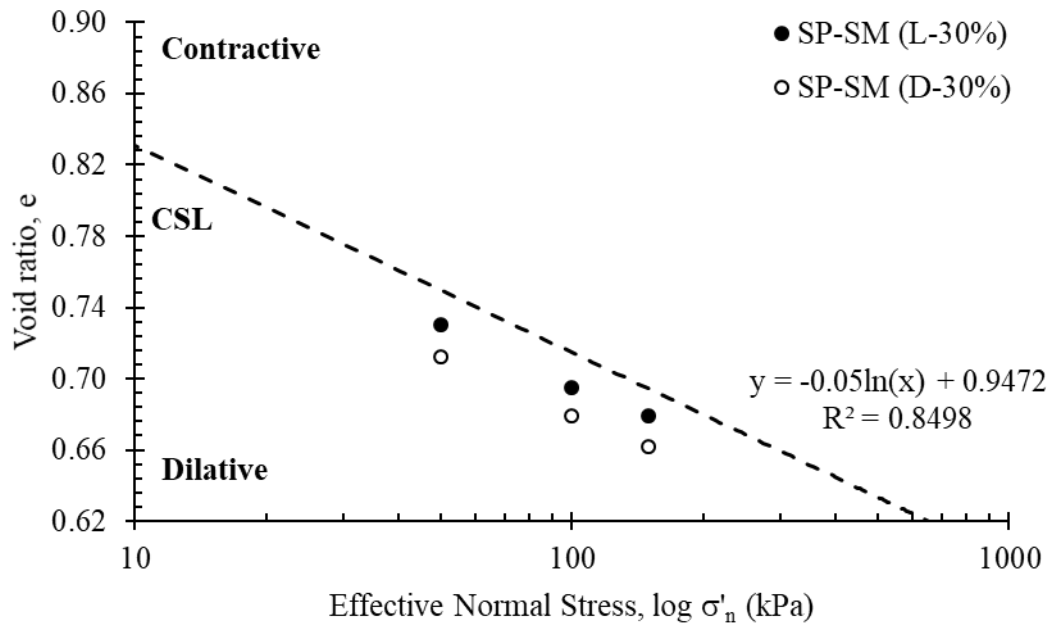


Figure 108: SP-SM (30%) consolidated void ratios and CSL plot.

4.3.4.4 Critical State Analysis of Silty-Sand Matrix

One of key assessment for prediction of liquefaction behaviour performed by using state parameter (Ψ). In Figures 109 and 110, the CSL's and state parameter for all silty sand proportions are illustrated respectively.

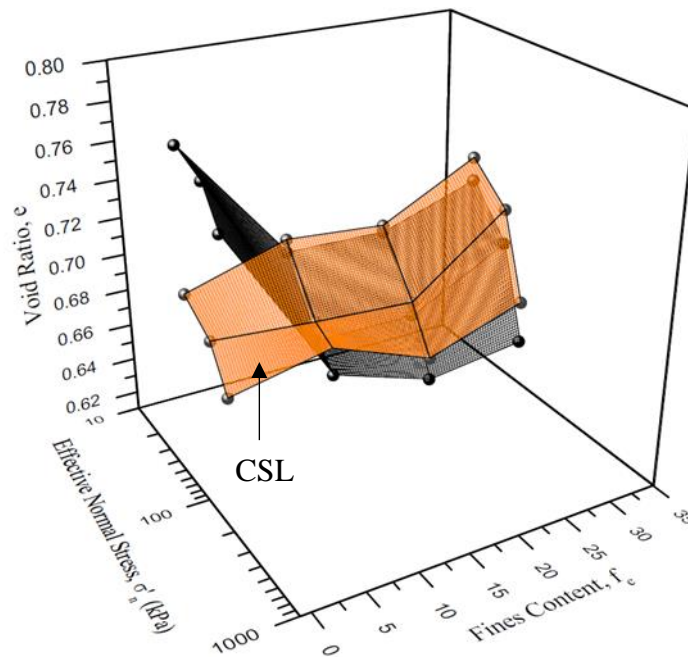


Figure 109: CSL plot of SP-SM-L Matrix with respect to e , σ'_n and f_c .

From CSL analysis of all soil groups containing silt fractions, both loose and dense specimens are plotted below the CSL after TFC content thus, indicating the stability which is reciprocal to dilative behaviour. From such plot, since theoretically the CSL is a unique parameter of soil, prediction of undrained behaviour can also be assessed from such analysis. The prediction analysis is supported in later section after validating the results from CU-Test. From state parameter plots, only loose sandy soil is exhibiting the contractive behaviour while as silt fraction increases the soil is in stable zone.

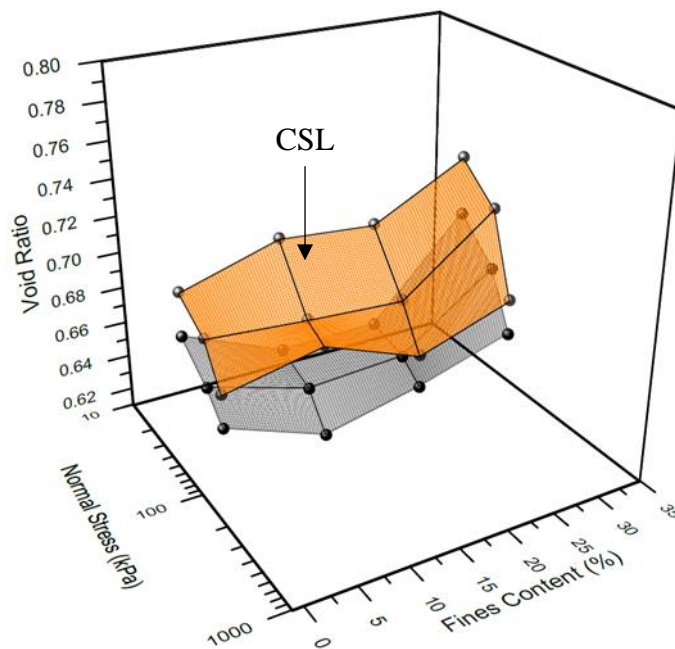


Figure 110: CSL plot of SP-SM-D Matrix with respect to e , σ'_n and f_c .

Based on CSL analysis, state parameters for all silty-Sand groups are established and presented in Figure 111. In state parameter analysis, the positive values indicating the contractive behaviour and vice versa. State parameter analysis is a beneficial indicator for a particular soil to assess the flow liquefaction behaviour. Since in drained testing, contractive and dilative behaviours are obtained whereas, such behaviour for undrained behaviour are termed as flow and non-flow behaviours. By analysing loose

Sand, state parameter is plotting in contractive zone thus, indicating the potential of Sand as liquefiable under restricted drainage conditions. In Table 11, the state parameter of each group is tabulated.

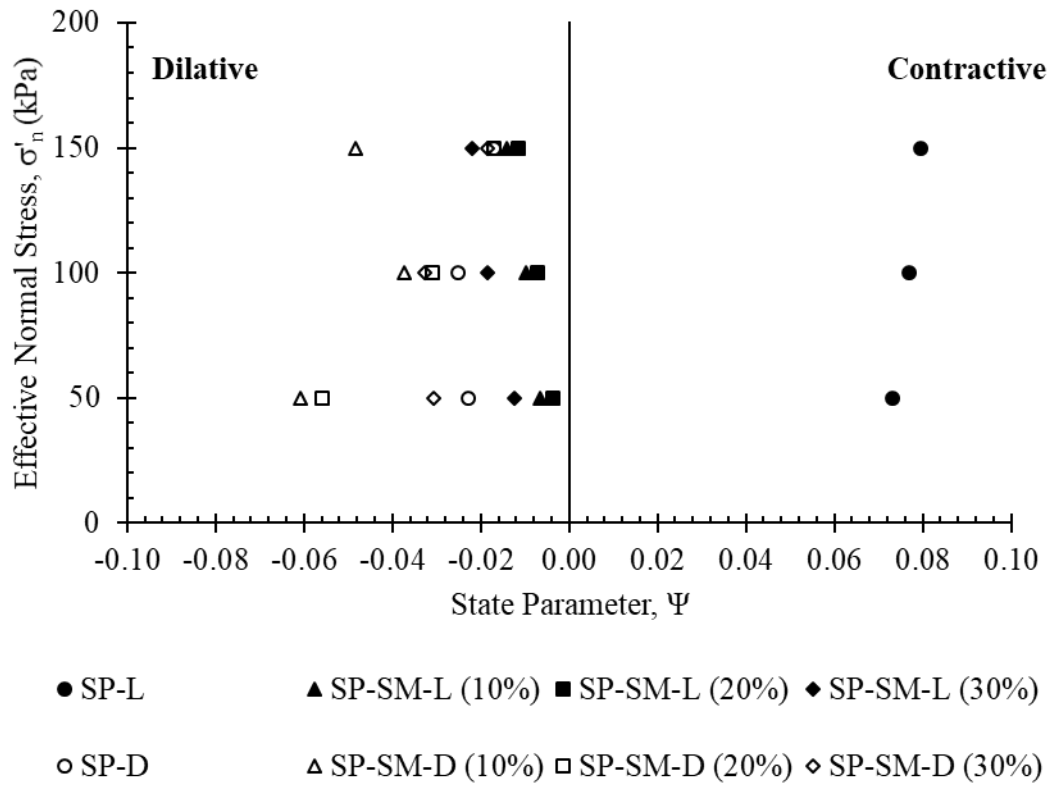


Figure 111: State parameters of SP-SM groups.

Table 11: SP-SM state parameters.

Effective Normal Stress, σ'_n (kPa)								
%	Loose				Dense			
	50	100	150	Remarks	50	100	150	Remarks
10	-0.007	-0.010	-0.014	Dilative	-0.068	-0.037	-0.048	Dilative
20	-0.004	-0.007	-0.012	Dilative	-0.056	-0.031	-0.017	Dilative
30	-0.012	-0.018	-0.022	Dilative	-0.031	-0.033	-0.019	Dilative

4.3.5 Drained Response of Clayey-Silty Sand Matrix

Effect of clays and silt with approximately equal proportions in sand matrix is presented in this section.

4.3.5.1 Effect of 10% Clay and Silt Fractions in Sand Matrix

In Figure 112, the internal frictional angle is plotted for loose and dense clayey-silty Sand group. In Figure 113, initial states of specimens are plotted with respect to CSL.

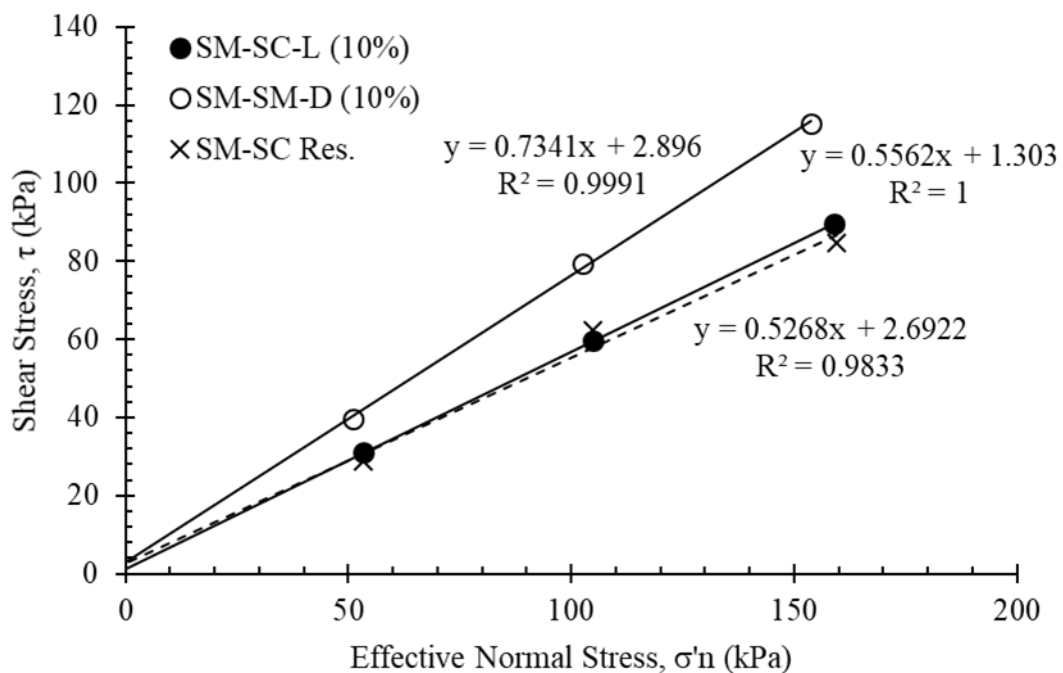


Figure 112: Drained frictional angle of SM-SC (10%) for loose, residual and dense.

From CSL plot observations (Figure 113), loose specimens are illustrating contractive behaviour. One of the primary reasons behind contractive behaviour is may due to complex fabric structure of specimen. Since similar results are obtained from Sand CSL plot, it can be assessed that clay and silt fractions are not contributing to shear strength properties at 10%.

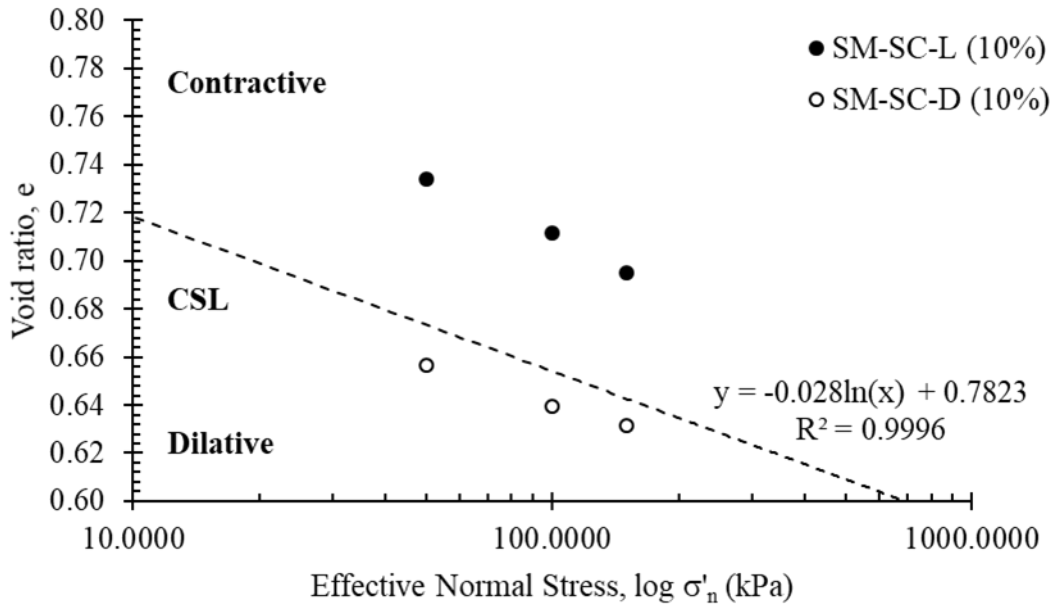


Figure 113: SM-SC (10%) consolidated void ratios and CSL plot.

4.3.5.2 Effect of 20% Clay and Silt Fractions in Sand Matrix

Figure 114 and Figure 115 presents the internal frictional angles and CSL plot for clayey-silty Sand (20%).

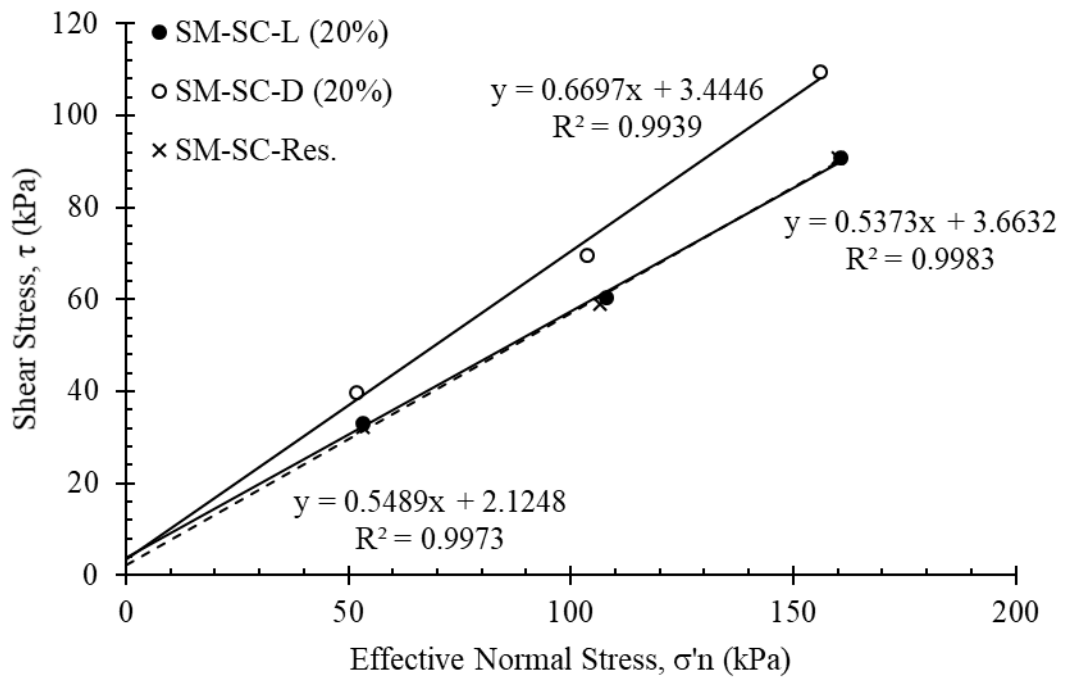


Figure 114: Drained frictional angle of SM-SC (20%) for loose, residual and dense.

From critical state approach, comparing with residual void ratios, approximately all the initial states are plotting below the line indicating the dilative behaviour. Although the initial points of initially loose specimens are plotting close to CSL, therefore the stable state difference is very small. Since the loose specimen are plotting on the CSL line, the soil will not exhibit significant contractive behaviour thus dilation will occur upon further shearing of specimen.

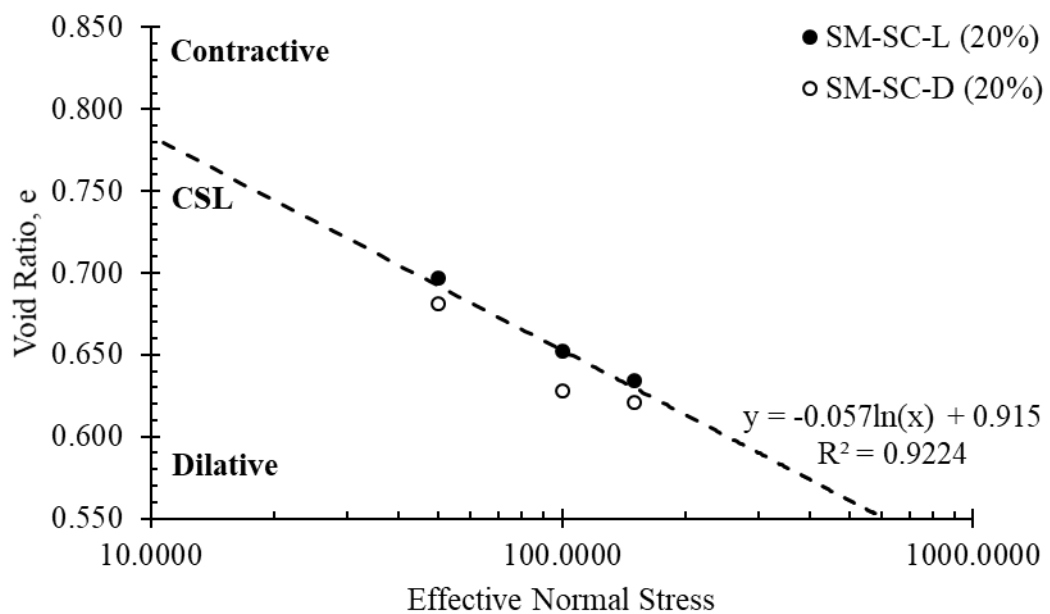


Figure 115: SM-SC (20%) consolidated void ratios and CSL plot.

4.3.5.3 Effect of 30% Clay and Silt Fraction in Sand Matrix

Effect of 30% inclusion of clay and silt fraction in Sand on internal frictional angles is presented in Figure 116. Among all soil groups, a unique behaviour is observed in CSL plot (Figure 117) where both loose and dense specimens are exhibiting similar characteristics. This behaviour is directly associated with fabric arrangement of both clays and silts. Since the specific surface is increased due to Illite mineral presence,

the friction between particles is further reduced due to increment in contact forces points between the individual particles thus, sliding of particles increased.

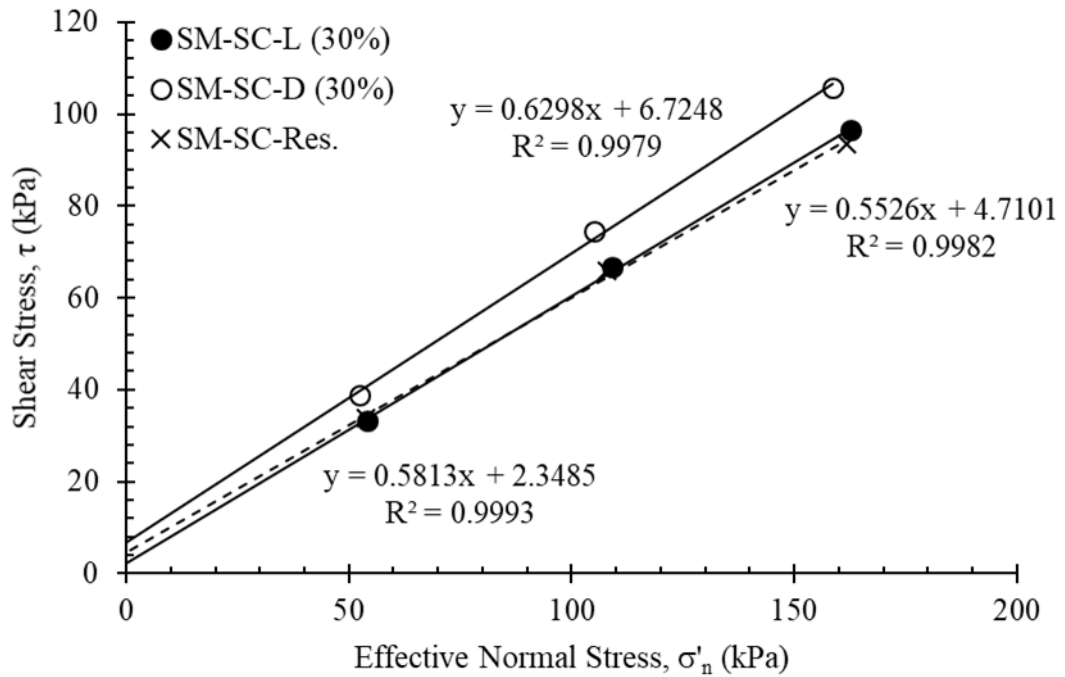


Figure 116: Drained frictional angle of SM-SC (30%) for loose, residual and dense.

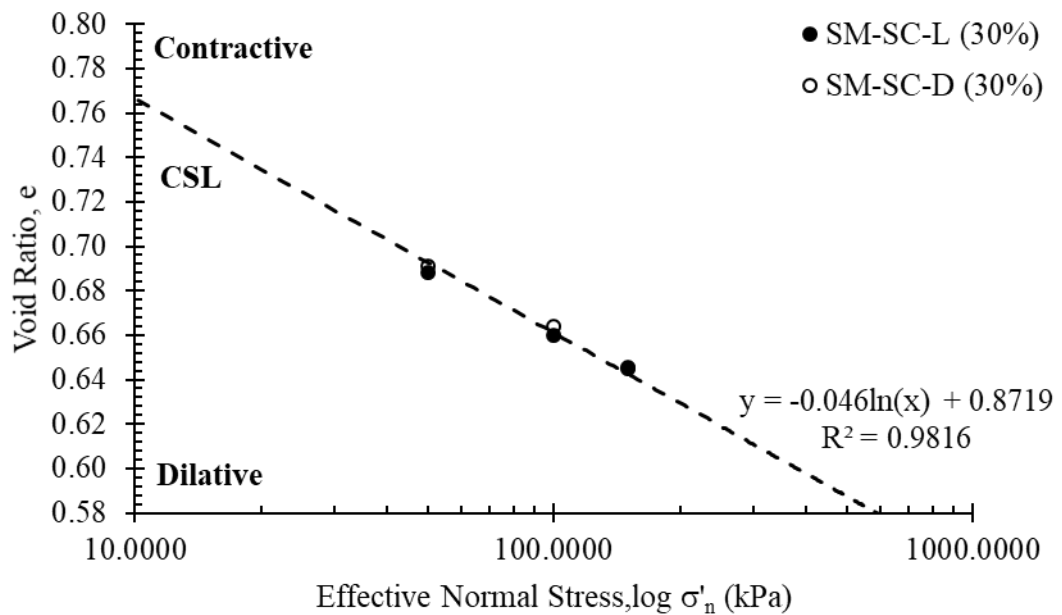


Figure 117: SM-SC (30%) consolidated void ratios and CSL plot.

4.3.5.4 Critical State Analysis of Clayey-Silty Sand Matrix

In Figures 118, 119 and 120, the CSL's and state parameter for all silty sand proportions are illustrated respectively. From CSL plot, it is observed that after TFC (10%), the soil groups are exhibiting stable behaviour where the initial state parameters are plotting either below or close to CSL line.

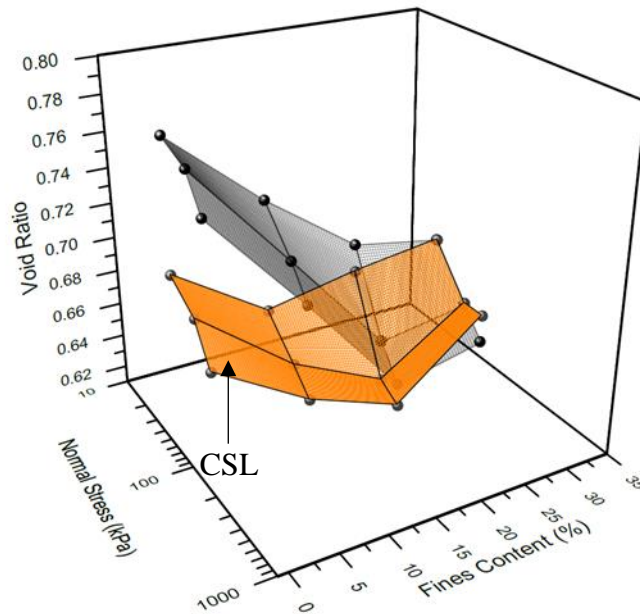


Figure 118: CSL plot of SP-SM-L Matrix with respect to e , σ'_n and f_c .

Despite from Figure 113, Figure 115 and Figure 117, in some cases for 20% and 30% of loose specimens are plotting in near proximity of CSL where identification of contractive and dilative behaviour with respect to normal stress applied is difficult to assess. Therefore, state parameter is an effective parameter to predict the overall behaviour of soil-fines pattern. In Figure 120 and Table 12, state parameters for all clayey-silty Sand groups are illustrated.

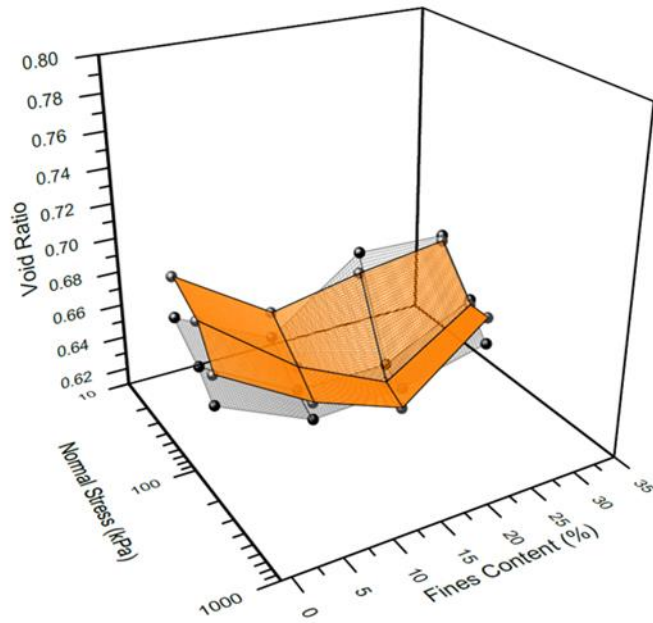


Figure 119: CSL plot of SP-SM-L Matrix with respect to e , σ'_n and f_c .

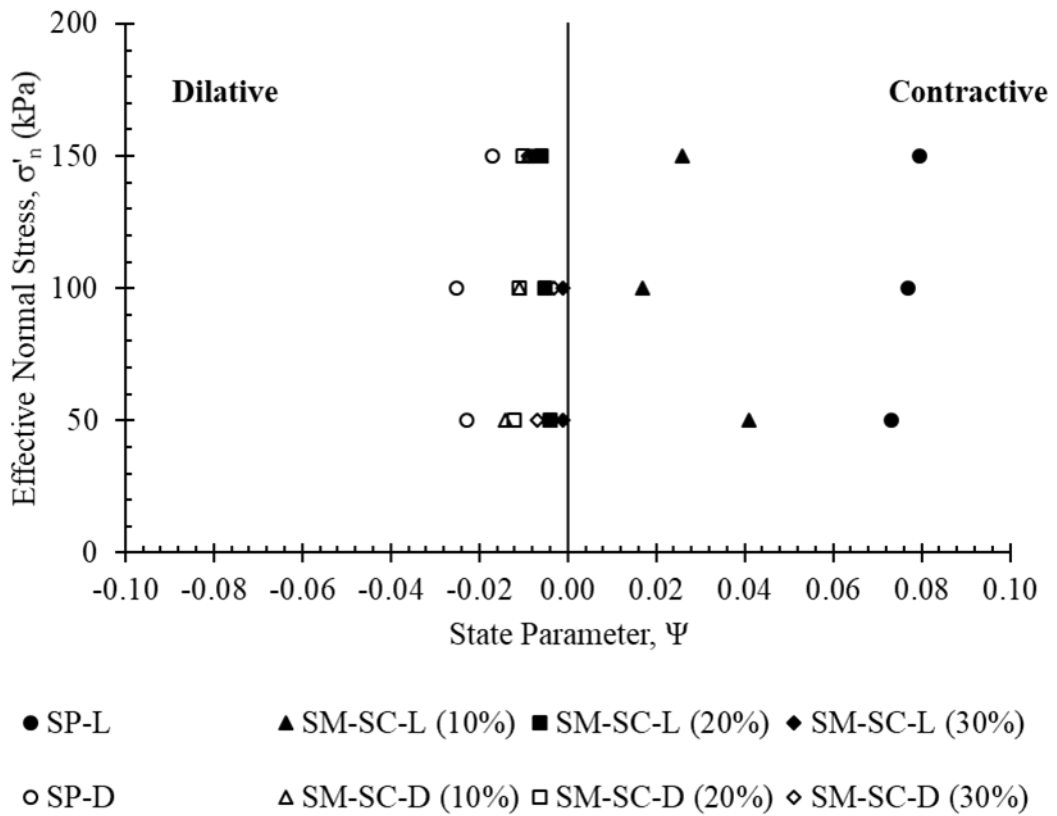


Figure 120: State parameters of SM-SC groups.

Table 12: SM-SC State parameters.

Effective Normal Stress, σ'_n (kPa)								
%	Loose				Dense			
	Fines	50	100	150	Remarks	50	100	150
10	+0.041	+0.017	+0.026	Contractive	-0.014	-0.011	-0.009	Dilative
20	-0.004	-0.005	-0.006	Dilative	-0.012	-0.011	-0.010	Dilative
30	-0.001	-0.001	-0.008	Dilative	-0.007	-0.003	-0.009	Dilative

From state parameter plot (Figure 120), since the boundary conditions are well defined between contractive and non-contractive zones, the clear perception is obtained for 20% and 30% SM-SC groups as both groups (initially loose states) are exhibiting non-contractive behaviour based on state parameter theory.

4.3.6 Drained Response of Clayey Sand Matrix

Effect of clays particles specifically Illite mineral in sand matrix is presented in this section.

4.3.6.1 Effect of 10% Clay Fractions in Sand Matrix

Internal frictional angles and critical state plots of SP-SC (10%) group is presented in Figure 121 and Figure 122 respectively.

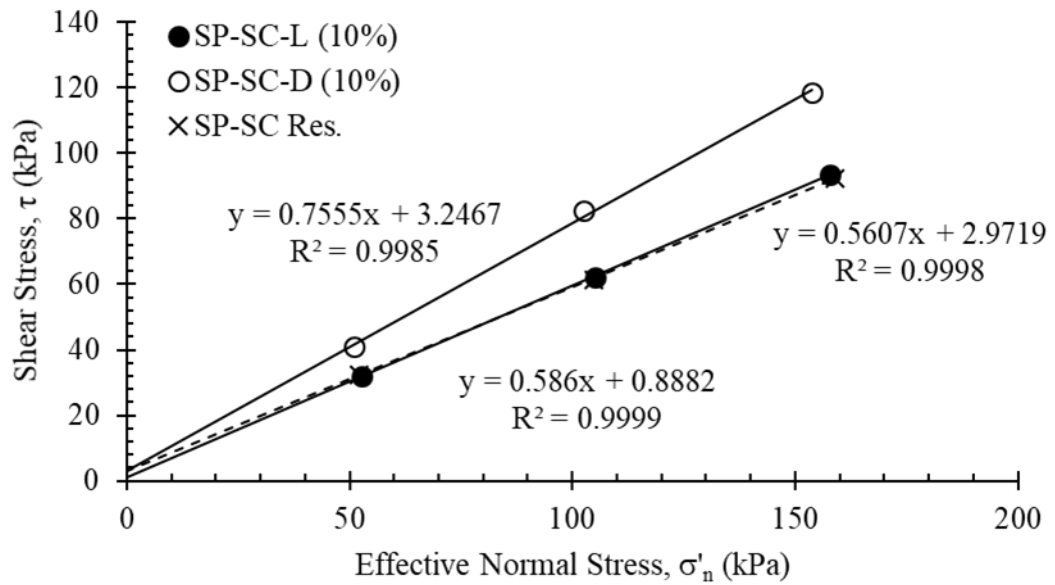


Figure 121: Drained frictional angle of SP-SC (10%) for loose, residual and dense.

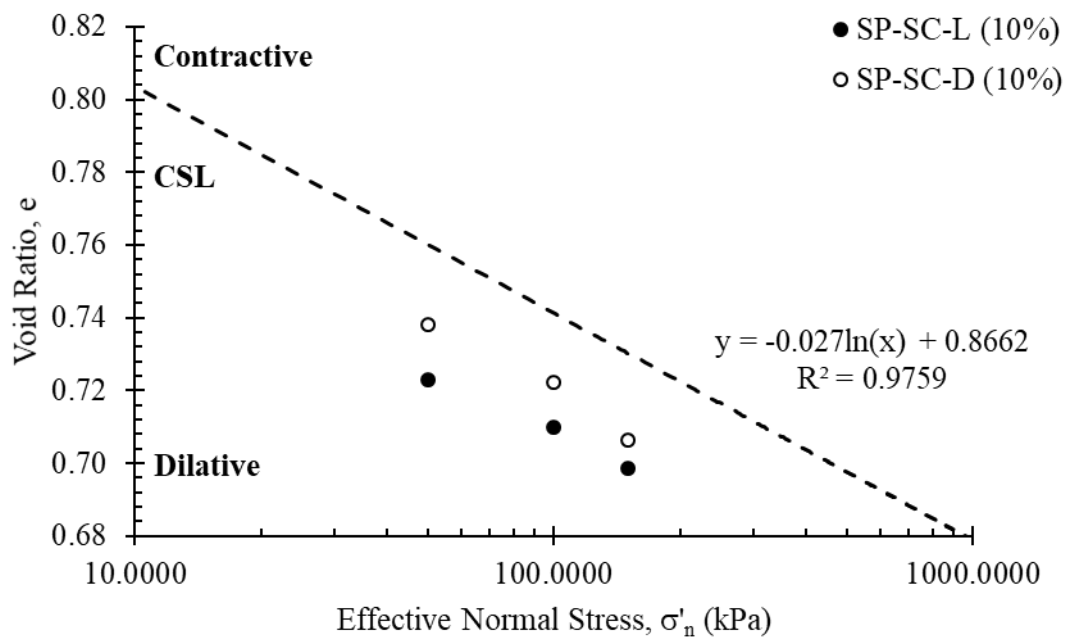


Figure 122: SP-SC (10%) consolidated void ratios and CSL plot.

Critical state mechanics of 10% clay presence indicates that all the specimens are plotting in dilative zone. This phenomenon is directly associated with the particle size as 10% partial replacement of sand is significance and it is a threshold fines content,

therefore volumetric composition of clay particles is very high causing increase in compressibility of soil with further increment of proportions.

4.3.6.2 Effect of 20% Clay Fractions in Sand Matrix

Influence of 20% inclusion of clay particles is illustrated in Figure 123 and 124.

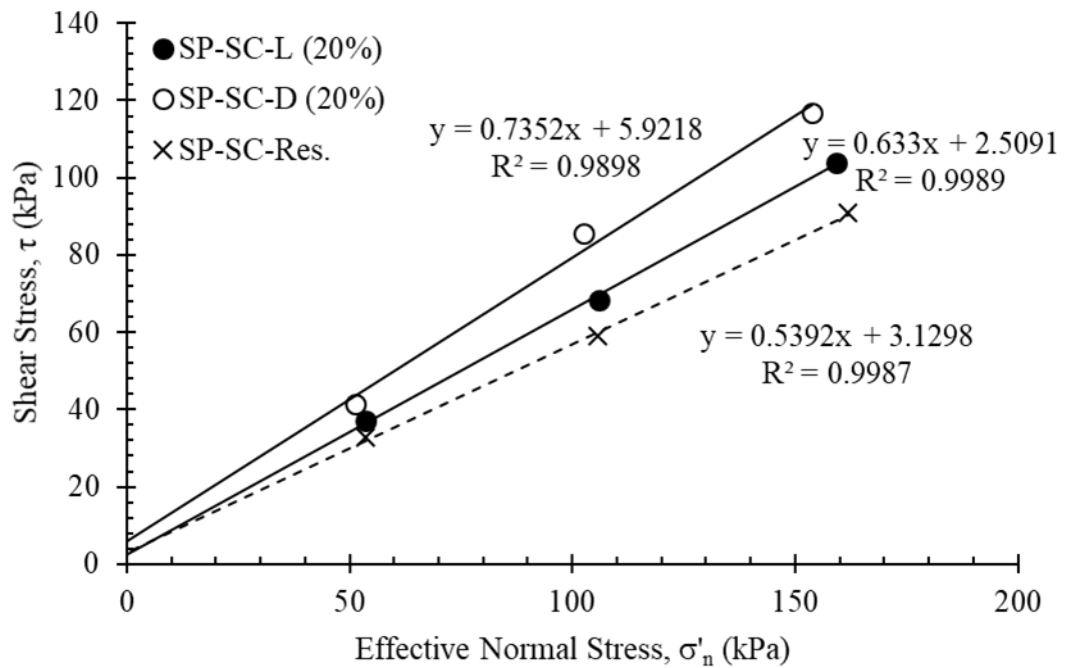


Figure 123: Drained frictional angle of SP-SC (20%) for loose, residual and dense.

From Figure 124, 20% clay presence in sand matrix as previously observed, plotting in dilative zone. In addition to this, as the fine content increased, the initial state of loose specimen became closer to critical state indicating that increment of fines content beyond TFC, loose and dense behaviour will behave similar as the consolidated state will be close to residual state.

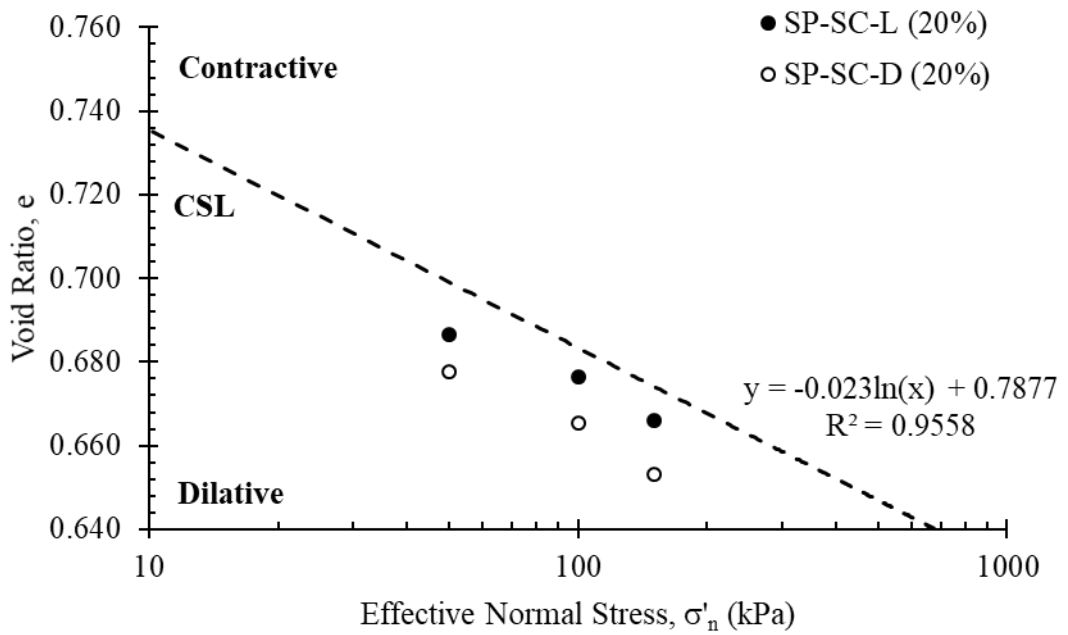


Figure 124: SP-SC (20%) consolidated void ratios and CSL plot.

4.3.6.3 Effect of 30% Clay Fractions in Sand Matrix

Evaluation of clay particles dominant matrix with 30% of sand particles partial replacement is illustrated in Figure 125 and Figure 126.

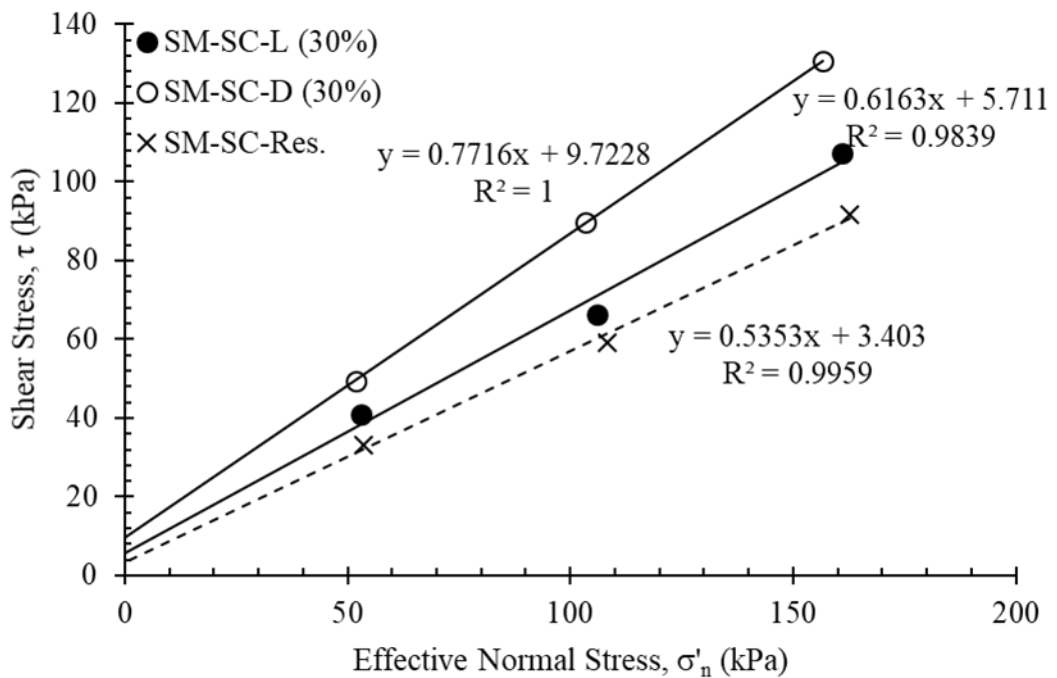


Figure 125: Drained frictional angle of SP-SC (30%) for loose, residual and dense.

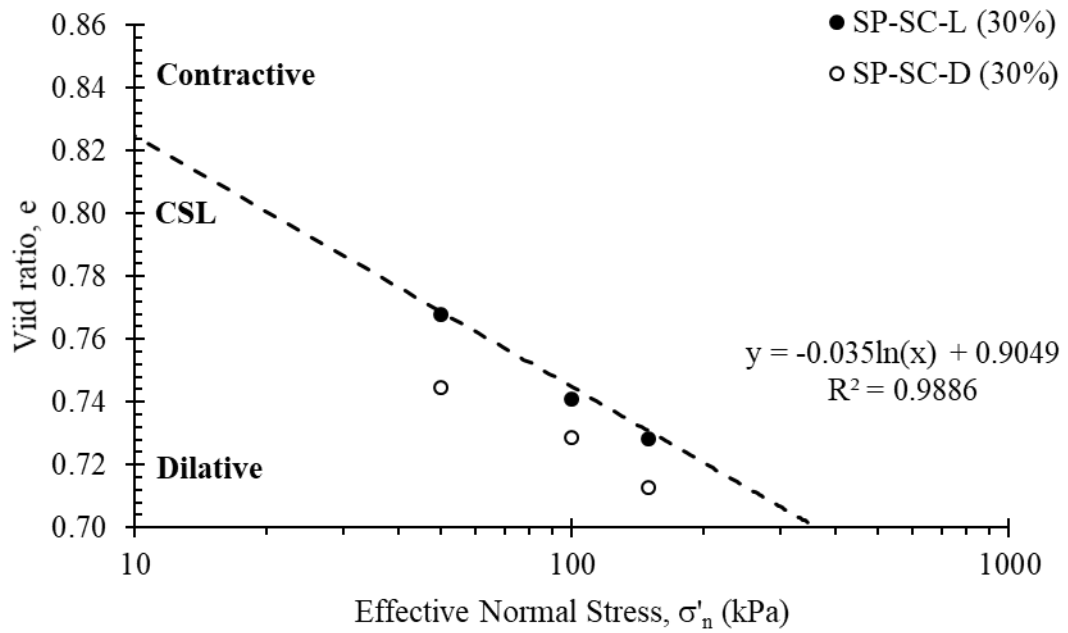


Figure 126: SP-SC (30%) consolidated void ratios and CSL plot.

The initial state of 30% clay presence for loose specimen as discussed earlier are plotting in contiguity of critical state and validating the predicting assessment of further inclusion of clay presence in sand-matrix. In addition, from CSL assessment, the results are also authenticating the gradation analysis significance indicating the susceptibility of flow behaviour reduction for undrained case.

4.3.6.4 Critical State Analysis of Clayey-Silty-Sand Matrix

Summarized critical state behaviour of all clayey-Sand matrix is illustrated in Figure 127, 128 and 129. Presence of clay fractions in sand matrix improves the stability as observed from Figure 127 and 128. A unique case for clayey-sand mixture as compared to other fines mixture is observed that at 10%, void ratios increased and significantly reduced at 20%. This phenomenon is associated with soil fabric as in threshold content (10%), sand particles are also contributing to fabric structure. Whereas, after TFC the fabric structure is rearranged by clay particles thus modifying the surface to surface contact of sand grains (Section 4.1.2).

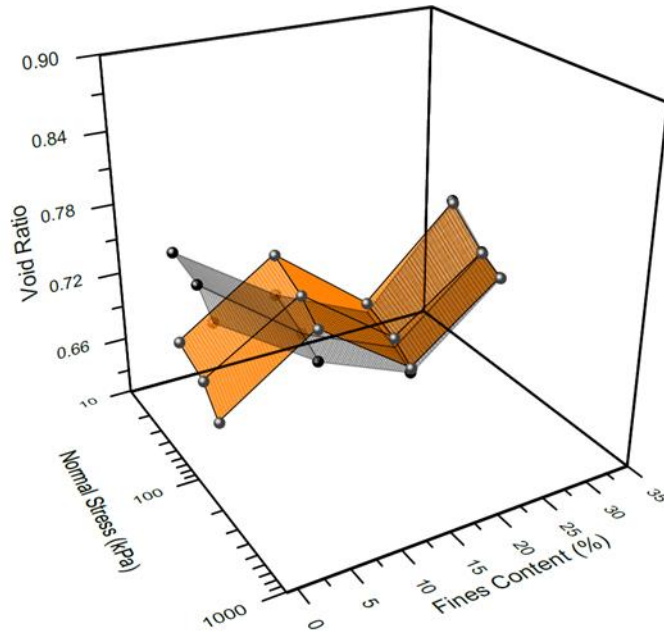


Figure 127: CSL plot of SP-SC-L Matrix with respect to e , σ'_n and f_c .

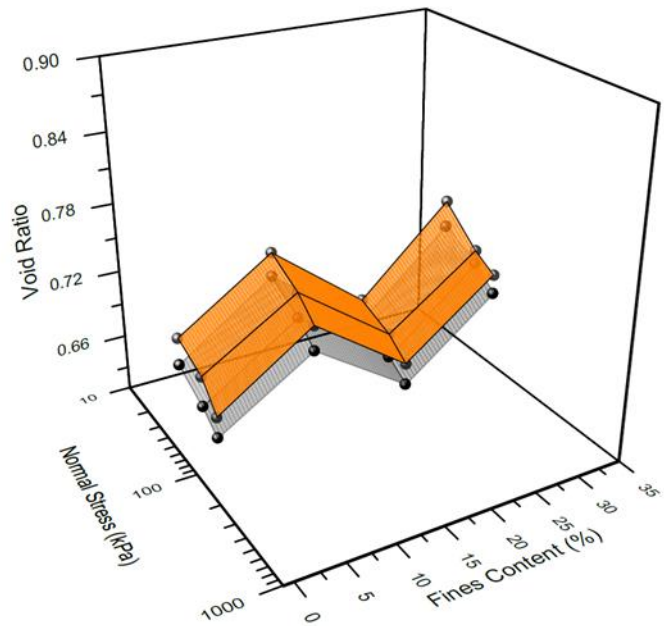


Figure 128: CSL plot of SP-SC-L Matrix with respect to e , σ'_n and f_c .

In Figure 129 and Table 13, state parameters of SP-SC groups are presented.

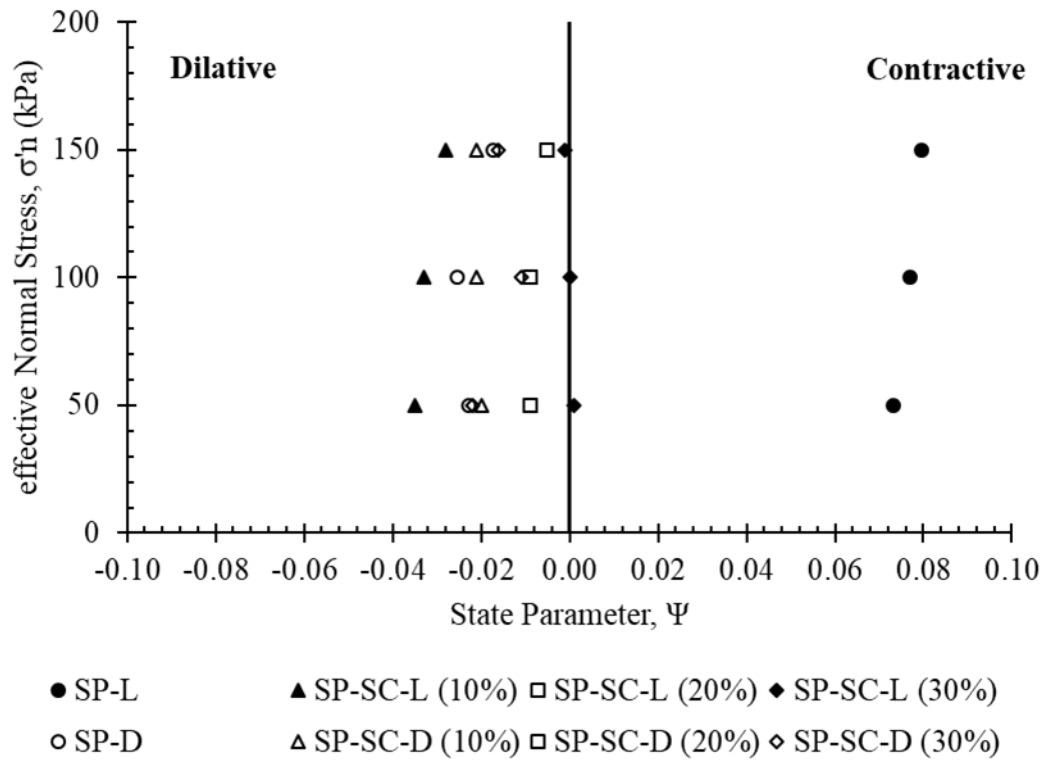


Figure 129: State parameter pf SP-SC groups.

State parameter of SP-SC groups are tabulated in Table 13.

Table 13: SP-SC state parameters.

Effective Normal Stress, σ'_n (kPa)								
%	Loose				Dense			
	50	100	150	Remarks	50	100	150	Remarks
10	-0.116	-0.139	-0.149	Dilative	-0.205	-0.220	-0.233	Dilative
20	-0.001	-0.002	-0.001	Dilative	-0.090	-0.082	-0.084	Dilative
30	-0.002	-0.003	0	Dilative	-0.091	-0.083	-0.084	Dilative

4.4.7 General Discussion of CD-DST Results.

The primary focus in evaluation of CD-DST results is based on CSL and state parameter. As CSL is influenced by sample preparation, void ratio, soil density (relative density) and applied normal stress. The state parameter as a result can capture peak shear strength as well as post peak response. From all group's observations, it is noticed that almost in all specimens, fines addition affected the compressibility behaviour and volume change during shearing due to partial replacement of sand by fines. A clear observation of this behaviour is demonstrated by high initial compression and the rise of CSL for silty Sand and clayey-Sand with respect to pure sand and the slope of the CSL line is steeper as compared to Sand (Figure 130). It is observed for clayey-silty Sand group that when 10% of fines are added, contractive behaviour is observed and the slope of the CSL is somewhat similar to Sand thus indicating that fines are acting as a filler material within the voids having no significant effect on the stability of soil matrix.

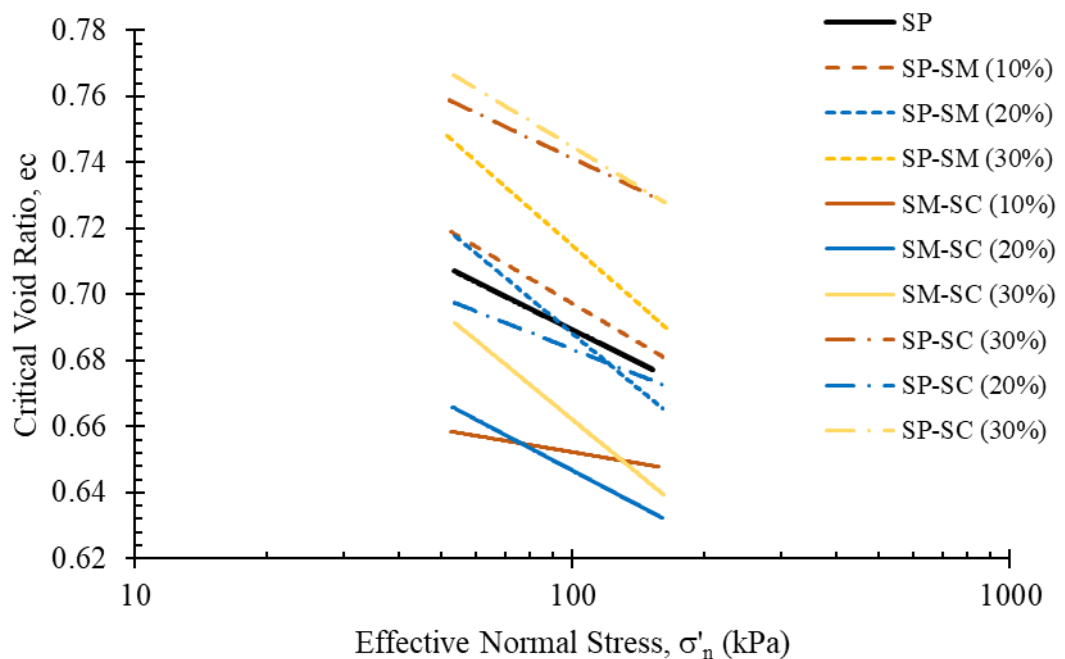


Figure 130: Variation of CSL lines of soil groups.

In Figure 131, variation of state parameter for loose specimens with respect to fines content is illustrated. It is observed as fines content increases, due to increase in compressibility behaviour of sand with fines, the tendency of dilatancy increases as compared with fines. Another interesting point is observed after TFC, at 20% all soil groups state parameters are approximately same. Such behaviour describes the transition behaviour of fabric structure for sand-fines to fine dominance and thereafter dilatancy starts to increase.

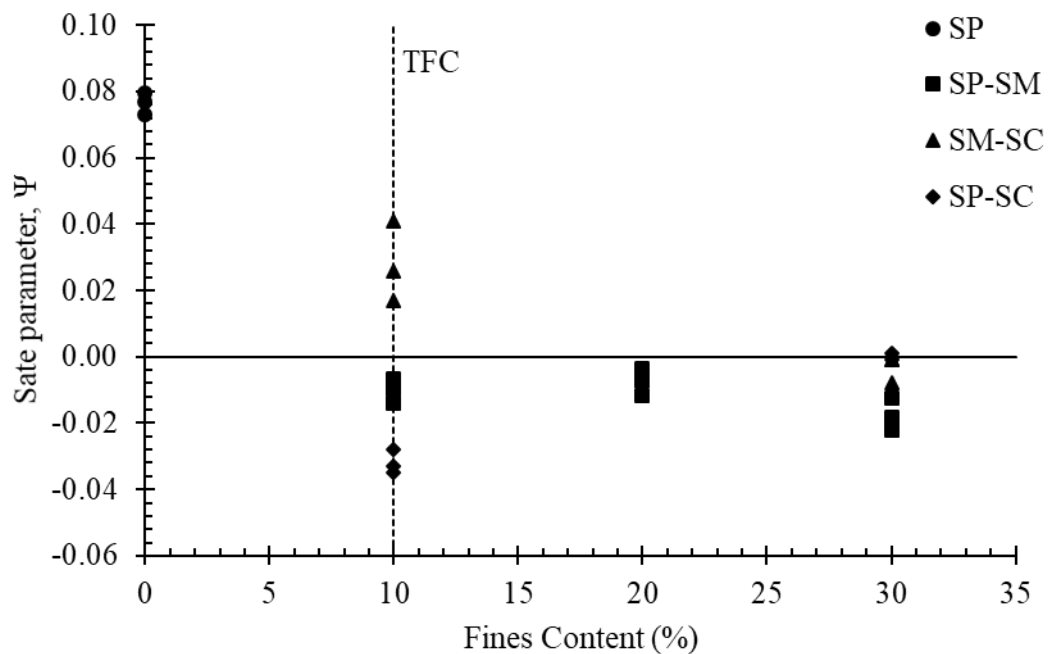


Figure 131: State parameter variation with fines (Loose state).

In terms of dense specimens (Figure 132), with an increment of fines content, the increasing tendency of state parameter is observed after TFC. Such behaviour illustrating the lowering of dilatancy of soil-matrix at the dense state and ultimately loose and dense specimen exhibiting similar behaviour at 30 % of fines addition. Similar behaviour is observed by Phan et al., 2016 where 60% of fines are added into Sand matrix.

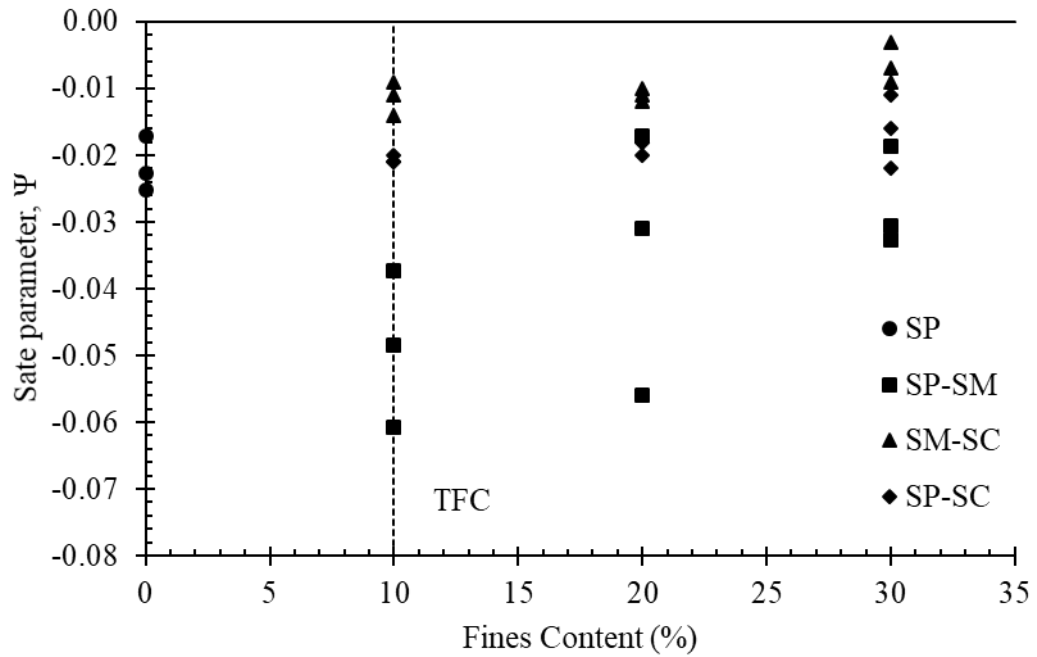


Figure 132: State parameter variation with fines (Dense state).

4.4 Cyclic Direct Shear Testing

In this section, the primary evaluation is based on assessment of the residual state for all soil groups for comparison with the monotonic direct shear box tests. Two methods are applied for shearing, 1- The specimen is sheared the specimen to box limit of 6.3mm in loops. 2- Shearing is performed for cycles of ± 3 mm. It is observed that five cycles are sufficient to achieve convergence in the mobilised shear stress.

The outcomes of method 1 are presented in Figure 147. From these plots, both ultimate and residuals are obtained. The results of second method are plotted in this section, which illustrates ± 3 mm residual hysteresis loops. It is considered that the results from method 2 are more representative of the cyclic response, hence they are used for further interpretation in this section. It is observed that as the fines content increases the ultimate mobilized shear stress is shifted and develops beyond 4 mm of horizontal displacement.

4.4.1 Residual behaviour of Sand

The residual hysteresis loops of Sand are presented in Figure 133. From the plot, it is observed that residual strength of initially loose sample after achieving ultimate strength is similar to monotonic direct shear box test and since the state parameter is dependent on critical state internal frictional angle, hence relying on translational results is validated since approximately 50% of axial strain rate is applied to the specimen. It is observed for dense specimens that after 1st cycle, the residual shear strength increases significantly up to 4th cycle. The residual shear strength is attained at 5th cycle similar to monotonic direct shear box test.

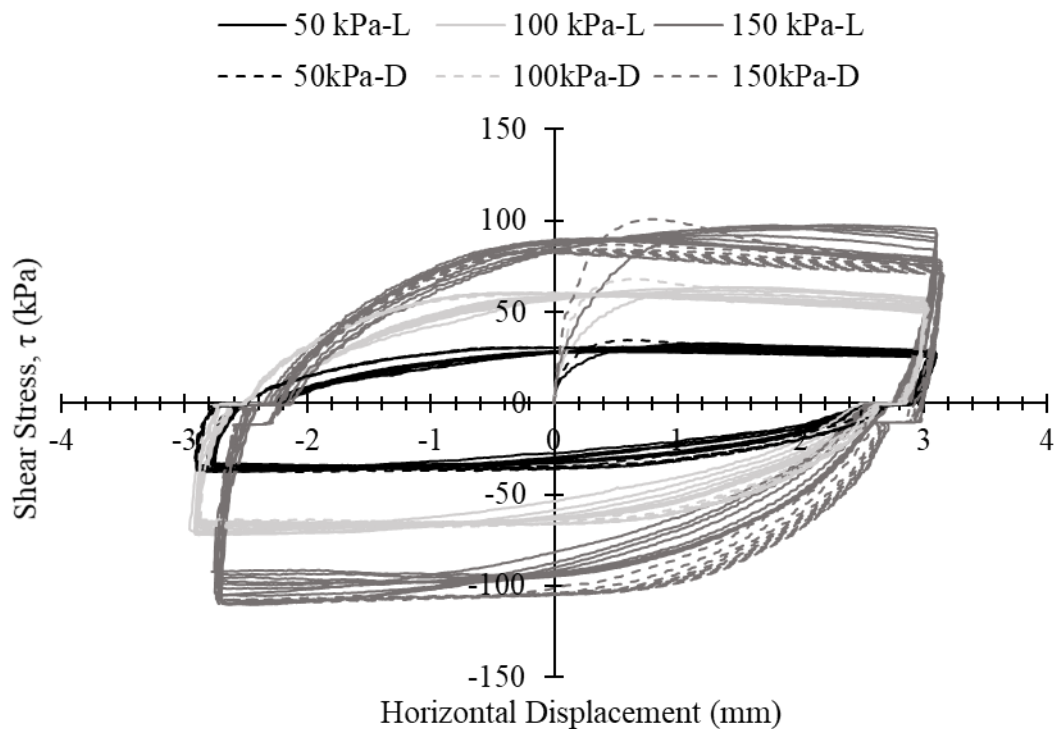


Figure 133: Residual hysteresis loops of SP.

4.4.2 Clayey-Sand Mixture

Effect of clay presence on residual strength of Sand is presented in Figures 134 – 136.

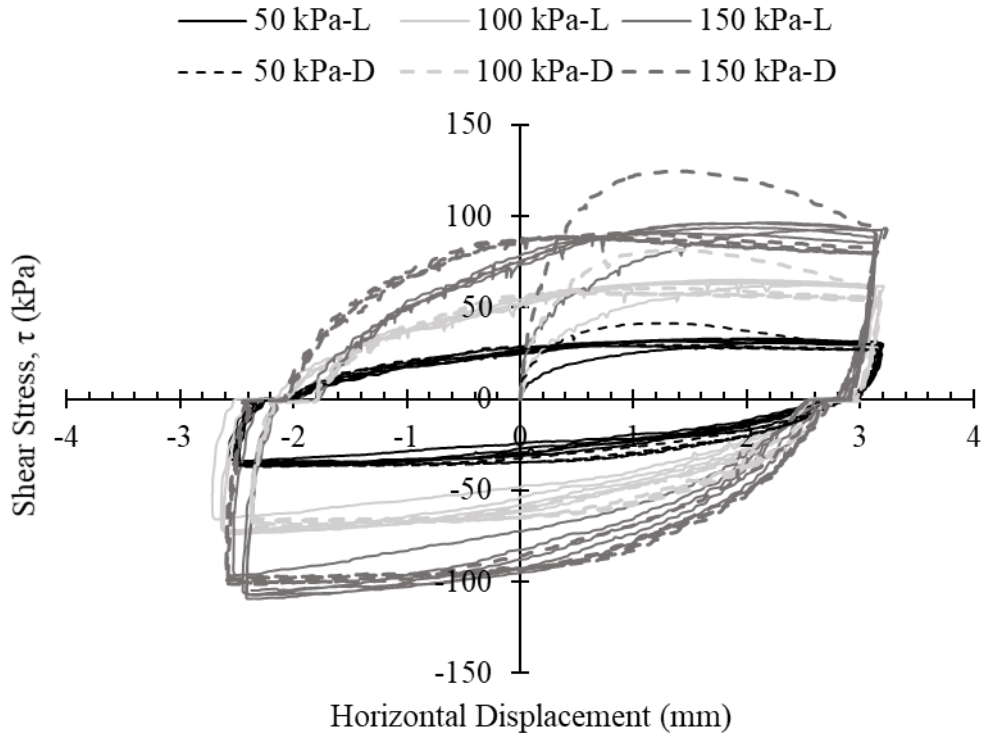


Figure 134: Residual hysteresis loops of SP-SC (10%).

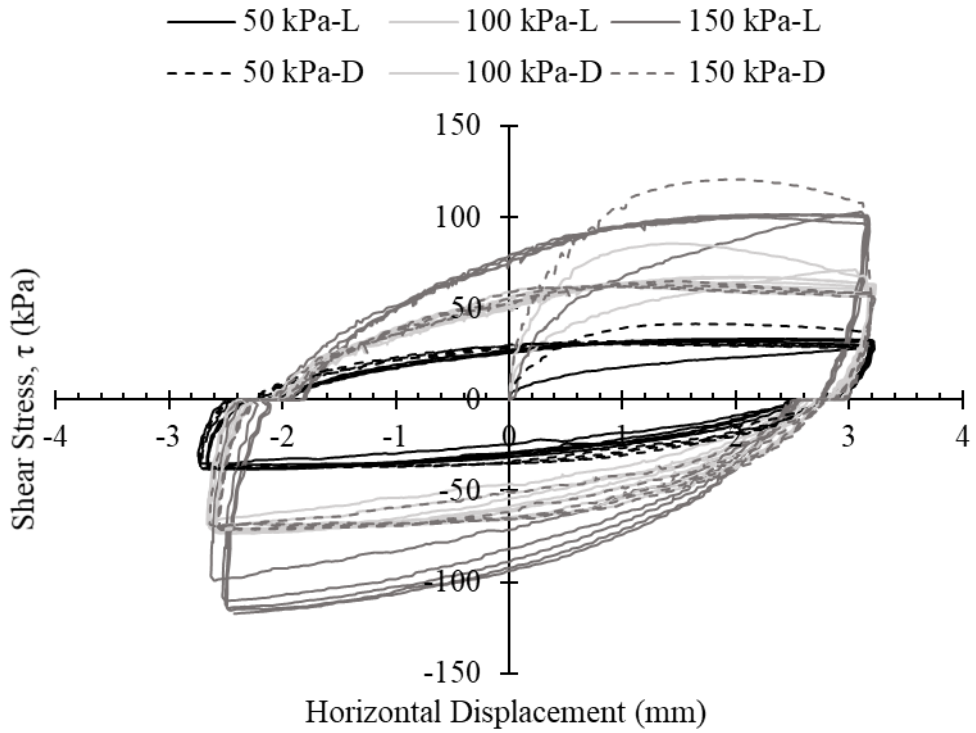


Figure 135: Residual hysteresis loops of SP-SC (20%).

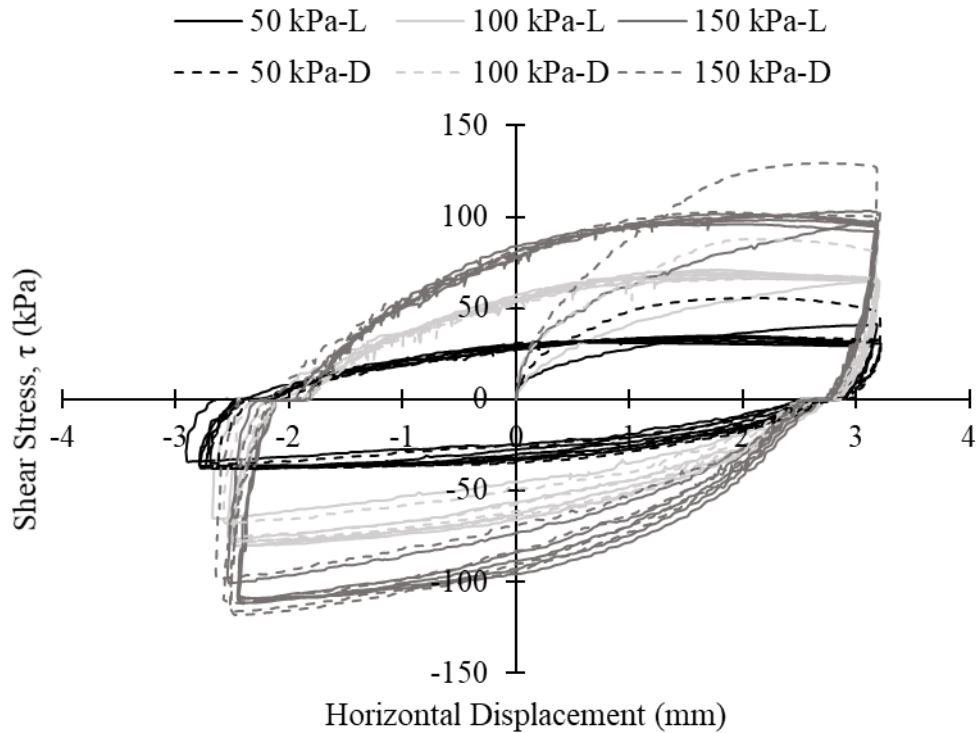


Figure 136: Residual hysteresis loops of SP-SC (30%).

Since the primary concern is to obtain residual strength of a soil, loops are used to evaluate the difference between peak stress and the residual stress. For dense specimens, in 1st cycle the peak strength is observed whereas, the residual strength is consistent in 2nd – 5th cycles. A noticeable difference is observed that as the fines content increases, peak shear strength shifts from 1.2 mm to 3 mm and is more prominent. A peak shear stress is prominent at loose state in 30% clay fractions addition in 1st cycle.

4.4.3 Silty- Sand Mixture

In Figures 137 - 139, silt fraction in sand matrix behaviour under reversal test is illustrated. The residual internal frictional angles obtained from all soil groups is from 4th cycle and are differing with one to three degrees from translational test. Since in cyclic testings, all tests are conducted in dry state and as compared to monotonic testings, the shear strength and state parameters obtained are validated. The similar

parameters also validate the fact that in 20% and 30% no excess pore water pressure is exhibited and no shift in shear plane is occurred in both testings. In Figure 135, 10% of silt-sand mixture hysteresis residual loops are illustrated. Another criteria to be satisfied here is regarding the axis of shear plane. Since the specimen is sheared forward and backward simultaneously, shifting of axis might occur. This shift is axis is monitored as while reversing, the negative shear stress values are in correspondence to positive values. In 20% silt-sand mixture (Figure 138), it is observed from monotonic testing analysis that ultimate point is occurred after 3mm and hence the ultimate point is not achieved in cyclic testing. Ultimately the required residual internal frictional angle obtained is differing only by 2 degrees. Similar case is obtained for 30% mixture and difference is obtained as 1 degrees.

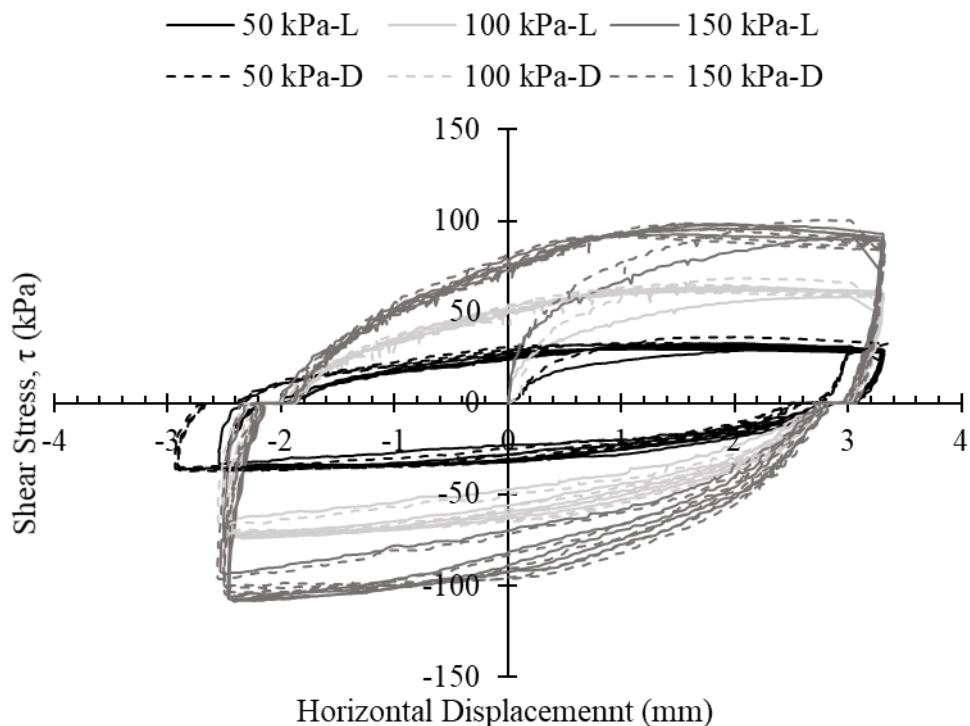


Figure 137: Residual hysteresis loops of SP-SM (10%).

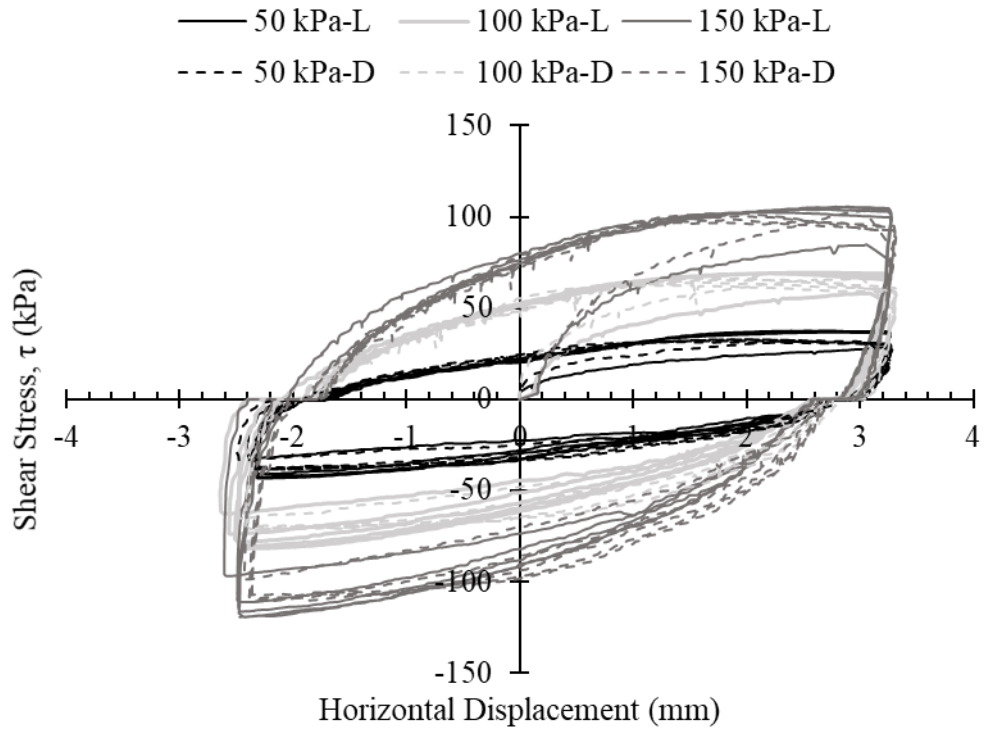


Figure 138: Residual hysteresis loops of SP-SM (20%).

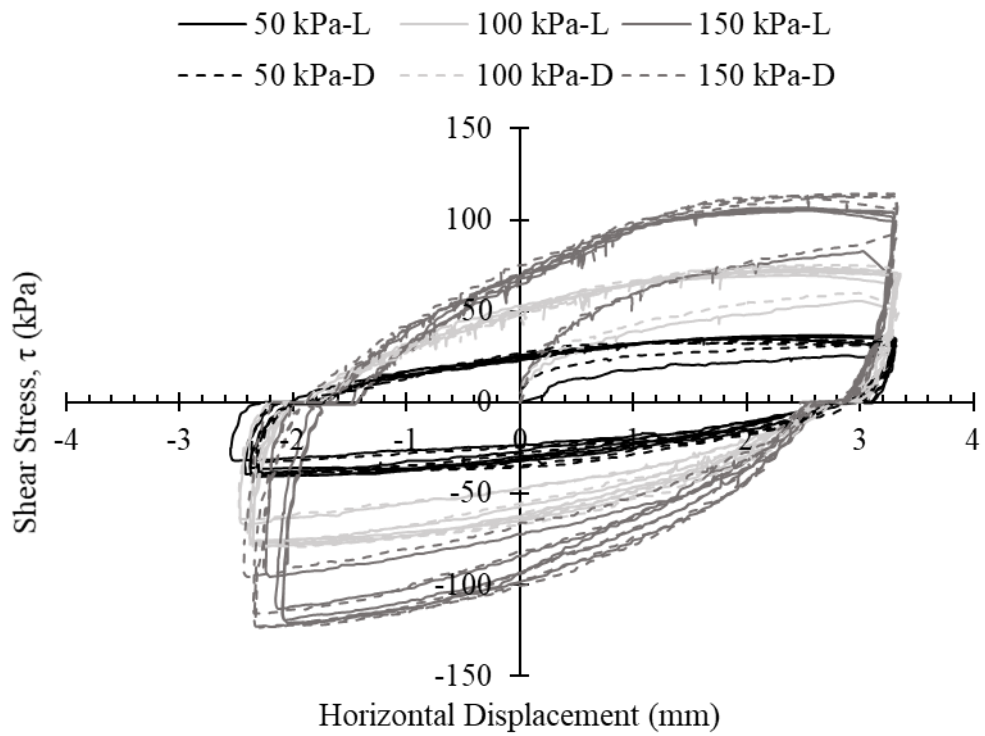


Figure 139: Residual hysteresis loops of SP-SM (30%).

4.4.4 Clayey-Silty- Sand Mixture

Residual hysteresis loops of SM-SC groups are illustrated in Figure 140 – 142.

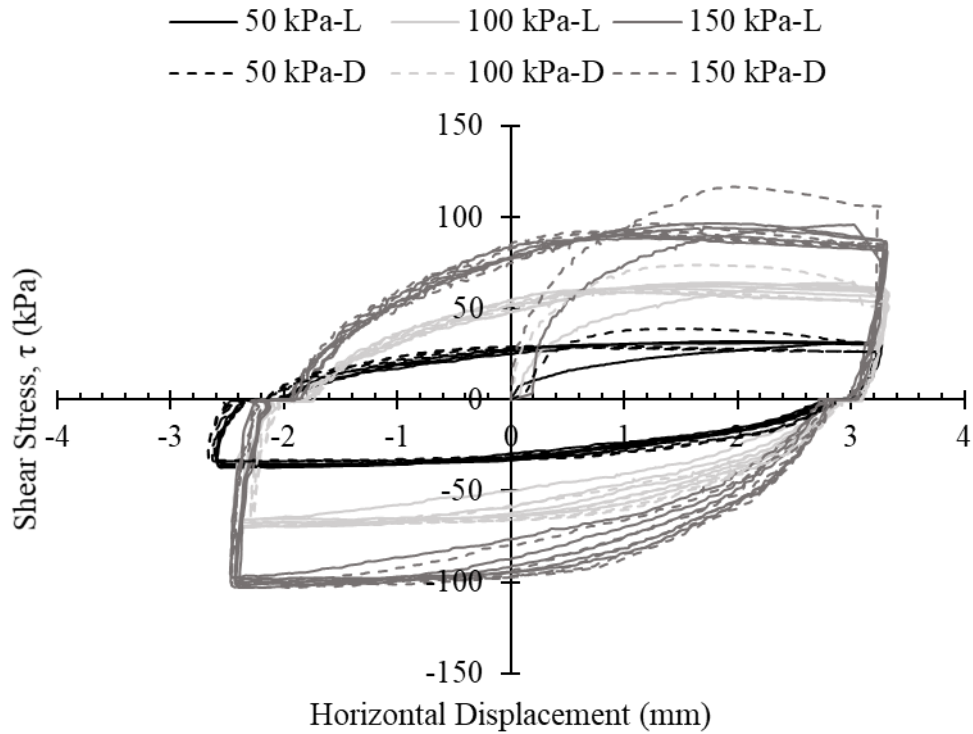


Figure 140: Residual hysteresis loops of SM-SC (10%).

It is observed from Figure 142, as the fines increases, the ultimate point and residual points are similar. This is due to shift of shear stress at large strain as observed from translational direct shear test.

The obtained plots from cyclic and translational direct shear tests are plotted as comparison plot in Figure 143 - 147. The results exhibiting similar results due to very small strain rate applied hence also validating no excess pore-pressure is generated during saturated sample shearin

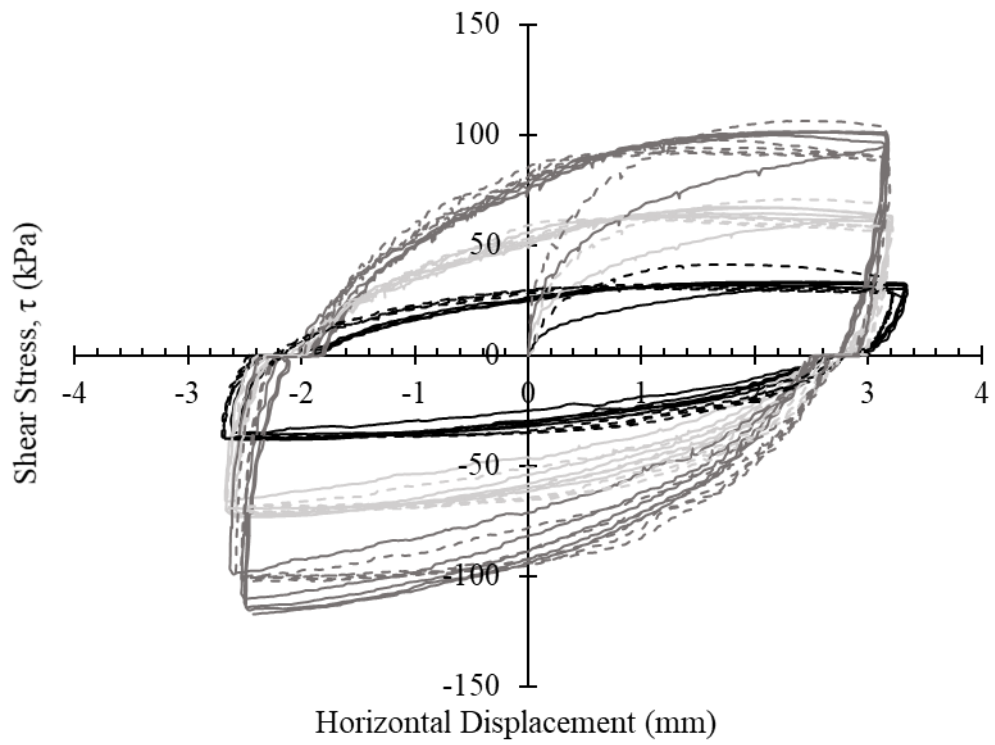


Figure 141: Residual hysteresis loops of SM-SC (20%).

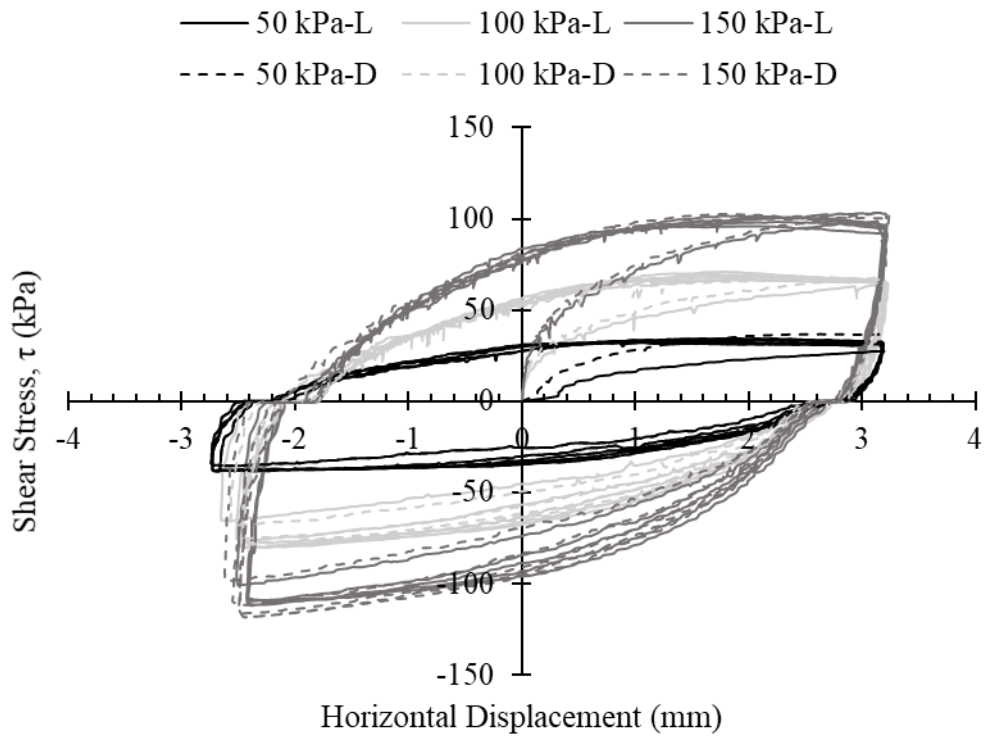


Figure 142: Residual hysteresis loops of SM-SC (30%).

4.5 Residual Behaviour Conclusive Remarks

Comparison plot of mobilized residuals between translational and cyclic shear tests are illustrated in Figures 143 – 145.

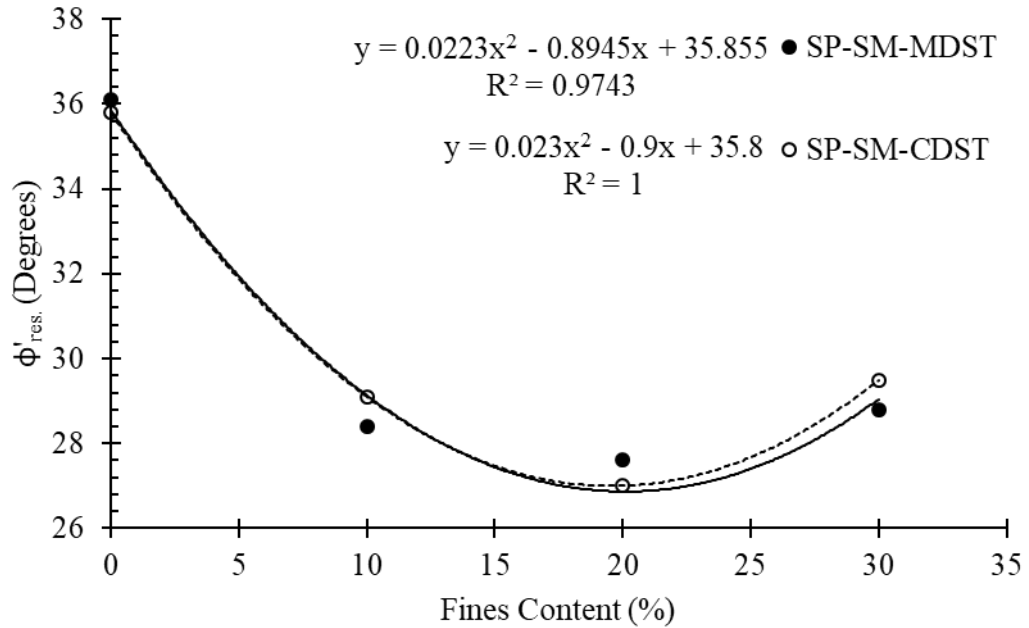


Figure 143: SP-SM groups MDST and CDST $\phi'_{res.}$ comparison.

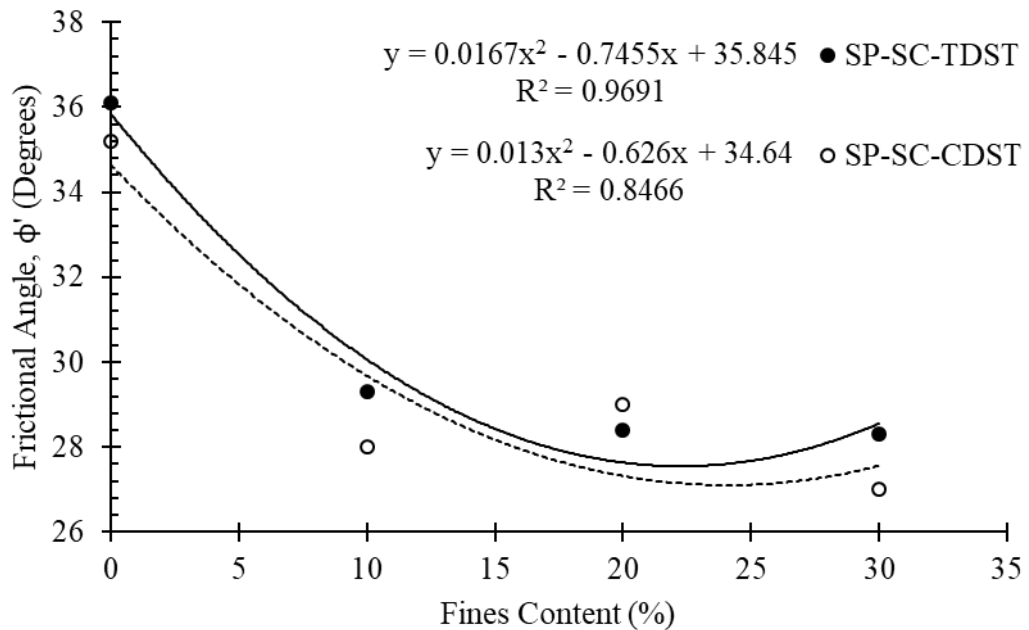


Figure 144: SM-SC groups MDST and CDST $\phi'_{res.}$ comparison.

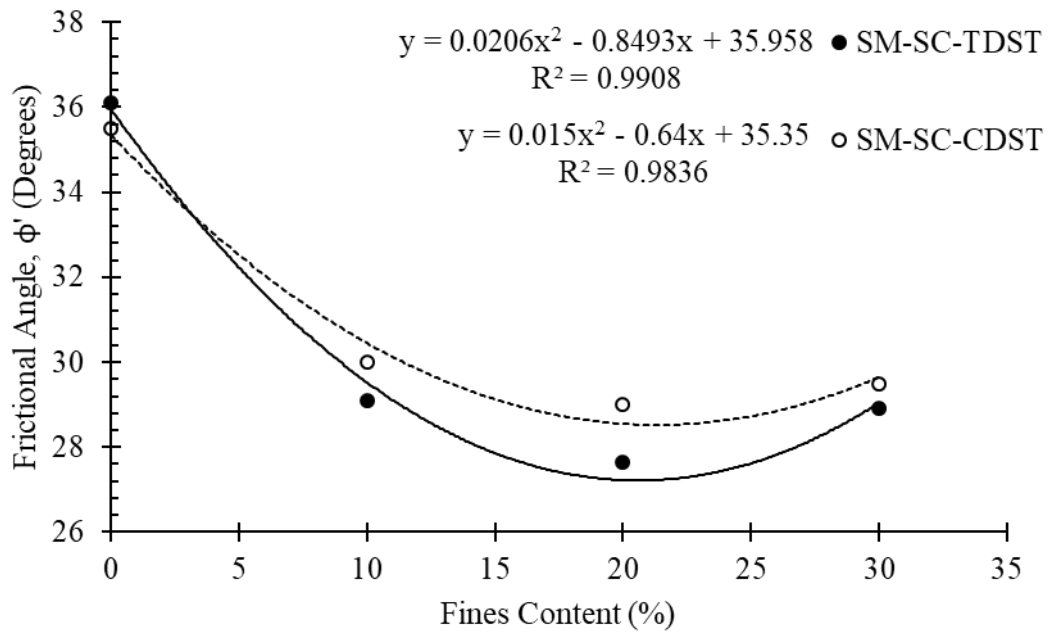


Figure 145: SP-SC groups MDST and CDST $\phi'_{res.}$ comparison.

The residual internal frictional angles obtained from both testing is exhibiting similar values therefore, conducting tests in dry state or saturated state with fines up to 30% will illustrate similar results. As aforementioned, critical state angle is reciprocal to critical void ratio, hence the state parameters obtained in monotonic direct shear box test can be considered for contractive behaviour. In Figure 146, residual internal frictional of all soil groups are plots obtained from MDST (moist tests) and CDST (dry tests) are plotted and in Figure 147, shear strength properties (ϕ'_{peak} , $\phi'_{res.}$ and c') obtained by considering all cases are plotted. The plot consists of frictional angles and cohesion values obtained by MDST (moist) and CDST (dry). The linear regression model (R^2) values in Figure 146 and Figure 147 indicating the variability of both testing cases are around its mean

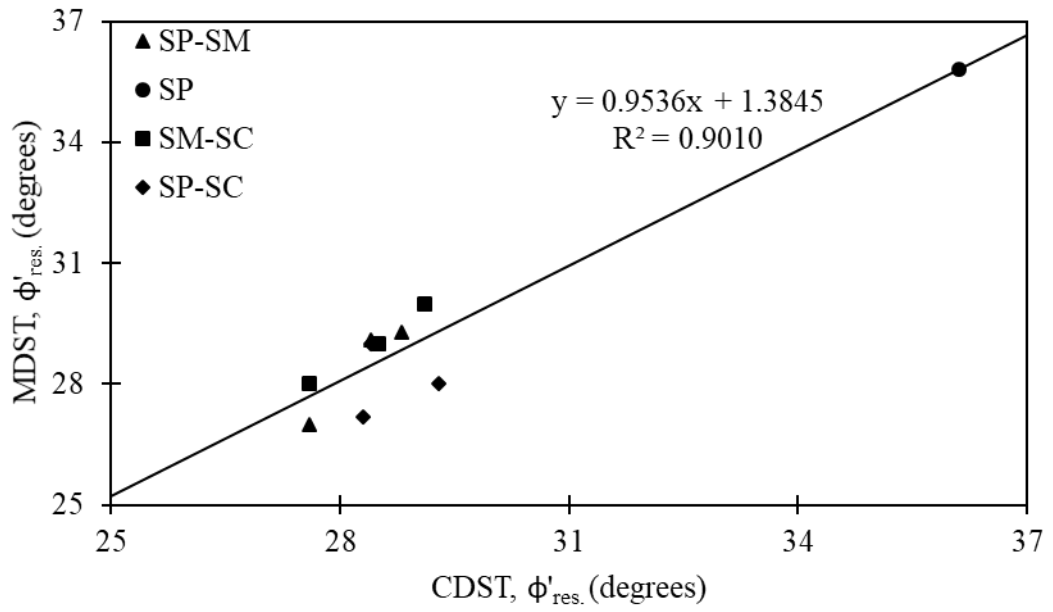


Figure 146: Residuals Comparison between TDST and CDST.

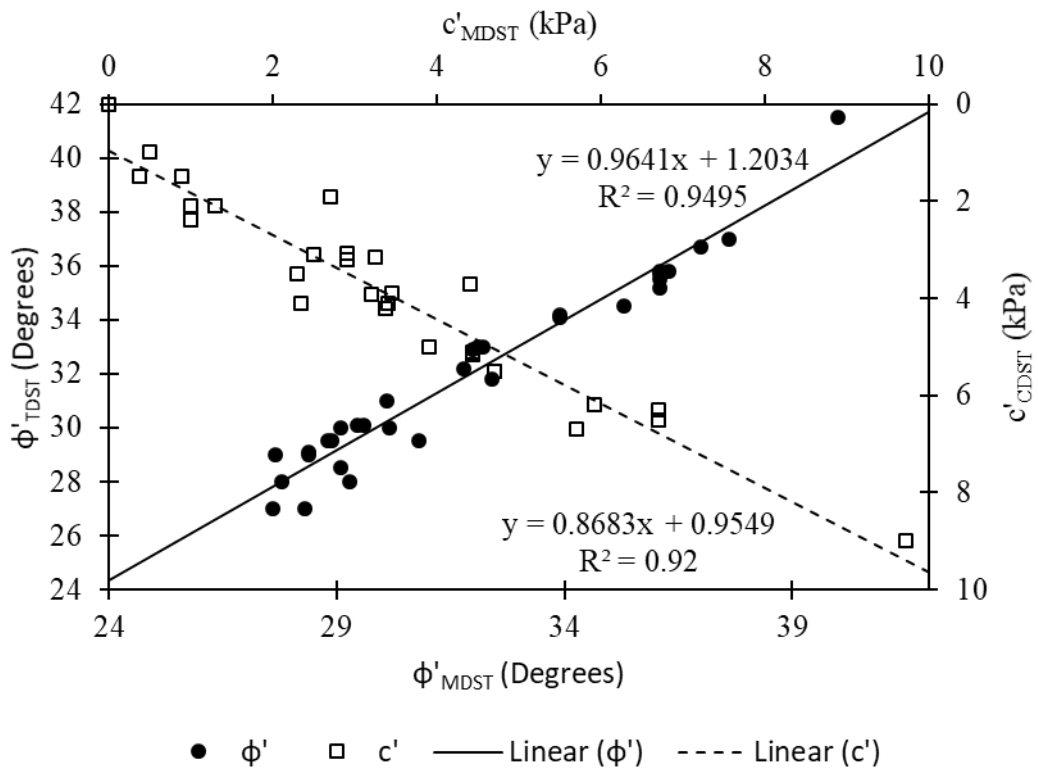


Figure 147: MDST and CDST shear strength properties comparison.

4.6 Drained Strength Parameters Conclusive Remarks

Figure 148 – 150 summarises the peak/ultimate and residual internal frictional angles outcomes for drained testing of all soil groups.

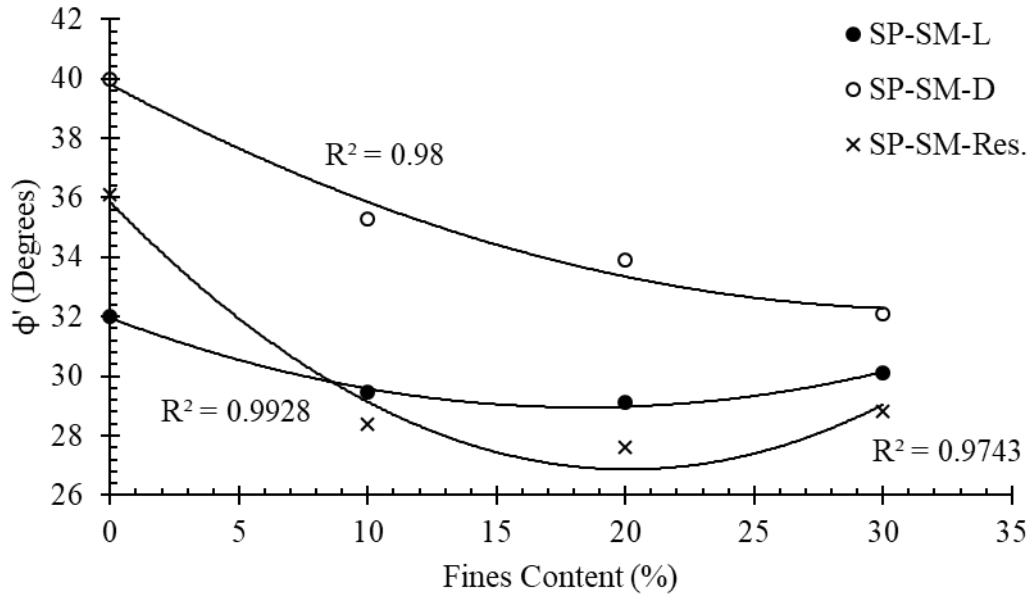


Figure 148: Variation in frictional angles of SP-SM groups.

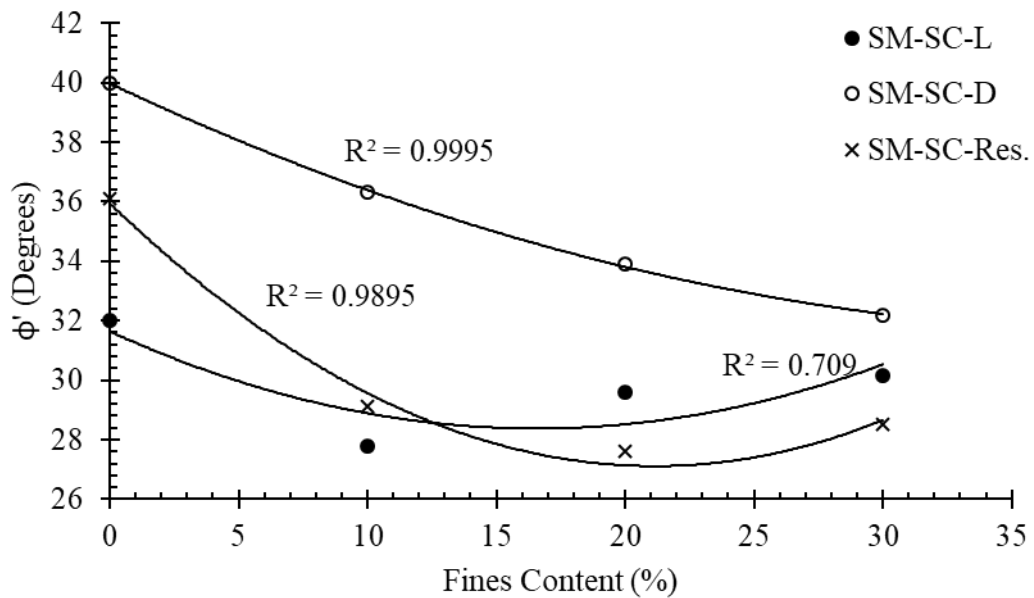


Figure 149: Variation in frictional angles of SM-SC groups.

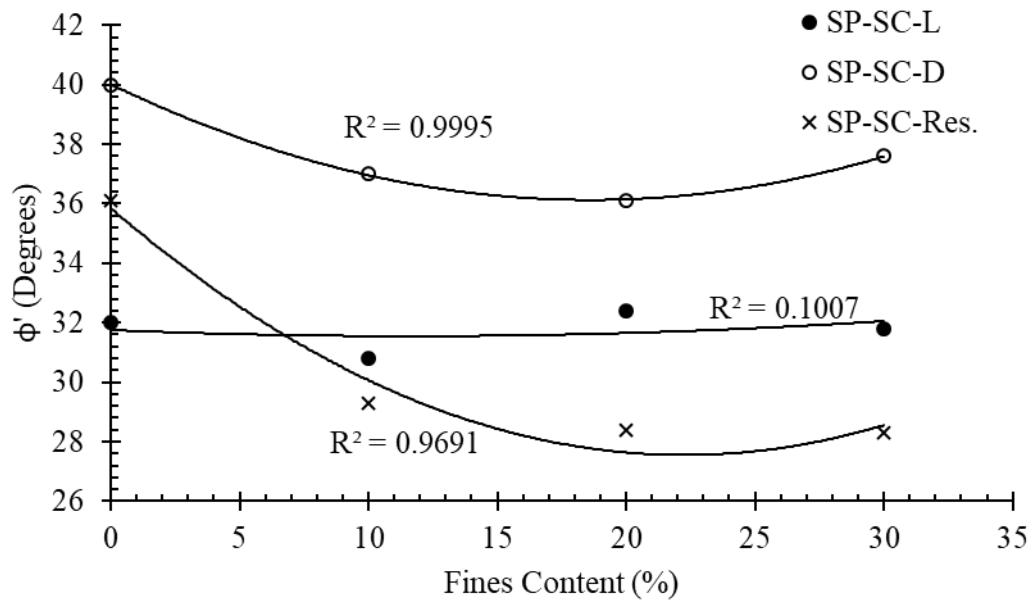


Figure 150: Variation in frictional angles of SP-SC groups.

Experimental results indicate that as the fines content increases, the mobilized peak shear stress shifts as compared to Sand. As the peak shear stress mobilizes at large strains the reduction in shear stress occurs resulting in decrease in ultimate/peak internal frictional as observed in Figures 148 – 150. Specimens reconstituted at dense state exhibiting similar characteristics of loose specimens for SP-SM and SM-SC groups. This phenomenon occurred due to change in initial states of soil. As aforementioned, all loose specimens are exhibiting high compressibility characteristics as fines content increases. Another phenomenon associated is due to cohesion factor. Since due to plastic nature of fines added, the fine particles act as lubricants between Sand grains which reduces the shearing resistance between Sand particles thus reducing friction between Sand particles. Similar results are obtained in another research study by (Umaharathi et al., 2018) where plastic fines are added to Sand up to 25%. In Figures 151 – 153, cohesion values are plotted against fines content. From Figure 151, it is observed that Sand in dense state also exhibiting a small cohesion factor which is due to presence of calcium carbonate (crushed seashells).

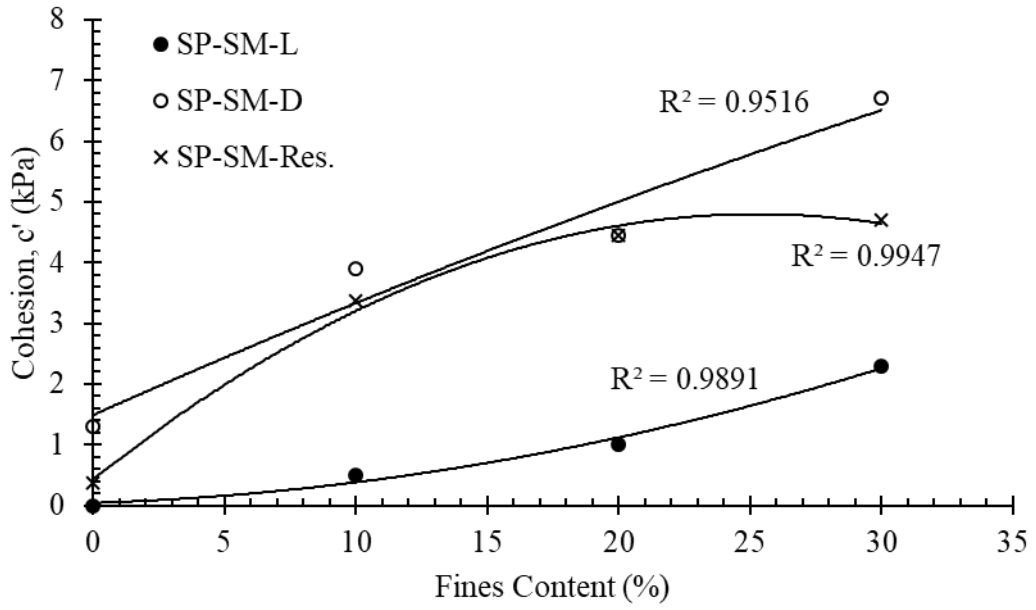


Figure 151: Variation in cohesion with respect to fines content of SP-SM.

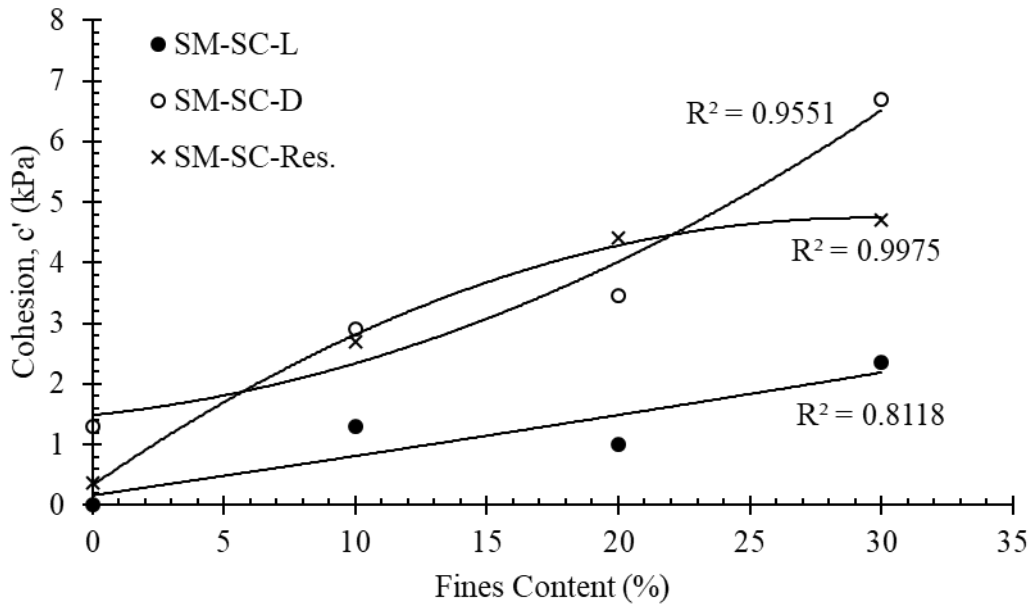


Figure 152: Variation in cohesion with respect to fines content of SM-SC.

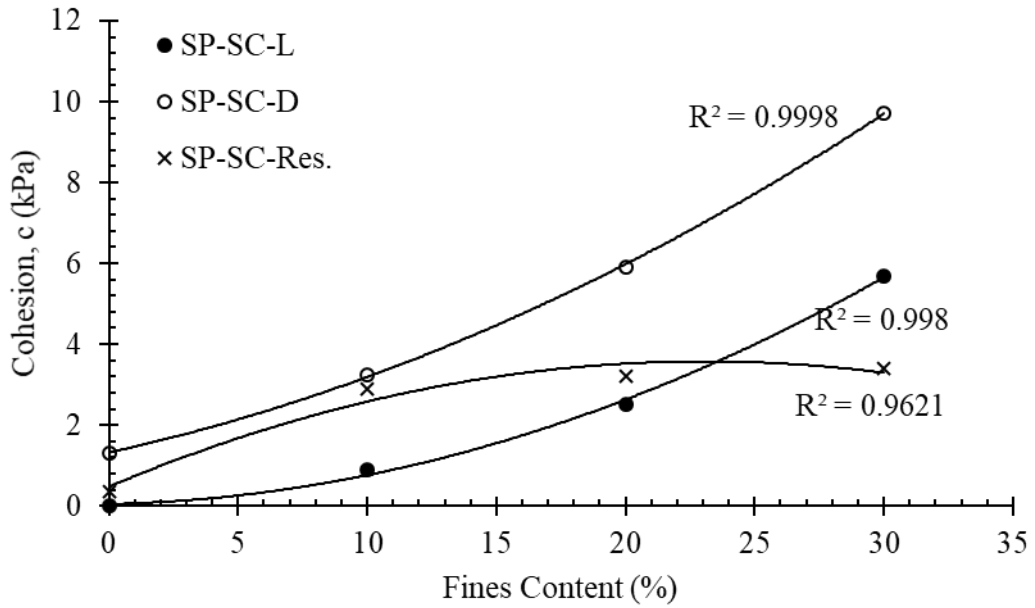


Figure 153: Variation in cohesion with respect to fines content of SP-SC.

4.7 Undrained Monotonic Behaviour

Flow and non-flow behaviour of all soil groups are illustrated in this section. Since from drained Direct Shear Box Testing's, contractive and dilative behaviour for tests soils are obtained, which are directly linked to flow and non-flow behaviour under undrained response. In order to validate the applicability of direct shear box testing to predict the flow and non-flow behaviour, the results obtained in this section are in harmony and in addition to this, evident behavioural response is obtained behind respective soils liquefaction triggering phenomenon. The samples prepared at particular densities are illustrated in section 4.1.

4.7.1 Initial State Analysis

Effect of confining stress on initial state is presented in Table 14. All soil groups are isotopically consolidated at confining stress of 50, 100 and 150 kPa. In Table 15, change in initial states and response of specimens under undrained static loading is summarized. It is observed that as the fines content increases, the compressibility of the soil increases resulting in increase in relative densities. Among all the soil groups,

sand-matrix composed of silt particles exhibiting higher compressibility. Similar observations are observed in direct shear testing where silty-Sand groups exhibited higher compressibility characteristics. In addition to this, the relative density values obtained from consolidating the specimens in triaxial resulted in lower values than direct shear box tests. The apparent reason reflecting the results involves two factors such as difference in specimen dimensions (height) and confinement conditions.

Table 14: Post confining stress effect on initial states.

Group	Initial mean effective stress, p'_o (kPa)					
	Loose			Dense		
	50	100	150	50	100	150
	Relative Density (%)					
SP	42	44	47	76	77	79
SP-SM (10%)	44	45	49	76	78	80
SP-SM (20%)	47	54	63	80	82	85
SP-SM (30%)	59	66	68	81	83	86
SM-SC (10%)	43	45	47	76	81	83
SM-SC (20%)	44	46	48	79	81	84
SM-SC (30%)	48	49	50	80	81	83
SP-SC (10%)	45	47	51	77	79	82
SP-SC (20%)	49	55	59	78	80	83
SP-SC (30%)	54	58	59	78	79	81

Comparison between initial states of direct shear box and triaxial tests after consolidation is illustrated in Figures 154– 159. The top surface plot relates to change in D_R in direct shear box test and vice versa.

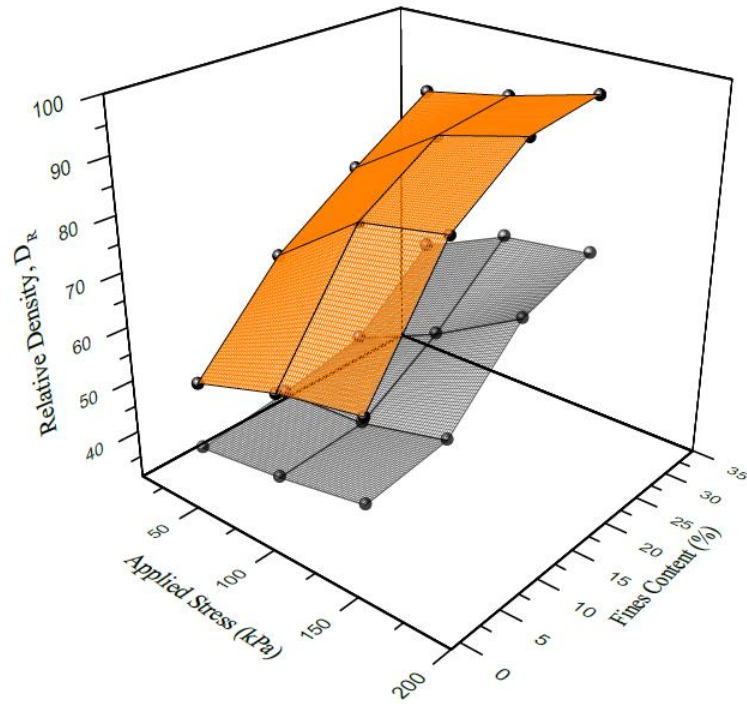


Figure 154: SP-SM direct shear and triaxial D_R comparison (Loose).

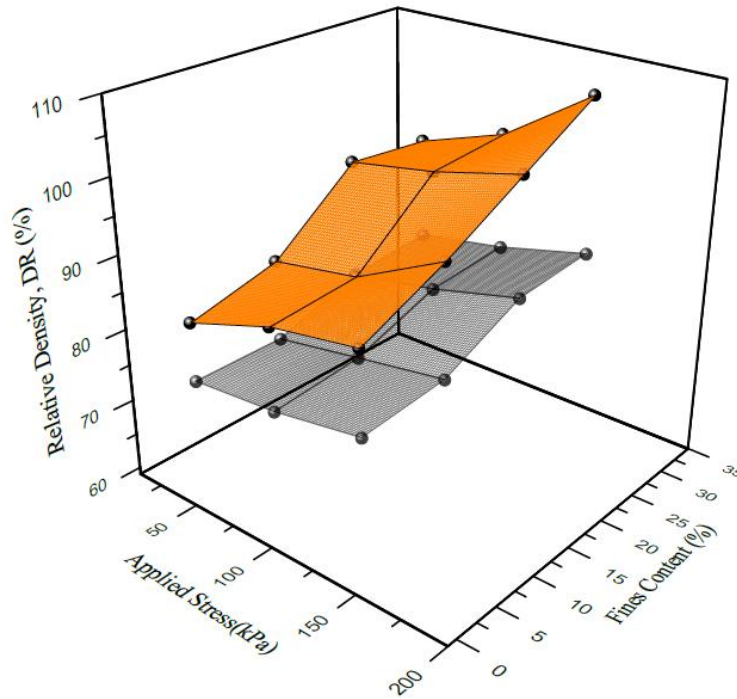


Figure 155: SP-SM direct shear and triaxial D_R comparison (Dense).

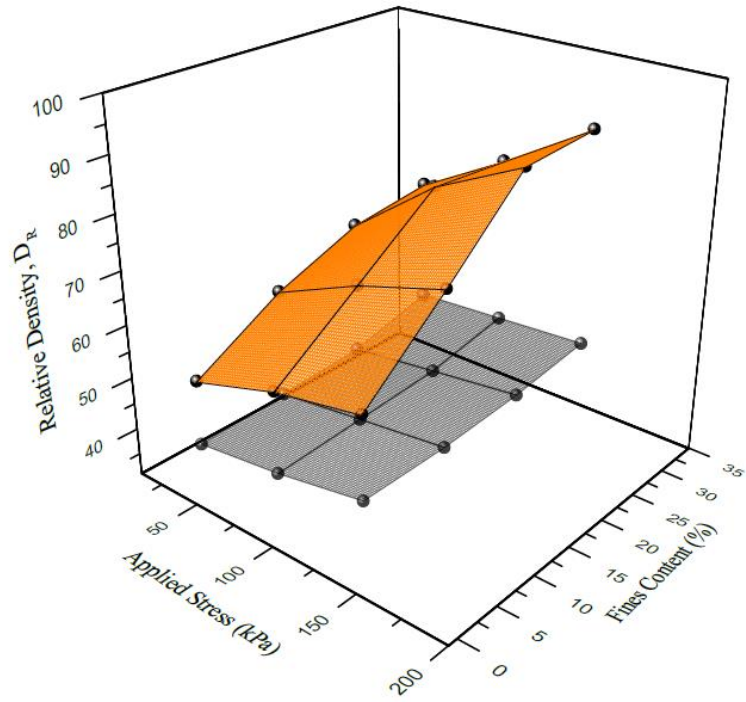


Figure 156: SM-SC direct shear and triaxial D_R comparison (Loose).

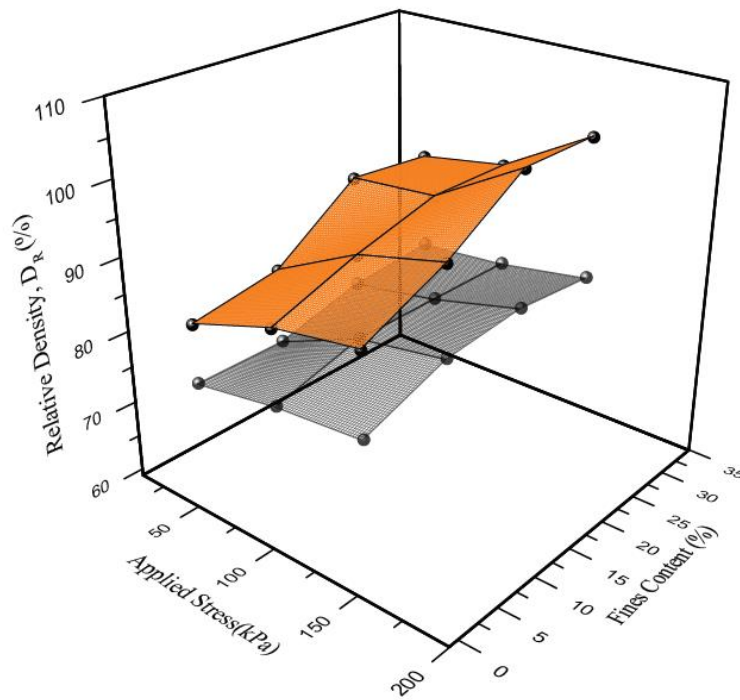


Figure 157: SM-SC direct shear and triaxial D_R comparison (Dense).

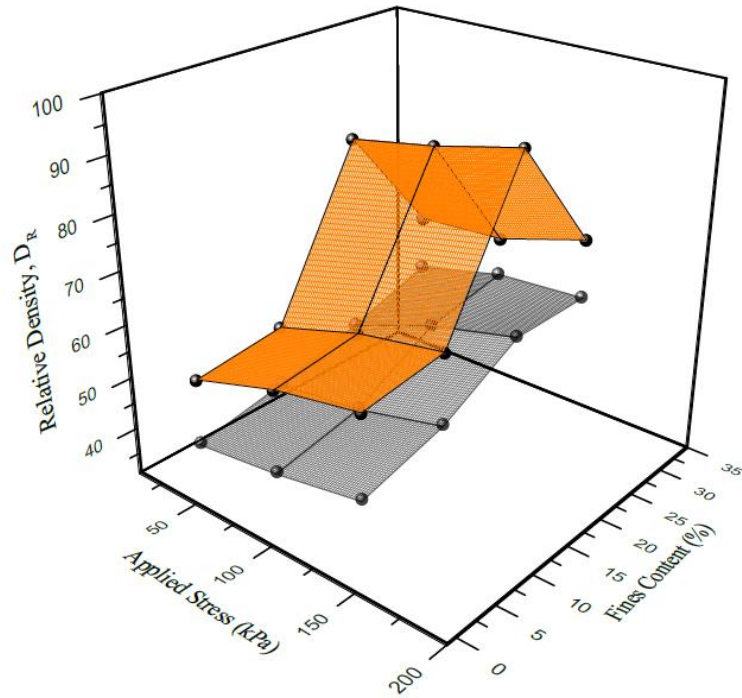


Figure 158: SP-SC direct shear and triaxial DR comparison (Loose).

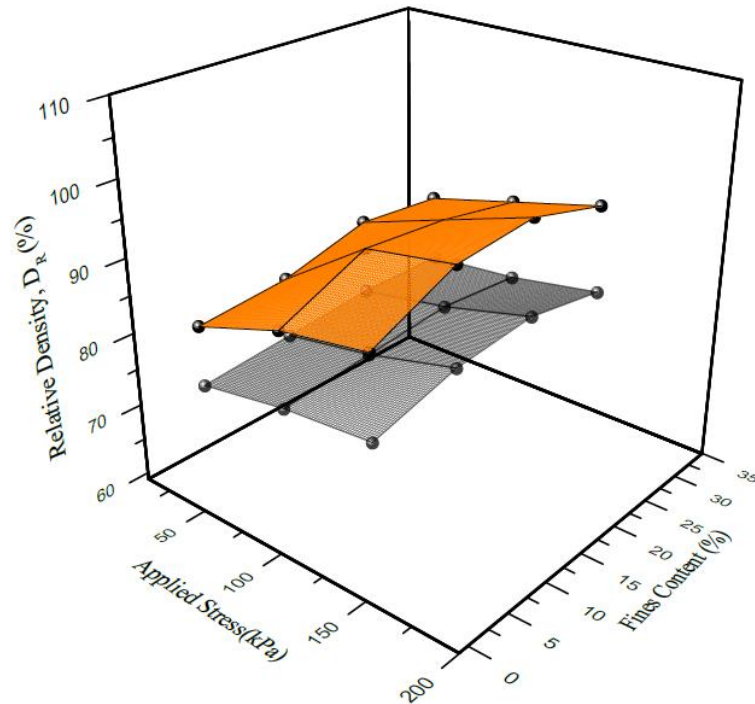


Figure 159: SP-SC direct shear and triaxial DR comparison (Dense).

The summarized undrained monotonic behaviour of soil groups is presented in Table 15.

Table 15: Undrained static response of sand-fines mixtures.

Soil groups	σ_3' (kPa)	Initial states, e_c		B-Values		Remarks	
		$D_R = 35$	$D_R = 70$	$D_R = 35$	$D_R = 70$	$D_R = 35$	$D_R = 70$
SP	50	0.793	0.707	0.94	0.91	<i>Flow</i>	Non-Flow
	100	0.790	0.703	0.96	0.91	<i>Flow</i>	Non-Flow
	150	0.779	0.698	0.94	0.88	<i>Flow</i>	Non-Flow
SP-SM (10%)	50	0.793	0.696	0.96	0.90	Non-Flow	Non-Flow
	100	0.790	0.687	0.96	0.89	Non-Flow	Non-Flow
	150	0.779	0.682	0.97	0.90	Non-Flow	Non-Flow
SP-SM (20%)	50	0.814	0.711	0.98	0.91	Non-Flow	Non-Flow
	100	0.792	0.705	0.98	0.93	Non-Flow	Non-Flow
	150	0.764	0.697	0.95	0.89	Non-Flow	Non-Flow

Table 15 (cont.): Undrained static response of sand-fines mixtures.

Soil groups	σ_3' (kPa)	Initial states, e_c		B-Values		Remarks	
		$D_R = 35$	$D_R = 70$	$D_R = 35$	$D_R = 70$	$D_R = 35$	$D_R = 70$
SP-SM (30%)	50	0.842	0.761	0.98	0.91	Non-Flow	Non-Flow
	100	0.815	0.755	0.98	0.93	Non-Flow	Non-Flow
	150	0.807	0.743	0.95	0.90	Non-Flow	Non-Flow
SM-SC (10%)	50	0.793	0.687	0.96	0.93	Non-Flow	Non-Flow
	100	0.786	0.672	0.96	0.91	Non-Flow	Non-Flow
	150	0.779	0.666	0.96	0.91	Non-Flow	Non-Flow
SM-SC (20%)	50	0.823	0.714	0.95	0.91	Non-Flow	Non-Flow
	100	0.819	0.710	0.94	0.90	Non-Flow	Non-Flow
	150	0.813	0.698	0.96	0.90	Non-Flow	Non-Flow

Table 15 (cont.): Undrained static response of sand-fines mixtures.

Soil groups	σ_3' (kPa)	Initial states, e_c		B-Values		Remarks	
		$D_R = 35$	$D_R = 70$	$D_R = 35$	$D_R = 70$	$D_R = 35$	$D_R = 70$
SM-SC (30%)	50	0.873	0.753	0.99	0.94	Non-Flow	Non-Flow
	100	0.868	0.751	0.99	0.95	Non-Flow	Non-Flow
	150	0.864	0.742	0.96	0.94	Non-Flow	Non-Flow
SP-SC (10%)	50	0.750	0.657	0.95	0.91	<i>Limited Flow</i>	Non-Flow
	100	0.743	0.650	0.95	0.91	<i>Limited Flow</i>	Non-Flow
	150	0.731	0.642	0.97	0.91	<i>Flow</i>	Non-Flow
SP-SC (20%)	50	0.798	0.709	0.98	0.90	Non-Flow	Non-Flow
	100	0.781	0.701	0.95	0.90	Non-Flow	Non-Flow
	150	0.767	0.694	0.95	0.92	Non-Flow	Non-Flow

Table 15 (cont.): Undrained static response of sand-fines mixtures.

Soil groups	σ_3' (kPa)	Initial states, e_c		B-Values		Remarks	
		$D_R = 35$	$D_R = 70$	$D_R = 35$	$D_R = 70$	$D_R = 35$	$D_R = 70$
SP-SC (30%)	50	0.840	0.750	0.97	0.94	Non-Flow	Non-Flow
	100	0.827	0.747	0.97	0.94	Non-Flow	Non-Flow
	150	0.823	0.739	0.96	0.91	Non-Flow	Non-Flow

4.7.2 Monotonic Loading Undrained Response of Sand

The undrained monotonic response of loose and dense sand is presented in this section.

In Figures 160 and Figure 161, q -axial strain and excess pore water pressure-axial strain is presented respectively. Stress paths of loose SP is illustrated in Figure 162.

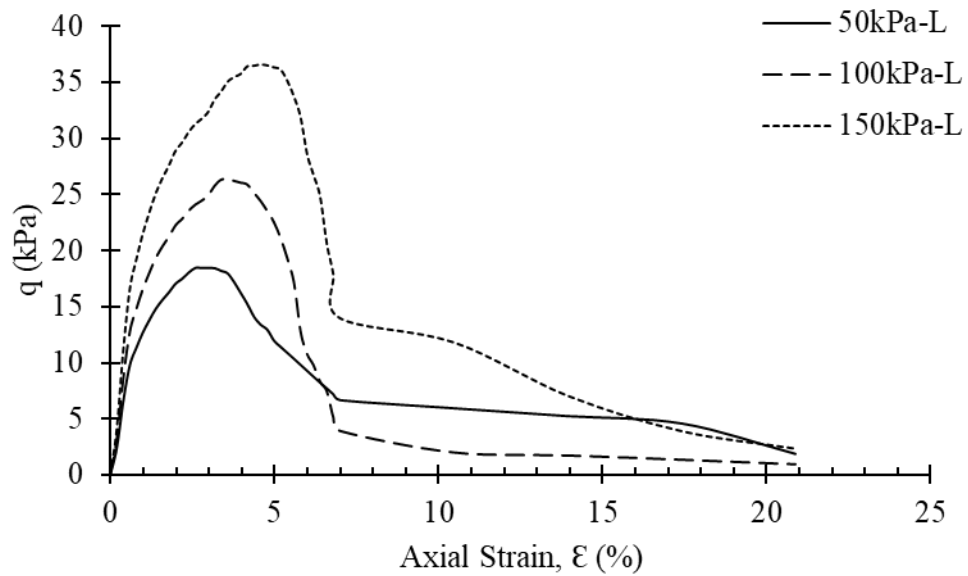


Figure 160: Undrained response of loose sand.

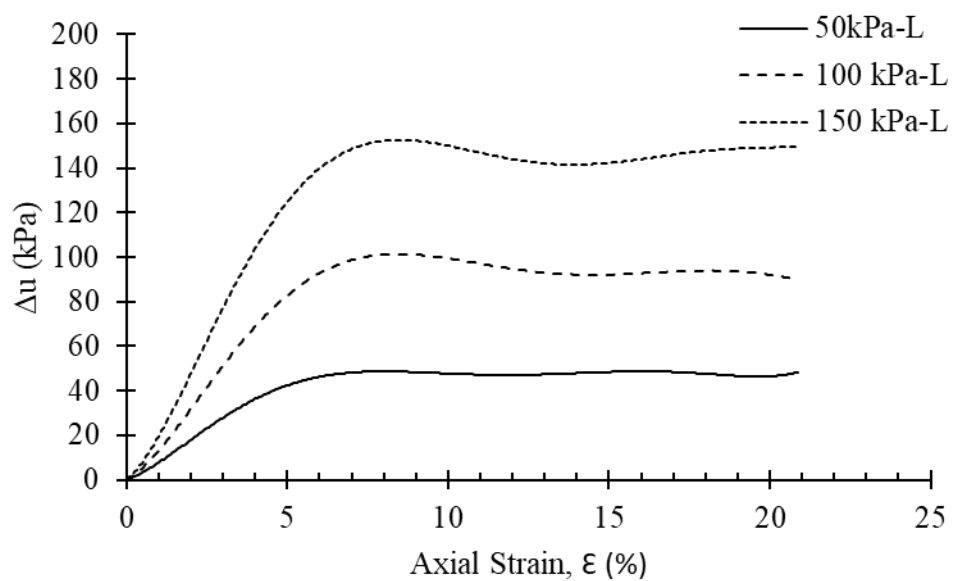


Figure 161: Excess pore-water pressure development in base sand.

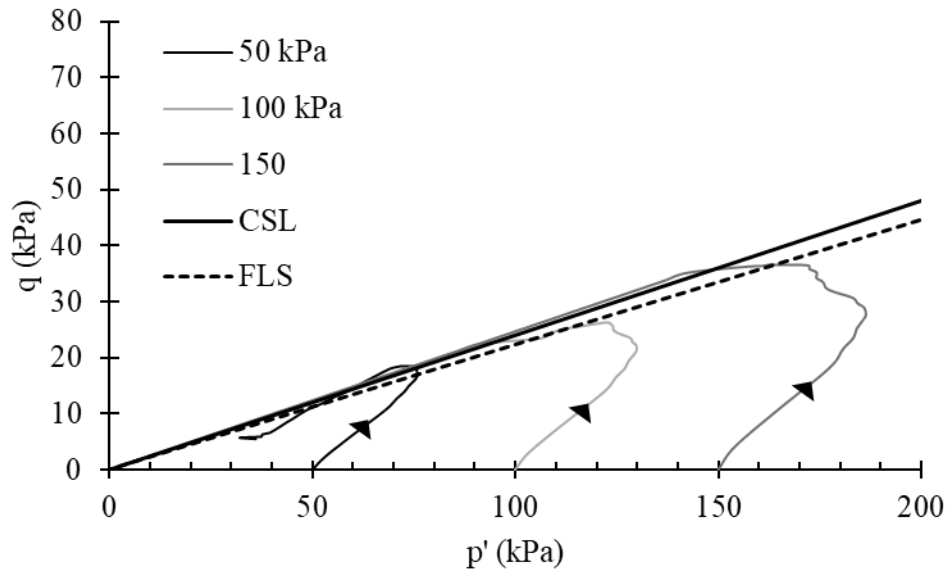


Figure 162: Stress paths for loose sand.

In Figure 163, dense specimen q-axial strain and Figure 164 illustrates pore water pressure- axial strain is plotted.

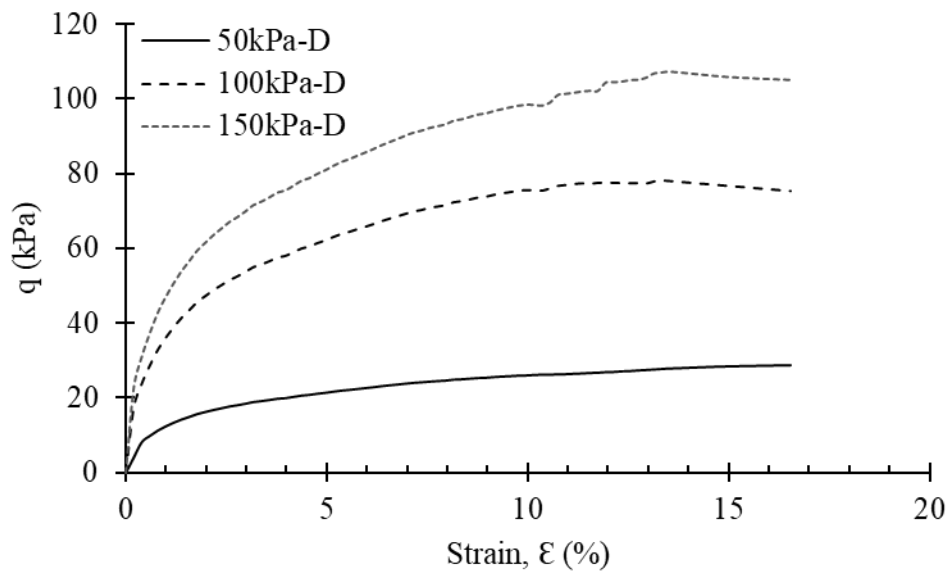


Figure 163: Undrained response of base sand.

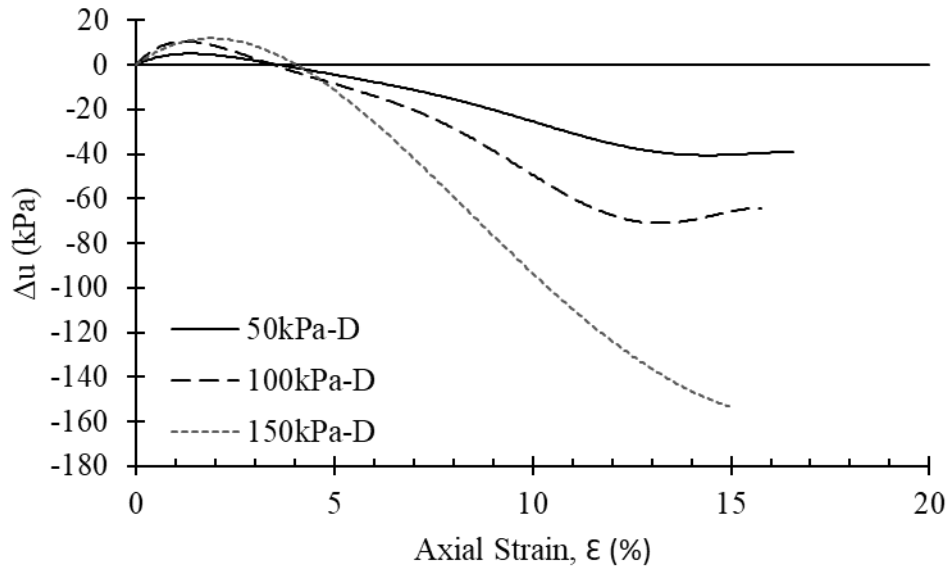


Figure 164: Pore-water pressure development in dense sand.

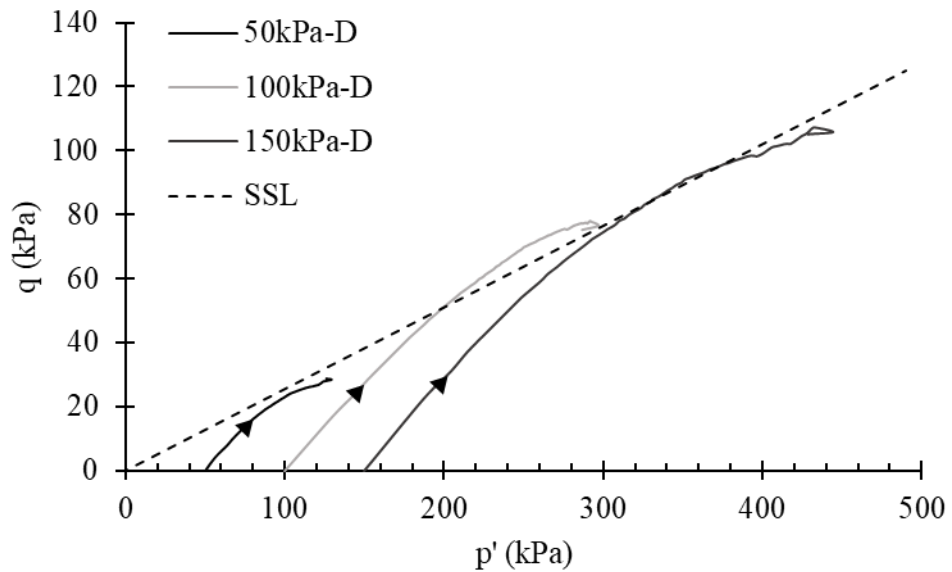


Figure 165: Stress paths for dense sand.

Loose sand subjected to monotonic loading showed instable response for all three confining stress applications (Figure 162). It is observed that as the confining stress increased, instability is more pronounced. At low confining stress (50kPa) the specimen is exhibiting limited flow liquefaction. In all confining stress application, the sample is exhibiting strain-hardening phenomenon approximately 3 – 6% of axial

strain level and afterwards, deviator stress (q) significantly drops (Figure 160). This phenomenon is directly linked with pore-pressure generation as observed in Figure 161. At initial strain levels, pore-pressure generation in specimen is slow therefore, peak deviator stress is observed and afterwards pore water pressure keeps on generating until reaches equilibrium. Pore-pressure generation related to 100 and 150 kPa of confining stresses illustrates a drop in pore-pressure after reaching peak value for a short period of strain level and sudden increment in pore-pressure reaching back to its ultimate point (Figure 161). It is also noted for 150 kPa of confining stress where pore-pressure reduces, a quasi-steady state is obtained directly linked to previous statement and deviator stress ultimately drops further. Since the test is terminated due to limitation of data recording, it is observed that if further axial strain levels are applied, deviator stress ultimately reaches to zero hence, total liquefaction phenomenon can be associated. Stress-paths of the loose sand (Figure 162) also shows interesting behaviour as the critical state and stability lines (Flow liquefaction Surface, FLS) are very close indicating the sudden collapse of the stable state, if the soil is subjected to further static loads. Another case can be associated here regarding the ultimate points in loose specimens is for liquefiable soils, the ultimate is achieved immediately at low strain levels for liquefied specimen and in this case ultimate point is shifted at 3 – 6% strain (Figure 160) and this phenomenon might be related to particle shape. Since the Silver Beach Sand is composed of mainly angular to sub-rounded shaped particles (Figure 43), therefore initially angular particles are primarily contributing to the strength.

In terms of dense specimens, all three specimens are exhibiting stable condition (Figure 163 and 165). From Figure 163, it is observed that at 100 and 150 kPa of

confining stresses, after achieving steady state, strain-hardening phenomenon is observed ($\epsilon_{100\text{kPa}} = 10\%$ and $\epsilon_{150\text{kPa}} = 11\%$) due to dilation of dense sand. Regarding the steady state, the peak deviator stresses are observed in all three σ_3 ' stresses and Steady State Line (SSL) is plotted (Figure 165). With reference to pore-pressure evaluations (Figure 164), negative pore pressure occurrence is observed due to dilation of densely packed particles (dense state).

4.7.3 Critical and Steady State Analysis SP-Group

In Figure 166, based on the observed behaviours of loose and dense Sand. SSL and FLS are plotted. By establishing SSL (Figure 165), it is observed that loose specimens are plotting above the SSL directing to flow liquefaction for all three specimens. In Figure 165, CSL [$e_{ss} = \Gamma - \lambda \ln p'$] and Normal Consolidation Line (NCL) [$e_c = N - \lambda \ln p'$] are plotting in contrast with each other for both states of Sand (Loose and Dense). The CSL and NCL parameters (Γ , N and λ) are tabulated in Appendix E. By establishing CSL and NCL, state parameter can be obtained.

In Table 16, summarized outcomes such as state parameter, pore-pressure ratio, flow potential, steady state are presented.

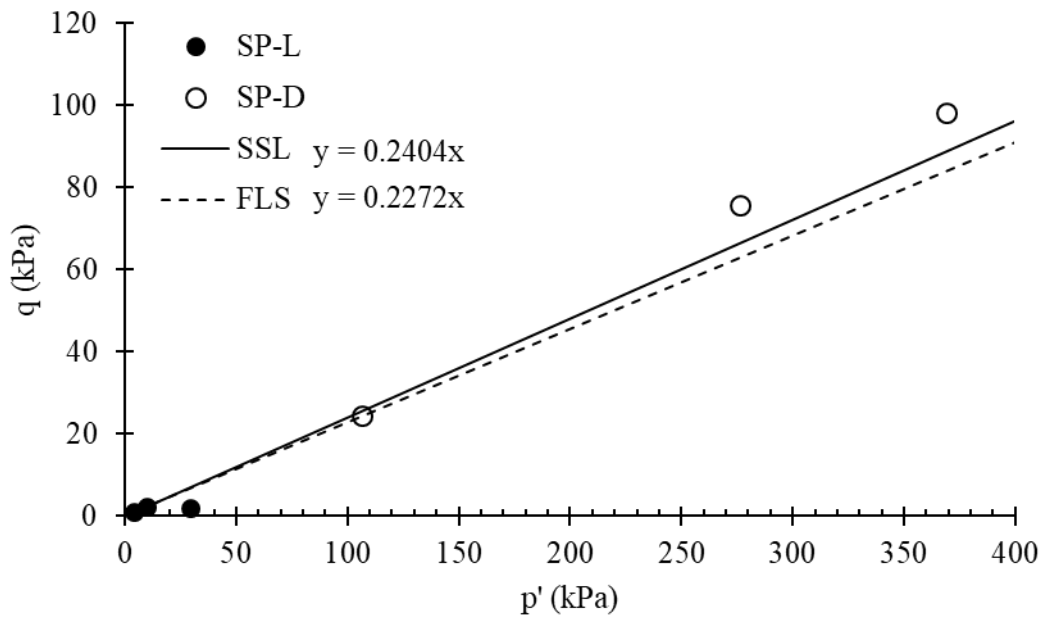


Figure 166: SSL and FLS of Sand.

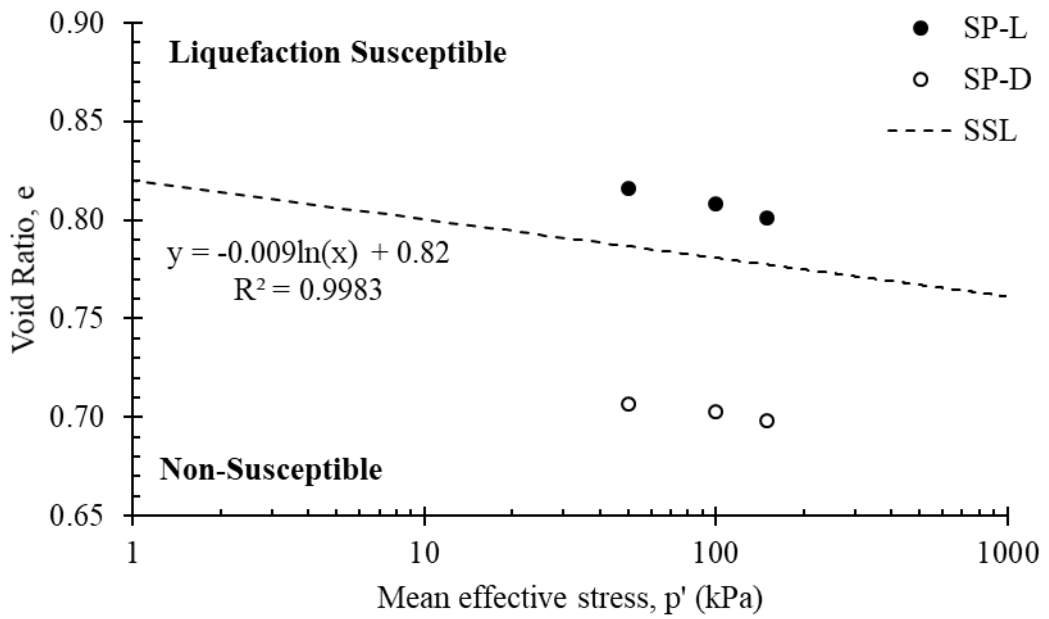


Figure 167: Steady state liquefaction susceptibility analysis.

Table 16: Steady state parameters of loose and dense sand.

Parameters	Loose			Dense		
	50	100	150	50	100	150
Ψ	+0.031	+0.029	+0.026	-0.077	-0.0755	-0.076
r_u	0.96	1	1.03	-0.91	-0.87	-1.10
u_f (%)	26.4	96.1	100	-	-	-
ϕ_{ss} (Degrees)		12.8			14.9	

4.7.4 Monotonic Loading Undrained Response of Silty-Sand

4.7.4.1 Loose State

The undrained response of SP-SM group is presented in this section. The undrained behaviour of sand at loose state ($D_R = 35\%$) is simulating the flow liquefaction behaviour for all confining stresses. In comparison, initially 10% of fines in this groups are added to observe the stability improvement of sand-fines structure. In Figure 168 stress-strain curve and in Figure 169, excess pore water pressure generated during monotonic loading is presented. In Figure 170, stress paths are plotted for loose silty-Sand specimens.

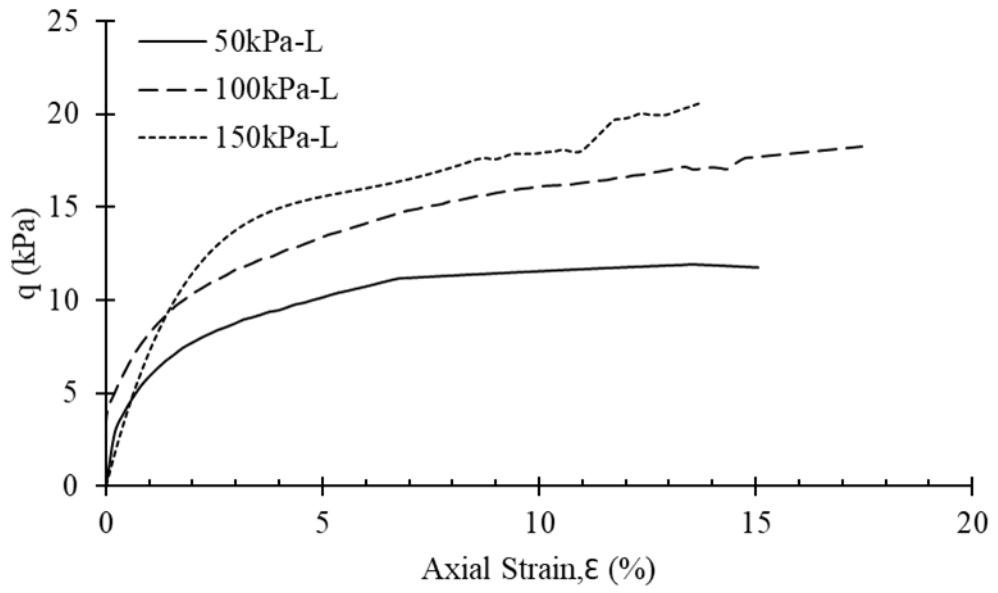


Figure 168: Undrained response of loose SP-SM (10%).

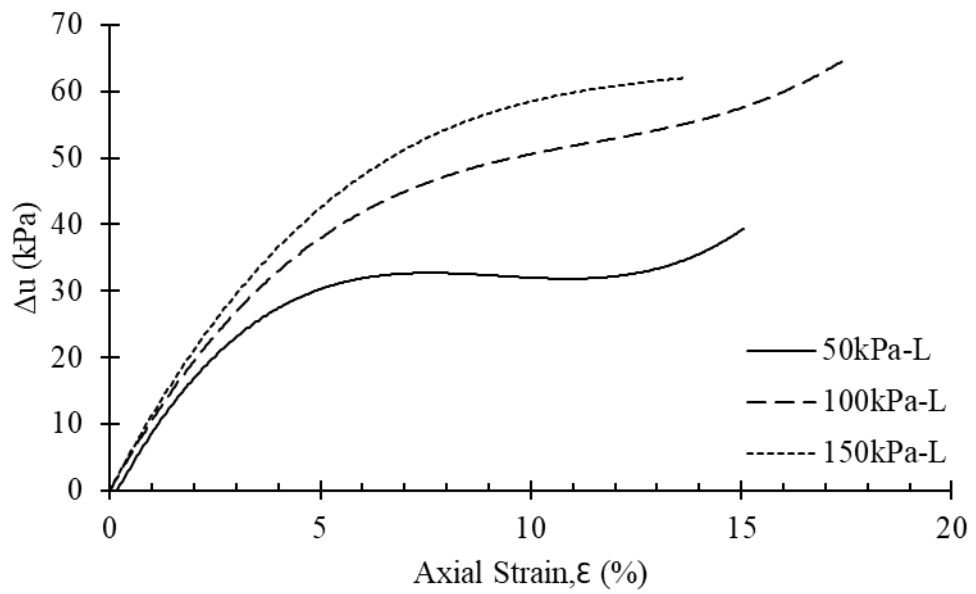


Figure 169: Pore-water pressure development in loose state SP-SM (10%).

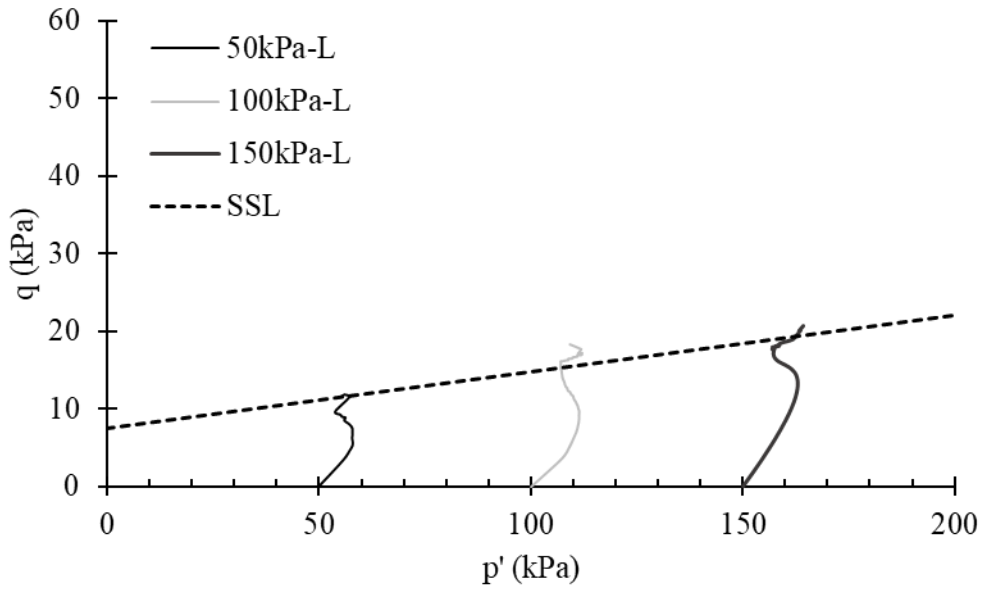


Figure 170: Stress paths of loose specimen SP-SM (10%).

In Figures 171 – 173, effect of 20% inclusion silt in Sand matrix is presented.

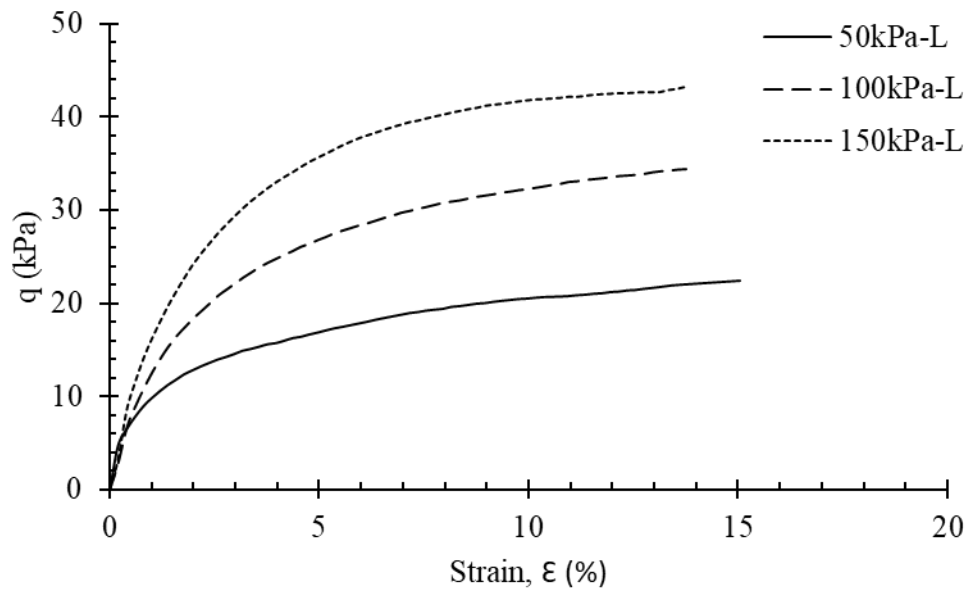


Figure 171: Undrained response of loose base SP-SM (20%).

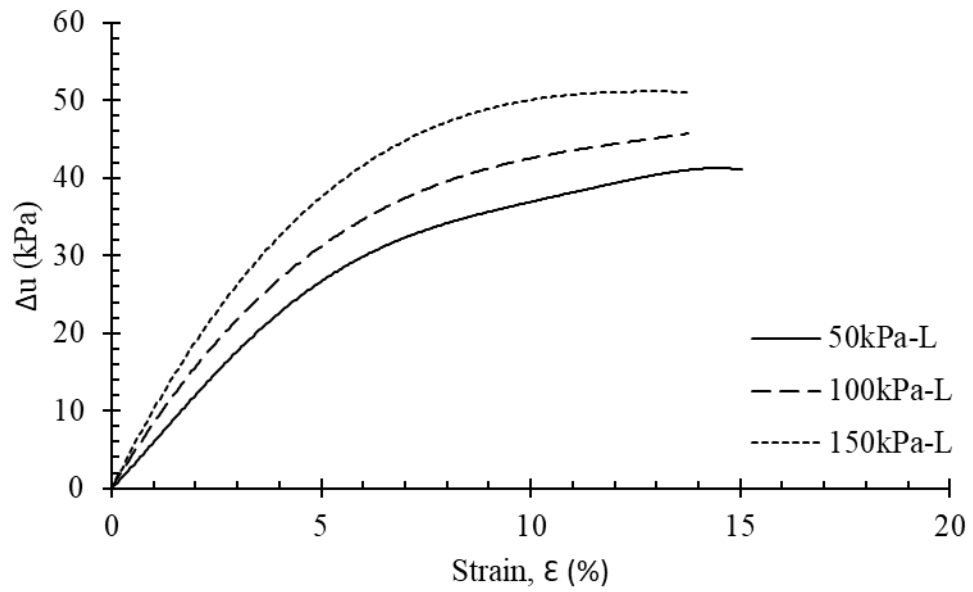


Figure 172: Pore-water pressure development in loose state SP-SM (20%).

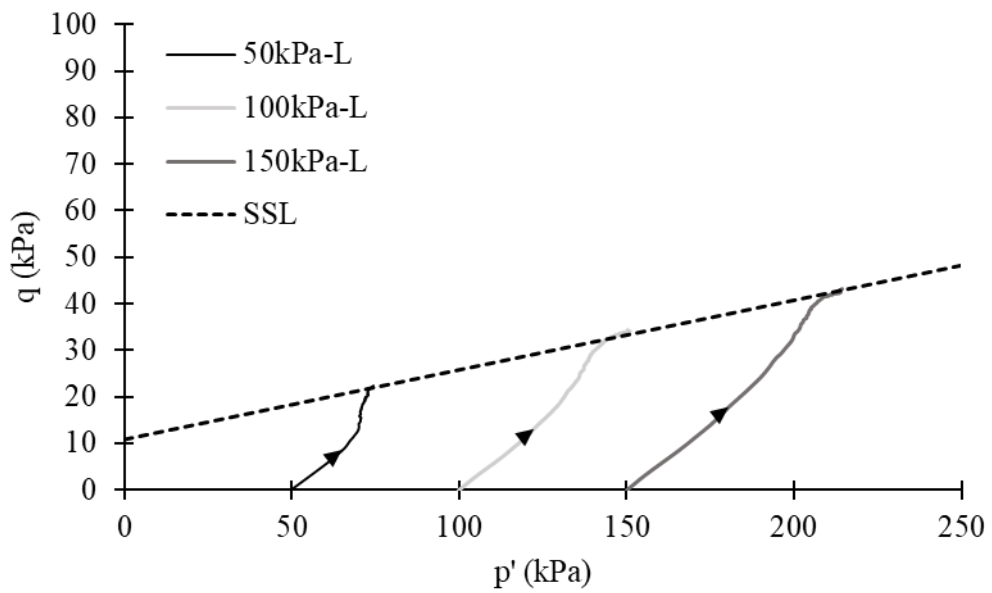


Figure 173: Stress paths of loose specimen SP-SM (20%).

The effect of 30% inclusion of silt fraction in Sand matrix on stress-strain, pore water pressure development is illustrated in Figure 174 and Figure 175 respectively.

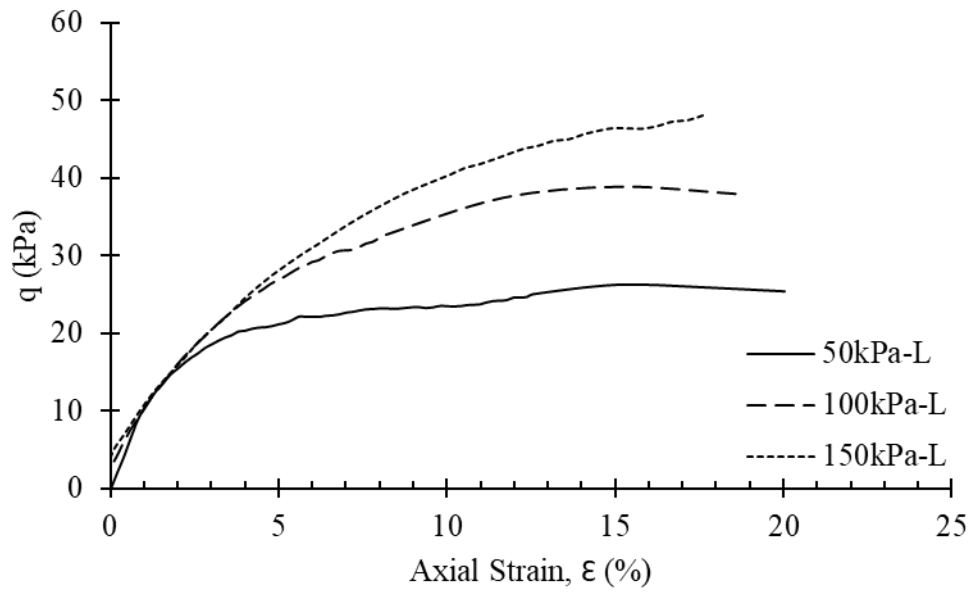


Figure 174: Undrained response of loose base SP-SM (30%).

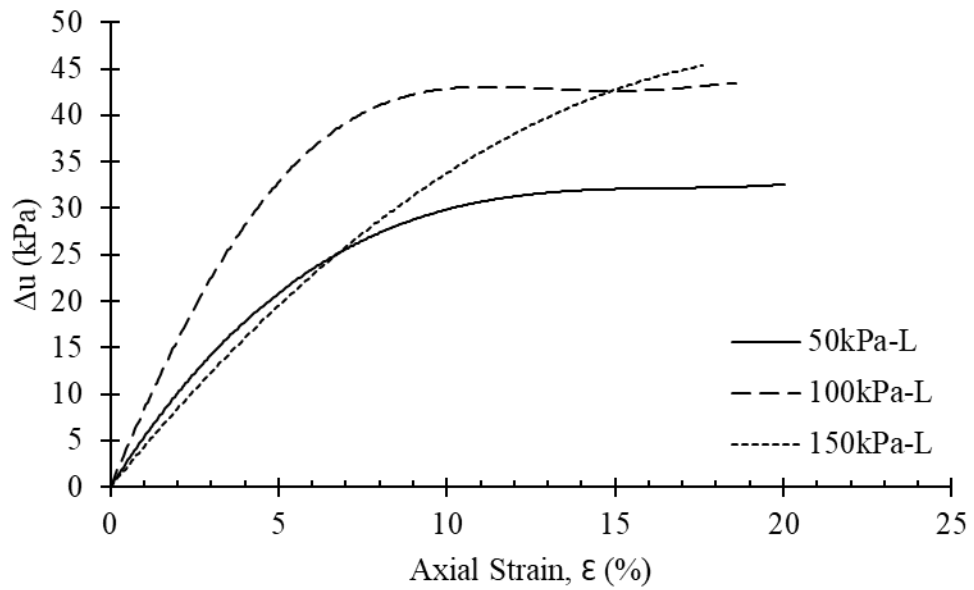


Figure 175: Pore-water pressure development in loose state SP-SM (30%).

In Figure 176, q - p' space (Stress path) of 30% SP-SM group is illustrated.

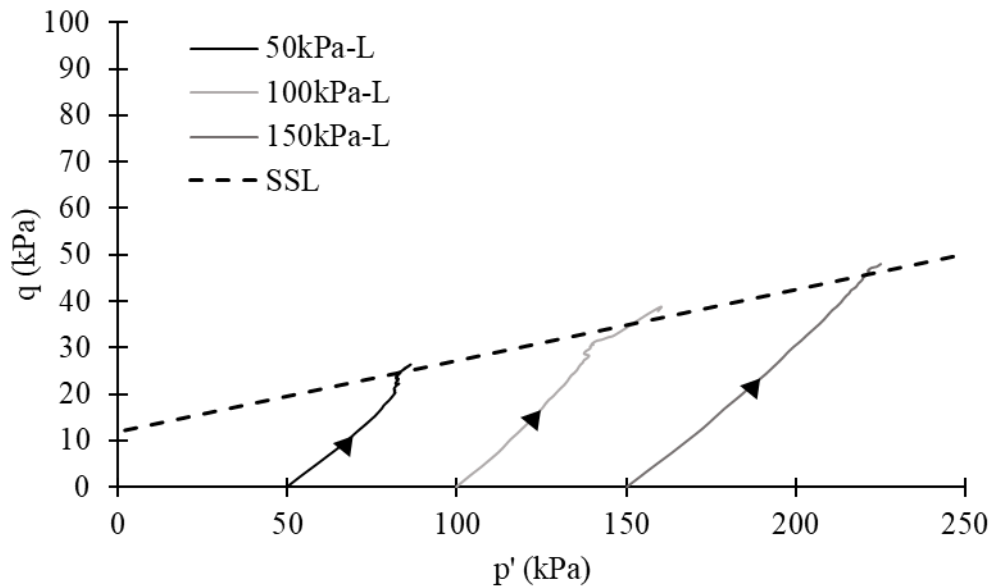


Figure 176: Stress paths of loose specimen SP-SM (30%).

Silty-sand mixture with all proportions are exhibiting stable state. In terms of pore-pressure development, it is observed that as the silts fractions increase, excess pore-pressure reduces. Three primary factors can be associated with such phenomenon, such as water-absorption capacity of fines increases, secondly permeability reduces therefore build up pore-pressure is only observed at low fines content and thirdly initial state (post-consolidation void ratio).

In Figure 168, at 10% of fines content, it is observed that for 100 and 150 kPa of confining stresses after approximately 11% of strain level, strain hardening is observed for loose specimens. The strain hardening occurred due to transformation of sample state from loose to medium state. Another reason can be associated in terms of behavioural aspect is since 10% of fines is threshold fines content where pores between the sand grains are filled with silt particles and as the deviator stress increases, it can assumed that at larger strains the sand particles are dominating over fines where

contact forces between sand grains are close enough to transfer the applied forces, hence exhibiting strain hardening or non-flow behaviour.

4.7.4.2 Dense State

Dense specimen behaviour of silty-sand mixture with 10% fines presence is illustrated in Figures 177 – 179.

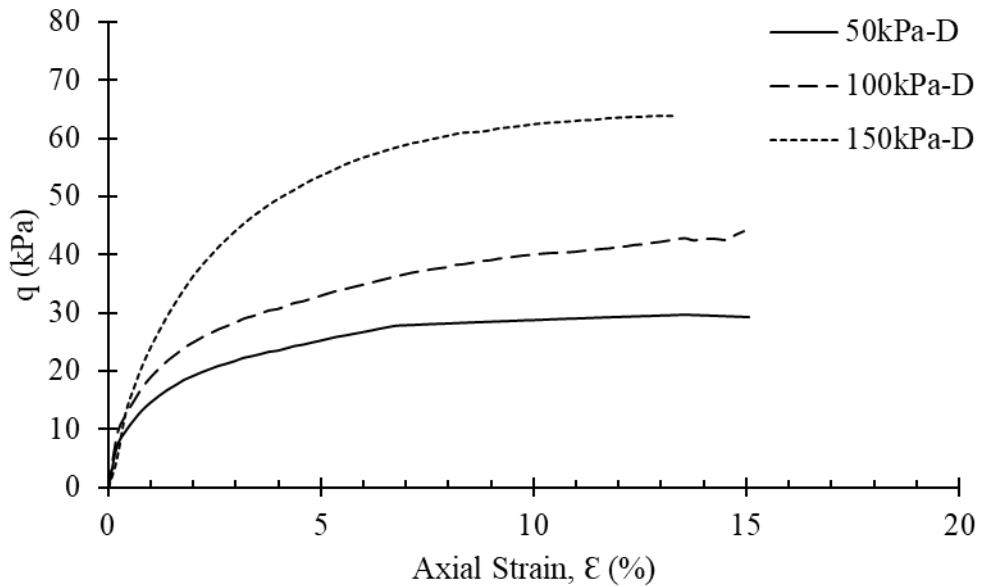


Figure 177: Undrained response of dense SP-SM (10%).

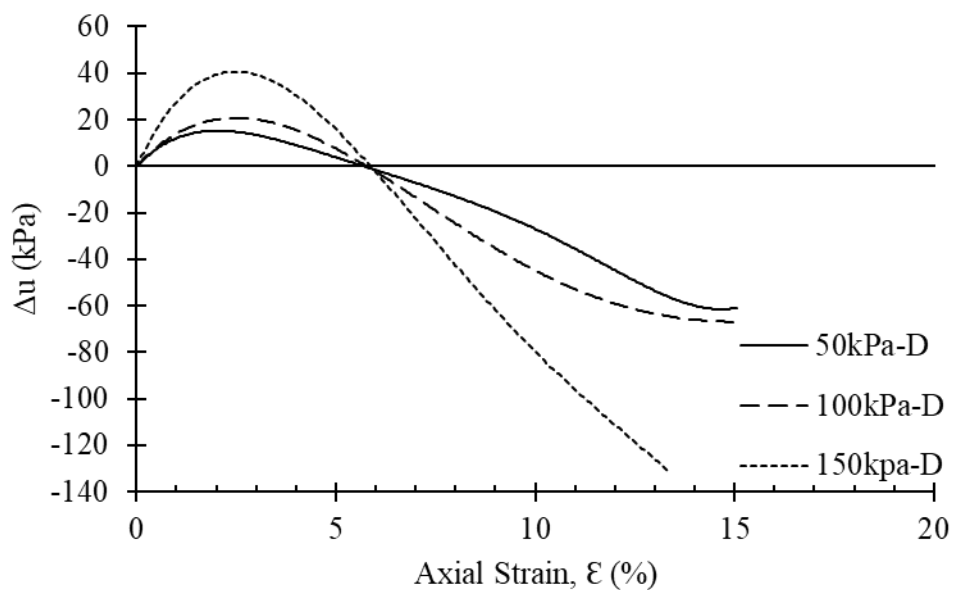


Figure 178: Pore-water pressure development in dense state SP-SM (10%).

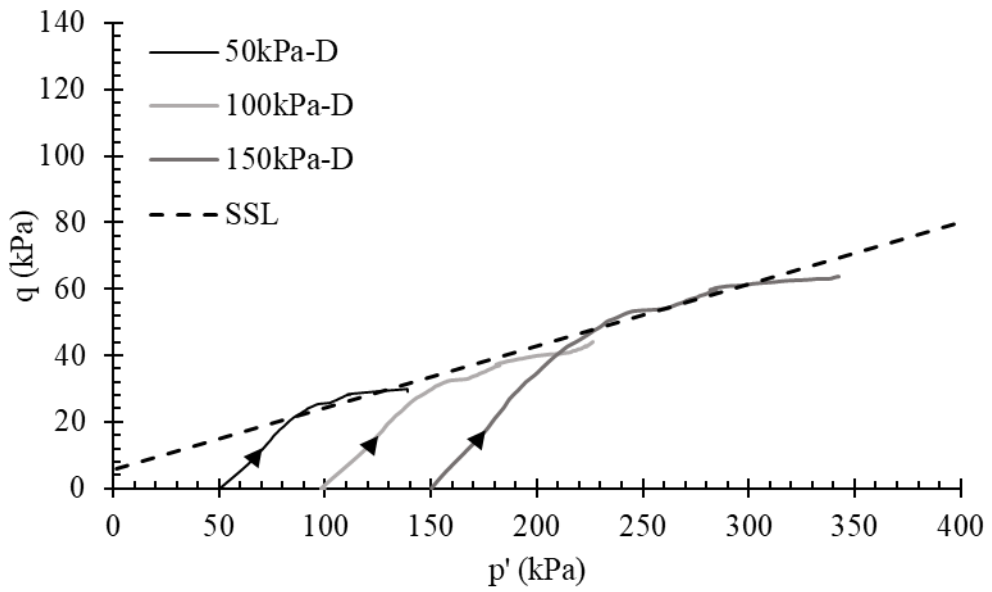


Figure 179: Stress paths of dense specimen SP-SM (10%).

In Figures 180 – 182, fine dominant group composed of 20% silt fractions in sand-matrix is presented.

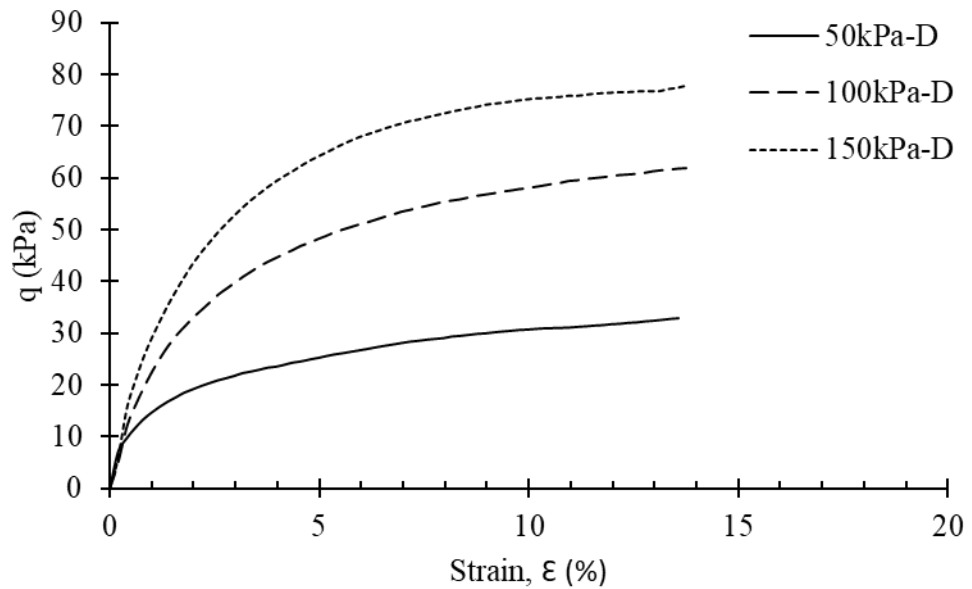


Figure 180: Undrained response of dense SP-SM (20%).

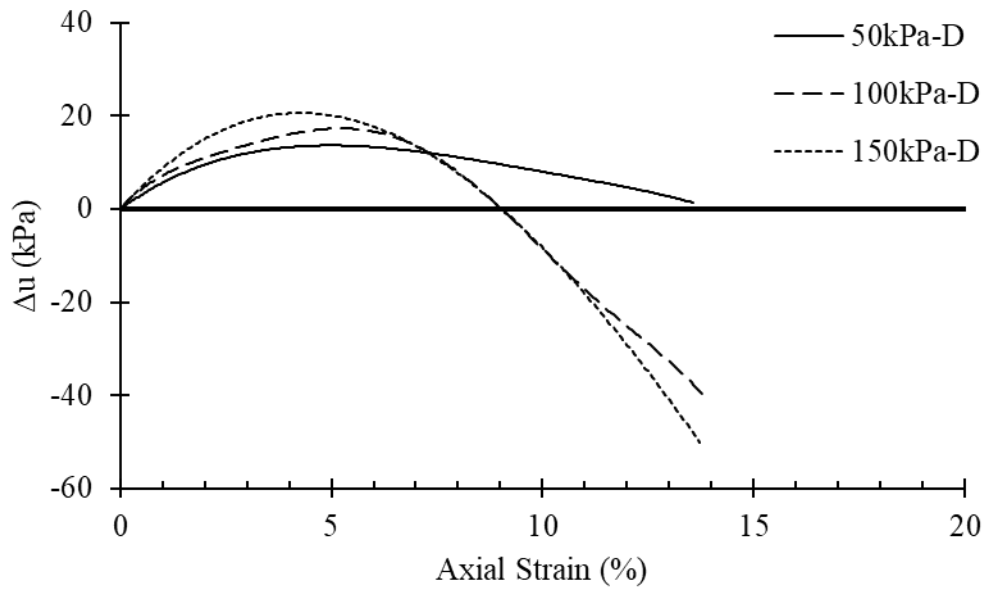


Figure 181: Pore-water pressure development in dense state SP-SM (20%).

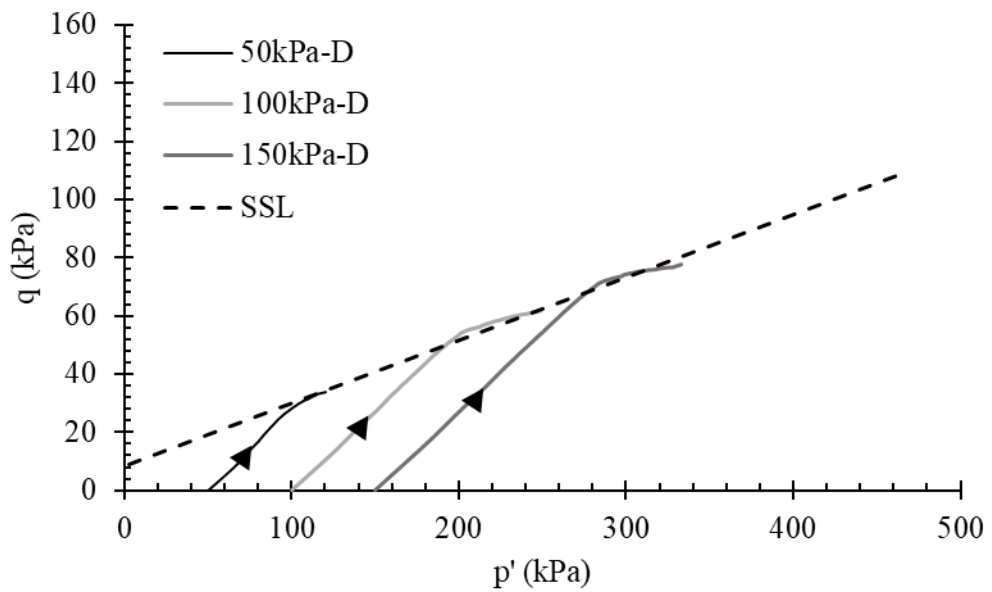


Figure 182: Stress paths of dense specimen SP-SM (20%).

Undrained behaviour of Dense silty-Sand mixtures is exhibiting similar characteristics as of dense Sand (Figure 163). In terms of pore-pressure development in SP-SC (20%), an initial increase in pore-pressure is generated up to 5% of axial strain within specimen and starts to decrease for 100 and 150 kPa of confining stresses (Figure 181) due dilation.

Partial replacement of 30% sand particles by silt fractions behaviour is illustrated in Figures 183 - 185.

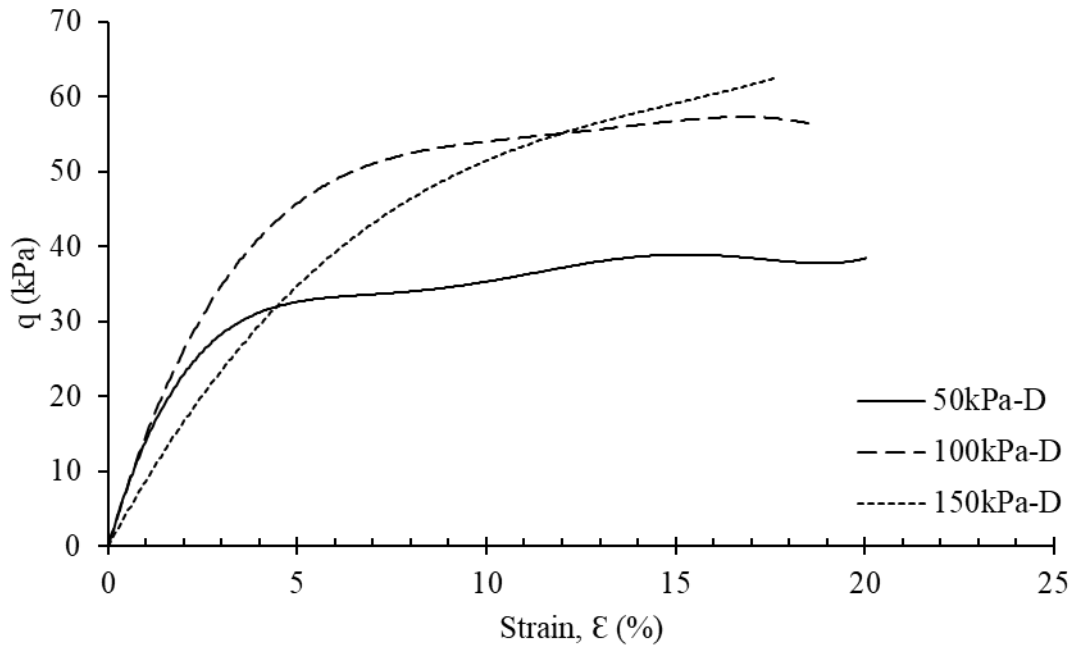


Figure 183: Undrained response of dense SP-SM (30%).

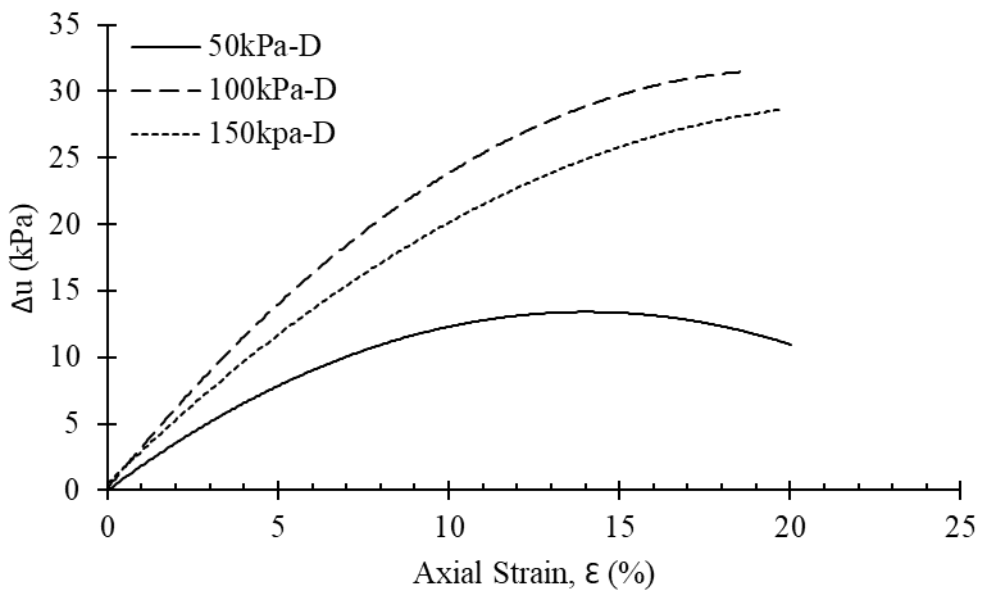


Figure 184: Pore-water pressure development in dense state SP-SM (30%).

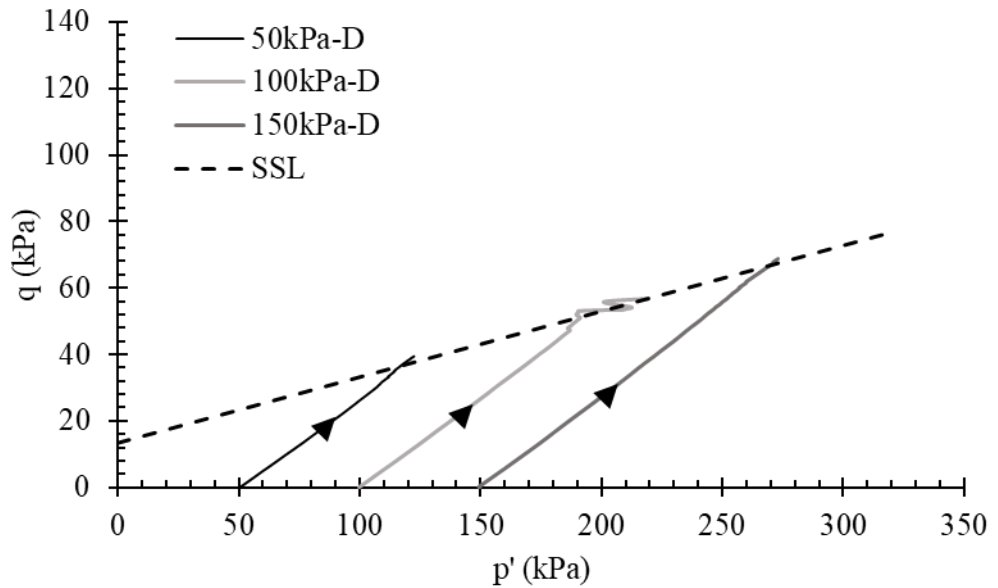


Figure 185: SP-SM (30%) stress paths of dense specimen.

The undrained behaviour of 30% differs from the first two groups. Although the specimen is prepared at dense state, positive pore-pressure is developed in all cases (Figure 184). Since 30% of fines inclusion is directly associated to volume increase of silt fractions indicating the role of microstructure for pore water pressure development. Again, the pore-pressure development in SP-SM 30% in dense state as compared to loose state, the pore water pressure development is not significance. Such phenomenon can be associated to reduction in permeability of sample where the pore sizes are small enough and irregular travel path of fluid within the sample is developed.

Steady state analysis of SP-SM groups is presented in next sub-section along with the comparison with base sand.

4.7.4.3 Critical and Steady State Analysis SP-SM Groups

The steady state line of all silt groups is plotted in Figure 188 with comparison to Sand. In Figure 186, the steady state points observed SP-SM at loose state are plotted and it is observed that SSL slope of Sand is steeper as compared to silt groups. From such observations it is noted that gradual incline in SP-SM groups reduces the steady state angle. Although reduction in SSL angles corresponds to instability factor, but cohesion factor is more pronounced. By observing the shear stress equation ($\tau = c' + \sigma_n' \tan \phi'$), as the increment of excess pore water generation reduces the effective stress, the plasticity of the soil will prevent instability in soil. Such behaviour is observed in the experimental evaluations of SP-SM groups.

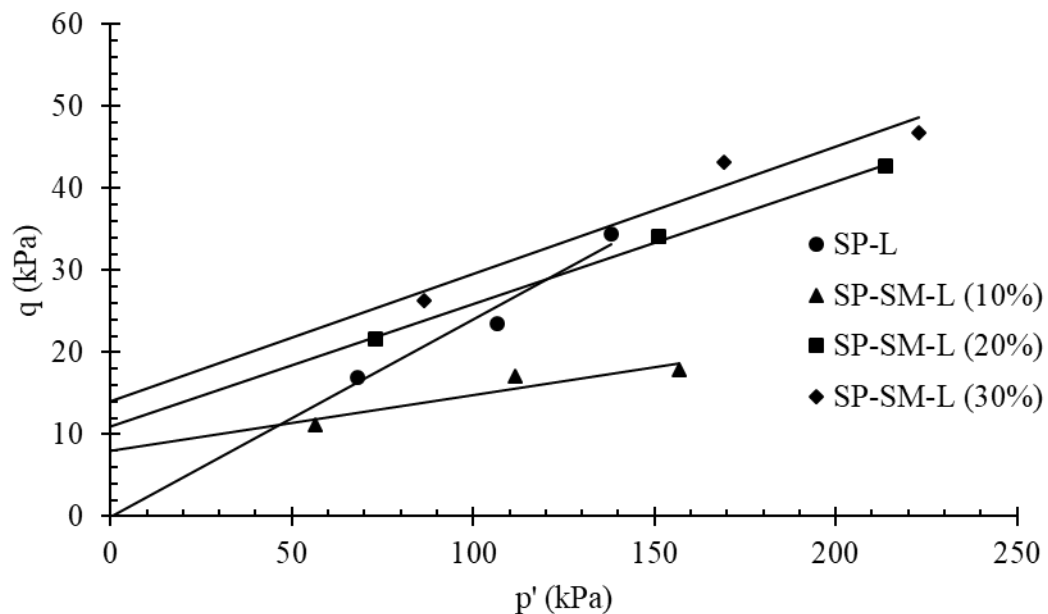


Figure 186: SSL comparison of SP-SM-L groups.

In Figure 187, the SSL obtained from dense specimens are presented.

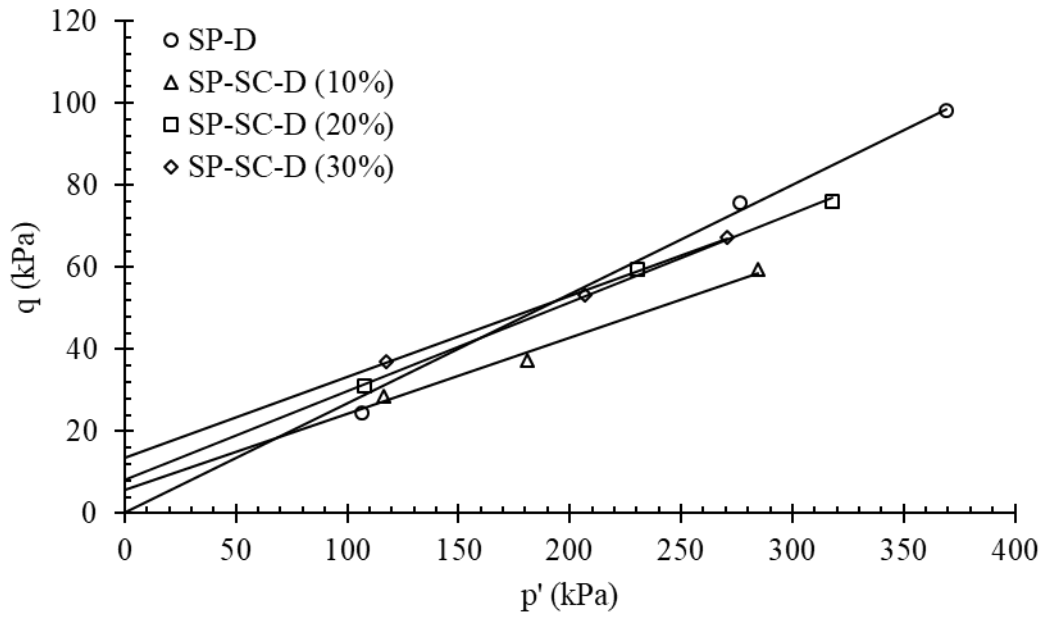


Figure 187: SSL comparison of SP-SM-D groups.

Since the SSL is a unique parameter for a soil, by observing Figure 186 and Figure 187, cumulative plot of SSL is established for both loose and dense states of all silty-Sand soil groups (Figure 188). The steady state points obtained from each state (loose and dense) are in good congruence by analysing linear regression analysis.

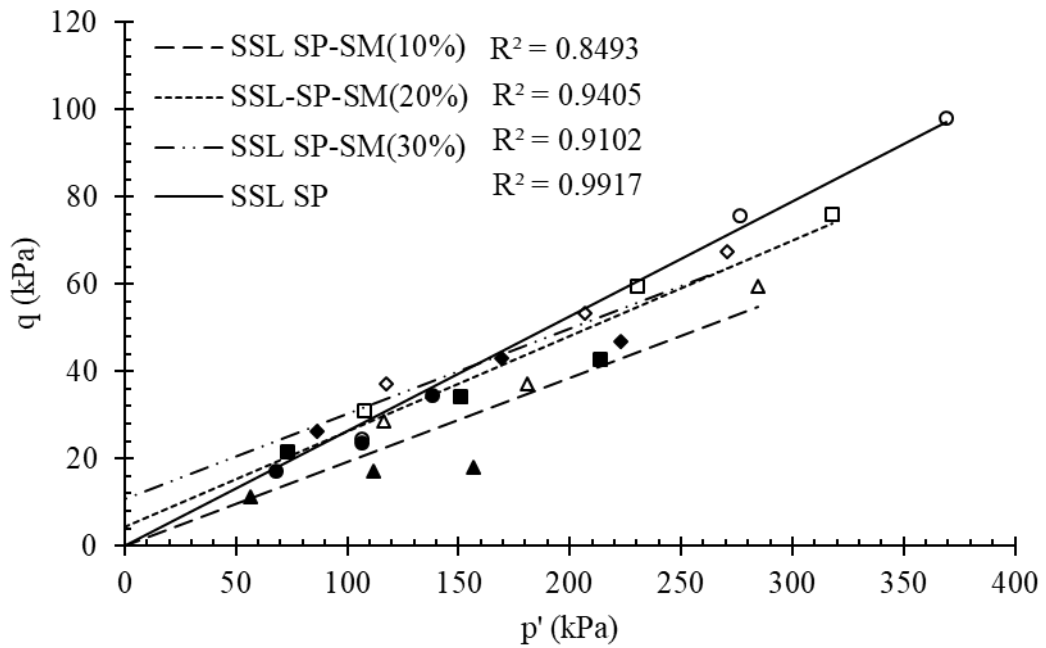


Figure 188: SSL cumulative plot of SP-SM groups.

Based on SSL theory, in Figures 189 – 191, initial states of soil groups are plotted to analyse the liquefaction susceptibility.

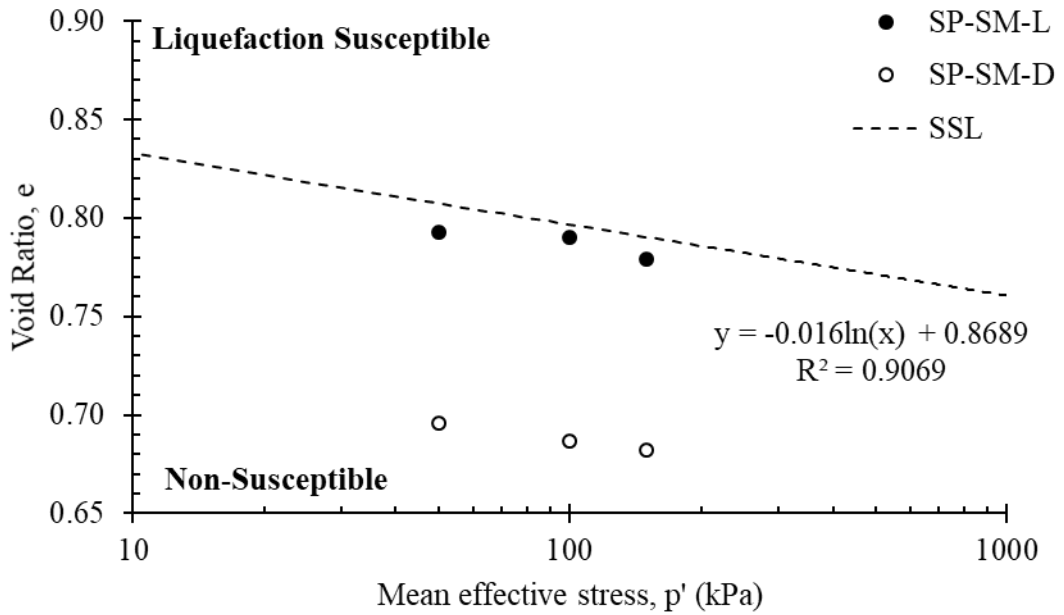


Figure 189: SSL liquefaction susceptibility SP-SM (10%).

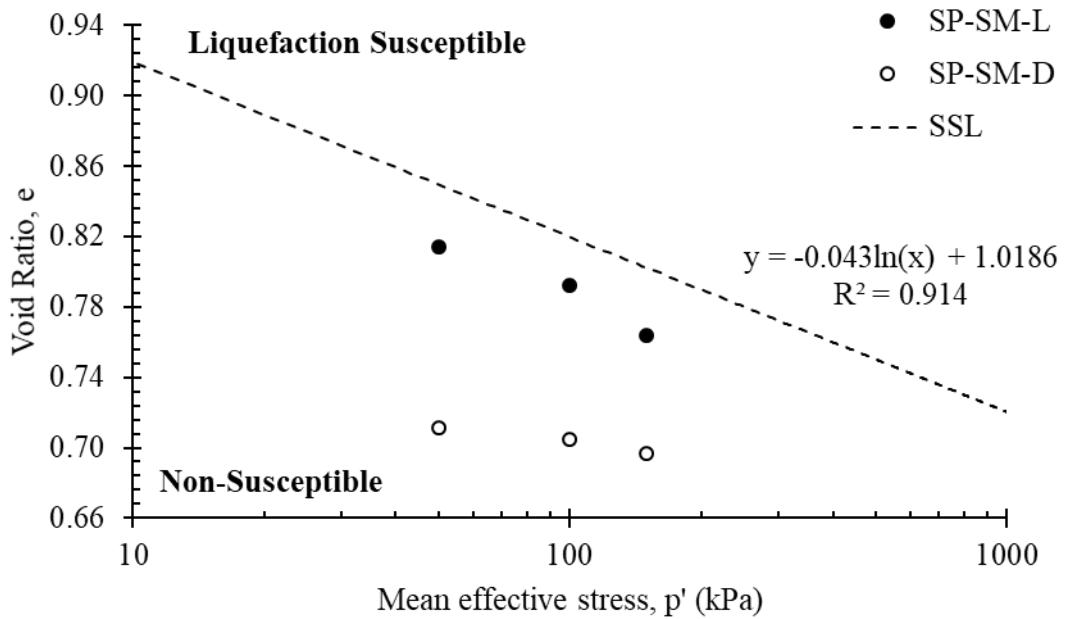


Figure 190: SSL liquefaction susceptibility SP-SM (20%).

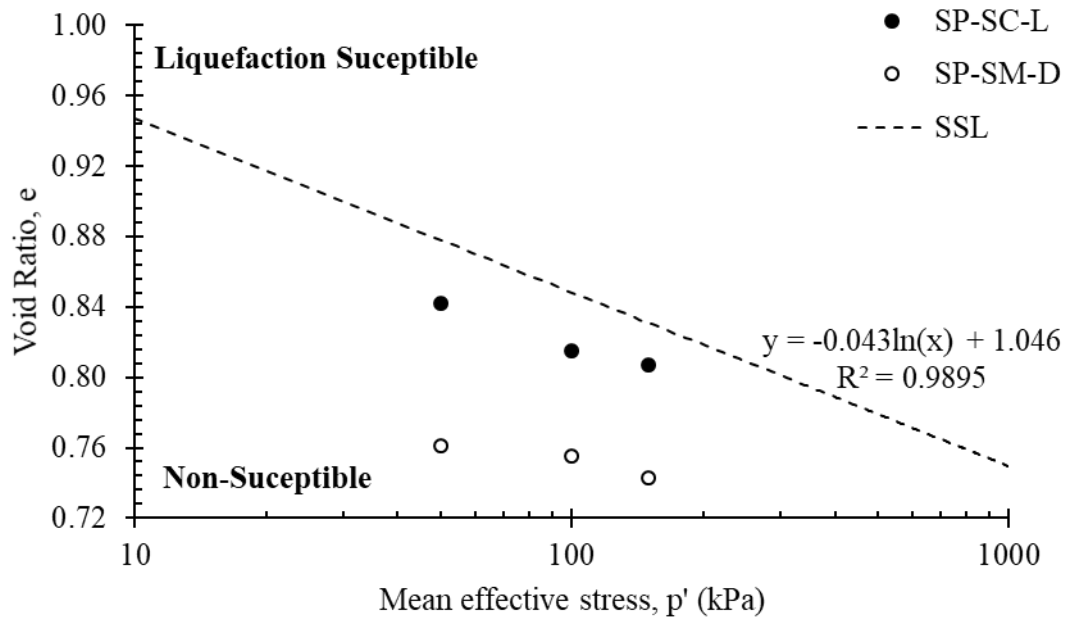


Figure 191: SSL liquefaction susceptibility SP-SM (30%).

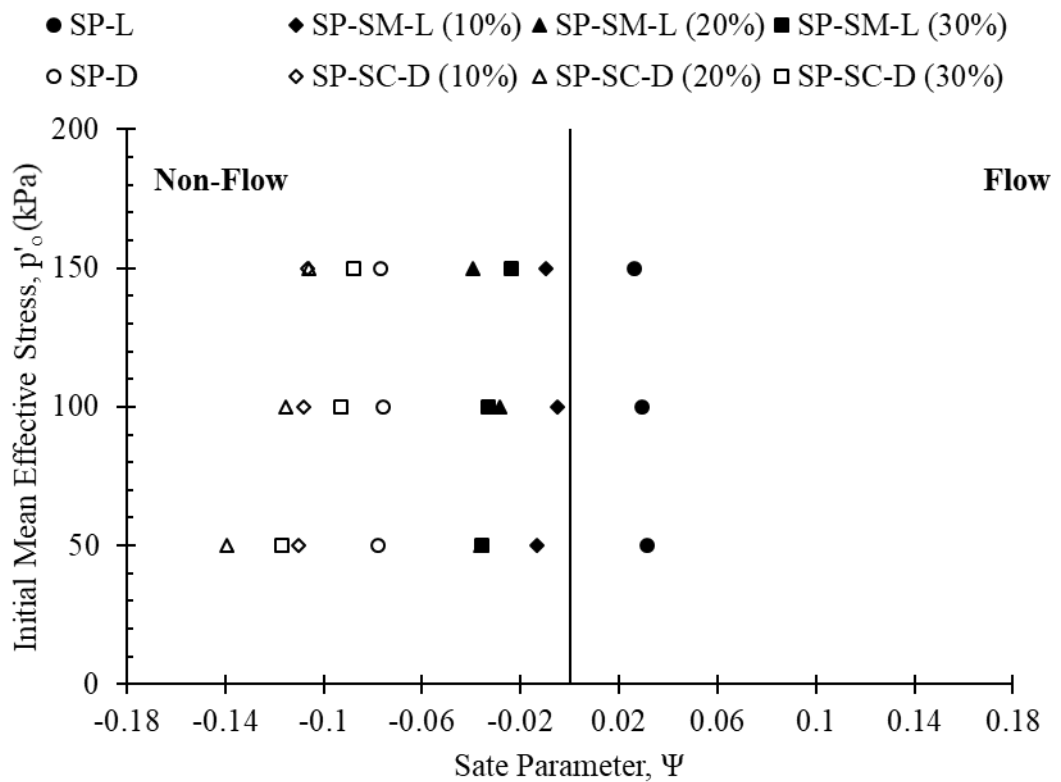


Figure 192: SP-SM state parameter.

Steady state limit analysis of all SP-SM groups and their respective initial states are plotting below the SSL, thus indicating the non-flow behaviour. A notable difference is observed that 10% of fines are plotting very close to SSL indicating the significance of flow potential analysis (Figure 192). Another assessment criterion is the evaluation of state parameter ($\Psi = e - e_{ss}$) in undrained testing, flow behaviour is associated with positive value and non-flow or strain hardening behaviour is associated with negative value. State parameter for various SP-SM soil groups and SP is illustrated in Figure 189. Since 10% silt fractions in Sand matrix are plotting very close to SSL, state parameter value will provide an accurate representation of flow or non-flow aspect as given in Table 17.

As discussed earlier due to positive pore-pressure development, flow potential analysis is necessary. In Figure 193, variation of pore-pressure ratio with fines are plotted. Since the negative r_u value is directly associated with non-flow aspect, therefore flow potential analysis (u_f) is applied to only those specimens exhibiting positive r_u values which are close to 1 or greater than 1.

Table 17, summarizes the critical state outcomes of undrained SP-SM behaviour.

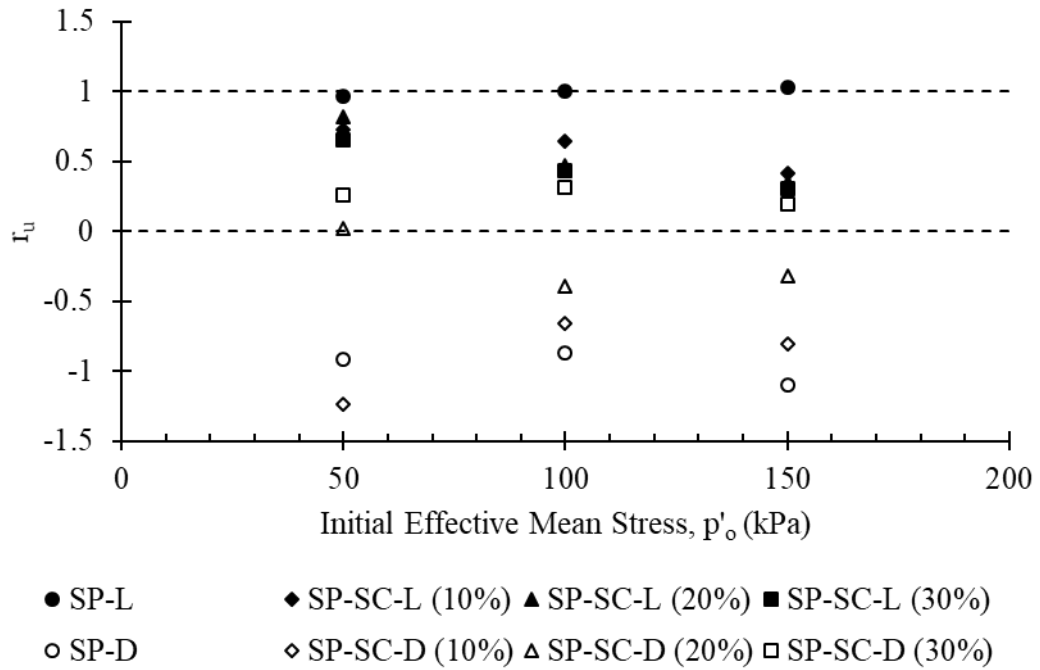


Figure 193: SP-SM pore pressure ratio variation.

Table 17: Steady state parameters of silty-sand groups.

p'_o (kPa)	State	Fines Content (%)					
		10		20		30	
		Ψ	r_u	Ψ	r_u	Ψ	r_u
50		-0.013	0.724	-0.036	0.82	-0.036	0.650
100	Loose	-0.005	0.648	-0.029	0.468	-0.033	0.434
150		-0.010	0.414	-0.039	0.350	-0.024	0.309
50		-0.110	-1.238	-0.139	0.241	-0.117	0.26
100	Dense	-0.108	-0.662	-0.116	-0.3922	-0.093	0.311
150		-0.107	-0.808	-0.106	-0.3186	-0.088	0.195

4.7.5 Monotonic Loading Undrained Response Clayey-Silty-Sand

4.7.5.1 Loose State

Effect of 10% clays and silts presence by dry mass in sand matrix is explained is

Figures 194 – 196.

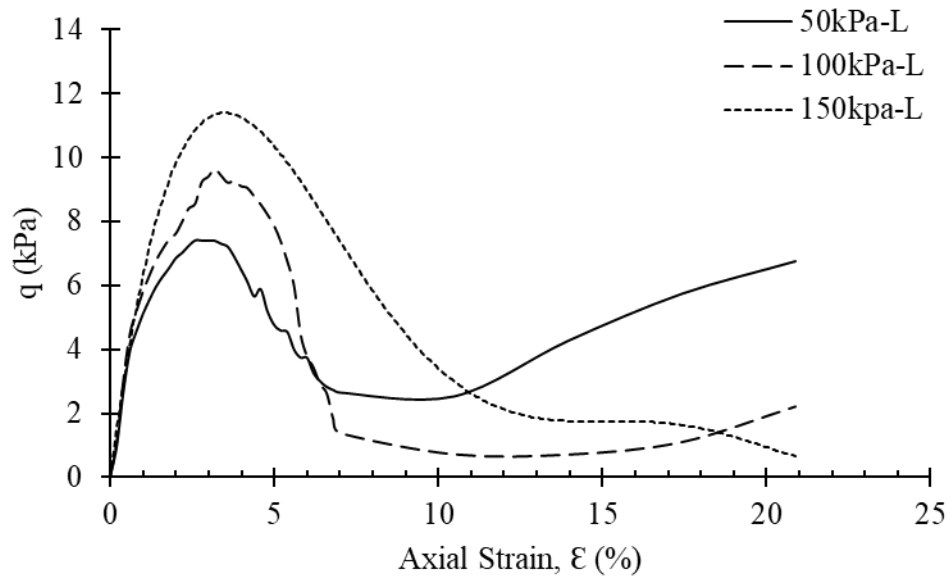


Figure 194: Undrained response of loose SM-SC (10%).

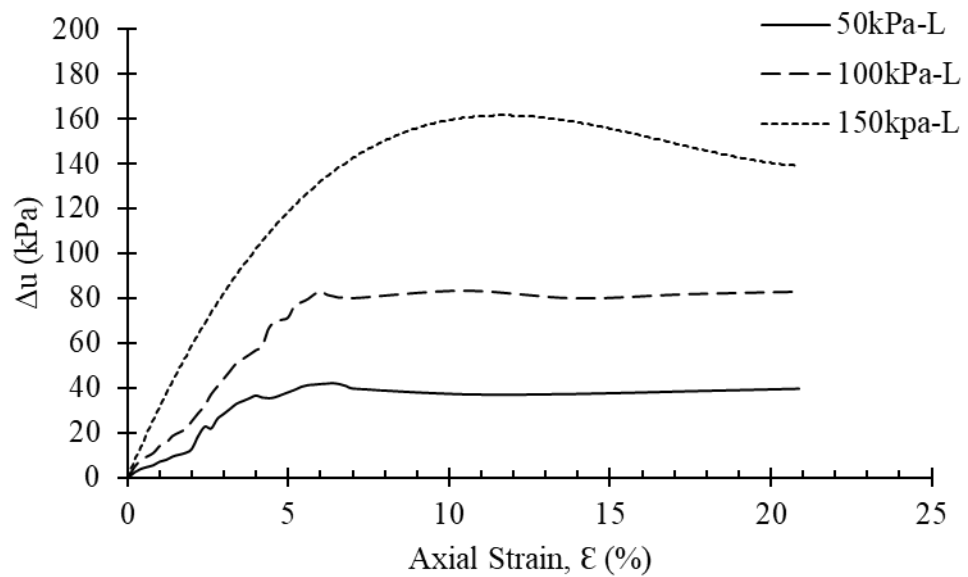


Figure 195: Pore-water pressure development in loose state SM-SC (10%).

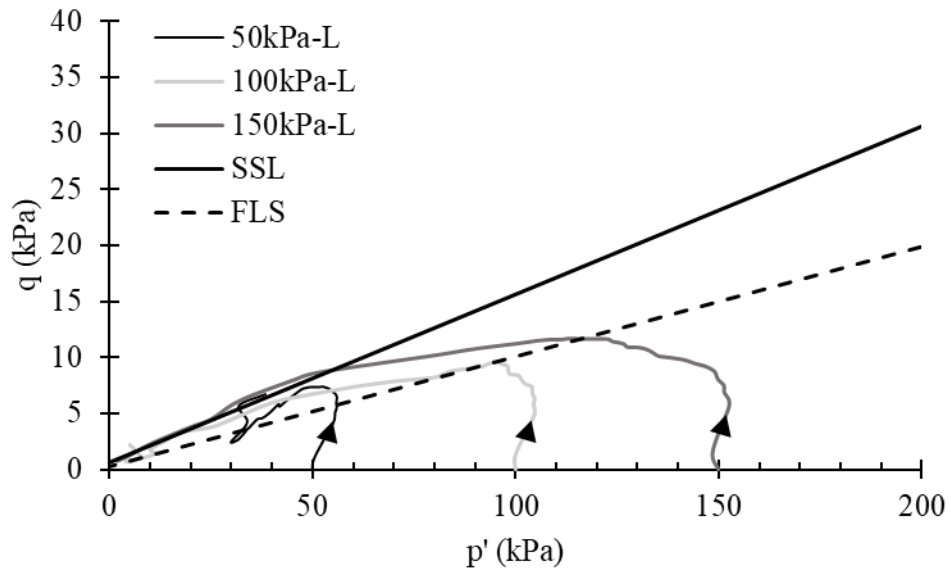


Figure 196: Stress paths of loose specimen SM-SC (10%).

From Figure 194, specimens at 50 and 100 kPa of confining stress is exhibiting limited liquefaction where quasi steady state is observed at 7% of axial strain level. Total flow liquefaction is observed at axial strain level of 16% for higher confining stress of 150 kPa. Prior to flow liquefaction, quasi-steady state is observed at strain level of 14%. The primary reason behind such phenomenon is observed by visual inspection as due to complex fabric structure, the mixed layers were transformed to individual layers for limited liquefaction case. This phenomenon occurred due to excessive pore water pressure generation, as the pressure is strong enough resulting in separation of layers (silt and clay fractions). From layers inspection it is observed that sand grains are not present in top layer and clay fractions are pumped out (Figure 248). Such phenomenon is termed as clay pumping from sand matrix. Intermediate layer is partially intact whereas, lower layer is composed of only sand grains. This phenomenon is explained in detail in section 4.8.

Figures 197 - 199, are the graphical plots of 20% silty-clayey fines influence in Sand matrix is presented.

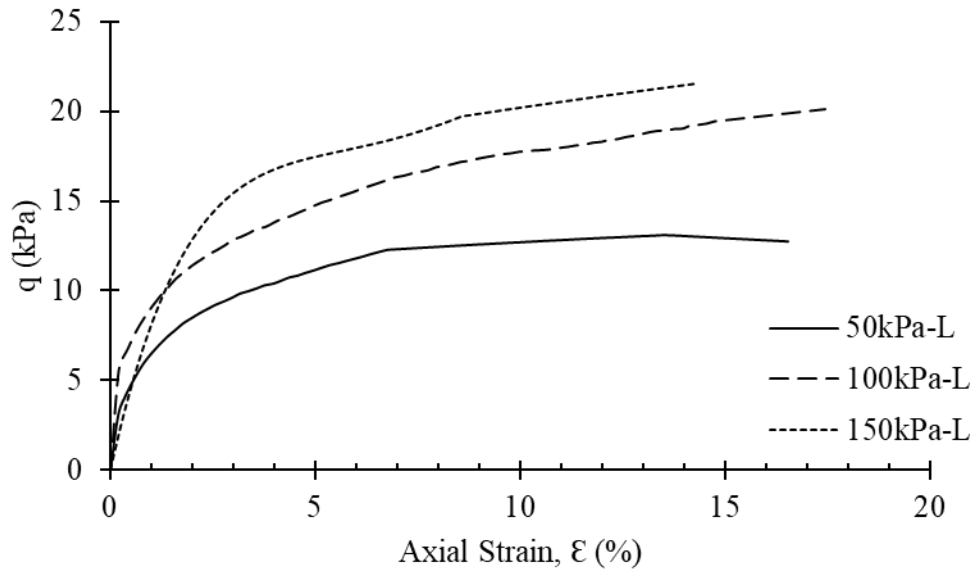


Figure 197: Undrained response of loose SM-SC (20%).

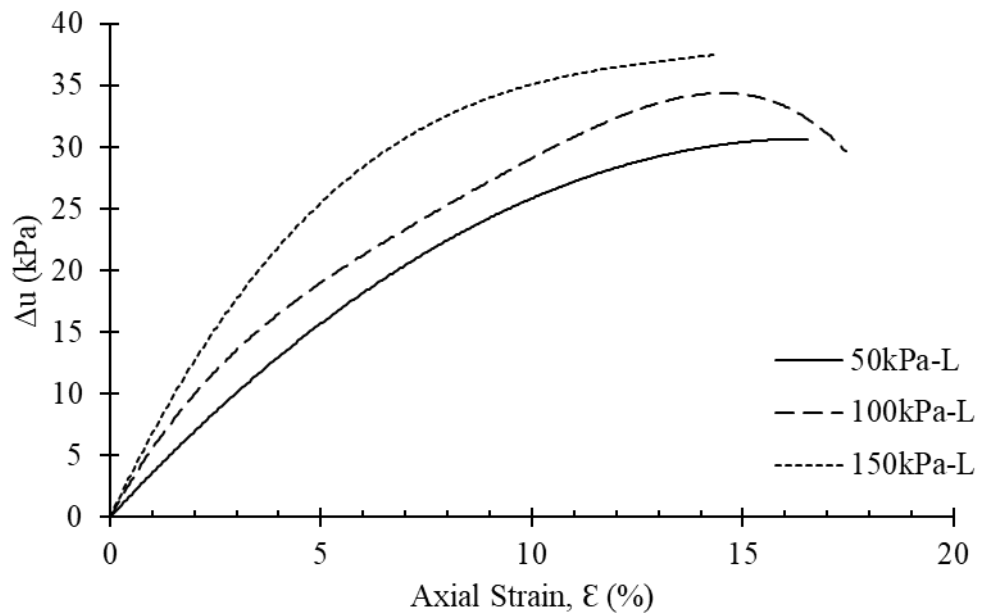


Figure 198: Pore-water pressure development in loose state SM-SC (20%).

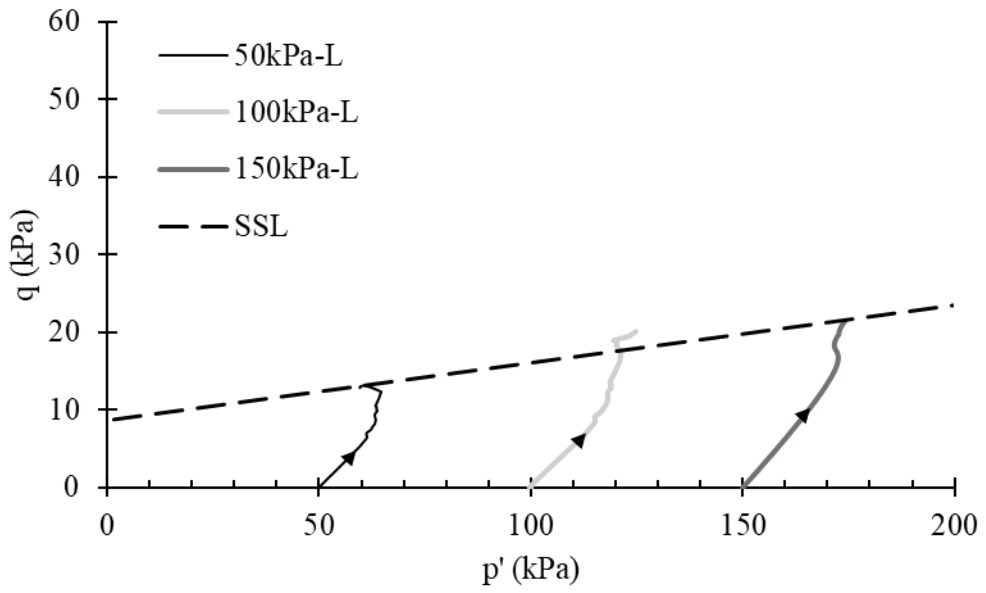


Figure 199: Stress paths of loose specimen SM-SC (20%).

Effect of 30% silt and clays with equal proportions in sand-matrix is illustrated in Figures 200 – 202.

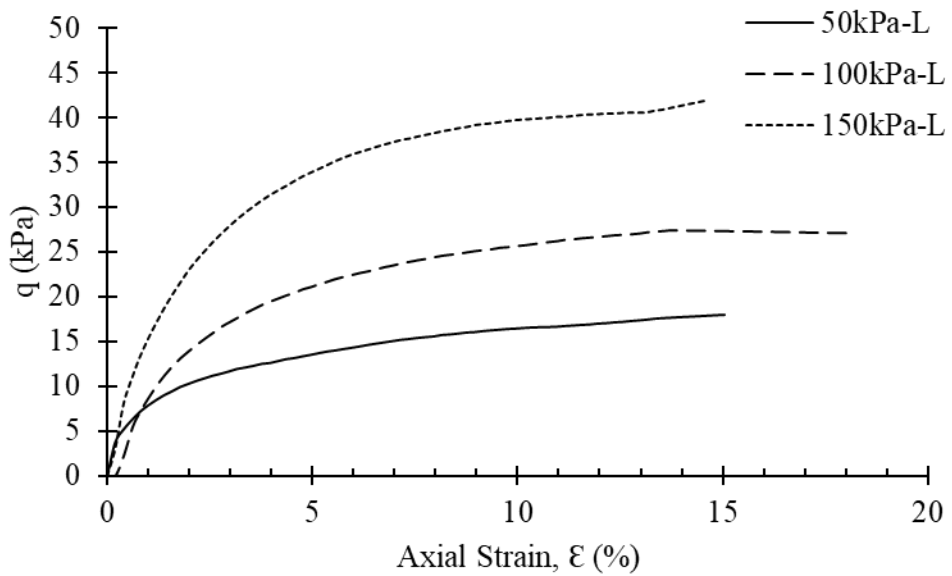


Figure 200: Undrained response of loose SM-SC (30%).

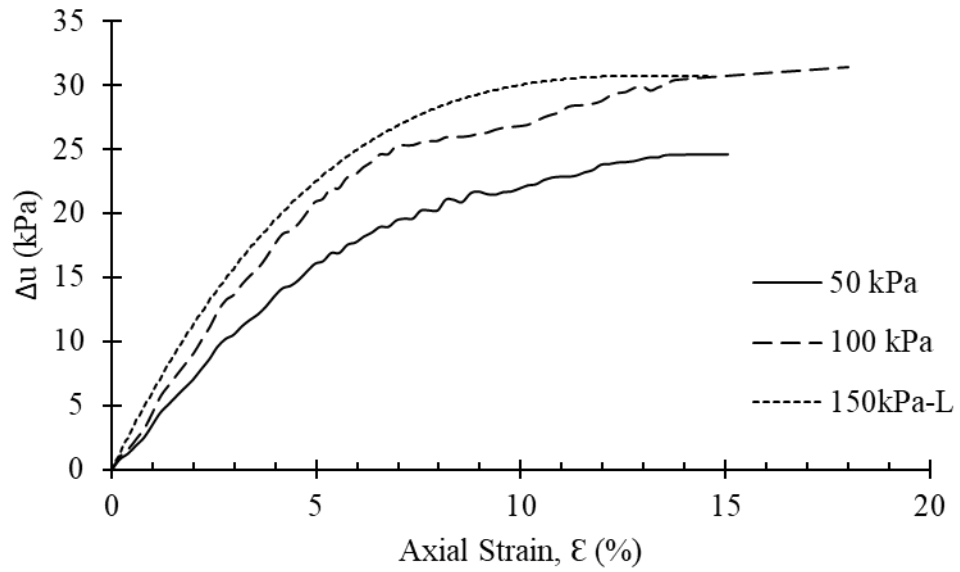


Figure 201: Pore-water pressure development in loose state SM-SC (30%).

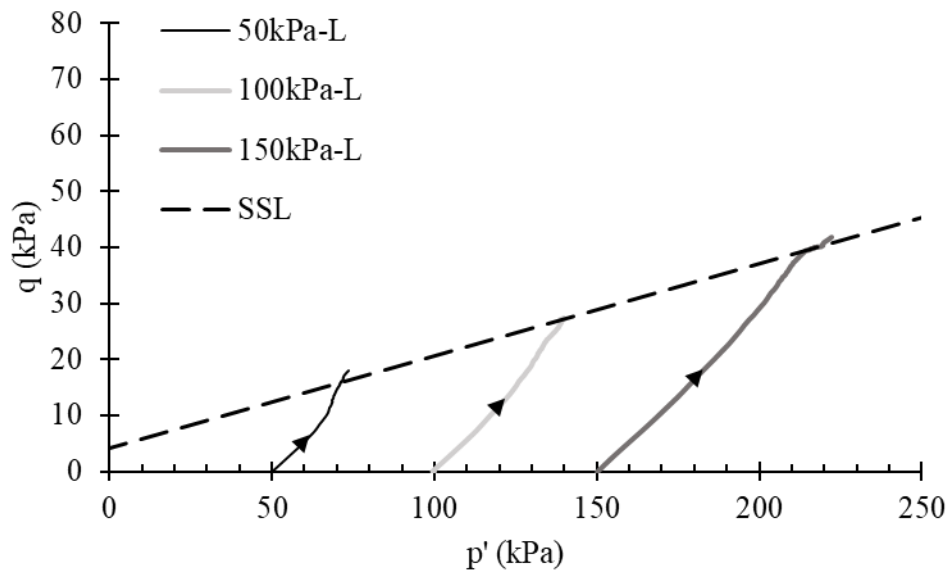


Figure 202: Stress paths of loose specimen SM-SC (30%).

Inclusion of 20 and 30 percentageS of fines improves the stability of sand-matrix. All specimens are exhibiting non-flow characteristics. Since after threshold fines content (TFC = 10%), the sand-matrix is completely transformed to fine-grained soil structure.

4.7.5.2 Dense State

In Figures 203 – 205, static behaviour of dense specimen under undrained conditions is emphasized for SM-SC (10%) group.

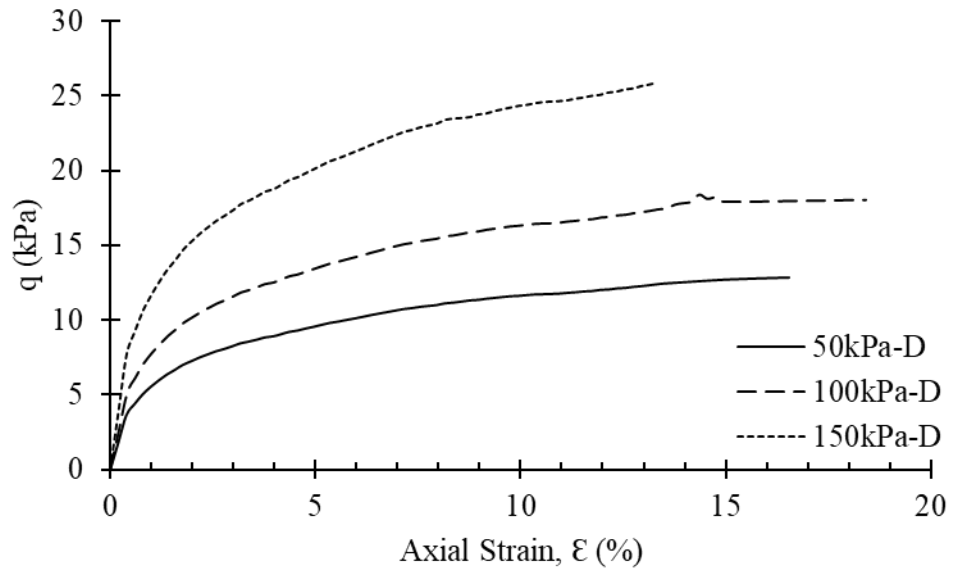


Figure 203: Undrained response of dense SM-SC (10%).

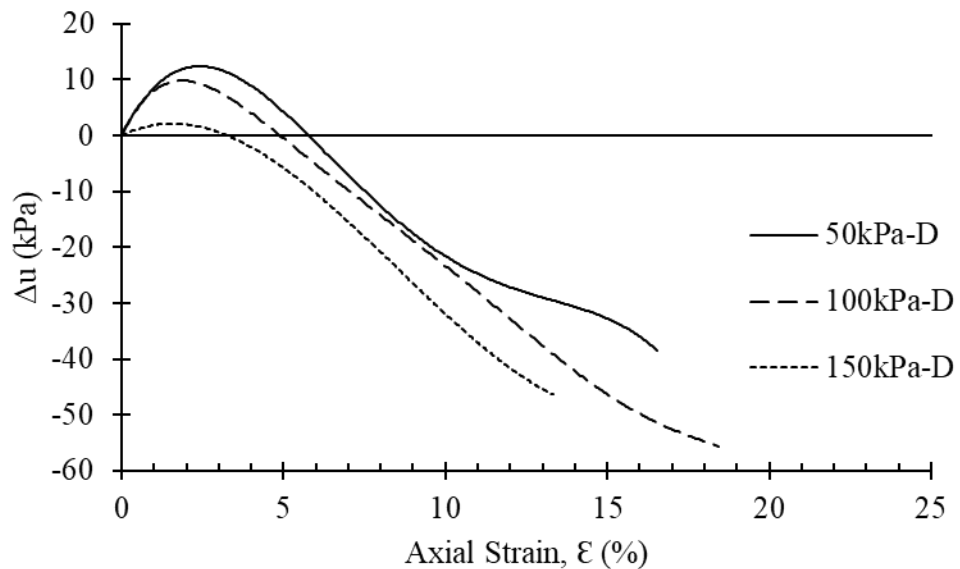


Figure 204: Pore-water pressure development in dense state SM-SC (10%).

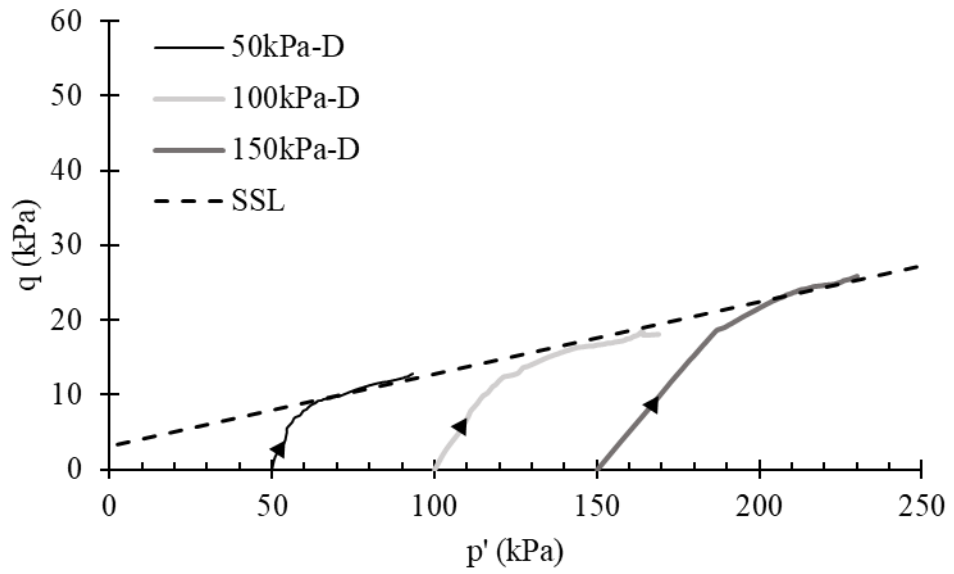


Figure 205: Stress paths of dense specimen SM-SC (10%).

Effect of 20% silty-clayey fines in sand-matrix is shown in Figures 206 – 208.

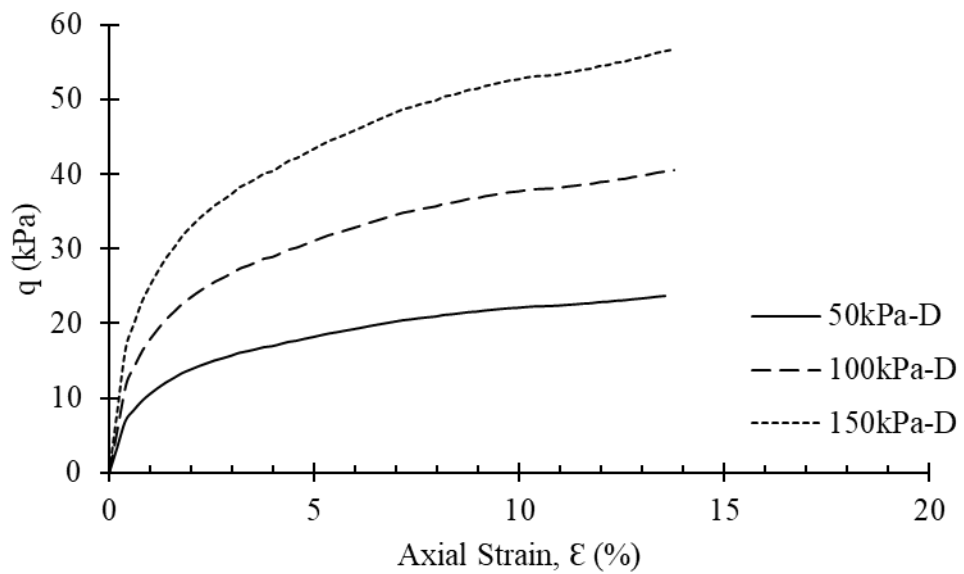


Figure 206: Undrained response of dense SM-SC (20%).

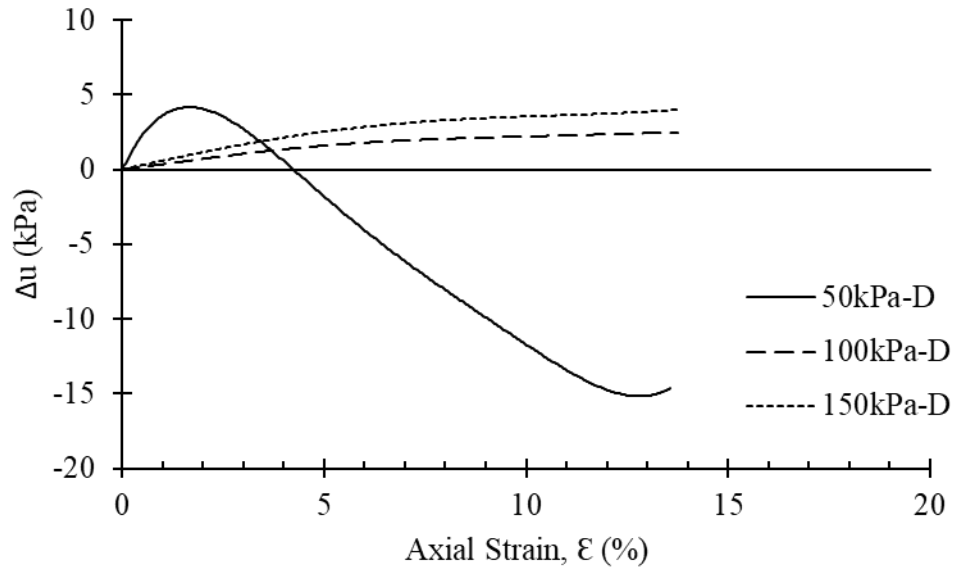


Figure 207: Pore-water pressure development in dense state SM-SC (20%).

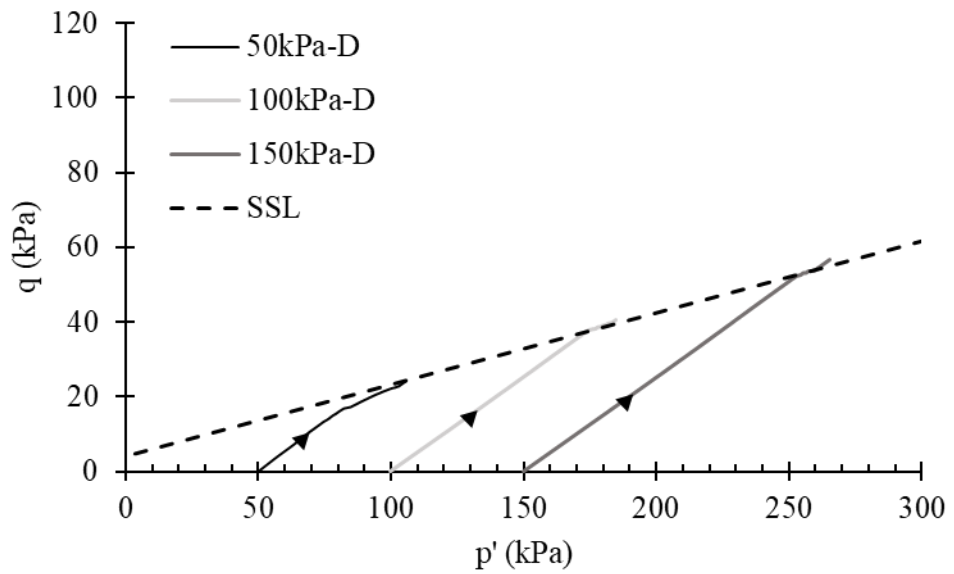


Figure 208: Stress paths of dense specimen SM-SC (20%).

Dense SM-SC (30%) soil group shear-strain curve, pore-pressure and stress-paths behaviours are illustrated in Figures 209 – 211 respectively.

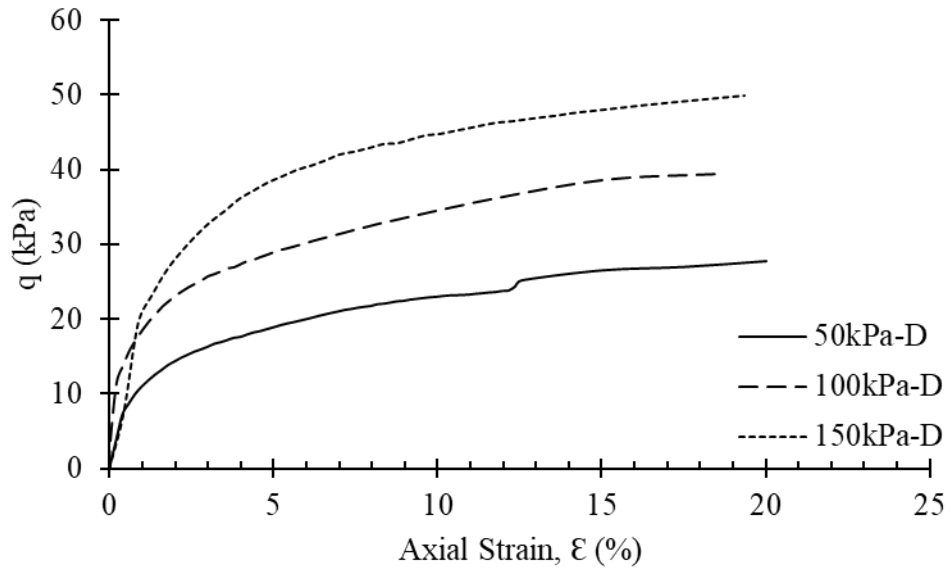


Figure 209: Undrained response of dense SM-SC (30%).

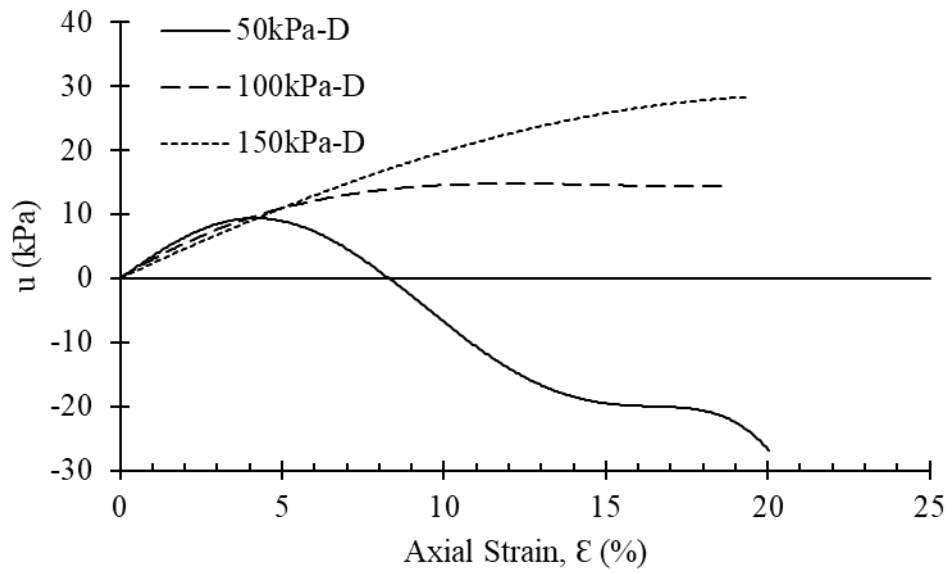


Figure 210: Pore-water pressure development in dense state SM-SC (30%).

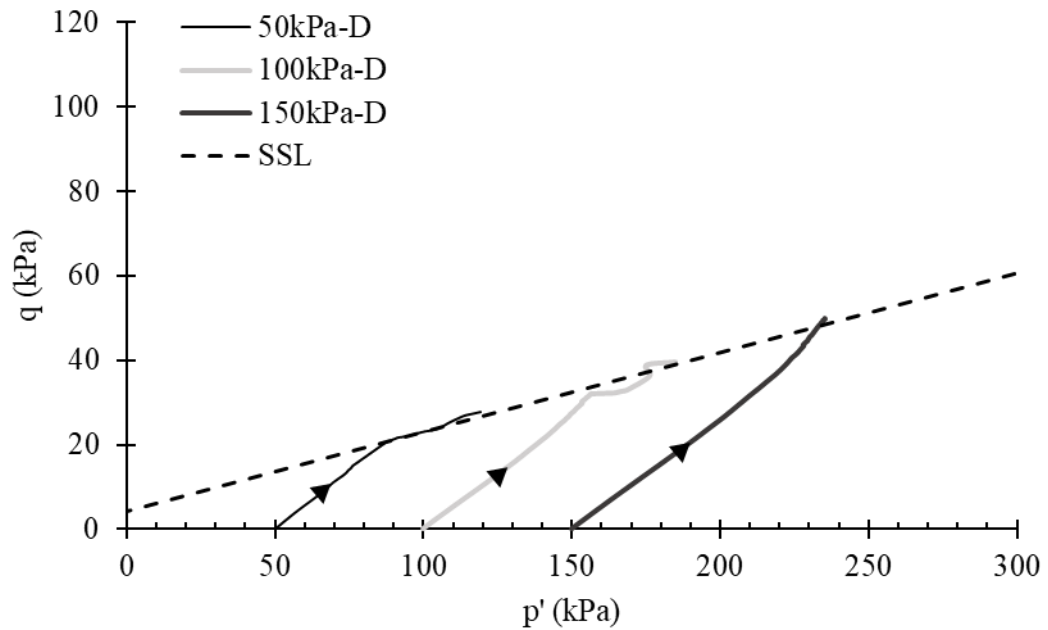


Figure 211: Stress paths of dense specimen SM-SC (30%).

Undrained dense behaviour of SM-SC groups illustrating stable behaviour with all proportions. Similar behaviour is observed for 30% SM-SC as for SP-SM (30%) as at higher confining stresses, the positive pore-water pressure is generated (Figure 210). One of the reasons that can be associated behind such phenomenon is due to high SSA of fines. Since SSA is an intrinsic property and governs the microstructural behaviour, therefore, the water absorption capacity of clays is increases leading to positive pore-water generation. In terms of 10% fines inclusion in Sand matrix, negative pore water pressure is observed due to dilation (Figure 204). As compared to 20% and 30% groups, it can be assessed that although at TFC, the fines are not participating absorption of water as of other groups. At 20% fines inclusion from pore water pressure plot (Figure 207), at 50 kPa of confining stress, negative pore water pressure is observed due to dilation and although at 100 kPa and 150 kPa of confining stress, positive pore water is generated, the increase in excess pore water pressure is not significant.

4.7.5.3 Critical and Steady State Analysis SM-SC Group

Clayey-silty Sand groups steady state lines at loose state are plotted in Figure 212 with comparison to Sand SSL. From Figure 212, the SSL for SM-SC at loose state as compared to Sand is less steep. From such observations it is noted that gradual incline in SM-SC groups reduces the steady state angle. As discussed earlier for SP-SM groups, the reduction in SSL angles corresponds to instability factor, but cohesion factor is more pronounced. It is noted from Figure 212 that at 30% of Fines inclusion, the SSL slope is merging towards SP SSL. The clear picture can be obtained regarding the effect of 30% fines in Sand by analysing the plot of initial state as shown in Figure 217.

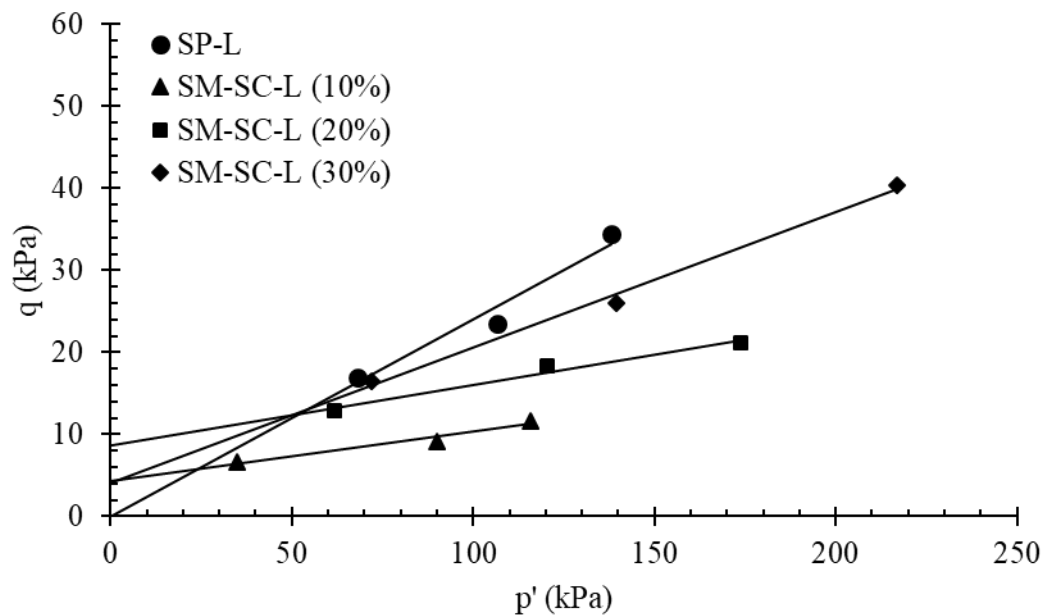


Figure 212: SSL comparison of SM-SC-L groups.

In Figure 213, SM-SC dense specimens SSL are presented.

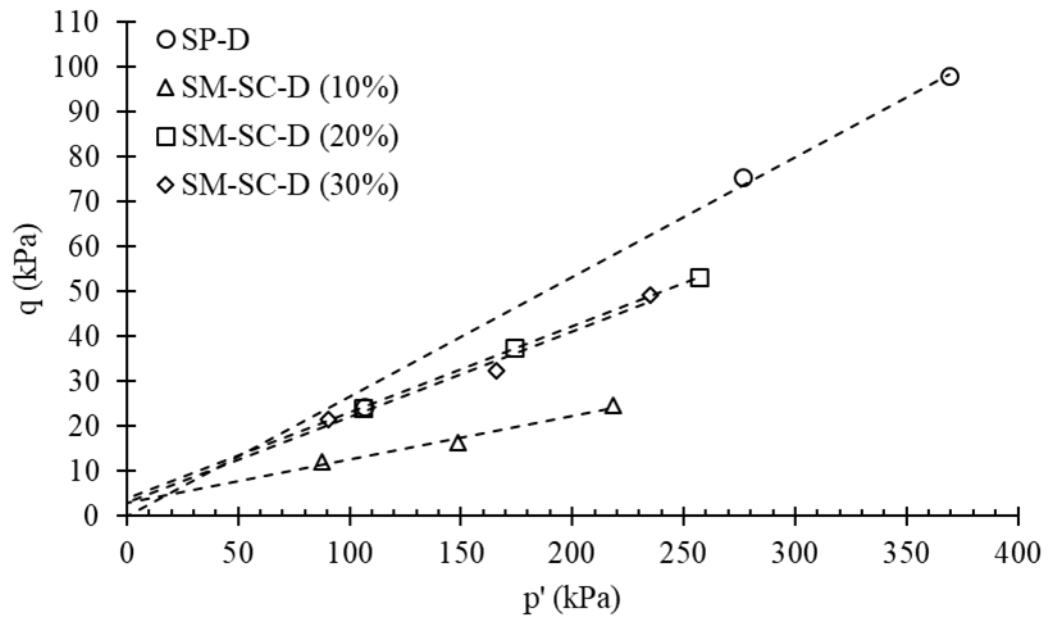


Figure 213: SSL comparison of SM-SC-D groups.

Analysis of SSL illustrates that approximately all soil groups in undrained testing reached to steady state for both initially loose and dense specimens. By observing the trend in Figure 212 and Figure 213 plots, in Figure 215 – 217, evaluation of initial state based on SSL is evaluated to analyse flow or non-flow behaviour of groups. Since the SSL is unique for a soil, by observing Figure 212 and Figure 213, cumulative plot of SSL is established for both loose and dense states of all SM-SC groups (Figure 214). By analysing linear regression analysis (R^2) the steady state points obtained from each state (loose and dense) are in conformance.

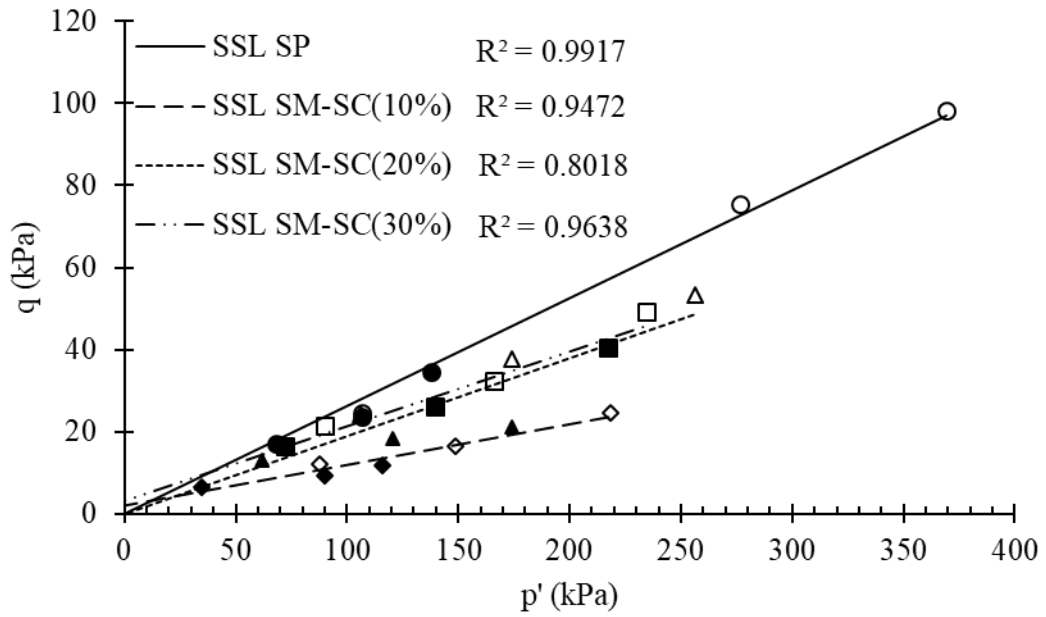


Figure 214: SSL cumulative plot of SM-SC groups.

Based on the SSL theory, liquefaction susceptibility of SM-SC soil groups is illustrated in Figures 215 – 217.

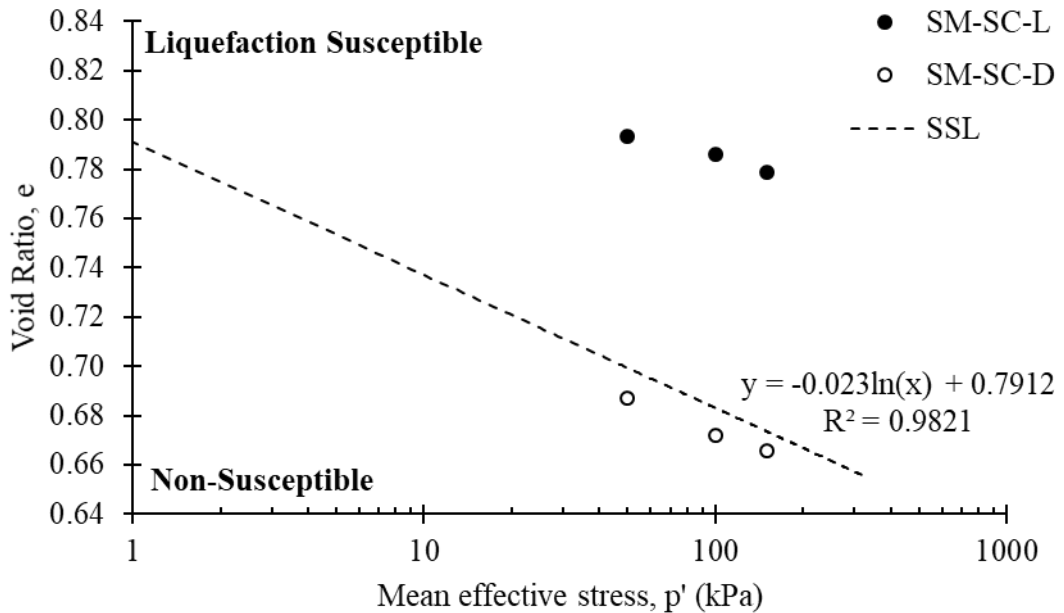


Figure 215: SSL liquefaction susceptibility SM-SC (10%).

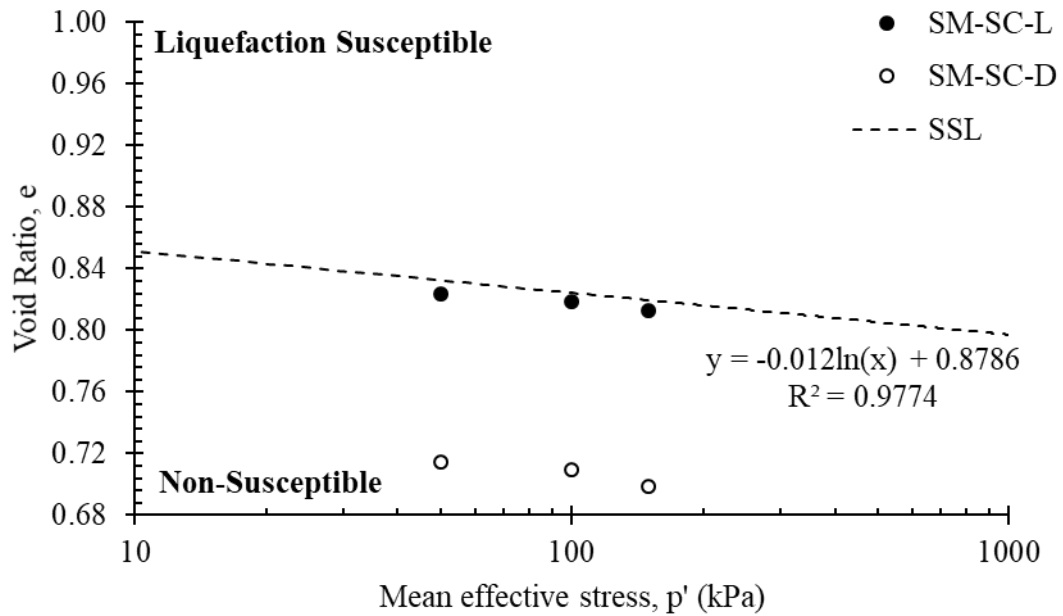


Figure 216: SSL liquefaction susceptibility SM-SC (20%).

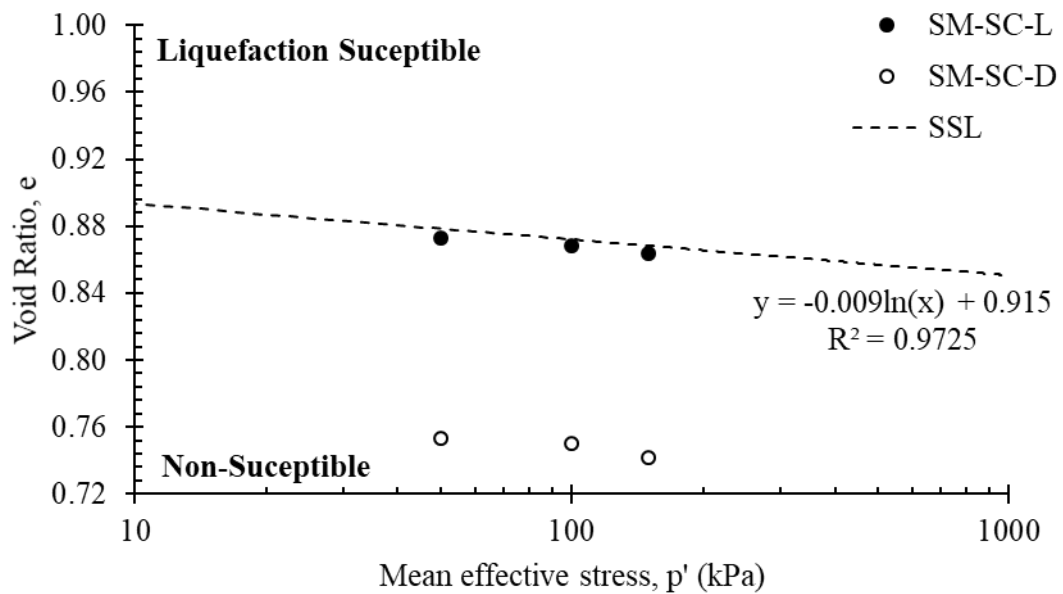


Figure 217: SSL liquefaction susceptibility SM-SC (30%).

From SSL analysis, 10% of clayey-silty Sand mixture, non-flow behaviour is observed and the dense specimens are exhibiting strain hardening (non-flow) behaviour. This phenomenon is also observed by plotting SSL. A great difference is observed between initial and critical states (Figure 215 – 217). As it observed from Figure 216 and Figure

217, SM-SC-L (20%) and SM-SC-L (30%) are plotting in close proximity of SSL, therefore, in such case state parameter evaluation is necessary and provides clear perception for flow or non-flow behaviour (Figure 218).

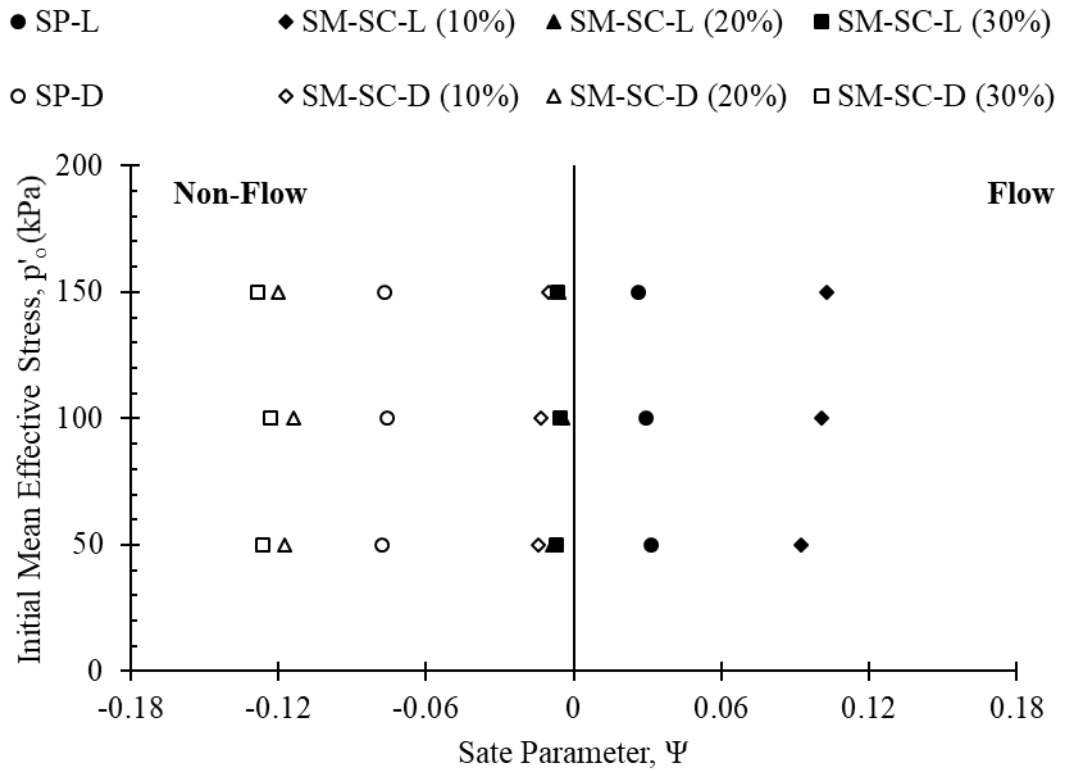


Figure 218: SM-SC state parameter.

In Figure 219, pore water ratio with variation of fines content in Sand is presented and in Table 18, steady state parameters obtained from test results are tabulated.

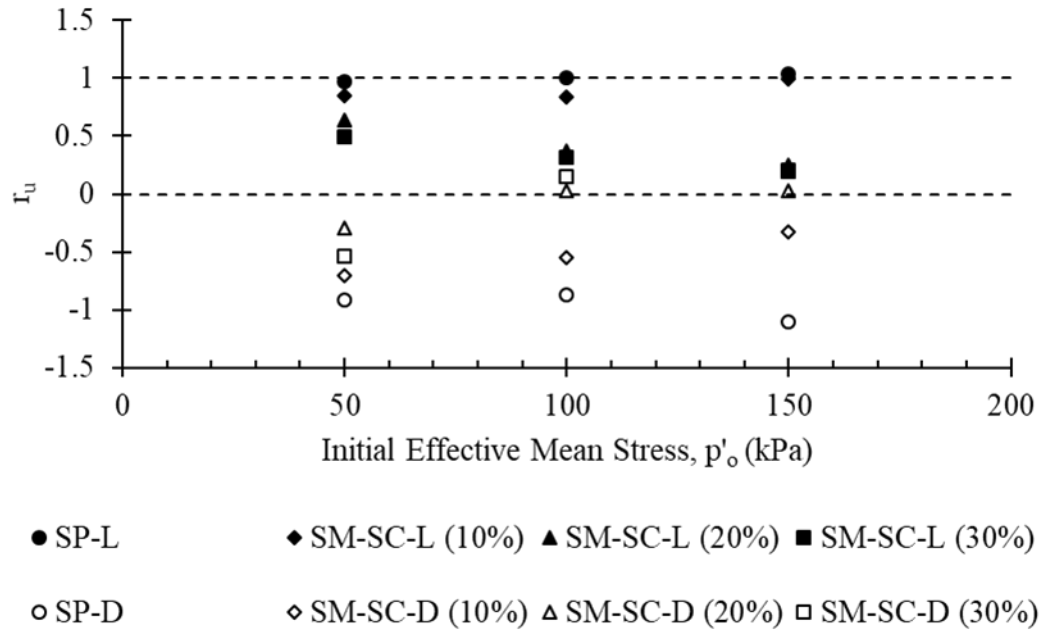


Figure 219: SM-SC pore pressure ratio variation.

Table 18: Steady state parameters of clayey-silty sand mixture.

p'_o (kPa)	State	Fines Content (%)					
		10		20		30	
		Ψ	r_u	Ψ	r_u	Ψ	r_u
50		+0.092	0.844	-0.008	0.643	-0.007	0.492
100	Loose	+0.101	0.834	-0.005	0.366	-0.005	0.315
150		+0.103	0.992	-0.006	0.250	-0.006	0.210
50		-0.014	-0.699	-0.117	-0.298	-0.126	-0.541
100	Dense	-0.013	-0.551	-0.004	0.025	-0.123	0.145
150		-0.010	-0.322	-0.120	0.026	-0.128	0.194

4.7.6 Monotonic Loading Undrained Response of Clayey-Sand

The effect of highly plastic clay particles (Illite mineral) presence in sand matrix with different proportions are highlighted in this section.

4.7.6.1 Loose State

The samples initial states are indicated in Section 4.7.1. In Figures 220 - 222, stress-strain, p' - q pore-water pressure generation and p' - q (stress-paths) curves are illustrated for 10% partial replacement of sand particles with clay fractions.

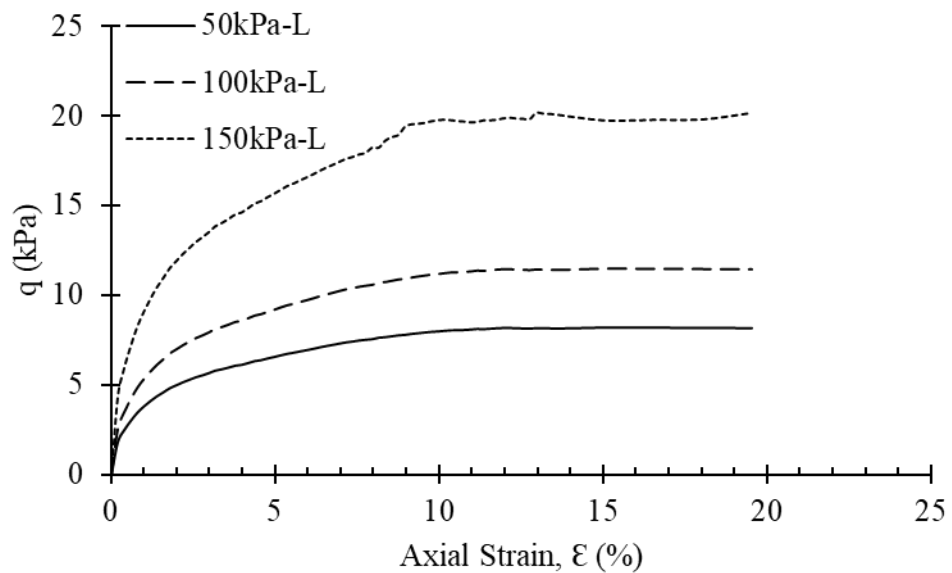


Figure 220: Undrained response of loose SP-SC (10%).

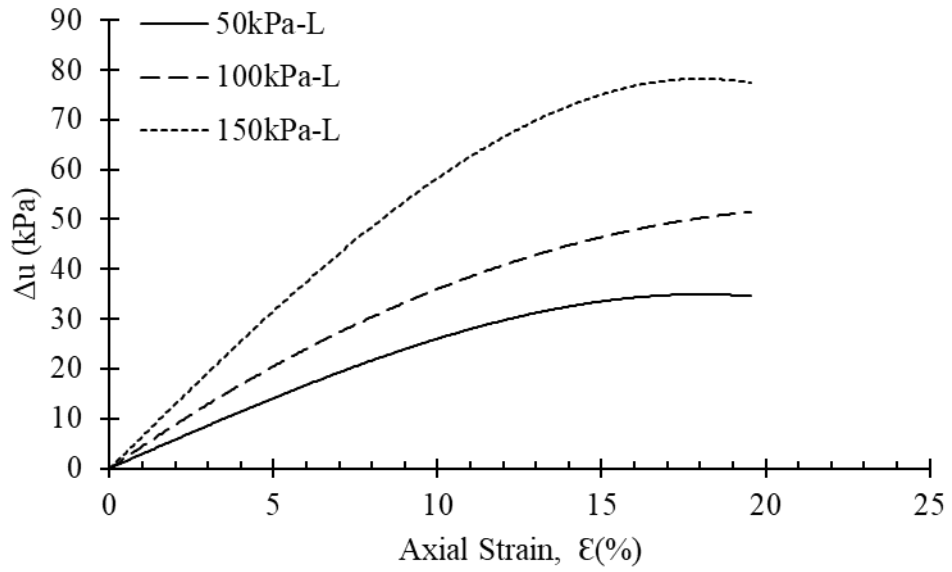


Figure 221: Pore-water pressure development in loose state SP-SC (10%).

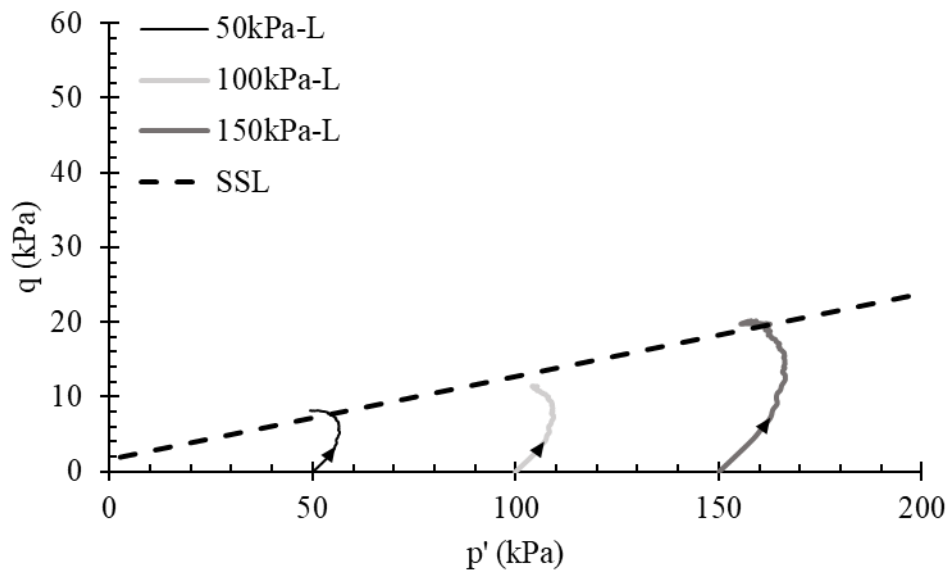


Figure 222: Stress paths of loose specimen SP-SC (10%).

Undrained response of 20% clay-sand mixture is presented in Figures 223 – 225.

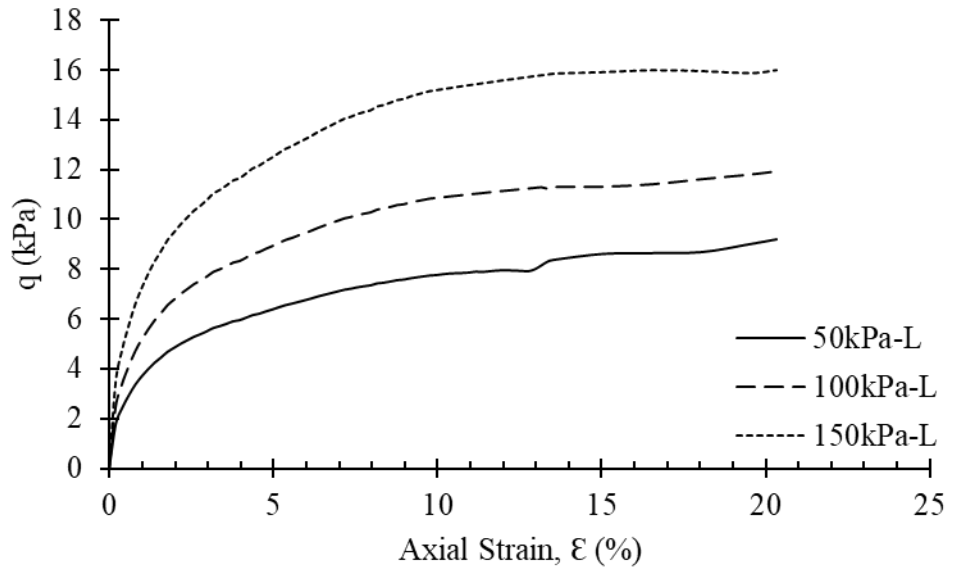


Figure 223: Undrained response of loose SP-SC (20%).

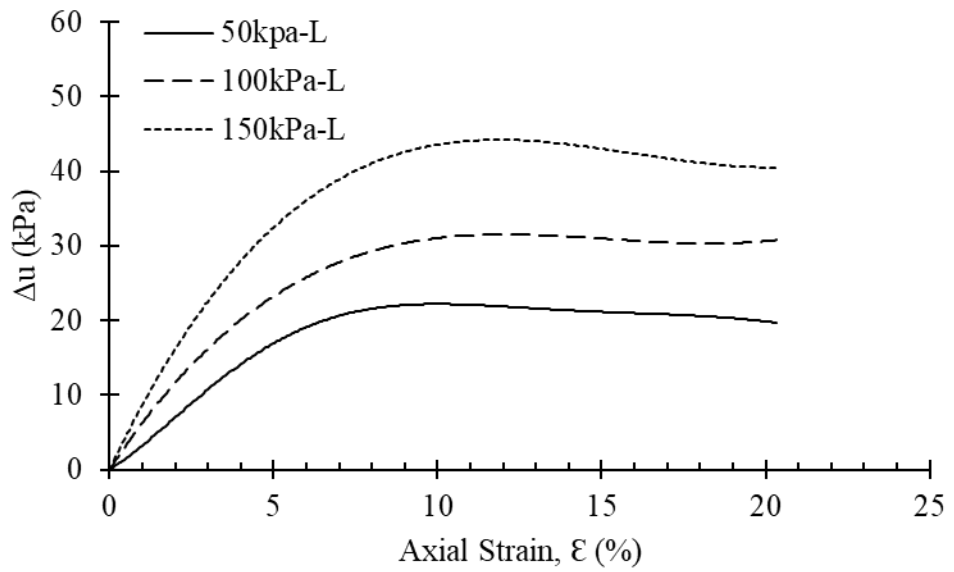


Figure 224: Pore-water pressure development in loose state SP-SC (20%).

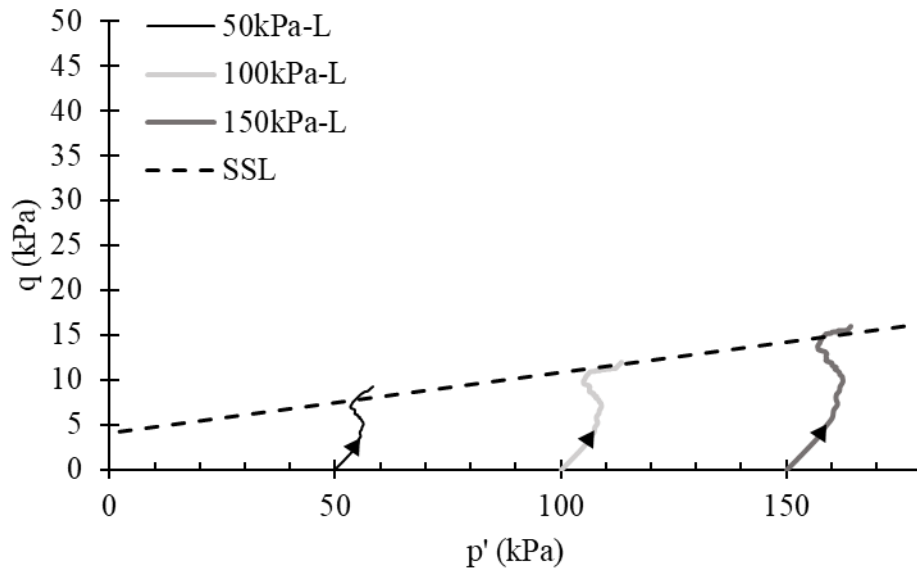


Figure 225: Stress paths of loose specimen SP-SC (20%).

Influence of 30% clay fractions is illustrated in Figures 226 – 228.

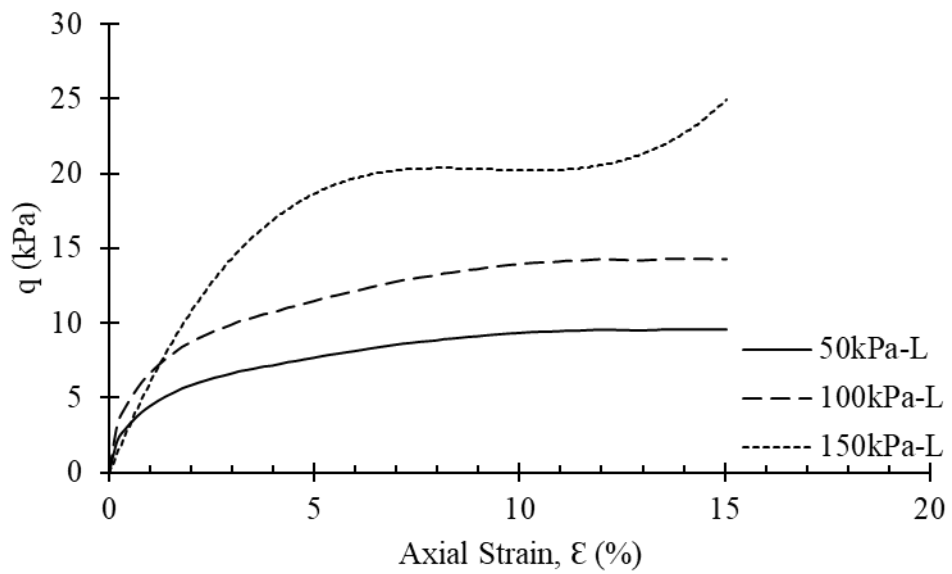


Figure 226: Undrained response of loose SP-SC (30%).

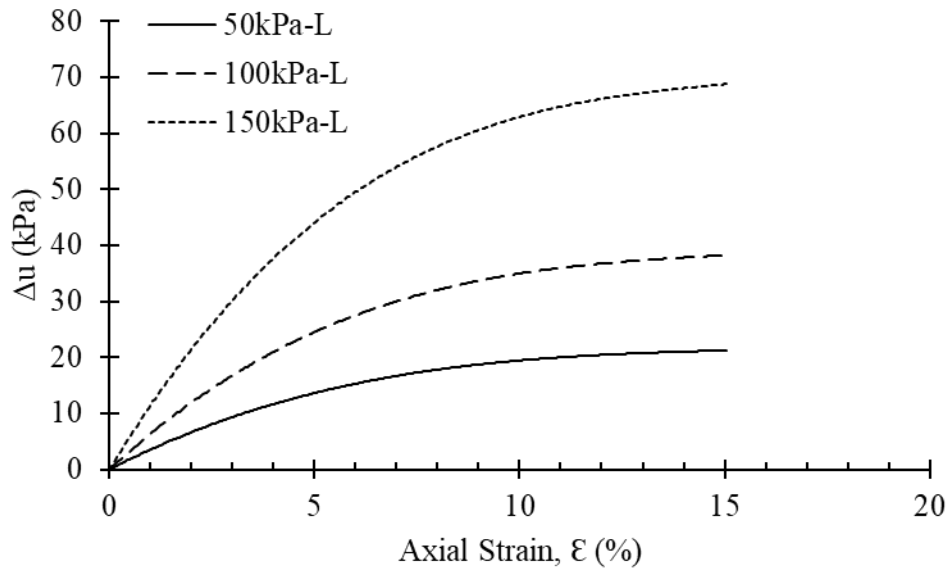


Figure 227: Pore-water pressure development in loose state SP-SC (30%).

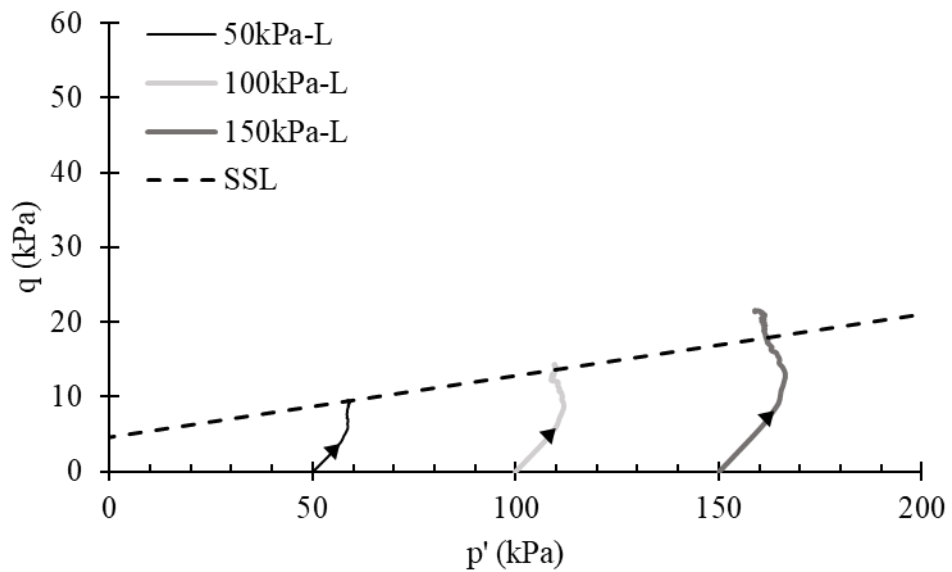


Figure 228: Stress paths of loose specimen SP-SC (30%).

Presence of clay fractions in sand-matrix strongly influences the mechanical behaviour even at lower threshold content. The presence of clay fraction as compared to Sand reduces the liquefaction susceptibility as the fines content increases. Another important factor influencing liquefaction susceptible is considered in terms of SSA of soil is observed that compared to other soil groups, the presence of clay fractions

increases SSA of clay group significantly indicating the presence of higher negative charged cations. Thus, resulting in decrease in pore-pressure generation due to increase in water retention capacity of clay particles because of the change in the mineralogical nature of clays, reduction in the internal frictional angle of soil particles and resulting in the steady state presence at larger strain levels (Figure 220, 223 and 226).

4.7.6.2 Dense State

The undrained response of 10% clayey Sand mixture with varying proportions at dense state is illustrated in Figures 229 – 231.

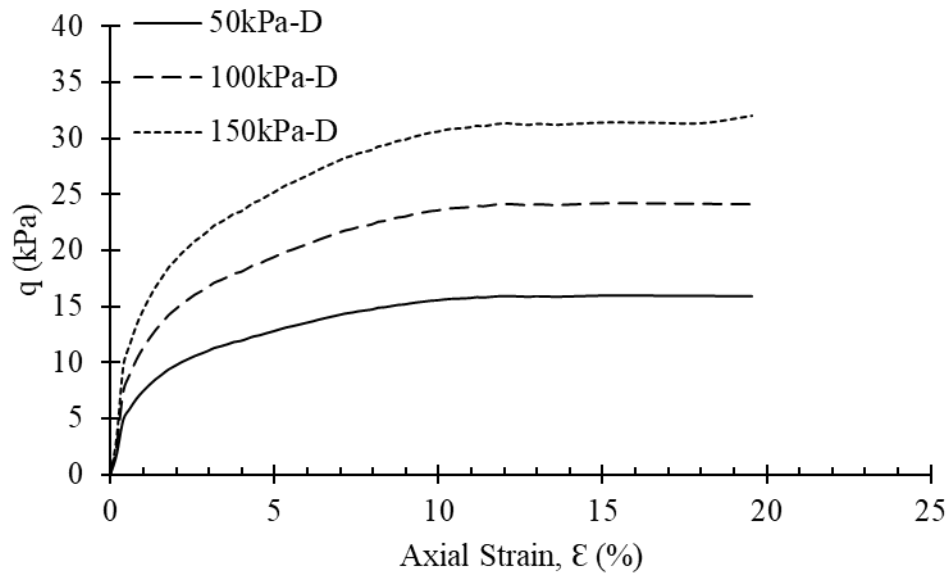


Figure 229: Undrained response of dense SP-SC (10%).

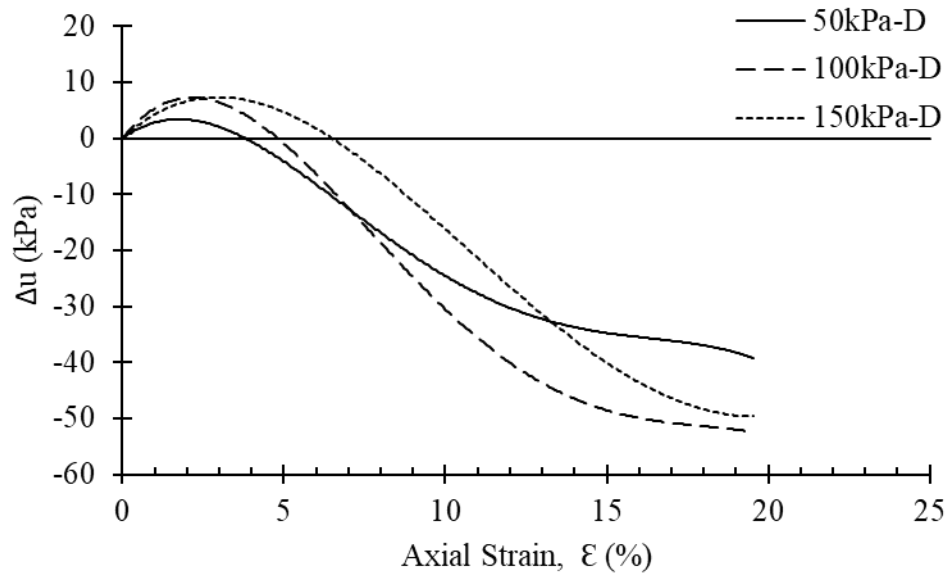


Figure 230: Pore-water pressure development in dense state SP-SC (10%).

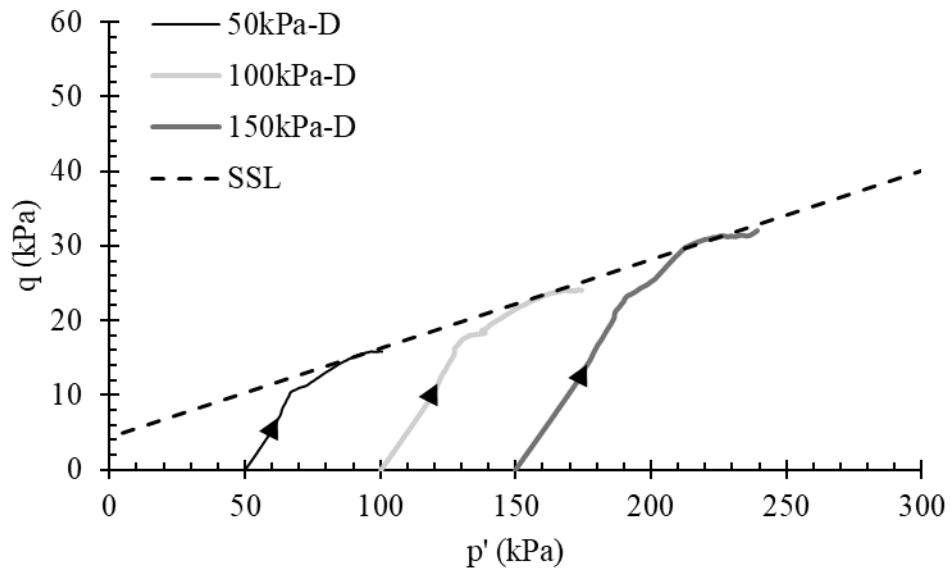


Figure 231: SP-SC (10%) stress paths of loose specimen.

Effect of 20% clay fractions in Sand matrix is presented in Figures 232 – 234.

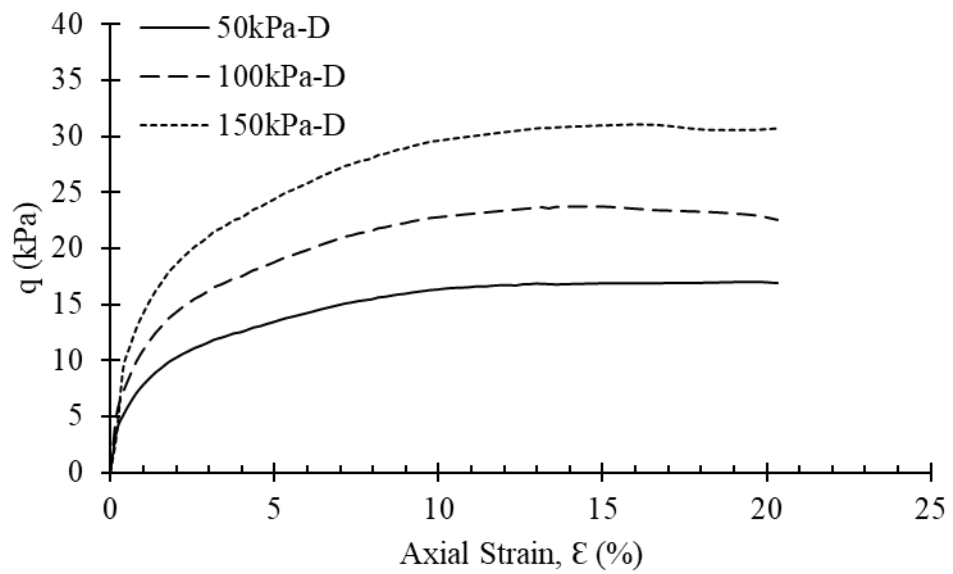


Figure 232: Undrained response of dense SP-SC (20%).

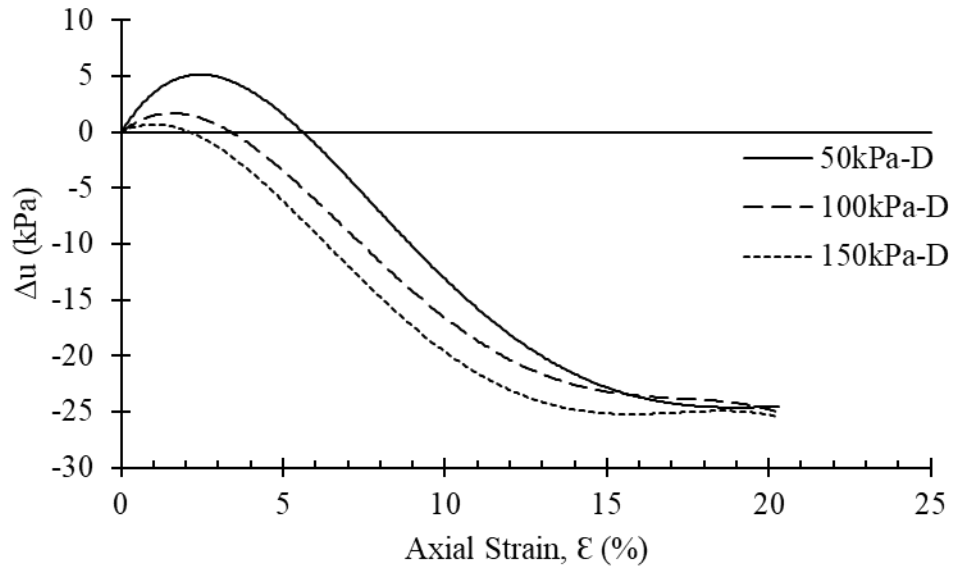


Figure 233: Pore-water pressure development in dense state SP-SC (20%).

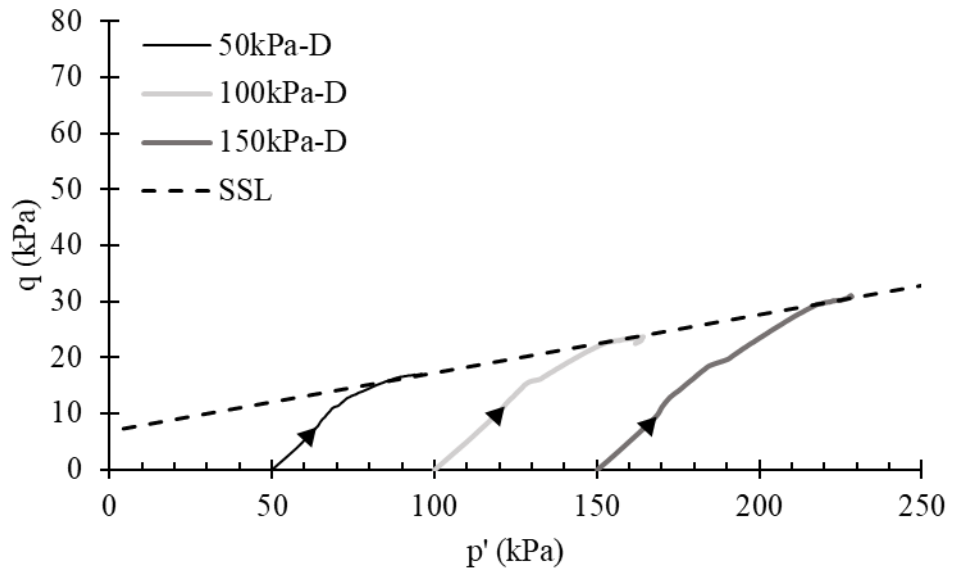


Figure 234: Stress paths of dense specimen SP-SC (20%).

Undrained static loading response of 30% clayey-Sand is presented in Figures 235 – 237.

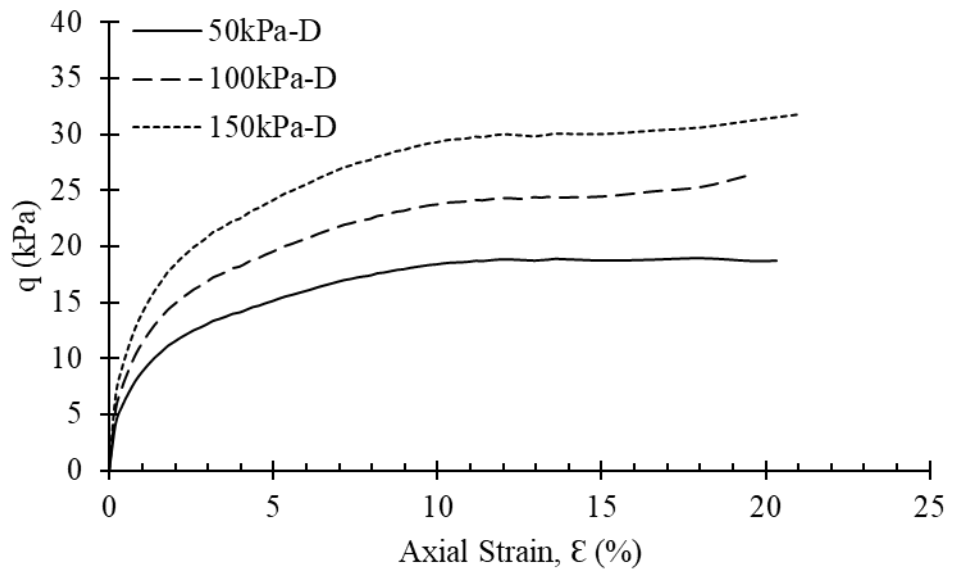


Figure 235: Undrained response of dense SP-SC (30%).

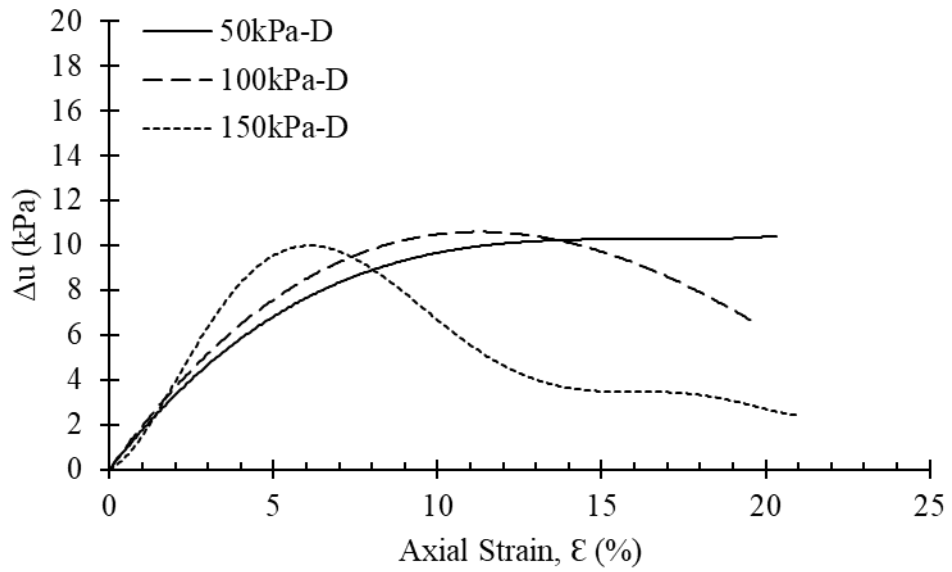


Figure 236: Pore-water pressure development in dense state SP-SC (30%).

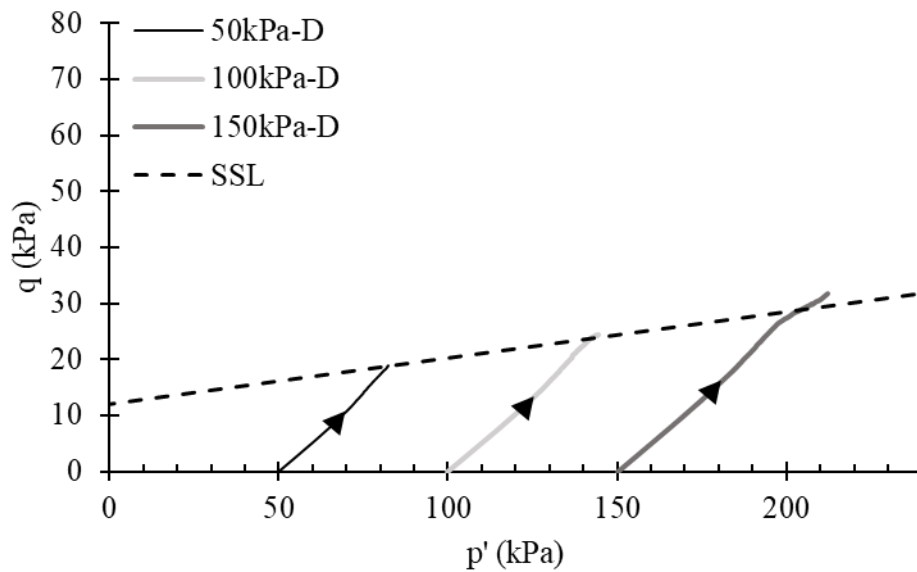


Figure 237: Stress paths of dense specimen SP-SC (30%).

Dense specimens at threshold fines content (10%) indicating the effective role of sand-grains influence on shear strength development (Figure 229) and negative pore-pressure is developed due to dilation of dense sand. Since the initial state of soil influences the shear strength parameters, it is observed from Figure 233, that as the clay content increases, the negative pore-pressure or drop in pore-water pressure is

lower as compared to SP-SC (10%) due to increase in water absorption capacity of clay particles thus contributing to pore-water pressure generation. In terms of shear strength development, the steady states is achieved at lower strain levels for low percentage of clay fractions (Figure 220, 223 and 226). Similar trend is observed for dense SP-SC groups that as the clay percentages increases, the steady state shifts to large strain levels (Figure 229, 232 and 235). From p' - q space (stress paths), all soil groups (loose and dense) are exhibiting stability of soil.

4.7.6.3 Critical and Steady State Analysis SP-SC Groups

In this section, the steady state parameters obtained from undrained static loading of clayey-Sand groups are presented. Steady state lines are plotted in Figures 238 and Figures 239 for each respective state of soil (loose and dense).

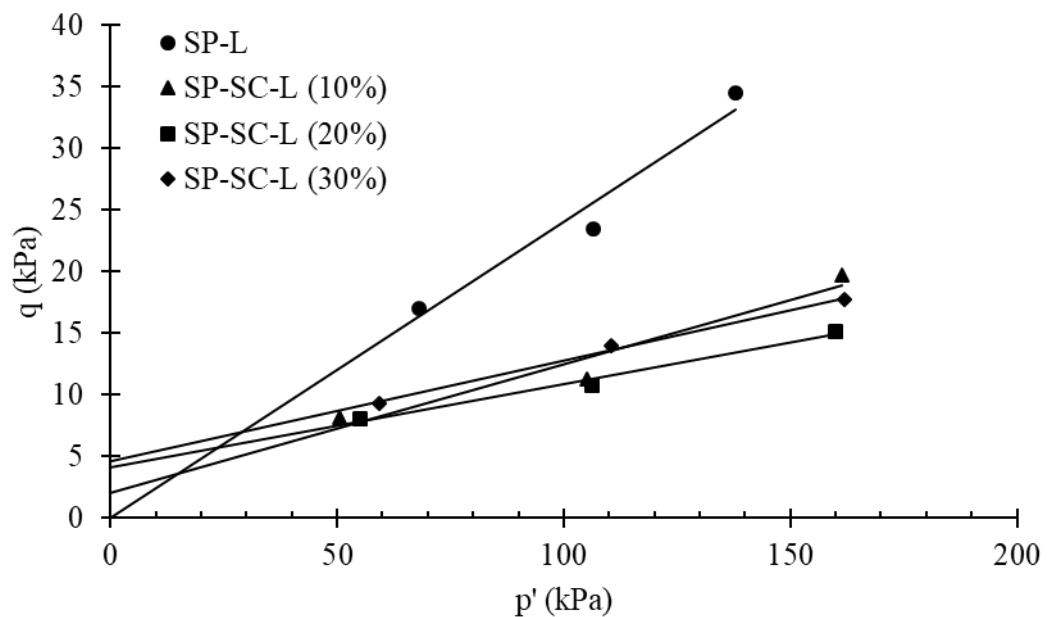


Figure 238: SSL comparison of SP-SC-L groups.

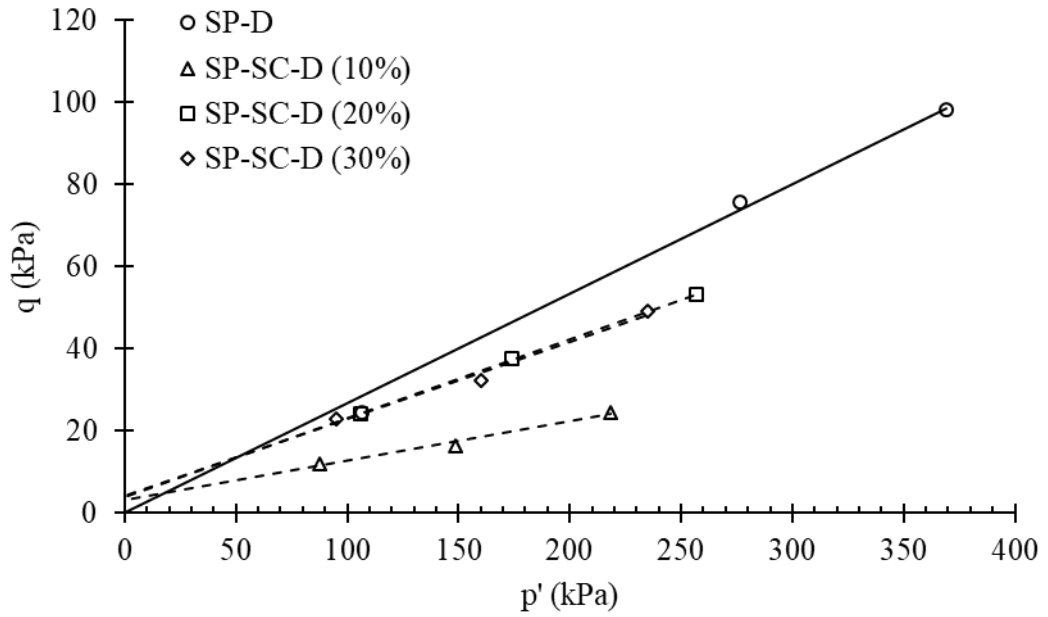


Figure 239: SSL comparison of SP-SC-D groups.

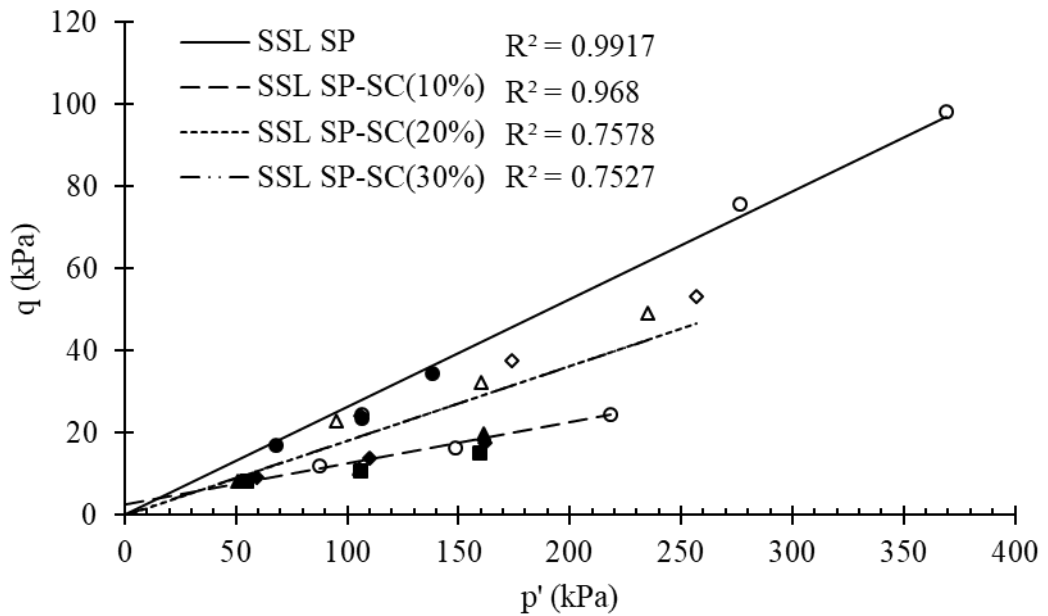


Figure 240: SSL cumulative plot of SP-SC groups.

The SSL of SP-SC (10%) in both state (loose and dense) are achieved as observed in undrained response. Whereas, for SP-SC (20%) and SP-SC (30%) the steady states at

dense states are not pronounced from p' - q space analysis. Therefore, for initial state analysis for liquefaction susceptibility is based on loose state SSL (Figures 241 – 243).

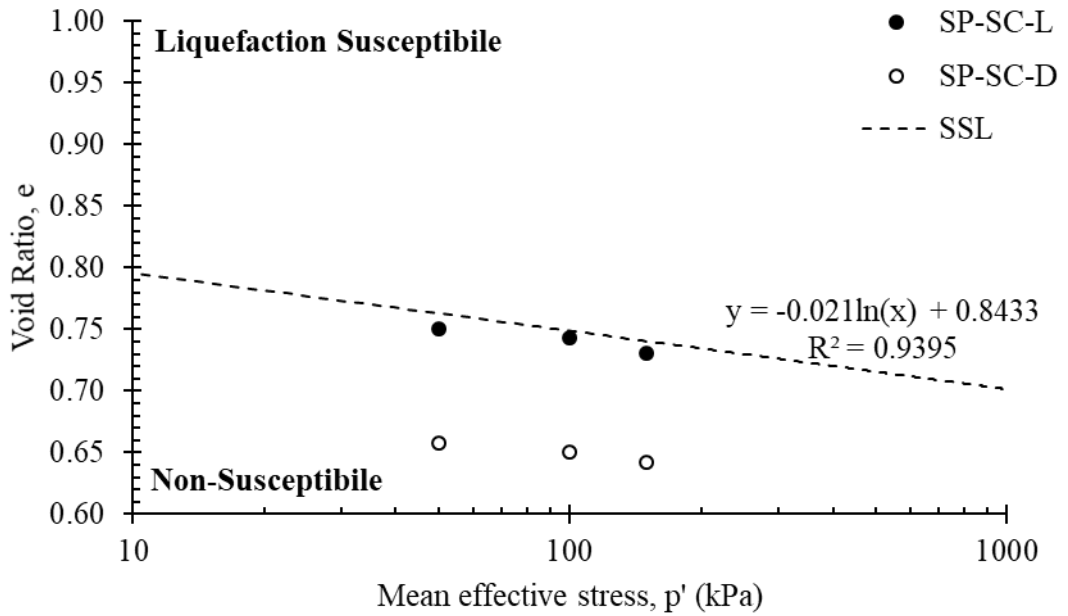


Figure 241: SSL liquefaction susceptibility SP-SC (10%).

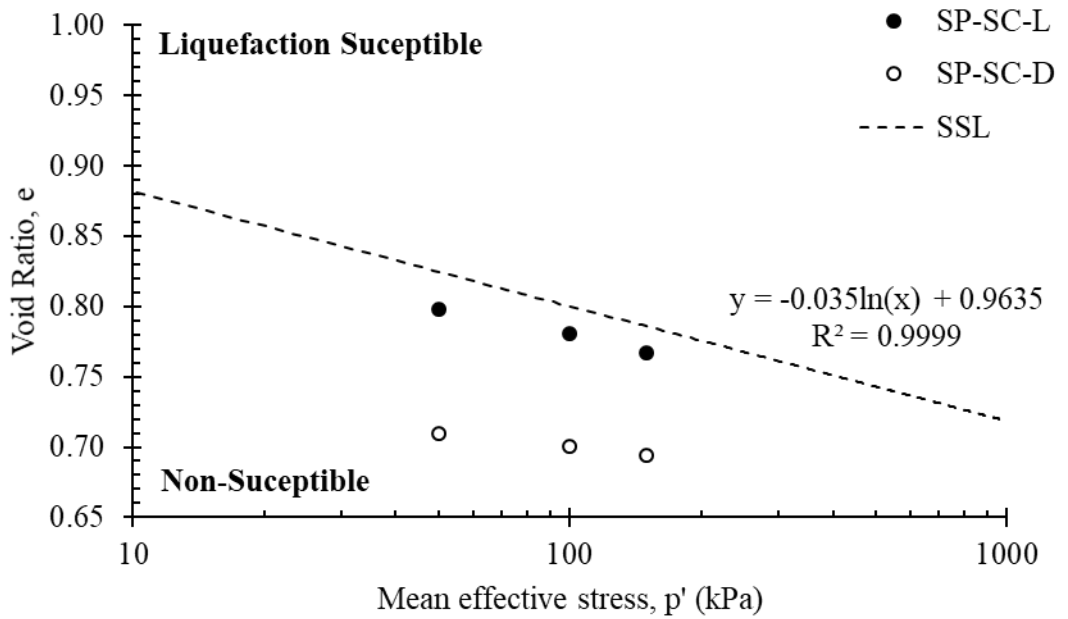


Figure 242: SSL liquefaction susceptibility SP-SC (20%).

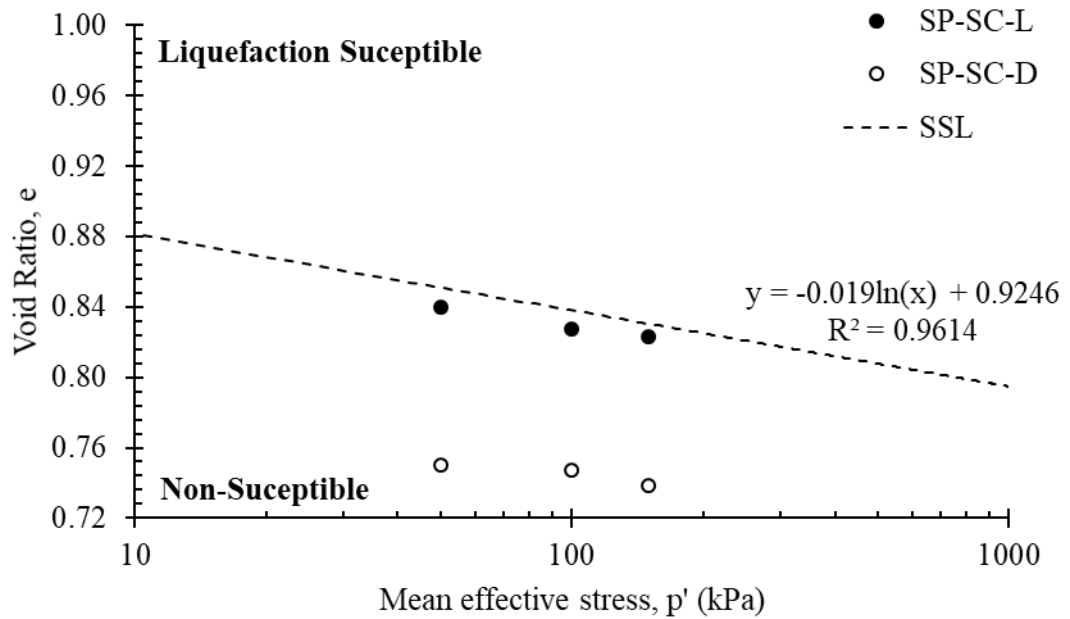


Figure 243: SSL liquefaction susceptibility SP-SC (30%).

From initial state of soil with respect to steady states, all SP-SC groups are exhibiting non-flow behaviour as their respective initial states are plotting below the SSL. As it is observed as the fines content increases, the initial states are plotting closer to SSL (Figure 243), thus it can be assessed that further inclusion of fines might lead to instability of soil. In Figure 244, based on the initial state analysis with respect to steady state, state parameter is analysed.

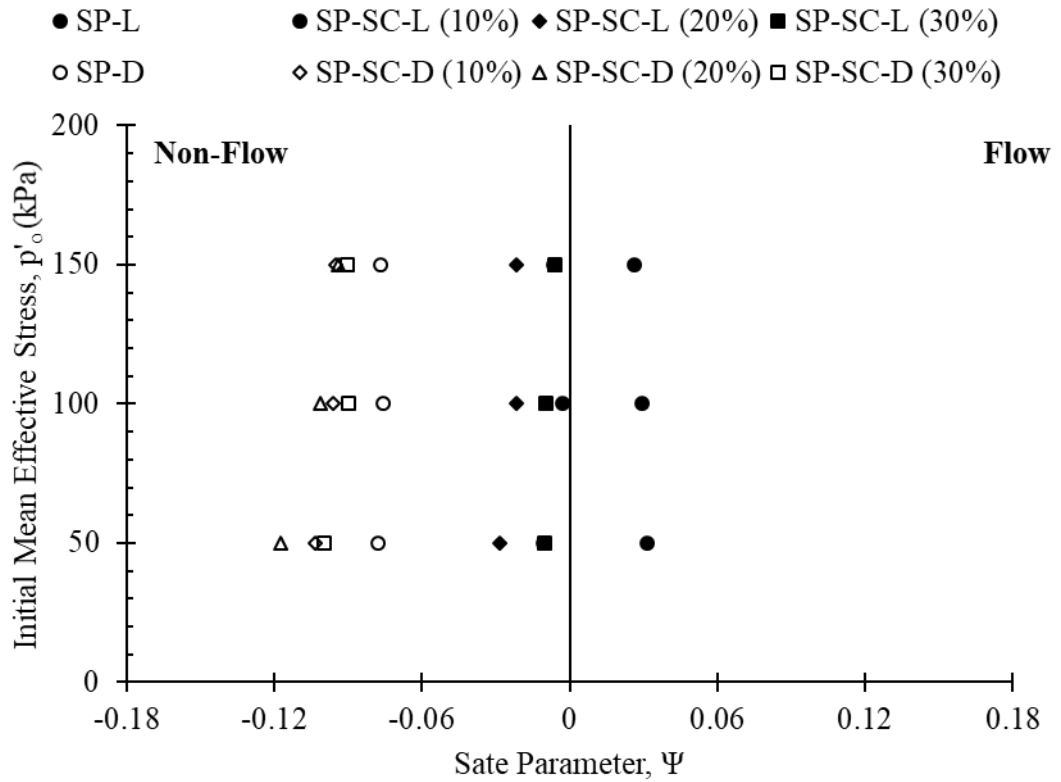


Figure 244: SP-SC state parameter.

To assess the viability of flow potential analysis, in Figure 245 variation of pore-pressure ratio is illustrated. In Table 19, steady state parameters are illustrated.

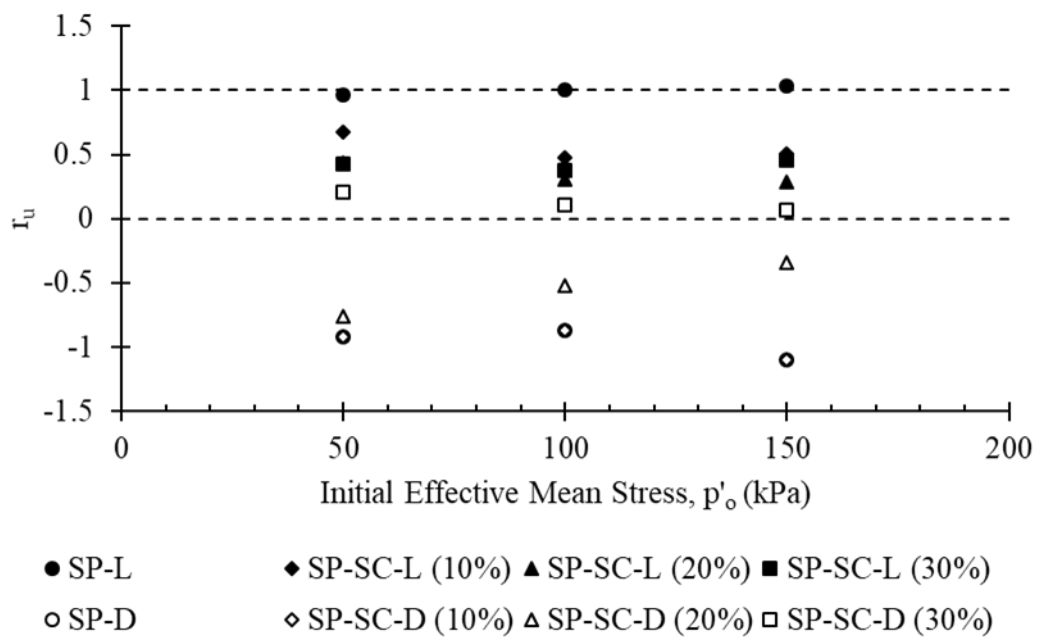


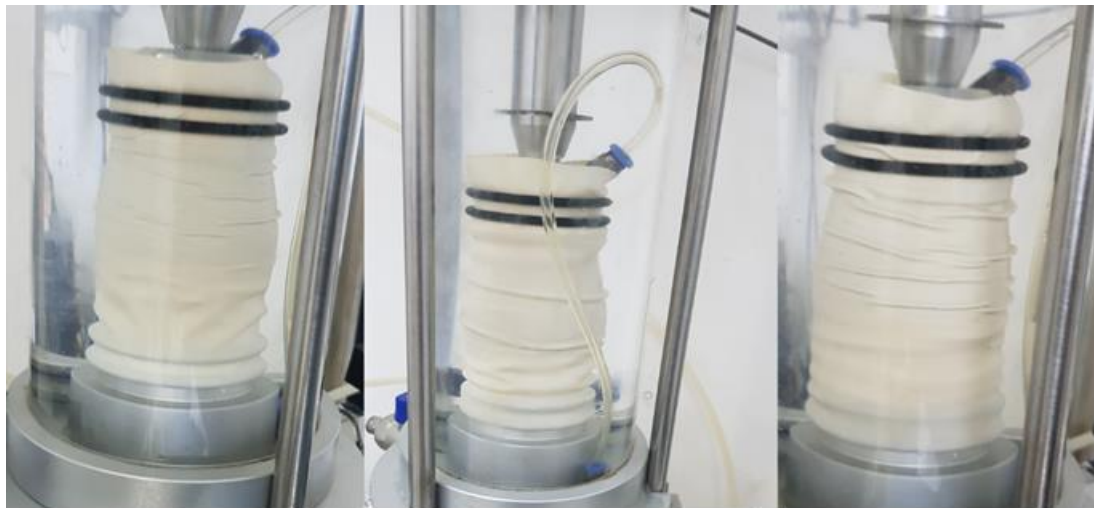
Figure 245: SP-SC pore pressure variation.

Table 19: Steady state parameters of clayey-sand groups.

p'₀	State	Fines Content (%)					
		10		20		30	
		Ψ	r _u	Ψ	r _u	Ψ	r _u
50		-0.011	0.690	-0.029	0.437	-0.010	0.422
100	Loose	-0.002	0.476	-0.022	0.310	-0.010	0.380
150		-0.007	0.507	-0.022	0.289	-0.006	0.455
50		-0.104	-0.76	-0.117	-0.500	-0.100	0.208
100	Dense	-0.100	-0.522	-0.101	-0.252	-0.089	0.11
150		-0.100	-0.337	-0.094	-0.179	-0.091	0.073

4.8 Visual Analysis of Liquefied and Non-Liquefied Groups

Experimental outcomes of SP and SM-SC (10%) soil groups exhibited liquefaction phenomenon and beside experimental evaluations, the liquefied soil exhibited different visual characteristics. As discussed earlier and observed in experimental analysis, the pore-pressure development in specimen is the key factor behind flow characteristics. One of the indications of high pore water pressure generation in specimen is the excessive development of wrinkles around rubber membrane as can be seen in Figure 246, whereas, in non-liquefied specimens, such behaviour is not observed. In Figure 246, development of wrinkles at different stages of testing is illustrated.



Liquefaction initiation

Quasi-steady state

Liquefied

Figure 246: Development of wrinkles on rubber membrane.

The development of wrinkles observed is in context with other researchers (Amini & Qi, 2000) and in addition to such observed behaviour, the researchers also specify that taking into consideration the membrane correction factors in necessary evaluation for liquefied specimens has no effect on experimental outcomes.

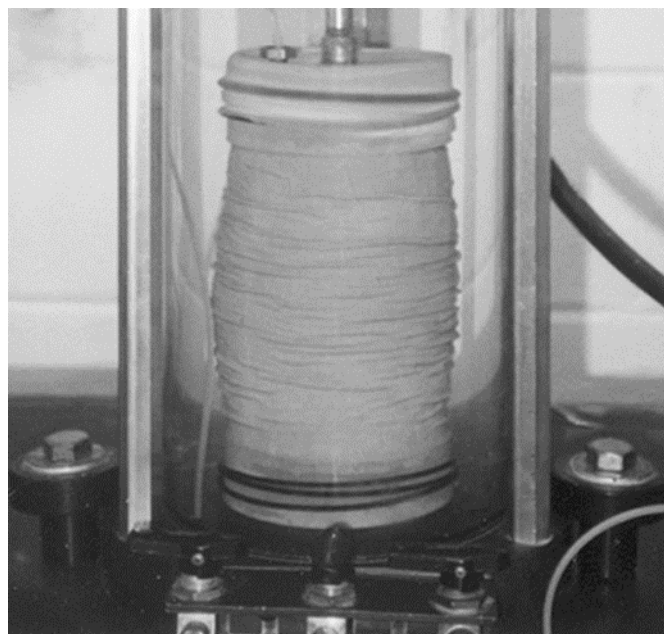


Figure 247: Soil specimen after liquefaction (Amini & Qi, 2000).

One of the cases as discussed above is observed for 10% clayey-silty Sand mixture and is illustrated in Figure 248. Figure 248, illustrates the limited liquefied soil behaviour of SM-SC (10%) tested under 100 kPa of confining stress and Figure 249 illustrates liquefied soil tested under 100 and 150 kPa of confining stress.

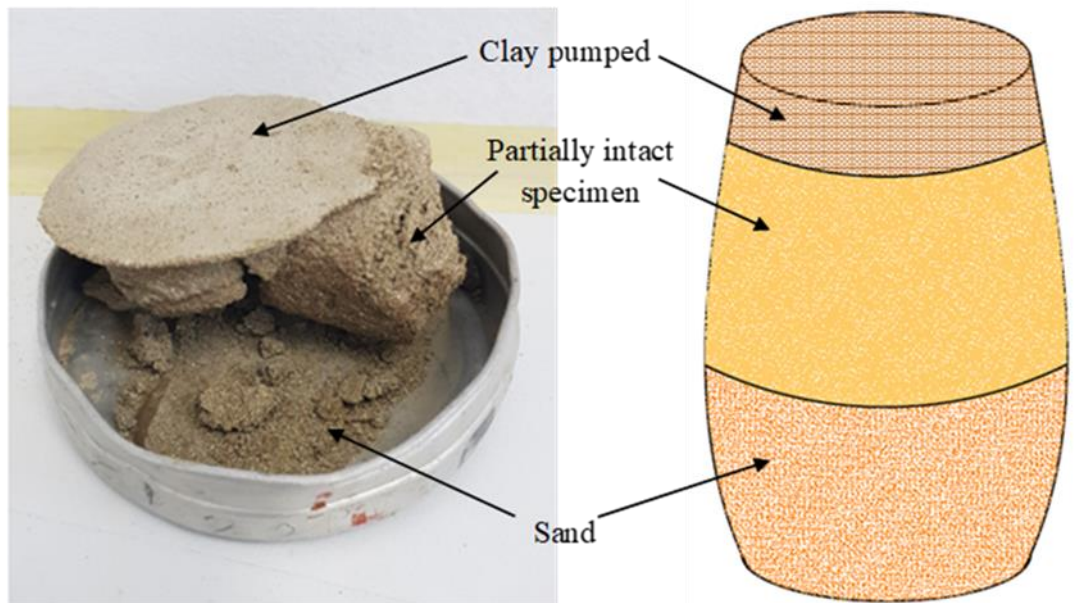


Figure 248: SM-SC (10%) limited liquefaction observation.

A comparison is made between SM-SC groups (10%, 20% and 30%) under same confining stress, ($\sigma'_3 = 150$ kPa) are illustrated in Figure 250. The microstructure analysis is performed to understand clearly the separation of layers occurred in 10% clayey-silty-sand matrix and illustrated in Figure 252.

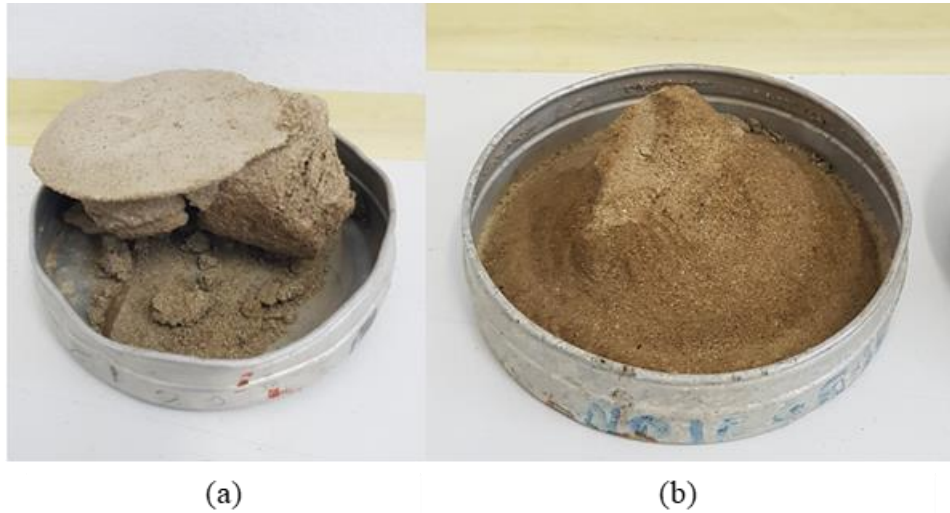


Figure 249: SM-SC liquefied soil at (a) 100 kPa and (b) 150 kPa.

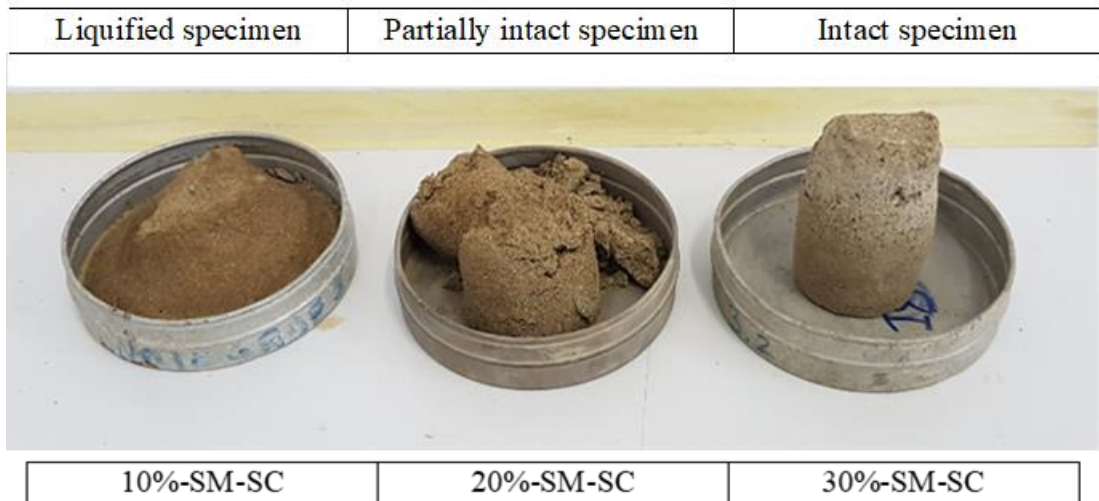


Figure 250: SM-SC groups visual comparison.

A well-known concept regarding shearing of loose specimen resulting in bulging is shown in Figure 251 for SM-SC (10%) and SM-SC (30%) groups. A noticeable difference between liquefied and non-liquefied bulged shapes of loose specimens are compared in Figure 251. As seen in Figure 251, non-liquefied specimen exhibit bulged behaviour while in liquefied soil tilting of the specimen is observed.

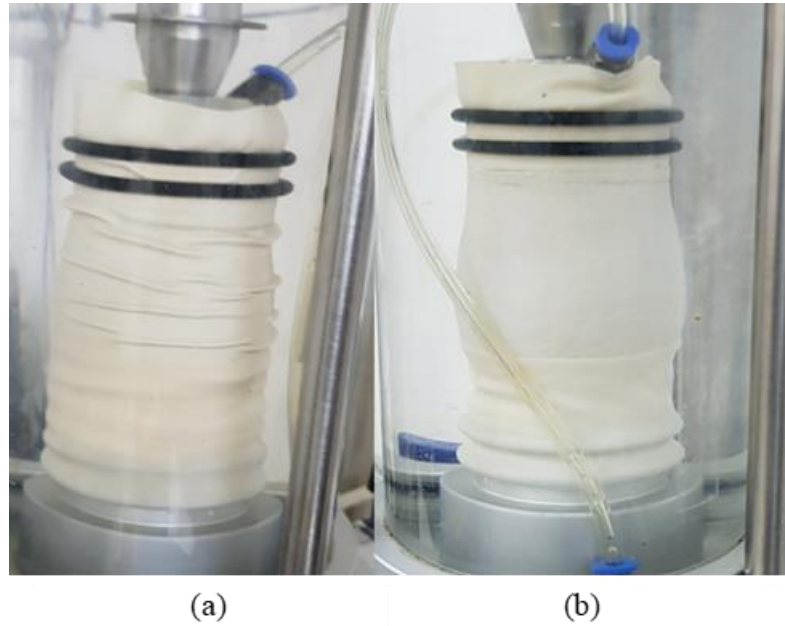


Figure 251: (a) Liquefied SM-SC (10%) and (b) Non-liquified SM-SC (30%) loose specimens bulging.

In Figure 252, optical microscopic images of SP-SM (10%) images are presented. Figure 252(a) shows that fine particles are separated from the Sand matrix and accumulated at top of the specimen. This is mainly occurring due to development of excess pore water pressure which results in increment in pore sizes (Figure 252-b: Intermediate layer) creating a pathway for fines to travel within the microstructure and accumulating at top. From such analysis it can be assessed that at 150 kPa of confining stress, the pore water pressure developed significantly resulting in non-structured soil fabric (Figure 249-b).

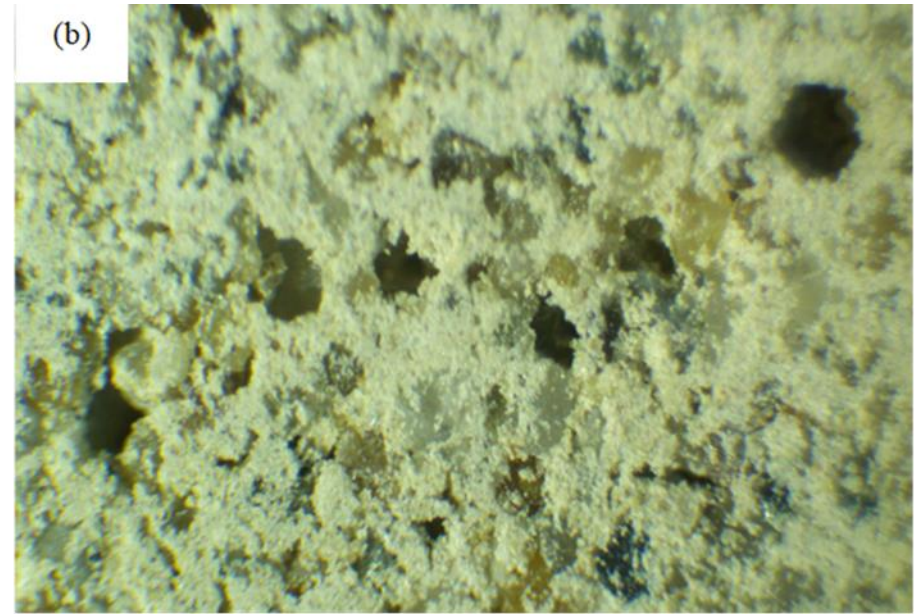
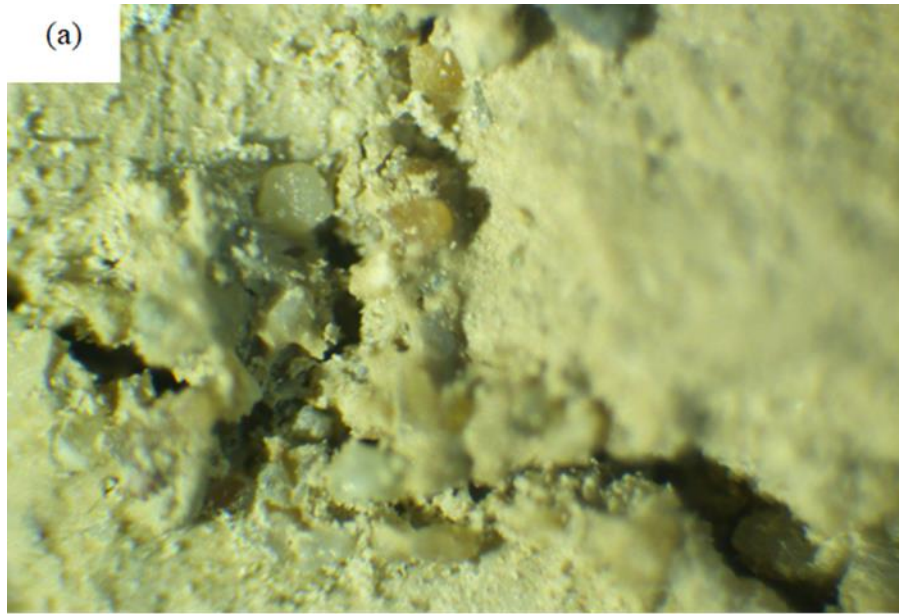


Figure 252: Clayey-Silty-Sand particle separation: Microstructure analysis of soil specimen under 150kPa confining stress.
(a) Fines accumulation at top of specimen (b) Intermediate layer.

4.9 General Discussion of CU-Triaxial Test

Flow liquefaction susceptibility of all soil groups are primarily assessed by considering state parameter to obtain the plot in either flow or non-flow region. It is observed that among all soil groups, Sand and clayey-silty Sand (10%) exhibited flow behaviour. From steady state analysis, in Figure 253, SSL obtained from all soil groups are presented for comparison purpose.

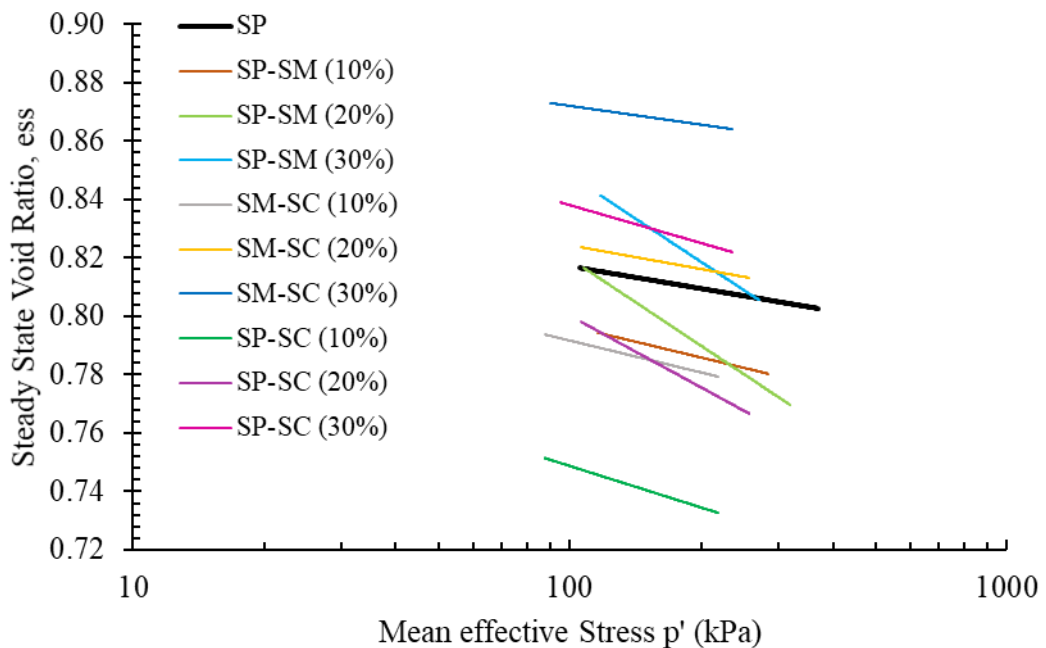


Figure 253: Variation of SSL of soil groups.

From Figure 253, it is observed that with addition of fines in Sand matrix, SSL are steeper. Such indicator directs to the fact the stability of the soil will reach at lower effective stresses whereas, in contrast to the liquified soil groups, the slope of the SSL is lower. Based on the observed behaviour of state parameters, in Figures 254 and 255, state parameter with respect to fines content is plotted.

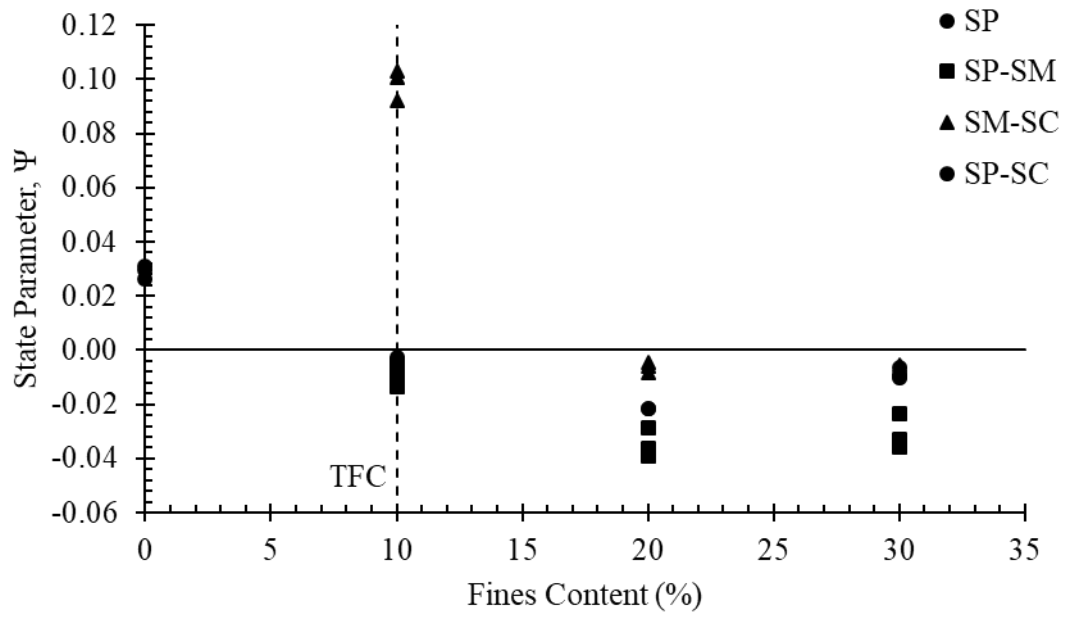


Figure 254: State parameters variation with fines at loose state.

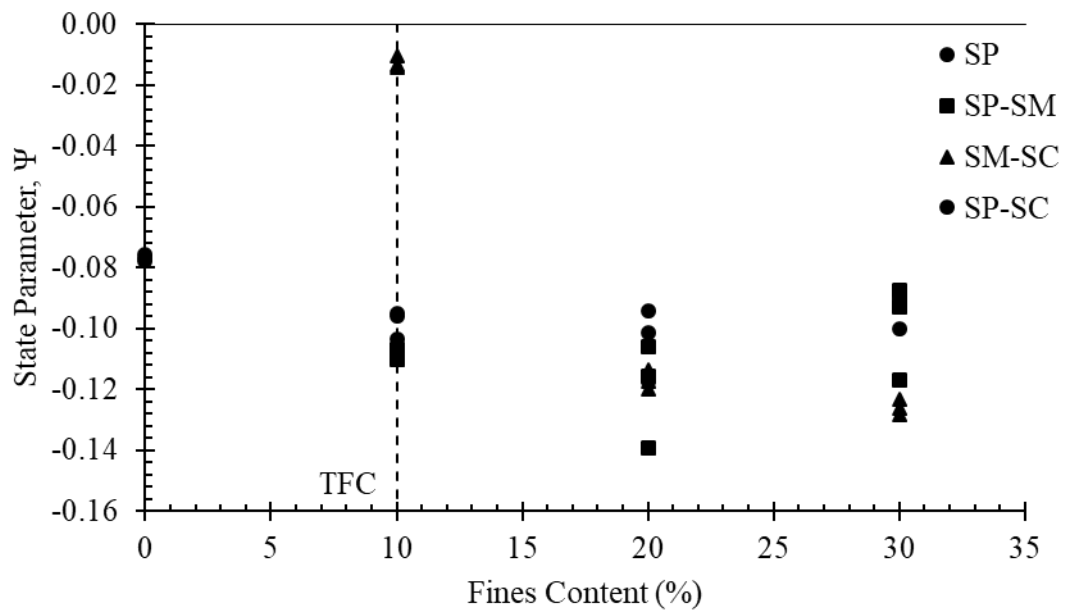


Figure 255: State parameters variation with fines at dense state.

From Figures 254 and Figure 255, it is observed that as fines content increases, the dilatancy tendency increases, with an exception for 10% SM-SC (loose and dense). Such a tendency of dilatancy is observed for stable soil groups, and similar results are

obtained as compared to study done on critical state of Sand with fines by Phan et al. 2016.

4.10 Data Comparison of Direct Shear & Triaxial Test Results

The primary objective of this research involves evaluating contractive (flow) and dilative (non-flow) behaviour of sand with varying percentages of fines. The state parameters obtained from both testings' [Direct Shear Box Test (DST) and Triaxial Test (TT)] are plotted in Figures 256 – 258.

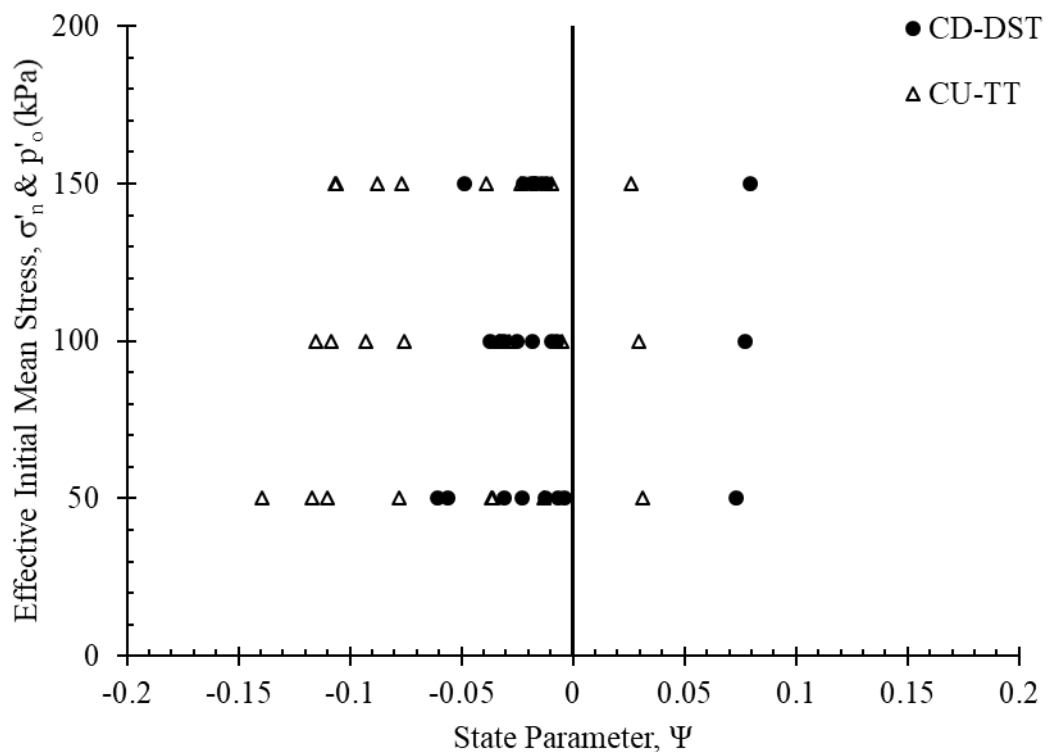


Figure 256: SP-SM state parameters comparison between CD (DST) and CU (TT).

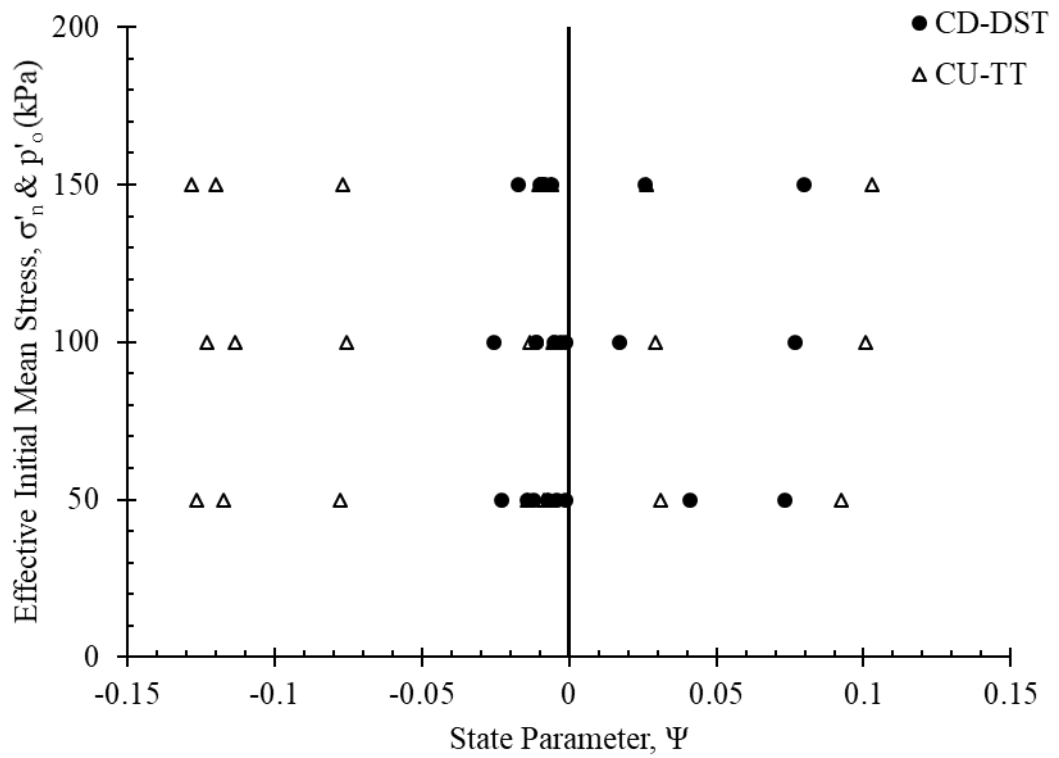


Figure 257: SM-SC state parameters comparison between CD (DST) and CU (TT).

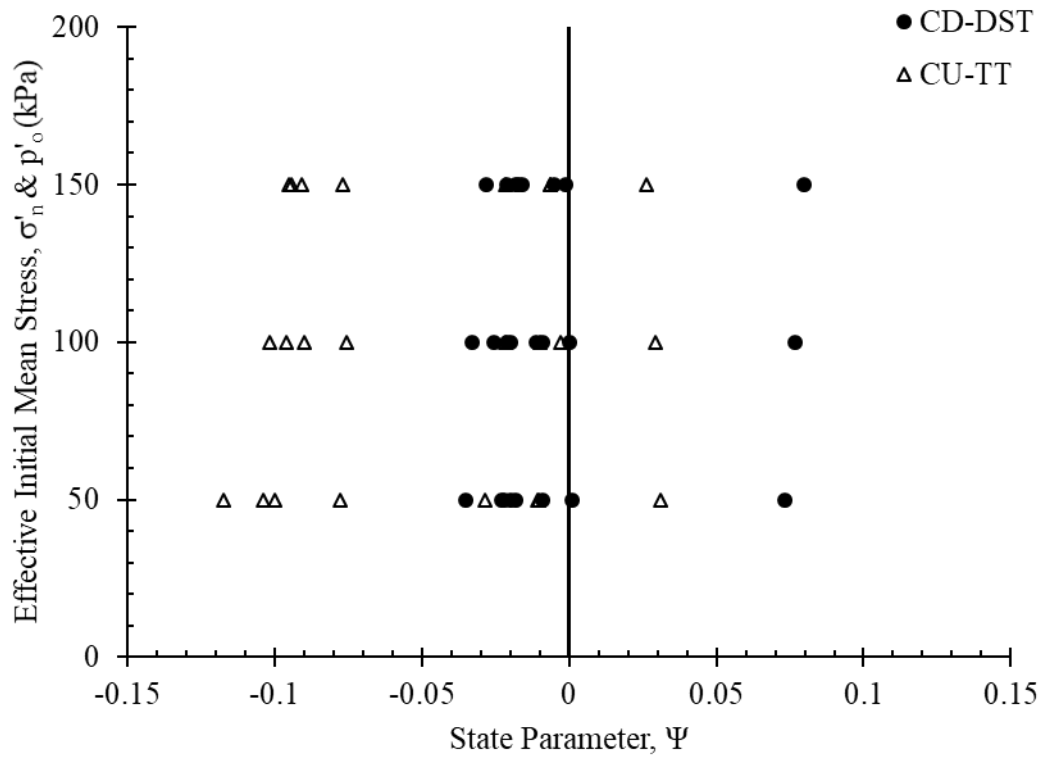


Figure 258: SM-SC state parameters comparison between CD (DST) and CU (TT).

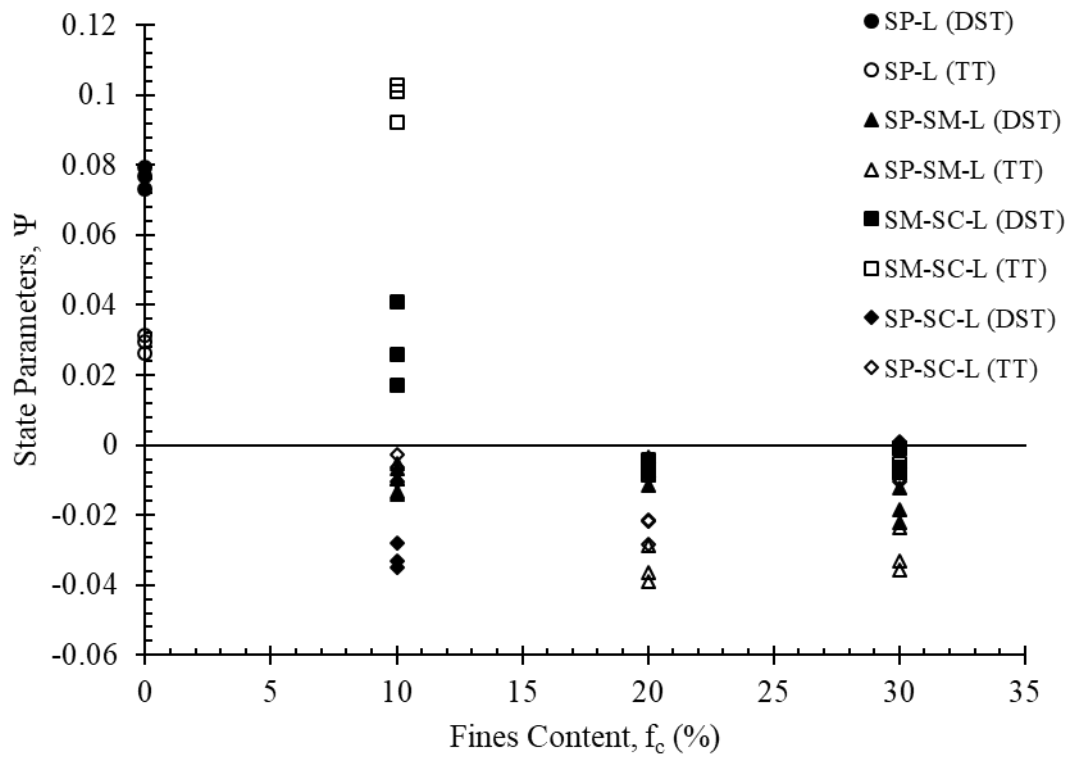


Figure 259: CD (DST) and CU (TT) SM-SC-L state parameters comparison with f_c .

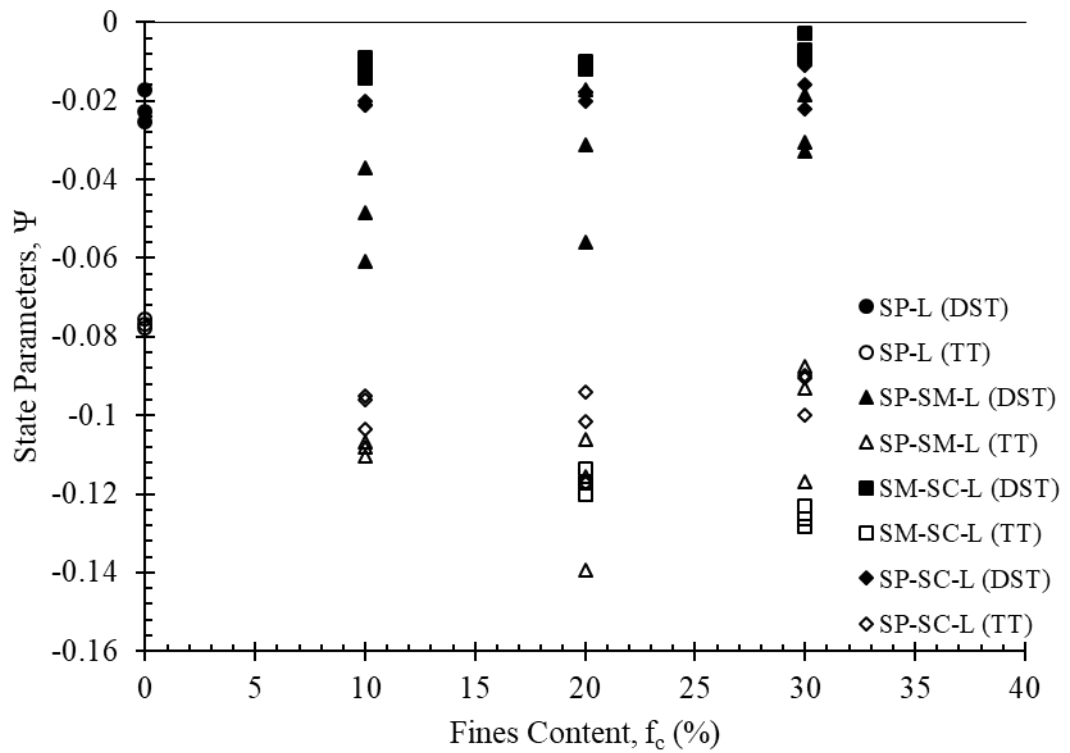


Figure 260: CD (DST) and CU (TT) SM-SC-D state parameters comparison with f_c .

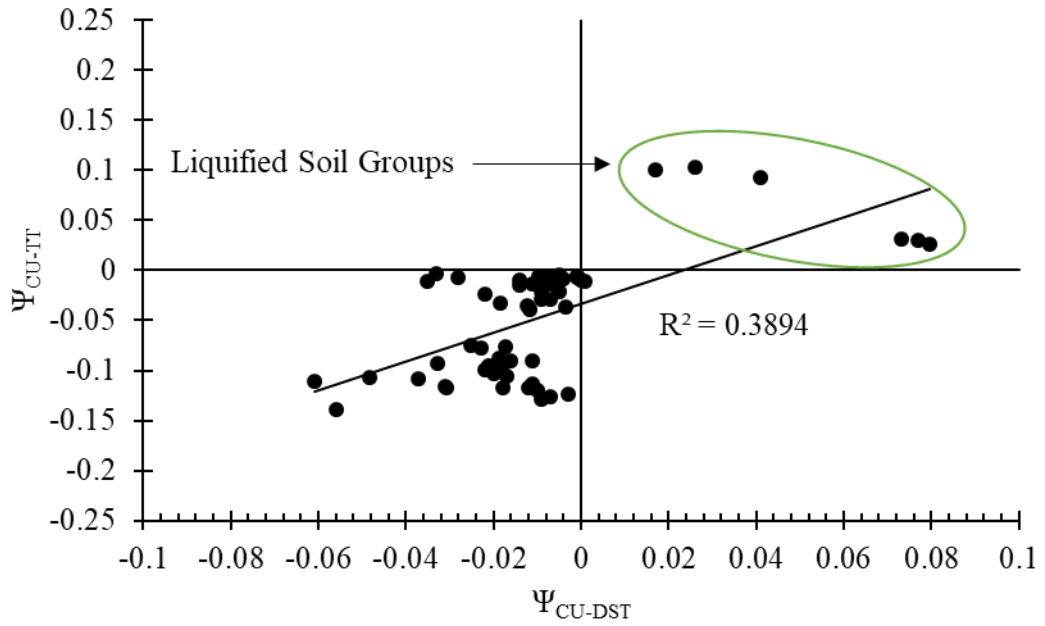


Figure 261: CD-DST & CU-TT Ψ comparison.

The state parameters obtained from both testings' indicating a good correlation since both testings' findings give similar behaviour and are plotting in the same quadrant (Figure 261). Although the regression value corresponding to linear fit is low, the P-value significance analysis indicating very low variation among both testing's (DST and TT) state parameter outcomes. The P-value analysis is presented in Table 20. In contrast to state parameters obtained in Figures 259 and Figure 260, similar results are obtained regarding the tendency of dilatancy as discussed in critical state analysis sections.

Table 20: P-value significance analysis of Ψ for CD-DST and CU-TT.

Regression Statistics					
Multiple R					0.555219
R Square					0.308269
Adjusted R Square					0.296342
Standard Error					0.021609
Observations					60
ANNOVA					
	DF	SS	MS	F	Significance F
Regression	1	0.01207	0.0120	25.84757	4.14E-06
Residual	58	0.027084	0.000467		
Total	59	0.039154			
	Coefficients	Standard Error	t Stat	P-value	
Intercept	0.001636	0.003581	0.456996	0.649381	
CT	0.185713	0.003581	5.084051	4.14E-06	< 0.05

Chapter 5

CONCLUSIONS AND RECOMMENDATIONS

5.1 Conclusions

In this section, conclusive remarks are presented based on the experimental results and analyses performed.

- A laboratory scale fines separation technique developed to obtain different types of fines from parent soil followed by incorporation of separated fines into sand-matrix. The fundamental objective to separate parent soil (Alluvial clay) is to obtain clay and silt fractions and to incorporate the separated fractions into sand-matrix with different proportions to form a set of manufactured sand-fines mixtures to depict the variation of natural deposits.
- The set of sand-fines mixtures are reconstituted for testing using employing dry funnel pluviation technique. The reconstituted specimens are reflecting initial relative densities of 35 and 70 percentages. The consolidated states of the specimens are carried out in two different testing setups, Direct Shear Box and Triaxial. Specimens are isotropically consolidated in triaxial under confining pressures of 50, 100 and 150 kPa. In terms of direct shear box test, specimens are consolidated under same effective normal stresses.
- In drained and undrained tests, primary evaluation criteria to assess contractive and dilative behaviour is based on state parameters since the said terminologies are associated to flow and non-flow behaviour affiliated to undrained behaviour. The evaluations of the experimental outcomes indicate the sand prepared at initially

loose state is exhibiting contractive behaviour and when the drainage conditions are constrained, limited flow behaviour is exhibited. Flow liquefaction behaviour is also observed when 10% of clays and silts with equal proportions are added to sand-matrix. At low confining stresses, specimens exhibited limited deformation while at 150 kPa of confining stress, total liquefaction phenomenon is observed. Based on the visual observations, in the said soil group, at low confining stresses, if the specimen is subjected to large strains total liquefaction phenomenon is observable. Since limited deformations is observed an interesting phenomenon is observed where fines are separated within the sand-matrix presenting the clear picture of soil fabric structure before total liquefaction.

- Sand matrix consisting of silt fractions, exhibiting stable behaviour for fine-dominated groups where it is observed that at threshold fines content, at loose state the initial states are plotting in the proximity of critical state lines.
- Presence of clay and silt fractions with equal proportions in sand matrix at threshold fines content exhibited strain-softening behaviour whereas, afterwards the stability of the soil is not prominent since the initial states are plotting on and very near to critical state limit lines. From the assessed behaviour it is noticed that 40% of fines inclusion evaluation became necessary since beyond this content proportion, the classification of the soil will be completely transformed to fine-grained soil.
- Clay particles (Illite mineral) presence in sand-matrix exhibited stable behaviour at 10 and 20 percentages and at 30 percentage of clay inclusion indicating similar characteristics of 20% where no improvement is observed. Such phenomenon again illustrating the significance of testing 40% fines and concluding the overall behaviour.

- Soil groups reconstituted at dense state is exhibiting stable or strain-hardening of all soil groups. A noticeable difference is observed in all 30% inclusion of fines groups, that no significance improvement in terms of engineering behaviour is observed simulating similar characteristics of 20% of fines in undrained testing. Similar characteristics are observed in drained testing.

5.2 Recommendations

Liquefaction topic in geotechnical earthquake engineering is one of the vast topics in research field. The possible future works can be performed on the existing evaluations and following are recommendations by the author:

- Analysing the behaviour of sand-matrix with 40 and 50 percentages fines inclusion.
- Expanding analysis of soil groups with different percentages of fines sub-groups such as 75% clay and 25% silt and vice versa.
- Employing different reconstitution technique such as wet pluviation.
- Analysing the sand dominated and fine dominated soils individually by employing dry funnel pluviation technique for sand dominated region and wet pluviation technique for fine-dominated region.
- Post shearing particle gradation analysis of tested soil groups and microstructural analysis of the particles.
- Application of high effective stresses to analyse the potential crushing and breakage of particles and surface area analysis under microscope.
- Analysing the cyclic mobility of non-liquefied soil groups since lateral spreading can occur in both loose and dense states.

- The undrained behaviour is highly dependent on mechanisms laboratory testings especially at high void ratios therefore, analysing the liquefaction potential of soil groups by triaxial extension tests.
- Shearing the specimen at different shearing rates and analysing the peak mobilized shear stress and rate of excess pore water generation of both liquefied and non-liquefied soil groups.
- Apart from free-field liquefaction analysis, effect of surcharge or structures influence (soil-structure interaction) on potential liquefaction analysis.

REFERENCES

- Alarcon-Guzman, A., Leonards, G. A., & Chameau, J. L. (1988). Undrained Monotonic and Cyclic Strength of Sands. *Journal of Geotechnical Engineering*, 1089-1109.
- Amini, F., & Qi, G. Z. (2000). Liquefaction Testing of Stratified Silty Sands. *Journal Of Geotechnical and Geoenvironmental Engineering*, 208-217.
- Araujo, W., & Ruiz, G. (2018). Prediction Methods of Liquefaction Phenomenon And Mitigation Strategies. *16th LACCEI International Multi-Conference for Engineering, Education, and Technology*. Lima, United States. : Innovation in Education and Inclusion.
- Baker, M., Baas, J. H., Malarkey, J., Silva, J. R., Craig, M., Kane, I., & Barker, S. (2017). The Effect of Clay Type On the Properties of Cohesive Sediment Gravity Flows and Their Deposits. *Journal of Sedimentary Research*, 1176-1195.
- Benghalia, Y., Bouafia, A., & Canou, J. (2014). Liquefaction Susceptibility Study of Sandy Soils: Effect of Low Plastic Fines. *Saudi Society for Geosciences*, 605-618.
- Bouferra, R., & Shahrour, I. (2004). Influence of fines on the resistance to liquefaction of a clayey. *Proceedings of the Institution of Civil Engineers - Ground Improvement*, 1-5.

- Cagnan, Z., & Tanircan, G. (2010). Seismic Hazard Assessment for Cyprus. *Journal of Seismology*, 225-246.
- Cerato, A. B., & Lutenegeger, A. J. (2002). Determination of Surface Area of Fine-Grained Soils by the Ethylene Glycol Monoethyl Ether (EGME) Method. *Geotechnical Testing Journal*, 315-321.
- Chang, N. Y. (1987). *Liquefaction Susceptibility of Fine-Grained Soils Preliminary Study Report*. Washington DC: Department of the Army US Army Corps of Engineers.
- Chien, L. K., Oh, Y. N., & Chang, C. H. (2002). Effects of Fines Content on Liquefaction Strength and Dynamic Settlement of Reclaimed Soil. *Canadian Geotechnical Journal*, 254-265.
- Cokca, E., & Birand, A. (1993). Determination of Cation Exchange Capacity of Clayey Soils by the Methylene Blue Test. *Geotechnical Testing Journal*, 518-524.
- Das, B. M., & Sobhan, K. (2014). Plasticity Chart Engineering. In *Principles of Geotechnical* (8th ed., pp. 112-113). Stamford: Cengage Learning.
- Della, N., Arab, A., Belkhatir, M., & Missoum, H. (2009). Identification of the Behaviour of the Chelf Sand to Static Liquefaction. *Science Direct*, 282-290.

Dillerstone, J. (2011, May 10). *Liquefaction: Land Sinkage from Earthquakes*.

Retrieved from Janette Dillerstone:

<https://janettedillerstone.wordpress.com/tag/liquefaction/>

Geo-Slope International Limited. (n.d.). *GeoSlope*. Retrieved from Seequent:

<http://downloads.geoslope.com/geostudioresources/8/0/examples/QuakeW/Lower%20San%20Fernando%20Dam.pdf>

Guo, T., & Prakash, S. (1999). Liquefaction Of Silts and Silt-Clay Mixtures. *Journal Of Geotechnical and Geoenvironmental Engineering*, 706-710.

Head, K. H., & Epps, R. J. (2011). Drained Strength and Residual Strength Shearbox Tests. In *Manual of Soil Laboratory Testing* (pp. 274-276). Scotland: Whittles Publishing.

Hershel Friedman. (2010). *Minerals.net*. Retrieved from

https://www.minerals.net/gemstone/quartz_gemstone.aspx

Holtz, R. D., & Kovacs, W. D. (1981). Identification of Clay Minerals. In *An Introduction to Geotechnical Engineering* (p. 89). Parentice Hall.

Ishihara, K. (1993). Liquefaction and Flow Failure During Earthquake. *Geotechnique*, 351-415.

Ishihara, K. (1996). Residual strength of fines-containing sand. In *Soil Behaviour in Earthquake Geotechnics* (pp. 268-269). New York: Oxford University Press.

- Ishihara, K. (1996). Sand Behaviour Under Monotonic Loading. In *Soil Behaviour in Earthquake Geotechnics* (pp. 247-248). New York: Oxford University Press.
- Jefferies, M., & Been, K. (2016). *Soil Liquefaction; A Critical State Approach*. Boca Raton: CRC Press.
- Kim, U., Kim, D., & Zhuang, L. (2016). Influence Of Fines Content on The Undrained Cyclic Shear Strength of Sand–Clay Mixtures. *Soil Dynamics and Earthquake Engineering*, 124-134.
- Koester, J. P. (1988). *Earthquake Induced Liquefaction of Fine-Grained Soils*. Washington DC: Department of the Army US Army Corps of Engineers.
- Kramer, S. L. (2014). Liquefaction. In *Geotechnical earthquake Engineering* (pp. 361-362). Edinbrugh: UK.
- Kuerbis, R., Negussey, D., & Vaid, Y. (1988). Effect of Gradation and Fines Content on the Undrained Response of Sand. *ASCE Geotechnical Special Publication No. 21*.
- Ladd, S. R. (1977). Specimen Preparation and Cyclic Stability of Sands. *Journal of the Geotechnical Engineering Division*, 535-547.
- Lade, P. V., & Yamamuro, J. A. (1997). Effects of Nonplastic Fines on Static Liquefaction of Sands. *Canadian Geotechnical Journal*, 918-928.

- Lade, P. V., Liggio, C. D., & Yamamuro, J. A. (1998). Effects of Non-Plastic Fines on Minimum and Maximum Void Ratios of Sand. *Geotechnical Testing Journal*, 336-347.
- Marto, A., Tan, C. S., Makhtar, A. M., Wen, S. U., & Yen, L. M. (2015). Effect of Plasticity on Liquefaction Susceptibility of Sand-Fines Mixtures. *Applied Mechanics and Materials*, 1407-1411.
- Monkul, M. M. (2013). Influence of Gradation on Shear Strength and Volume Change Behavior of Silty Sands. *Geomechanics and Engineering*, 401-417.
- Monkul, M. M., Etminan, E., & Şenol, A. (2017). Coupled Influence of Content, Gradation and Shape Characteristics of Silts on Static Liquefaction of Loose Silty Sands. *Soil Dynamics and Earthquake Engineering*, 12-26.
- Mulilis, P. J., Seed, B. H., Chan, C., Mitchell, JK., K. J., & Arulanandan, K. (1997). Effect of Sample Preparation on Sand Liquefaction. *Journal of the Geotechnical Engineering Division*, 91-109.
- Novikova, T., Papadopoulos, G., & Karastathis, V. (2006). Evaluation of Ground Motion Characteristics, Effects of Local Geology and Liquefaction Susceptibility. *Springer Science*.
- Olson, S. M., & Stark, T. D., (2003). Yield Strength Ratio and Liquefaction Analysis of Slopes and Embankments. *Journal of Geotechnical and Geoenvironmental*. 842-853.

- Park, S.-S., & Kim, Y.-S. (2013). Liquefaction Resistance of Sands Containing Plastic Fines With Different Plasticity. *Journal of Geotechnical and Geoenvironmental Engineering*, 825-830.
- Phan, V. T.-A., Hsiao, D. H., & Nguyen, P. T.-L. (2016). Critical State Line and State Parameter of Sand-Fines Mixtures. *Procedia Engineering*, 299-306.
- Polito, C. P., & Martin, J. R. (2001). Effects of Nonplastic Fines on the Effects of Nonplastic Fines on the. *Journal of Geotechnical and Geoenvironmental Engineering*, 408-415.
- Rahman, M. M., & Lo, S. R. (2014). Undrained Behavior of Sand-Fines Mixtures and Their State Parameter. *Journal of Geotechnical and Geoenvironmental Engineering*, 1-12.
- Saputra, W. (2016). Problem Encountered When Producing Carbonate Sand Reservoir.
- Seed, H. B. (1981). Earthquake Resistant Design of Earth Dams. *International Conferences on Recent Advances in Geotechnical Earthquake Engineering and Soil Dynamics*. St. Louis Missouri.
- Tana, C. S., Marto, A., Makhtar, A. M., Chong, S. Y., & Pakir, F. (2015). Liquefaction Resistance of Sand Matrix Soils. *Jurnal Teknologi (Sciences & Engineering)*, 67-72.

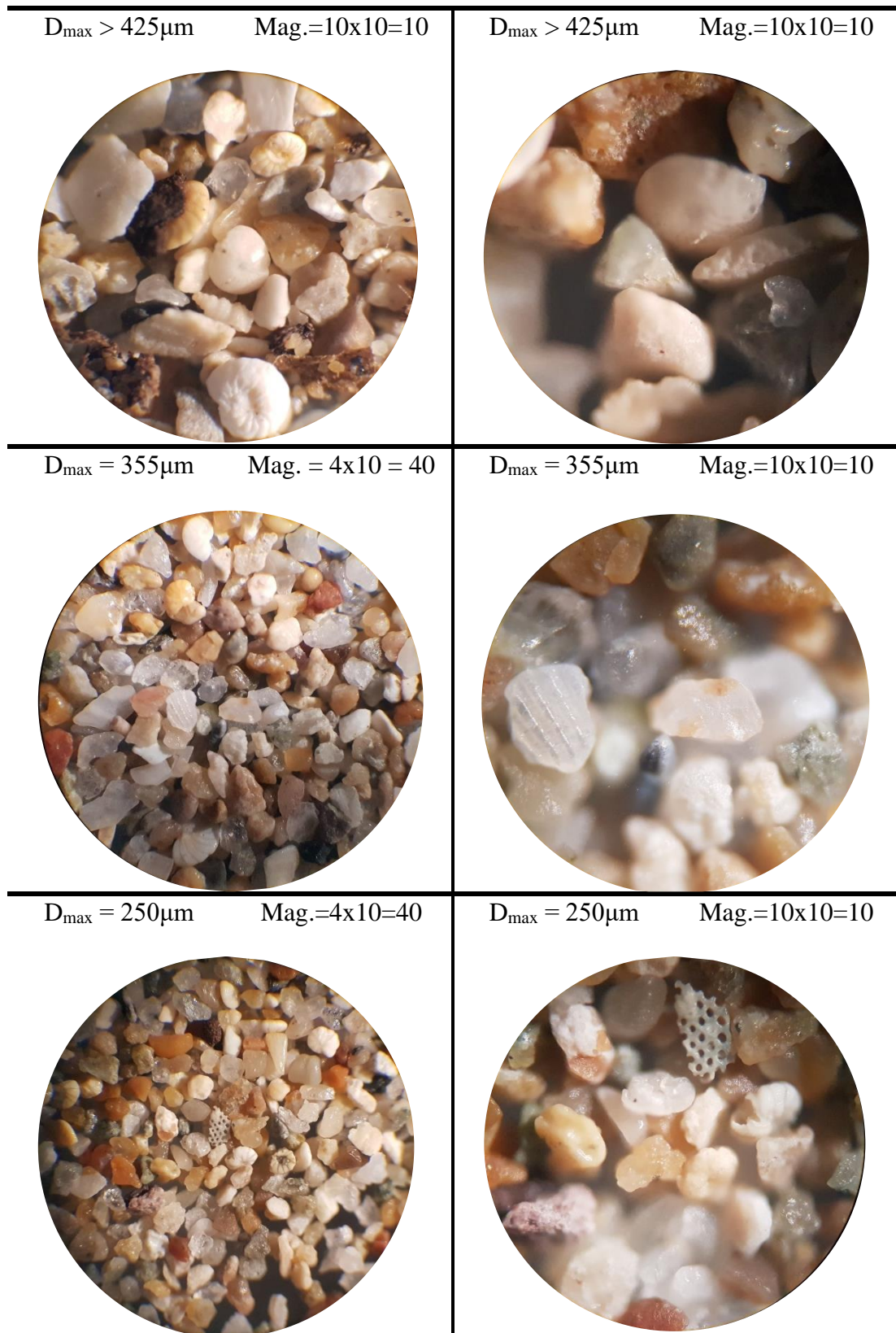
- Thevanayagam, S. (1998). Effect of Fines and Confining Stress on Undrained Shear Strength of Silty Sands. *Journal of Geotechnical And Geoenvironmental Engineering* , 479-491.
- Thevanayagam, S., Shenthan, T., Mohan, S., & Liang, J. (2002). Undrained Fragility of Clean Sands, Silty Sands, and Sandy Silts. *Journal of Geotechnical and Geoenvironmental Engineering*, 849-859.
- Umaharathi, N., Bhargav, K. P., & Balunaini, U. (2018). Effect of Plastic Fines on Shear Strength of Sands. *Geotechnical Characterisation and Geoenvironmental Engineering*, 51-58.
- Vallejo, L. E., & Mawby, R. (2000). Porosity Influence on The Shear Strength of Granular Material-Clay Mixtures. *Engineering Geology*, 125-136.
- Wang, Y., & Wang, Y. (2010). Study of Effects of Fines Content on Liquefaction Properties of Sand. *Soil Dynamics and Earthquake Engineering* (pp. 272-277). Shanghai: GeoShanghai 2010 International Conference.
- Xenaki, V., & Athanasopoulos, G. (2003). Liquefaction Resistance of Sand–Silt Mixtures: An Experimental Investigation of The Effect Of Fines. *Soil Dynamics and Earthquake Engineering*, 183-194.
- Yamamuro, J. A., Wood, F. M., & Lade, P. V. (2008). Effect of Depositional Method on the Microstructure of Silty Sand. *Canadian Geotechnical Journal*, 1538-1555.

- Yang, S. L., Sandven, R., & Grande, L. (2006). Instability of Sand–Silt Mixtures. *Soil Dynamics and Earthquake Engineering*, 183-190.
- Yang, S., Lacasse, S., & Sandven, R. (2006). Determination of the Transitional Fines Content of Mixtures of Sand and Non-plastic Fines. *ASTM Geotechnical Testing Journal*, 102-107.
- Yoshimine, M., & Ishihara, K. (1998). Flow Potential of Sand During Liquefaction. *Japanese Geotechnical Society*, 189-198.
- Zlatovic, S., & Ishihara, K. (1997). Normalized Behaviour of Very Loose Non-Plastic Soils. *Soils and Foundations*, 47-56.





APPENDICES

Appendix A: Optical Microscopic Analysis of Silver Beach Sand

A-1: SBS microscopic image [Range 425 – 250 μm]



A-2: SBS microscopic analysis [Range 212 – 150 μm]

$D_{\text{max}} = 212\mu\text{m}$ $\text{Mag.}=4\times 10=40$	$D_{\text{max}} = 212\mu\text{m}$ $\text{Mag.}=10\times 10=100$
	
$D_{\text{max}}=180\mu\text{m}$ $\text{Mag.}=4\times 10=40$	$D_{\text{max}}=180\mu\text{m}$ $\text{Mag.}=10\times 10 =100$
	
$D_{\text{max}} = 150\mu\text{m}$ $\text{Mag.} = 4\times 10 =40$	$D_{\text{max}}=150\mu\text{m}$ $\text{Mag.}=10\times 10 =100$
	

A-3: SBS microscopic analysis [Range 125 – 90 μm]

$D_{\max}=125\mu\text{m}$ $\text{Mag.} = 4 \times 10 = 40$	$D_{\max}=125\mu\text{m}$ $\text{Mag.}=10 \times 10 = 100$
	
$D_{\max}=106\mu\text{m}$ $\text{Mag.} = 4 \times 10 = 40$	$D_{\max}=106\mu\text{m}$ $\text{Mag.}=10 \times 10 = 100$
	
$D_{\max}=90\mu\text{m}$ $\text{Mag.} = 4 \times 10 = 40$	$D_{\max}=90\mu\text{m}$ $\text{Mag.}=10 \times 10 = 100$
	

A-4: SBS microscopic analysis [Range < 75 μm]

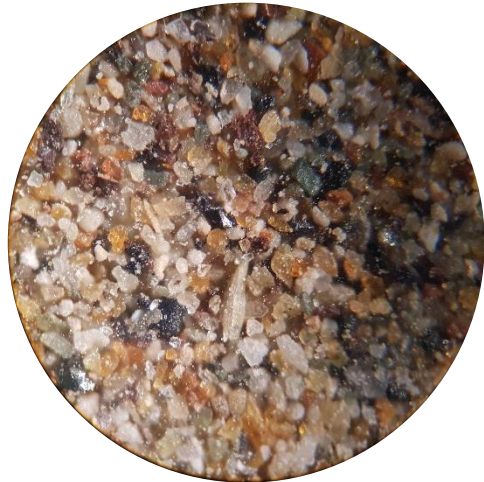
D < 75 μm

Mag. = 4x10 = 40



D < 75 μm

Mag. = 10x10 = 100



Appendix B: Separated Soil Liquid Limit Linear Regression Analysis

B-1: Alluvial Clay

No. of blows	15	30	32
w.c (%)	56	52	49
Equation	$w.c (\%) = -5.634 \ln (\text{no. of blows}) + 70.842$		
R²	0.9998		
LL (%)	53		

B-2: Separated Silt

No. of blows	14	16	20	29
w.c (%)	59	56	54	51
Equation	$w.c (\%) = -10.07 \ln (\text{no of blows}) + 84.483$			
R²	0.9457			
LL (%)	52			

B-3: Separated Clay

No. of blows	13	15	20	44
w.c (%)	59	58	57	54
Equation	$w.c (\%) = -3.812 \ln (\text{no. of blows}) + 68.542$			
R²	0.9694			
LL (%)	56			

B-4: Clay and Silt with Equal Proportions

No. of blows	18	28	36
w.c (%)	55	51	48
Equation	$w.c (\%) = -10 \ln (\text{no. of blows}) + 84.072$		
R²	0.9943		
LL (%)	52		

Appendix C: Direct Shear Box Test Experiment Outcomes

C-1: CD-DST experimental outcomes summary of Sand

Parameters	Applied Effective Normal Stress, σ'_n (kPa)								
	Loose			Residual			Dense		
	50	100	150	50	100	150	50	100	150
e_i	0.778	0.762	0.753	0.705	0.694	0.673	0.682	0.669	0.661
ϕ'_{max} (°,deg)	32.2	31.7	32.0	35.9	36.3	36.1	40.1	39.9	40.1
Equation	$\tau = 0.67 + 0.6243\sigma'_n$			$\tau = 0.36 + 0.7301\sigma'_n$			$\tau = 1.33 + 0.8412\sigma'_n$		
R^2	1.00			0.9998			0.9997		
ϕ'_{avg} (°,deg)	32			36			40		
c' (kPa)	0.67			0.36			1.33		

C-2: CS-DST experimental outcomes summary of Silty-Sand (10%).

Parameters	Applied Effective Normal Stress, σ'_n (kPa)								
	Loose			Residual			Dense		
	50	100	150	50	100	150	50	100	150
e_i	0.714	0.680	0.670	0.721	0.690	0.684	0.660	0.652	0.636
ϕ'_{max} (°,deg)	29.1	29.8	29.3	28.3	28.6	28.4	36.4	34.1	35.6
Equation	$\tau = 0.53 + 0.5656\sigma'_n$			$\tau = 3.38 + 0.5416\sigma'_n$			$\tau = 3.86 + 0.7066\sigma'_n$		
R^2	0.9994			0.9999			0.9950		
ϕ'_{avg} (°,deg)	29			28			35		
c' (kPa)	0.53			3.4			3.9		

C-3: CD-DST experimental outcomes summary of Silty-Sand (20%).

Parameters	Applied Effective Normal Stress, σ'_n (kPa)								
	Loose			Residual			Dense		
	50	100	150	50	100	150	50	100	150
e_i	0.713	0.680	0.669	0.717	0.687	0.664	0.661	0.656	0.647
ϕ'_{max} (°,deg)	29.4	28.8	29.2	28.4	26.6	27.8	35.0	32.6	34.2
Equation	$\tau = 0.98 + 0.5561\sigma'_n$			$\tau = 4.44 + 0.5208\sigma'_n$			$\tau = 4.44 + 0.6697\sigma'_n$		
R^2	0.9996			0.9958			0.9939		
ϕ'_{avg} (°,deg)	29			28			34		
c' (kPa)	1.00			4.4			4.4		

C-4: CD-DST experimental outcomes summary of Silty-Sand (30%).

Parameters	Applied Effective Normal Stress, σ'_n (kPa)								
	Loose			Residual			Dense		
	50	100	150	50	100	150	50	100	150
e_i	0.731	0.718	0.706	0.743	0.725	0.681	0.707	0.692	0.662
ϕ'_{max} (°,deg)	29.8	30.6	30.0	28.3	29.5	28.7	31.5	32.9	31.9
Equation	$\tau = 2.35 + 0.5813\sigma'_n$			$\tau = 4.71 + 0.5526\sigma'_n$			$\tau = 6.72 + 0.6298\sigma'_n$		
R^2	0.9993			0.9982			0.9979		
ϕ'_{avg} (°,deg)	30			29			32		
c' (kPa)	2.4			4.7			6.7		

C-5: CD-DST experimental outcomes summary of Clayey-Silty-Sand (10%).

Parameters	Applied Effective Normal Stress, σ'_n (kPa)								
	Loose			Residual			Dense		
	50	100	150	50	100	150	50	100	150
e_i	0.728	0.706	0.689	0.658	0.653	0.647	0.654	0.634	0.627
ϕ'_{max} (°,deg)	29.1	29.1	29.1	25.9	29.5	27.2	35.8	36.8	36.1
Equation	$\tau = 1.30 + 0.5562\sigma'_n$			$\tau = 2.69 + 0.5268\sigma'_n$			$\tau = 2.9 + 0.7341\sigma'_n$		
R^2	1.00			0.9833			0.9991		
ϕ'_{avg} (°,deg)	29			28			36		
c' (kPa)	1.3			2.7			2.9		

C-6: CD-DST experimental outcomes summary of Clayey-Silty-Sand (20%).

Parameters	Applied Effective Normal Stress, σ'_n (kPa)								
	Loose			Residual			Dense		
	50	100	150	50	100	150	50	100	150
e_i	0.747	0.708	0.685	0.668	0.639	0.636	0.670	0.666	0.643
ϕ'_{max} (°,deg)	30.9	28.8	29.2	27.6	27.0	28.4	35	32.6	34.2
Equation	$\tau = 3.66 + 0.5373\sigma'_n$			$\tau = 2.12 + 0.5489\sigma'_n$			$\tau = 3.44 + 0.6697\sigma'_n$		
R^2	0.9983			0.9973			0.9939		
ϕ'_{avg} (°,deg)	28			29			34		
c' (kPa)	3.66			2.12			3.44		

C-7: CD-DST experimental outcomes summary of Clayey-Silty-Sand (30%).

Parameters	Applied Effective Normal Stress, σ'_n (kPa)								
	Loose			Residual			Dense		
	50	100	150	50	100	150	50	100	150
e_i	0.786	0.753	0.718	0.690	0.662	0.637	0.708	0.697	0.672
ϕ'_{max} (°,deg)	29.8	30.6	30.0	28.3	29.5	28.7	31.5	32.9	31.9
Equation	$\tau = 2.35+0.5813\sigma'_n$			$\tau = 4.71+0.5526\sigma'_n$			$\tau = 6.72+0.6298\sigma'_n$		
R^2	0.9993			0.9982			0.9979		
ϕ'_{avg} (°,deg)	30			29			32		
c' (kPa)	2.4			4.7			6.7		

C-8: CD-DST experimental outcomes summary of Clayey-Sand (10%).

Parameters	Applied Effective Normal Stress, σ'_n (kPa)								
	Loose			Residual			Dense		
	50	100	150	50	100	150	50	100	150
e_i	0.723	0.710	0.699	0.758	0.743	0.727	0.738	0.722	0.706
ϕ'_{max} (°,deg)	30.4	30.2	30.4	29.5	29.1	29.3	36.5	37.7	36.9
Equation	$\tau = 0.89+0.5860\sigma'_n$			$\tau = 2.97+0.5607\sigma'_n$			$\tau = 3.25+0.7555\sigma'_n$		
R^2	0.9999			0.9998			0.9985		
ϕ'_{avg} (°,deg)	30			29			37		
c' (kPa)	1.0			2.9			3.2		

C-9: CD-DST experimental outcomes summary of Clayey-Sand (20%).

Parameters	Applied Effective Normal Stress, σ'_n (kPa)								
	Loose			Residual			Dense		
	50	100	150	50	100	150	50	100	150
e_i	0.687	0.676	0.666	0.696	0.685	0.671	0.678	0.665	0.653
ϕ'_{\max} (°,deg)	32.8	31.8	32.5	28.9	27.8	28.5	34.7	37.9	35.8
Equation	$\tau = 2.5 + 0.6330\sigma'_n$			$\tau = 3.13 + 0.5392\sigma'_n$			$\tau = 5.92 + 0.7352\sigma'_n$		
R^2	0.9989			0.9987			0.9898		
ϕ'_{avg} (°,deg)	32			28			36		
c' (kPa)	2.5			3.1			5.9		

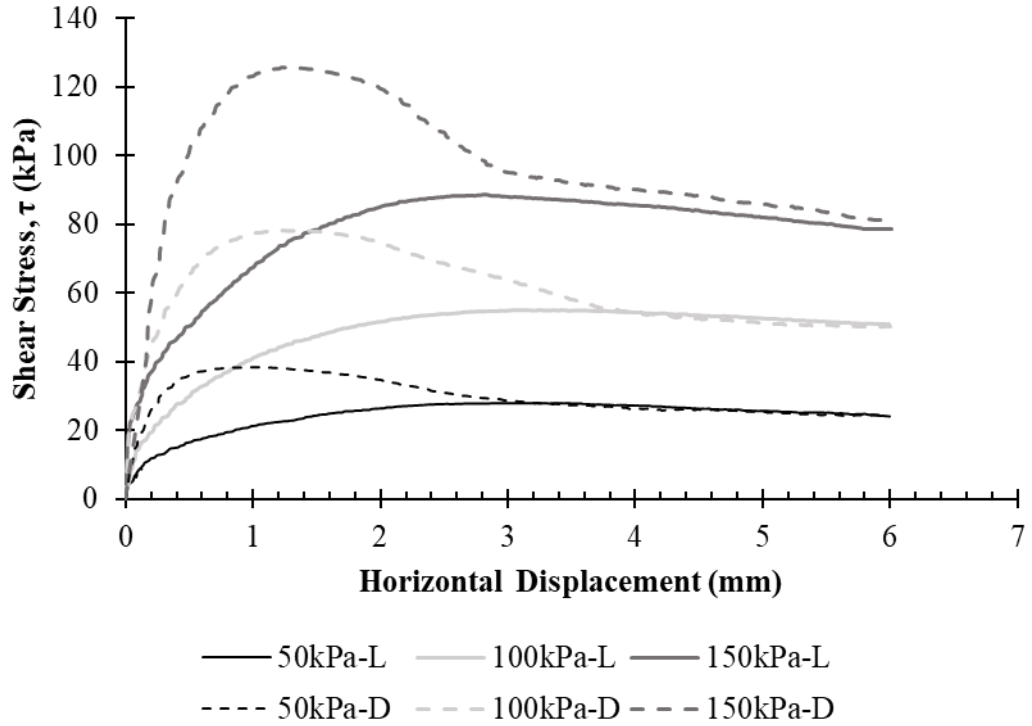
C-10: CD-DST experimental outcomes summary of Clayey-Sand (30%).

Parameters	Applied Effective Normal Stress, σ'_n (kPa)								
	Loose			Residual			Dense		
	50	100	150	50	100	150	50	100	150
e_i	0.768	0.741	0.728	0.767	0.740	0.729	0.745	0.729	0.713
ϕ'_{\max} (°,deg)	33.6	29.7	32.2	29.0	27.3	28.5	37.5	37.7	37.6
Equation	$\tau = 5.71 + 0.6163\sigma'_n$			$\tau = 3.40 + 0.5353\sigma'_n$			$\tau = 9.72 + 0.7716\sigma'_n$		
R^2	0.9839			0.9959			1.00		
ϕ'_{avg} (°,deg)	32			28			37		
c' (kPa)	5.7			3.4			9.7		

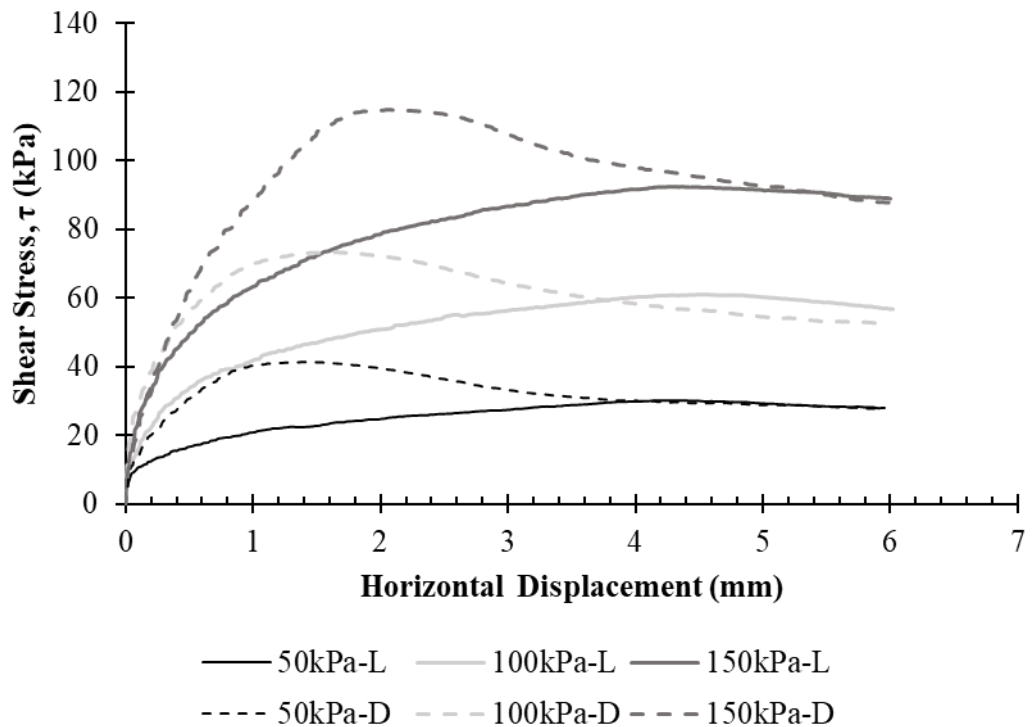
Appendix D: Direct Shear Box Test Shear Stress versus Displacement

Curves

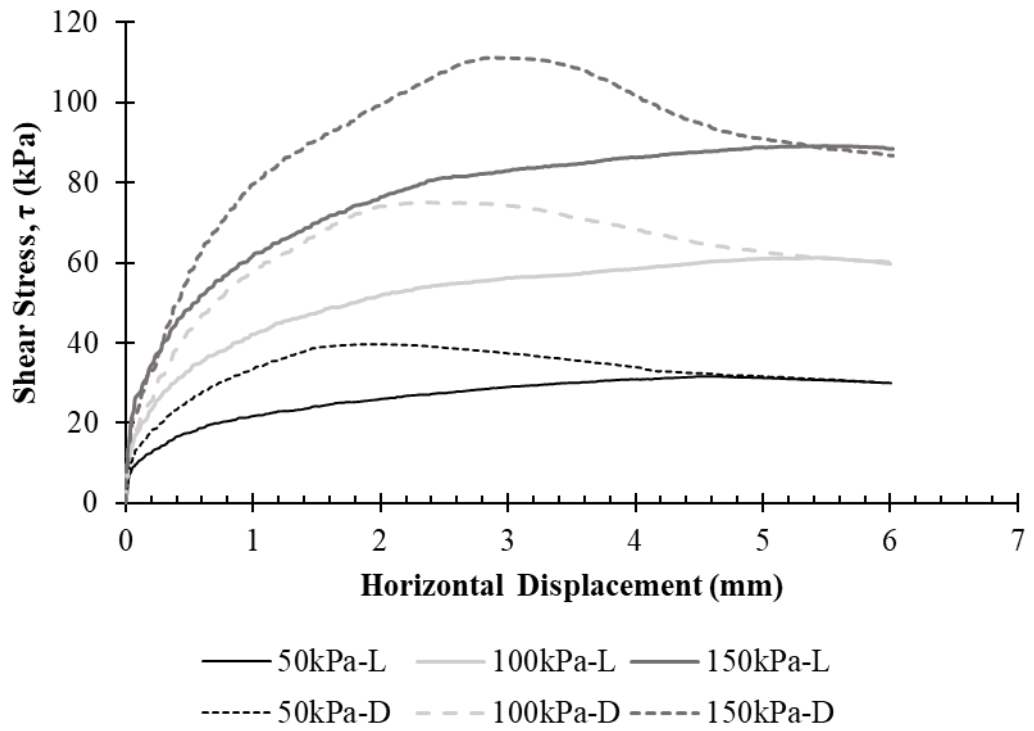
D-1: Loose and dense Sand plot.



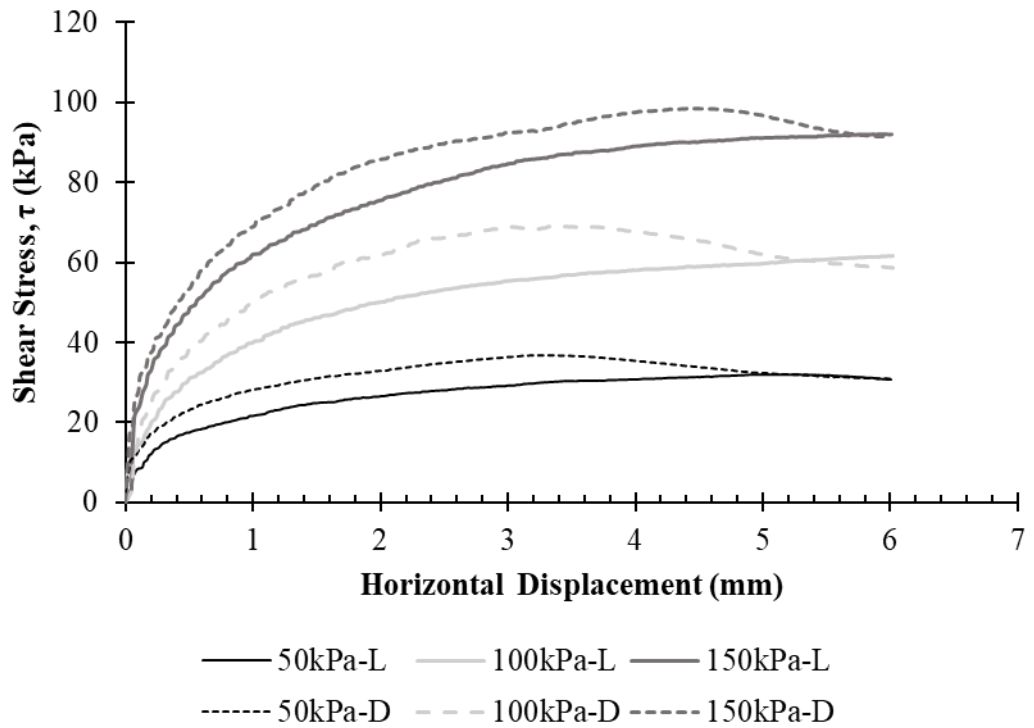
D-2: Loose and dense silty-Sand (10%) plot.



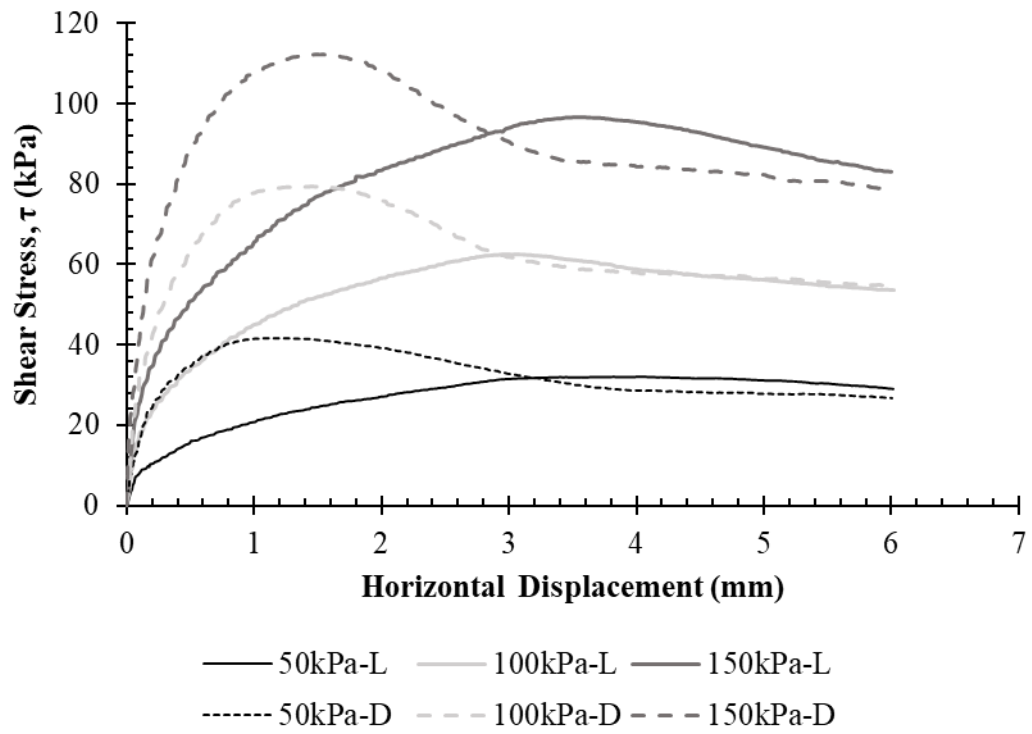
D-3: Loose and dense silty-Sand (20%) plot.



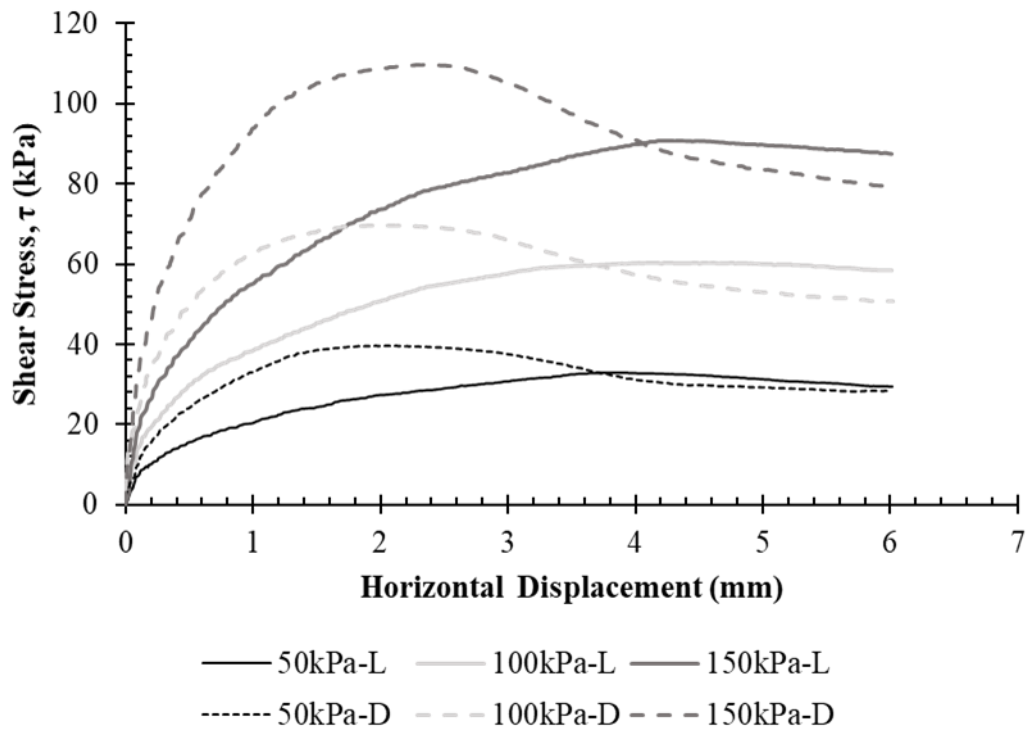
D-4: Loose and dense silty-Sand (30%) plot.



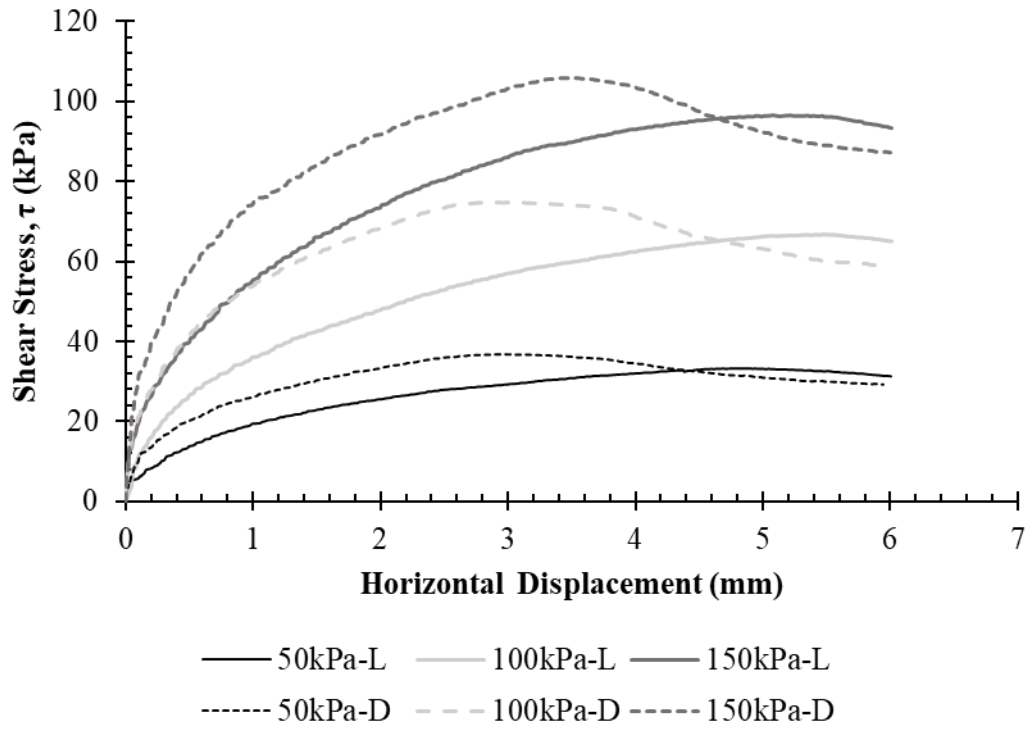
D-5: Loose and dense clayey-silty-Sand (10%) plot.



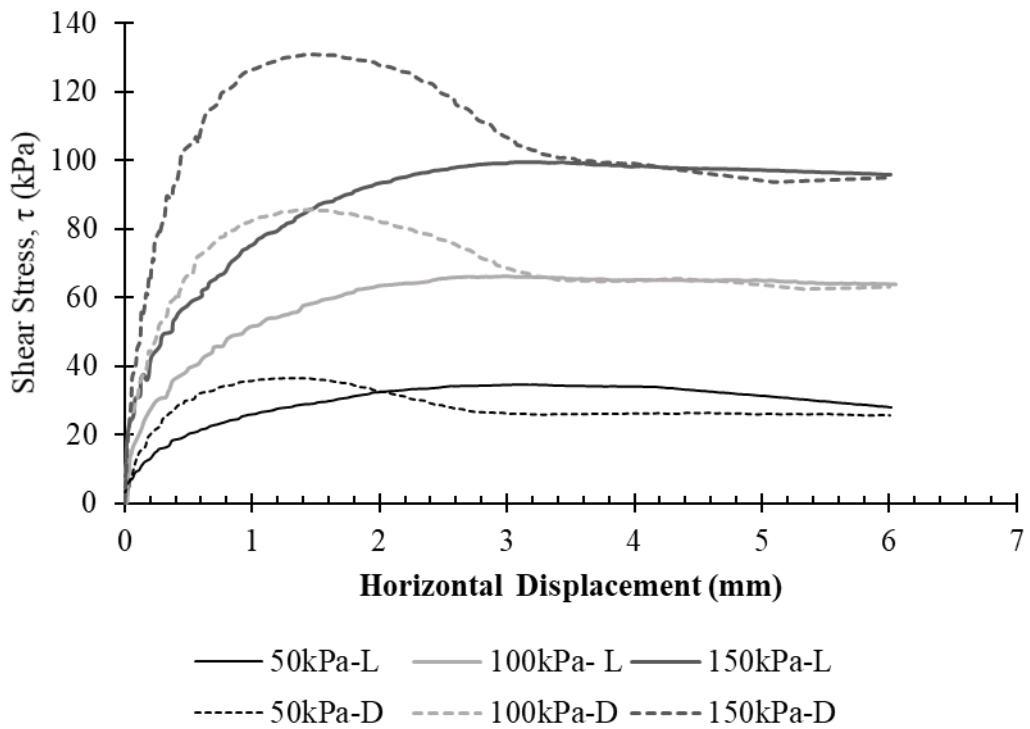
D-6: Loose and dense clayey-silty-Sand (20%) plot.



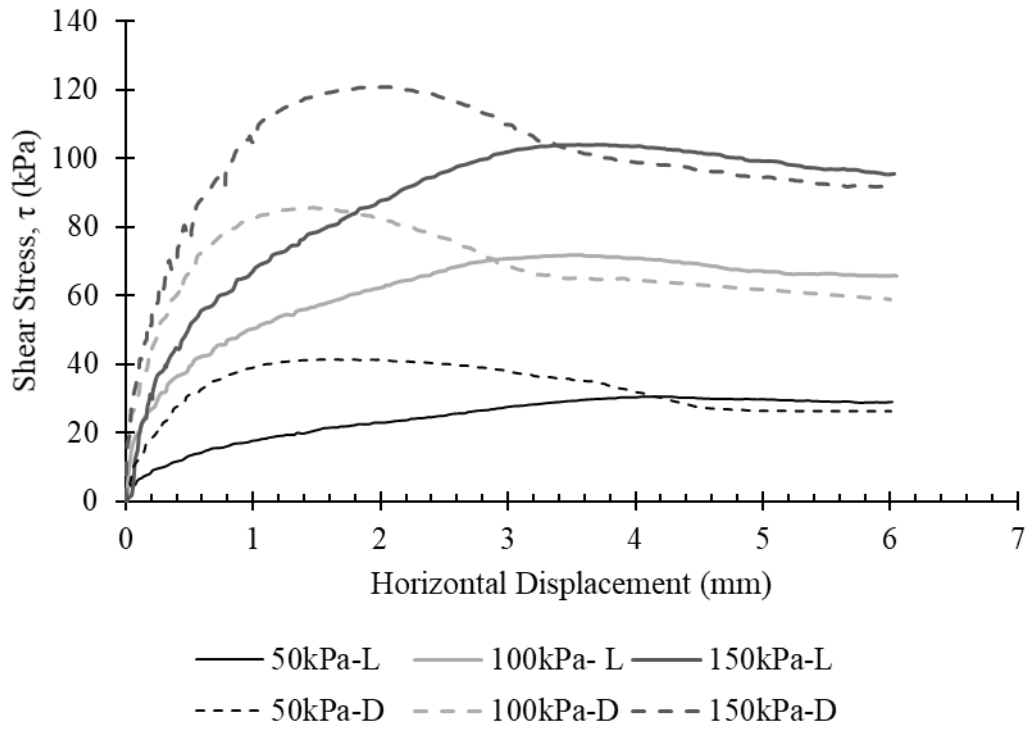
D-7: Loose and dense clayey-silty-Sand (30%) plot.



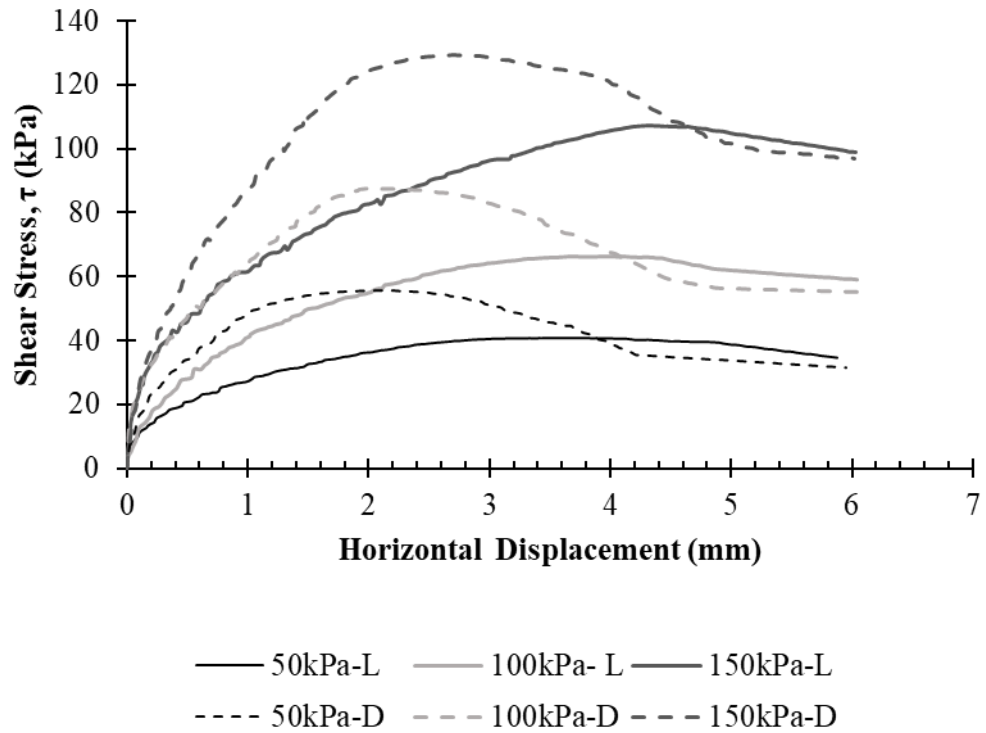
D-8: Loose and dense clayey -Sand (10%) plot.



D-9: Loose and dense clayey -Sand (20%) plot.



D-10: Loose and dense clayey -Sand (30%) plot.



Appendix E: Critical State Parameters CU-TT

E-1: SP CSL parameters.

State	N	λ	R^2	Γ	λ	R^2
NCL-L	0.87	0.013	0.9876			
CSL				0.82	0.009	0.9983
NCL-D	0.71	0.0001	0.9959			

E-2: SP-SM (10%) CSL parameters.

State	N	λ	R^2	Γ	λ	R^2
NCL-L	0.84	0.012	0.8			
CSL				0.87	0.016	0.9069
NCL-D	0.75	0.013	0.9998			

E-3: SP-SM (20%) CSL parameters.

State	N	λ	R^2	Γ	λ	R^2
NCL-L	0.98	0.044	0.9527			
CSL				1.02	0.043	0.9140
NCL-D	0.76	0.012	0.9470			

E-4: SP-SM (30%) CSL parameters.

State	N	λ	R^2	Γ	λ	R^2
NCL-L	0.82	0.016	0.9766			
CSL				1.04	0.043	0.9895
NCL-D	0.96	0.033	0.8887			

E-5: SM-SC (10%) CSL parameters.

State	N	λ	R^2	Γ	λ	R^2
NCL-L	0.84	0.013	0.9782			
CSL				0.79	0.023	0.9821
NCL-D	0.76	0.019	0.9946			

E-6: SM-SC (20%) CSL parameters.

State	N	λ	R^2	Γ	λ	R^2
NCL-L	0.86	0.009	0.9485			
CSL				0.88	0.012	0.9774
NCL-D	0.77	0.014	0.8533			

E-7: SM-SC (30%) CSL parameters.

State	N	λ	R^2	Γ	λ	R^2
NCL-L	0.90	0.008	0.9741			
CSL				0.92	0.009	0.9725
NCL-D	0.79	0.01	0.8266			

E-8: SP-SC (10%) CSL parameters.

State	N	λ	R^2	Γ	λ	R^2
NCL-L	0.82	0.017	0.9076			
CSL				0.84	0.021	0.9395
NCL-D	0.709	0.013	0.9682			

E-9: SP-SC (20%) CSL parameters.

State	N	λ	R^2	Γ	λ	R^2
NCL-L	0.91	0.028	0.9927			
CSL				0.96	0.035	0.9999
NCL-D	0.72	0.002	0.9966			

E-10: SP-SC (30%) CSL parameters.

State	N	λ	R^2	Γ	λ	R^2
NCL-L	0.90	0.016	0.9819			
CSL				0.92	0.019	0.9614
NCL-D	0.80	0.01	0.85			